

# Measurement of $J/\psi$ production cross-section in $pp$ collisions at $\sqrt{s} = 5 \text{ TeV}$

Z. Ren<sup>1</sup>, M. Wang<sup>1</sup>, L. Xu<sup>1</sup>, Z. Yang<sup>1</sup>, L. Zhang<sup>1</sup>, S. Zhang<sup>2</sup> and X. Zhu<sup>1</sup>.

<sup>1</sup>*Center for High Energy Physics, Tsinghua University, Beijing, China*

<sup>2</sup>*School of Physics State Key Laboratory of Nuclear Physics and Technology, Peking University, Beijing, China*

## Abstract

Production cross-sections of  $J/\psi$  mesons in proton-proton collisions at a centre-of-mass energy  $\sqrt{s} = 5 \text{ TeV}$  is measured, using a data sample with the integrated luminosity of  $9.13 \pm 0.18 \text{ pb}^{-1}$  collected by the LHCb detector in LHC operations in 2015. The double differential cross-sections, as functions of the transverse momentum  $p_T$  and the rapidity  $y$  of the  $J/\psi$  mesons, are determined separately for prompt  $J/\psi$  mesons and  $J/\psi$  mesons from  $b$ -hadron decays in the range  $0 < p_T < 14 \text{ GeV}/c$  and  $2 < y < 4.5$ . The production cross-sections integrated over the kinematic coverage are

$$\begin{aligned}\sigma(\text{prompt } J/\psi) &= 8.150 \pm 0.010(\text{stat}) \pm 0.283(\text{syst}) \mu\text{b}, \\ \sigma(J/\psi \text{ from } b) &= 0.817 \pm 0.003(\text{stat}) \pm 0.034(\text{syst}) \mu\text{b},\end{aligned}$$

assuming zero polarization of the  $J/\psi$  mesons.



# Contents

<b>1</b>	<b>Introduction</b>	<b>4</b>
<b>2</b>	<b>Data and Monte Carlo samples</b>	<b>5</b>
2.1	Data . . . . .	5
2.2	Monte Carlo . . . . .	5
<b>3</b>	<b>Cross-section determination</b>	<b>6</b>
<b>4</b>	<b>Candidate reconstruction and selection</b>	<b>7</b>
4.1	Trigger and Turbo stream selection . . . . .	7
4.2	Offline selection . . . . .	8
<b>5</b>	<b>Signal extraction</b>	<b>9</b>
5.1	Determination of the total $J/\psi$ signal yields . . . . .	9
5.2	Determination of the prompt and detached signal yields . . . . .	9
<b>6</b>	<b>Efficiency determination</b>	<b>13</b>
6.1	Acceptance . . . . .	15
6.2	Reconstruction-selection efficiency . . . . .	16
6.3	PID efficiency . . . . .	16
6.4	Trigger efficiency . . . . .	19
6.5	Total efficiency . . . . .	19
<b>7</b>	<b>Systematic uncertainties</b>	<b>20</b>
7.1	Signal model of mass fit . . . . .	20
7.2	Background model mass fit . . . . .	21
7.3	$t_z$ background shape . . . . .	22
7.4	Long tail in $t_z$ distribution . . . . .	22
7.5	Signal model of $t_z$ fit . . . . .	23
7.6	Tracking efficiency . . . . .	23
7.7	PID efficiency . . . . .	24
7.8	Trigger efficiency . . . . .	26
7.9	Polarisation . . . . .	28
7.10	Other sources . . . . .	29
7.11	Summary of systematic uncertainties . . . . .	30
<b>8</b>	<b>Results</b>	<b>31</b>
8.1	Cross-sections at 5 TeV . . . . .	31
8.2	Fraction of $J/\psi$ from $b$ . . . . .	32
8.3	Extrapolation to the total $b\bar{b}$ cross-section . . . . .	34
8.4	Comparison with results at 13 TeV . . . . .	34
8.5	Comparison with results at 8 TeV . . . . .	36
8.6	Comparison with theory models . . . . .	37
8.7	Nuclear modification factor . . . . .	40
<b>9</b>	<b>Conclusion</b>	<b>41</b>

<b>A</b>	<b>Tables of cross-section results</b>	<b>44</b>
<b>B</b>	<b>Tables of 2D fit results</b>	<b>48</b>
B.1	Check exchange of $\sigma_1$ and $\sigma_2$ . . . . .	53
<b>C</b>	<b>Tables of efficiencies</b>	<b>70</b>
<b>D</b>	<b>Plots of the <math>t_z</math> fit</b>	<b>75</b>
<b>E</b>	<b>Plots of the invariant mass fit</b>	<b>80</b>
<b>F</b>	<b>Plots of the <math>t_z</math> background fit</b>	<b>85</b>
<b>G</b>	<b>Different versions of full-simulation samples</b>	<b>90</b>
<b>H</b>	<b><math>p_T</math>-<math>y</math> spectrum correction</b>	<b>92</b>
<b>I</b>	<b>Plots of 2D pull distributions</b>	<b>95</b>
<b>J</b>	<b>Plots of <math>t_z</math> fit result in MC</b>	<b>100</b>
<b>K</b>	<b>Check the bias of the 2D fit</b>	<b>111</b>
	<b>References</b>	<b>115</b>

# <sup>1</sup> Preface

## <sup>2</sup> Version 2.0

<sup>3</sup> As suggested by Patrick, the toy MC test includes the pull result for  $\tau_b$ , shown in Fig.  
<sup>4</sup> K.2, Fig. K.3 and Fig. K.8.

## <sup>5</sup> Version 1.9

<sup>6</sup> As suggested by Patrick, the note is updated as follows:

- <sup>7</sup> • Modify some expressions and add the check for correlation between mass and  $t_z$  in  
<sup>8</sup> Sec. 3.
- <sup>9</sup> • The toy MC test is redone to check the bias for the 2D fit, detailed in Appendix K.

## <sup>10</sup> Version 1.8

<sup>11</sup> As suggested by Patrick and discussed between proponents, the note is updated as follows:

- <sup>12</sup> • Modify some expressions and add the reference for the previous study on simulation.
- <sup>13</sup> • Add the extrapolation to the total  $b\bar{b}$  cross-section in Sec. 8.3.

## <sup>14</sup> Version 1.7

<sup>15</sup> As suggested by Patrick, the note is updated as follows:

- <sup>16</sup> • The argument for  $n = 1$  in CB is added in Sec. 5.1.
- <sup>17</sup> • The date for the lumi Twiki page is added in the reference.
- <sup>18</sup> • The check for the exchange of  $\sigma_1$  and  $\sigma_2$  is shown in Appendix B.1.

## <sup>19</sup> Version 1.6

<sup>20</sup> Update the FCEL theory predictions for  $R_{p\text{Pb}}$  as a function of  $y$  in Fig. 8.19.

## <sup>21</sup> Version 1.5

<sup>22</sup> As suggested by Patrick and Shenzhen, and discussed between proponents, the note is  
<sup>23</sup> updated as follows:

- <sup>24</sup> • The luminosity is updated based on the twiki page, and the results is updated as  
<sup>25</sup> well. Since the new luminosity is determined run by run, we check that each run is  
<sup>26</sup> complete and the luminosity is reliably determined. A few runs are excluded and a  
<sup>27</sup> new dst file is included, and we redo the data extraction.
- <sup>28</sup> • The toy MC test is perfomed to check the bias for the 2D fit, detailed in Appendix  
<sup>29</sup> K.
- <sup>30</sup> • Add two data points in the Fig. 8.19.
- <sup>31</sup> • Modify some expressions and fix some typos.

<sup>32</sup> **Version 1.4**

<sup>33</sup> As suggested by Shanzhen, the  $R_{p\text{Pb}}$  as a function of  $p_{\text{T}}$  is added in Sec. 8.7.

<sup>34</sup> **Version 1.3**

<sup>35</sup> The FONLL theory results, provided by the FONLL author, are updated.

<sup>36</sup> As suggested by Shanzhen and discussed between proponents, the note is updated as  
<sup>37</sup> follows:

- <sup>38</sup>   • Change the binning schemes of the PID calibration sample and update the results.  
<sup>39</sup>    It is detailed in Sec. 7.7
- <sup>40</sup>   • Modify some expressions and fix some typos.

<sup>41</sup> **Version 1.2**

<sup>42</sup> Change the style of fit plots slightly and fix some typos.

<sup>43</sup> **Version 1.1**

<sup>44</sup> As suggested by Liupan, Andrii and Jibo, and discussed between proponents, the note is  
<sup>45</sup> updated as follows:

- <sup>46</sup>   • The systematic uncertainty due to the signal model of  $t_z$  fit is considered in Sec. 7.5.
- <sup>47</sup>   • Change the selection from  $2 < \eta < 5$  to  $2 < \eta < 4.9$  and update the results.
- <sup>48</sup>   • When performing the 2D fit, the parameters of mass shape are floated rather than  
<sup>49</sup>    fixed.
- <sup>50</sup>   • The 2D pull plots of the 2D fit are added in Appendix I.
- <sup>51</sup>   • The total cross-sections with  $0 < p_{\text{T}} < 20 \text{ GeV}/c$  are added in Sec. 8.1.
- <sup>52</sup>   • The power-low fit is performed with the cross-sections of all the energies in Sec. 8.7.
- <sup>53</sup>   • The  $p_{\text{T}}$  and  $y$  comparisons between data and MC after the reweight are added in  
<sup>54</sup>    Sec. H.

<sup>55</sup> **Version 1.0**

<sup>56</sup> As suggested by Liupan, Andrii and Jibo, and discussed between proponents, the note is  
<sup>57</sup> updated as follows:

- <sup>58</sup>   • Increase the generator level sample size to 10M and update the results.
- <sup>59</sup>   • Include new sim09h sample (4M) and update the results.
- <sup>60</sup>   • The comparison between sim09b and sim09h is added in Appendix G.
- <sup>61</sup>   • The single differential cross-sections result is added in Sec. 8.1.

- 62     ● The ratio between 13 TeV and 5 TeV is added in Sec. 8.4.
- 63     ● The ratio between 8 TeV and 5 TeV is added in Sec. 8.5.
- 64     ● The comparison with theory models is added in Sec. 8.6.
- 65     ● The introduction of  $R_{p\text{Pb}}$  is added and the  $R_{p\text{Pb}}$  result is updated in Sec. 8.7.
- 66     ● The power-law function used for interpolation in the  $p$ -lead measurement is checked  
67       in Sec. 8.7.
- 68     ● The fraction of  $J/\psi$  from  $b$  is added in Sec. 8.2.
- 69     ● The conclusion section is added in Sec. 9.
- 70     ● Follow the strategy applied in the previous  $J/\psi$  production measurements and give  
71       the change of results as a reference in Sec. 7.9.
- 72     ● Add another bin  $14 < p_{\text{T}} < 20 \text{ GeV}/c$  and  $2.0 < y < 4.5$ . For the  $d\sigma/dp_{\text{T}}$ , the  $p_{\text{T}}$   
73       range is extended to  $20 \text{ GeV}/c$ .
- 74     ● Merge prompt  $J/\psi$  and  $J/\psi$  from  $b$  when calculating the PID efficiency and the  
75       trigger efficiency.
- 76     ● A bug due to using wrong sample of PIDCalib was found in the PID efficiency  
77       calculation. We finally found the 5 TeV sample and used it after checking the Reco  
78       version. So, the result is updated.
- 79     ● The method to evaluate the systematic uncertainty due to the trigger efficiency is  
80       changed to the method used in the 13 TeV  $J/\psi$  production measurement, detailed in  
81       Sec. 7.8.
- 82     ● The comparison of the  $p_{\text{T}}$  and  $y$  distribution between data and MC is added in  
83       Appendix. We use the  $(p_{\text{T}}, y)$  distribution in data to correct that in MC, rather  
84       than consider it as the uncertainty, detailed in Appendix H.
- 85     ● The comment on the correlation of uncertainties between bins is added.

## 86     **Version 0.1**

87     Update the acceptance efficiencies and cross-section results after increasing the generator  
88       level sample size to 2M.

## 89     **Version 0.0**

90     First version of the analysis note.

# 91 1 Introduction

92 Quantum chromodynamics (QCD) is the fundamental theory describing strong interaction  
93 between coloured quarks and gluons. One of the most important features of QCD is  
94 that the coupling constant, which measures the strength of the interactions, becomes  
95 larger when the distance between the interacting quarks and gluons is larger, and the  
96 nonperturbative effects become more important. The study of the heavy quarkonium  
97 production in proton-proton ( $pp$ ) collisions could provide important information to probe  
98 QCD. The heavy quarkonium production involves the production of a heavy quark pair,  
99  $Q\bar{Q}$ , and the followed hadronisation of the  $Q\bar{Q}$  pair into the heavy quarkonium. The first  
100 step can be calculated with perturbative QCD, while the latter is nonperturbative and its  
101 mechanism is not fully understood. The physics process of heavy quarkonium production  
102 probes both perturbative and nonperturbative energy regions of QCD, which is helpful to  
103 test QCD models and improve our understanding of strong interactions. In Colour Singlet  
104 Model (CSM) [1–7], it is assumed that the intermediate  $Q\bar{Q}$  state is colourless and has the  
105 same  $J^{PC}$  quantum numbers as the final-state quarkonium. While in nonrelativistic QCD  
106 (NRQCD) approach [8–10], intermediate  $Q\bar{Q}$  states with all possible colour-spin-parity  
107 quantum numbers have probabilities to transform into the desired quarkonium. The  
108 transition probabilities, described by long distance matrix elements (LDME) in NRQCD,  
109 are nonperturbative and can be determined by fitting experimental data. These matrix  
110 elements are supposed to be universal, and their relative strength is ordered in powers  
111 of the velocity of heavy quarks,  $v$ , in the rest frame of the heavy quarkonium. For  
112 perturbative expansions, only a few matrix elements need to be taken into account for  
113  $J/\psi$  hadroproduction, and NRQCD coincides with CSM when only the leading  $v$  term is  
114 considered.

115 The CSM calculation at the leading order (LO) underestimates the  $J/\psi$  and  $\psi(2S)$   
116 production cross-sections by more than one order of magnitude in the range of transverse  
117 momentum ( $p_T$ ) higher than the masses of the charmonia [11]. The correction at the  
118 next-to-leading order (NLO) for CSM changes the  $p_T$  behaviour at high  $p_T$  [12, 13], and  
119 reduces the gap between predictions and experimental data significantly but still not  
120 satisfactory. Besides, the predicted  $J/\psi$  polarisation changes from transverse dominating at  
121 the LO to significantly longitudinal [14]. NRQCD, with the matrix elements determined by  
122 fitting CDF data, can describe the  $p_T$ -dependent  $J/\psi$  cross-section [15, 16]. These matrix  
123 elements can also well describe the magnitude and the  $p_T$  dependence of quarkonium  
124 cross-sections measured at LHC [17–19]. Despite the success of NRQCD in describing  
125 quarkonium hadronic production cross-sections, the predicted large transverse polarisation  
126 at high  $p_T$  [20–23] is not supported by experimental results [24–30].

127 In  $pp$  collisions,  $J/\psi$  mesons can be produced 1) directly from hard collisions of partons,  
128 2) through the feed-down of excited states, or 3) via decays of  $b$ -hadrons. The  $J/\psi$  mesons  
129 from the first two sources originate from the primary vertex of the  $pp$  collision, and are  
130 called prompt  $J/\psi$ , while those from the last source originate from vertices of  $b$ -hadrons,  
131 which are typically separated from the primary vertex, and are called  $J/\psi$  from  $b$ .

132 The  $J/\psi$  differential production cross-section has been measured with the LHC data  
133 in  $pp$  collisions at centre-of-mass energies of 2.76 TeV [31, 32], 7 TeV [33–37], 8 TeV [38]  
134 and 13 TeV [39]. The  $J/\psi$  polarisation was also measured by ALICE [26], CMS [27], and  
135 LHCb [40] in  $pp$  collisions at 7 TeV. Theoretical calculations with CSM and NRQCD  
136 were compared with the measurements for prompt  $J/\psi$  production. The production

137 cross-sections of  $J/\psi$  from  $b$ -hadron decays were compared to the calculations at Fixed  
138 Order plus Next-to-Leading Logarithms (FONLL) [41], which is a tool to calculate the  
139 heavy quark production cross-section.

140 In addition, the production cross-sections in  $pp$  collisions is necessary for nuclear effects  
141 study. Nuclear effects are usually characterized by the nuclear modification factor, defined  
142 as the production cross-section of a given particle per nucleon in  $pA$  collisions divided by  
143 that in  $pp$  collisions,

$$R_{pA}(k, \sqrt{s_{NN}} = 5 \text{ TeV}) \equiv \frac{1}{A} \frac{d\sigma_{pA}(k, \sqrt{s_{NN}} = 5 \text{ TeV})/dk}{d\sigma_{pp}(k, \sqrt{s_{NN}} = 5 \text{ TeV})/dk}, \quad (1.1)$$

144 where  $A$  is the atomic mass number of the nucleus,  $k$  is the rapidity  $y$  or transverse  
145 momentum  $p_T$  of the particle in the proton-nucleon centre-of-mass frame, and  $\sqrt{s_{NN}}$  is  
146 the centre-of-mass energy. The  $J/\psi$  production cross-section in proton-lead collisions  
147 at  $\sqrt{s_{NN}} = 5 \text{ TeV}$  has been measured by LHCb [42]. The measurement used a power  
148 law interpolation to get the cross-section in  $pp$  collisions. Since the  $J/\psi$  production  
149 cross-section in  $pp$  collisions has been measured directly, the nuclear modification factor is  
150 updated in this analysis.

151 This note describes details of the  $J/\psi$  cross-section measurement in  $pp$  collisions at  
152  $\sqrt{s} = 5 \text{ TeV}$ . The measurements include the differential production cross-sections of  
153 prompt  $J/\psi$  and  $J/\psi$  from  $b$  as functions of  $p_T$  and rapidity  $y$ , assuming zero polarisation  
154 of the  $J/\psi$  mesons, the integrated production cross-sections of prompt  $J/\psi$  and  $J/\psi$  from  
155  $b$  with  $p_T < 20 \text{ GeV}/c$  and  $2.0 < y < 4.5$ , the cross-section ratios between 13 TeV and  
156 5 TeV, between 8 TeV and 5 TeV, and the updated nuclear modification factor.

## 157 2 Data and Monte Carlo samples

### 158 2.1 Data

159 This analysis uses  $pp$  collision data collected by the LHCb detector at a centre-of-mass  
160 energy of 5 TeV in 2015, corresponding to an integrated luminosity of  $9.13 \pm 0.18 \text{ pb}^{-1}$  [43]  
161 (updated 2021-02-22). The data were taken with TCK 0x0115014E *MagDown*.

### 162 2.2 Monte Carlo

163 To study the efficiency, generator level samples with 10 M events and full-simulation  
164 samples with 6 M events (2 M for Sim09b version and 4 M for Sim09h version) are  
165 generated. The event type number is 24142001. In the simulation,  $pp$  collisions are  
166 generated using PYTHIA [44] with a specific LHCb configuration [45]. Decays of hadronic  
167 particles are described by EVTGEN [46], in which final-state radiation is generated using  
168 PHOTOS [47]. The interaction of the generated particles with the detector and its response  
169 are implemented using the GEANT4 toolkit [48, 49] as described in Ref. [50]. The prompt  
170 charmonium production is simulated in PYTHIA with contributions from both the leading  
171 order color-singlet and color-octet mechanisms [44, 51], and the charmonium is generated  
172 without polarization.

### 173 3 Cross-section determination

174 The double differential cross-section of  $J/\psi$  production in a given ( $p_T, y$ ) bin is defined as

$$\frac{d^2\sigma}{dp_T dy} = \frac{N(J/\psi \rightarrow \mu^+ \mu^-)}{\mathcal{L} \times \varepsilon_{\text{tot}} \times \mathcal{B}(J/\psi \rightarrow \mu^+ \mu^-) \times \Delta p_T \times \Delta y}, \quad (3.1)$$

175 where

- 176 •  $N(J/\psi \rightarrow \mu^+ \mu^-)$  is the number of  $J/\psi$  signals reconstructed through the  $J/\psi \rightarrow \mu^+ \mu^-$   
177 channel;
- 178 •  $\mathcal{L}$  is the integrated luminosity;
- 179 •  $\varepsilon_{\text{tot}}$  is the total efficiency in this ( $p_T, y$ ) bin, described in Sec. 6 in detail;
- 180 •  $\mathcal{B}(J/\psi \rightarrow \mu^+ \mu^-) = 5.961 \pm 0.033\%$  is the branching fraction of the decay  $J/\psi \rightarrow \mu^+ \mu^-$ , obtained from the PDG 2020 review [52];  
181
- 182 •  $\Delta p_T$  is the bin width of the  $J/\psi$  transverse momentum;
- 183 •  $\Delta y$  is the bin width of the  $J/\psi$  rapidity.

184 The following boundaries are used for the binning scheme of  $p_T$  and  $y$  of the  $J/\psi$   
185 mesons:

- 186 •  $p_T$  boundaries: 0, 1, 2, 3, 4, 5, 6, 7, 8, 10, 14 GeV/ $c$ ;
- 187 •  $y$  boundaries: 2.0, 2.5, 3.0, 3.5, 4.0, 4.5.

188 The cross-section of another bin that  $14 < p_T < 20$  GeV/ $c$  and  $2.0 < y < 4.5$  is measured  
189 as well. Thus for the  $d\sigma/dp_T$ , the  $p_T$  range is extended to 20 GeV/ $c$  with  $2.0 < y < 4.5$ ,  
190 while for the  $d\sigma/dy$ , the  $y$  range is from 2.0 to 4.5 with integrating the  $p_T$  bins that only  
191 less than 14 GeV/ $c$ .

192 To determine the double differential cross-section of prompt  $J/\psi$  and  $J/\psi$  from  $b$   
193 separately, the numbers of prompt  $J/\psi$  signals and  $J/\psi$  from  $b$  signals in bins of the  
194 kinematic variables  $p_T$  and  $y$  need to be extracted. They are obtained by a two-dimensional  
195 fit to the distributions of the dimuon invariant mass and the pseudo proper time  $t_z$  in each  
196 kinematic bin, described in Sec. 5 in detail. The pseudo proper time  $t_z$  of  $J/\psi$  mesons is  
197 defined as

$$t_z = \frac{z_{J/\psi} - z_{\text{PV}}}{p_z/m_{J/\psi}}, \quad (3.2)$$

198 where  $z_{J/\psi}$  is the  $z$  position of the  $J/\psi$  decay vertex,  $z_{\text{PV}}$  is the  $z$  position of the primary  
199 vertex,  $p_z$  is the measured  $J/\psi$  momentum along the beam axis  $z$ , and  $m_{J/\psi}$  is the known  
200  $J/\psi$  mass obtained from the PDG 2020 review [52]. This variable was found to give a  
201 good approximation of the  $b$ -hadron proper lifetime: given that  $b$ -hadrons are not fully  
202 reconstructed, the  $J/\psi$  momentum is used instead of the exact  $b$ -hadron momentum.  
203 The prompt  $J/\psi$  signals has zero lifetime, while the  $t_z$  distribution for  $J/\psi$  from  $b$  is  
204 approximately exponential as seen from simulation [53]. The pseudo proper time  $t_z$  allows  
205 us to statistically separate the prompt  $J/\psi$  from the  $J/\psi$  mesons created in decays of  
206  $b$ -hadrons.

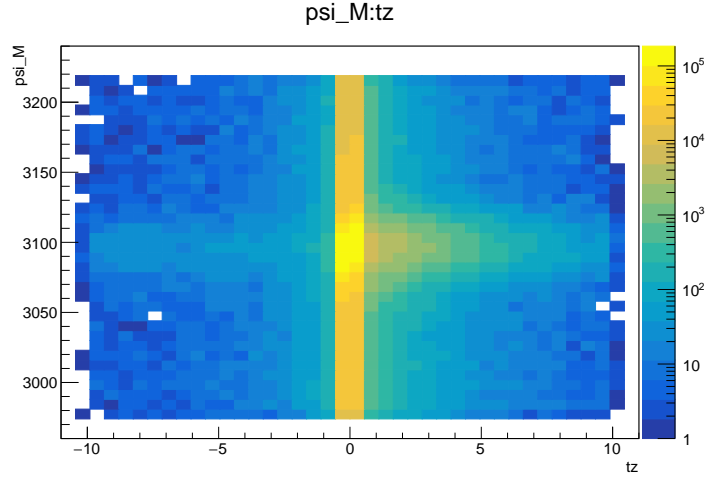


Figure 3.1: The 2D distribution of mass and  $t_z$  for data.

Table 3.1: The correlation factors between mass and  $t_z$  for each  $(p_T, y)$  bin.

$p_T$ ( GeV/c )	$2 < y < 2.5$	$2.5 < y < 3$	$3 < y < 3.5$	$3.5 < y < 4$	$4 < y < 4.5$
0-1	-0.004	0.001	0.002	0.009	0.016
1-2	0.004	0.003	0.003	0.010	0.022
2-3	-0.001	0.003	0.006	0.005	0.017
3-4	0.004	0.000	0.003	0.006	0.013
4-5	0.005	-0.001	0.006	0.016	0.017
5-6	-0.014	-0.003	0.005	0.005	0.045
6-7	-0.001	-0.006	-0.007	0.019	-0.009
7-8	0.026	-0.006	-0.012	0.025	0.033
8-10	-0.012	0.002	0.000	-0.007	0.067
10-14	-0.003	0.008	0.026	0.029	0.019
14-20			0.016( $2 < y < 4.5$ )		

To perform this 2D fit, it is assumed that the mass distribution and  $t_z$  distribution are uncorrelated. The 2D distribution for data is shown in Fig. 3.1 and the correlation factor is only 0.005. And the correlation factors for each  $(p_T, y)$  bin are shown in Table 3.1.

In each bin, the efficiency  $\varepsilon_{\text{tot}}$  is assumed to be constant. The efficiencies of prompt  $J/\psi$  and  $J/\psi$  from  $b$  are distinguished and compared when calculating.

## 4 Candidate reconstruction and selection

### 4.1 Trigger and Turbo stream selection

The reconstruction and preselection of  $J/\psi$  candidates for real data were based on the Turbo stream. The LHCb trigger system consists of three levels: L0, HLT1 and HLT2. The dedicated trigger lines used in this analysis are L0Muon, Hlt1DiMuonHighMass and Hlt2DiMuonJpsiTurbo. For events selected by Hlt2DiMuonJpsiTurbo, the cut "L0Muon\_TOS && Hlt1DiMuonHighMass\_TOS" is applied. The L0Muon trigger selects

Table 4.1: Hlt1DiMuonHighMass selection criteria

Variable	Value
track $p_T$	$> 500 \text{ MeV}/c$
track $p$	$> 3000 \text{ MeV}/c$
track $\chi^2/\text{ndf}$	$< 3$
track PID	IsMuon
$m_{\mu^+\mu^-}$	$> 2700 \text{ MeV}/c^2$

Table 4.2: Hlt2DiMuonJpsiTurbo selection criteria

Variable	Value
track $p_T$	$> 0 \text{ MeV}/c$
track $\chi^2/\text{ndf}$	$< 4$
$J/\psi$ $p_T$	$> 0 \text{ MeV}/c$
$J/\psi$ vertex $\chi^2/\text{ndf}$	$< 25$
$ m_{\mu^+\mu^-} - m_{J/\psi} $	$< 150 \text{ MeV}/c^2$

219 events with at least a muon candidate with high transverse momentum  $p_T > 900 \text{ MeV}/c$ .  
220 The selections of the Hlt1DiMuonHighMass line and the Hlt2DiMuonJpsiTurbo line are  
221 summarized in Table 4.1 and Table 4.2 respectively.

## 222 4.2 Offline selection

223 The offline selections are applied to  $J/\psi$  candidates to reduce the combinatorial background  
224 to a reasonable level and ensure the good quality of the signal-extraction fit. They are  
225 summarized in Table 4.3.

Table 4.3: Offline selection criteria

Variable	Value
number of PVs	$> 0$
track $p_T$	$> 650 \text{ MeV}/c$
track $p$	$> 3000 \text{ MeV}/c$
track $\eta$	$2 < \eta < 4.9$
track PID	IsMuon, $\text{DLL}_{\mu\pi} > 0$
track ghost probability $P(\text{ghost})$	$< 0.3$
$J/\psi$ vertex $\chi^2/\text{ndf}$	$< 8$
$ m_{\mu^+\mu^-} - m_{J/\psi} $	$< 120 \text{ MeV}/c^2$
$J/\psi$ $p_T$	$0 < p_T < 14 \text{ GeV}/c$
$J/\psi$ $y$	$2 < y < 4.5$
pseudo proper time $t_z$	$-10 \text{ ps} < t_z < 10 \text{ ps}$
uncertainty of $t_z$	$< 0.3 \text{ ps}$

## 226 5 Signal extraction

### 227 5.1 Determination of the total $J/\psi$ signal yields

228 The total number of  $J/\psi$  signals in each  $(p_T, y)$  bin is determined from an extended  
 229 unbinned maximum likelihood fit to the invariant mass distribution of the selected  $J/\psi$   
 230 candidates. The distribution of the background is modelled with an exponential function.  
 231 The signal is described by the sum of two Crystal Ball (CB) functions [54] with common  
 232 mean value ( $\mu$ ) and different widths ( $\sigma_1$  and  $\sigma_2$ ). Only one CB function is used in bins  
 233 with low statistics (number of events less than 30k). The CB function is defined as

$$f_{\text{CB}}(m; \mu, \sigma, \alpha, n) = \begin{cases} \left(\frac{n}{|\alpha|}\right)^n e^{-\frac{1}{2}\alpha^2} \left(\frac{n}{|\alpha|} - |\alpha| - \frac{m-\mu}{\sigma}\right)^{-n}, & \frac{m-\mu}{\sigma} < -|\alpha|; \\ \exp\left(-\frac{1}{2}\left(\frac{m-\mu}{\sigma}\right)^2\right), & \frac{m-\mu}{\sigma} > -|\alpha|. \end{cases} \quad (5.1)$$

234 The tails in CB functions are used to model the final-state radiation effects, which leads  
 235 to more  $J/\psi$  candidates with lower invariant masses.

236 The parameter  $n$  is fixed to 1 according to the talk by Jacques [55]. The argument  
 237 is as follows. The asymmetry of the  $J/\psi \rightarrow \mu^+ \mu^-$  mass shape is predominantly caused  
 238 by photo emission, which is a well-known QED phenomenon. In  $J/\psi \rightarrow \mu^+ \mu^-$ , the  
 239 probability to radiate a photon is given for each muon (in leading log approximation) by  
 240  $(\alpha/\pi) \ln(s/4m_\mu^2) \cdot (dx/x)[1 + (1-x)^2]/2$ , where  $x = E_\gamma/(M_{J/\psi}/2)$ . The first term is “an  
 241 equivalent radiator” of about 1.21% per muon, and the term  $(dx/x)[1 + (1-x)^2]/2$  is the  
 242 equivalent of the bremsstrahlung formula for this case. If the only cause for asymmetry  
 243 of the mass shape is photon emission then the crystal ball formula should have  $n = 1$ .

244  $\alpha$  is parameterized from simulation as a function of the  $\sigma$ ,

$$\alpha = -7.844 \times 10^{-5} \sigma^2 + 6.088 \times 10^{-3} \sigma + 2.082, \quad (5.2)$$

245 for  $\sigma$  in unit of  $\text{MeV}/c^2$ . This function is obtained using the generator level MC sample,  
 246 in which the invariant mass of dimuon differs from the true  $J/\psi$  mass due to the final-  
 247 state radiation effects. Then, the invariant mass of dimuon is smeared using a Gaussian  
 248 distribution with zero mean value and a constant standard deviation,  $\Sigma$ , which emulates  
 249 the Gaussian detector resolution. The smeared invariant mass distribution is fitted with a  
 250 CB function whose  $n = 1$  and all other parameters are free. By repeating this procedure  
 251 with different  $\Sigma$ , the relation between the  $\alpha$  and fitted  $\sigma$  can be determined, as shown in  
 252 Fig. 5.1.

253 In Fig. 5.2, the invariant mass distribution in the range of  $2 < p_T < 3 \text{ GeV}/c$ ,  $3 < y <$   
 254 3.5 is shown together with the fit. The invariant mass fit is performed in each  $(p_T, y)$  bin  
 255 of  $J/\psi$  candidates, and all the plots are shown in Sec. E. Through performing the fits,  
 256 the total number of  $J/\psi$  signals in each  $(p_T, y)$  bin is obtained, as well as all parameters  
 257 of the mass shape, which are useful to determine the prompt and detached signal yields.  
 258 The total numbers of  $J/\psi$  signals as a function of  $p_T$  in bins of  $y$  are shown in Fig. 5.3.  
 259 Integrating all bins, the total  $J/\psi$  signal yield is  $(1596.7 \pm 1.7) \times 10^3$ .

### 260 5.2 Determination of the prompt and detached signal yields

261 To determine the signal yields of prompt  $J/\psi$  and  $J/\psi$  from  $b$ , the pseudo proper time  $t_z$   
 262 distribution is used. In each kinematic bin, an unbinned extended maximum likelihood

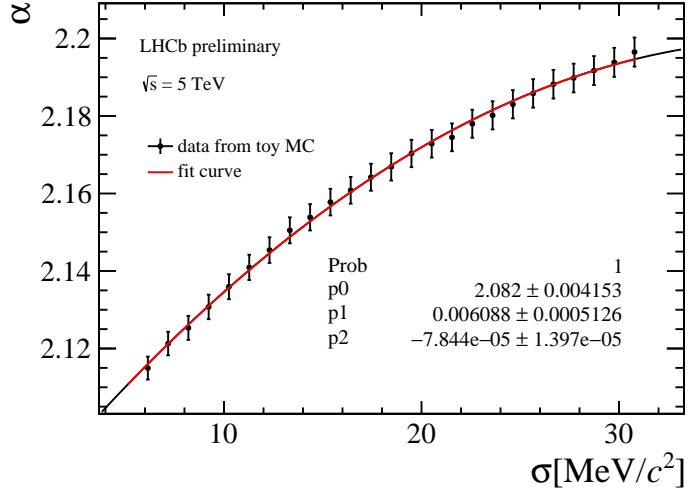


Figure 5.1: The relationship between the  $\alpha$  and fitted  $\sigma$ .

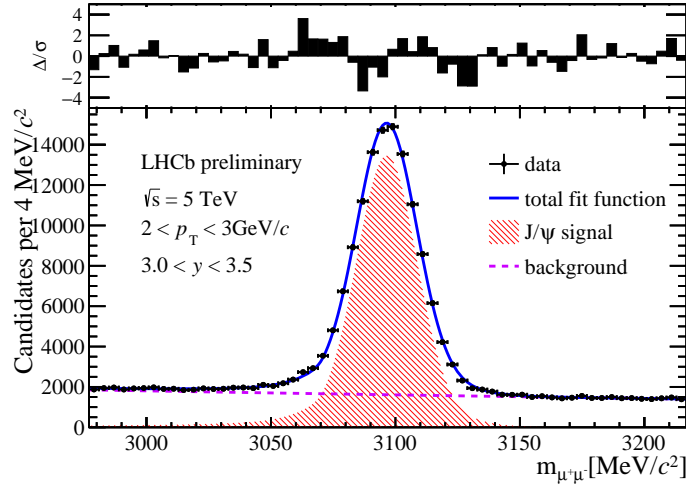


Figure 5.2: Invariant mass fit result of  $J/\psi$  candidates with  $2 < p_T < 3 \text{ GeV}/c$ ,  $3 < y < 3.5$ .

263 fit to the two-dimensional distribution of invariant mass  $m_{\mu^+\mu^-}$  and  $t_z$  is performed to  
 264 separate prompt  $J/\psi$  from the  $J/\psi$  mesons created in decays of  $b$ -hadrons.

265 At the generator level, the  $t_z$  distribution of the prompt  $J/\psi$  is a Dirac delta function,  
 266  $\delta(t_z)$ , while that of  $J/\psi$  from  $b$  follows an exponential function. For  $J/\psi$  signals, the  
 267 detector resolution is taken into account by convolving with a resolution function, which  
 268 is described by the sum of two Gaussian functions,

$$f_{\text{resolution}}(t_z; \mu, S_1, S_2, \beta) = \frac{\beta}{\sqrt{2\pi}S_1\sigma} e^{-\frac{(t_z-\mu)^2}{S_1^2\sigma^2}} + \frac{1-\beta}{\sqrt{2\pi}S_2\sigma} e^{-\frac{(t_z-\mu)^2}{S_2^2\sigma^2}}. \quad (5.3)$$

269 The parameter  $\sigma$  is the event-by-event uncertainty of  $t_z$ , calculated by combining the  
 270 estimated uncertainties of the  $J/\psi$  decay vertex and the associated PV. Besides,  $S_1$  and  
 271  $S_2$  are two scale factors to correct the imperfect estimation of the  $t_z$  uncertainty. The  
 272 parameter  $\mu$  is the bias of the  $t_z$  measurement, and  $\beta$  is the proportion of one Gaussian

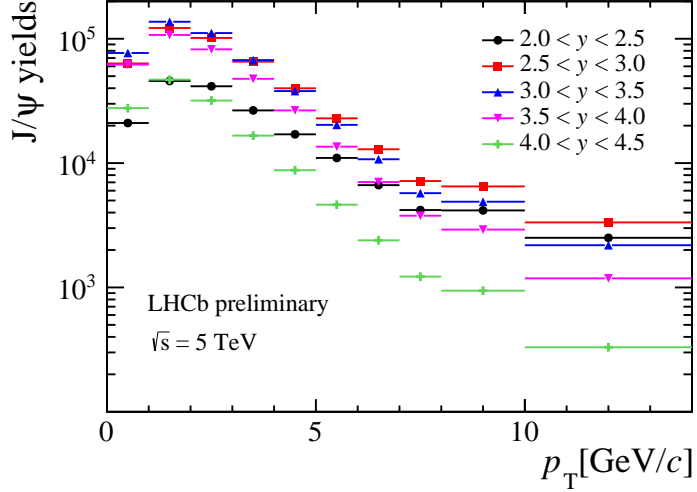


Figure 5.3: The total  $J/\psi$  yields as a function of  $p_T$  in bins of  $y$ .

function in the resolution function. In the fitting procedure, all the resolution parameters are floated.

It is possible that the reconstructed  $J/\psi$  candidate is associated to a wrong PV. There are two cases that an event is named wrong PV event:

- The  $J/\psi$  candidate is associated to a wrong PV in the case that the reconstructed PVs are accidentally close to each other.
- The PV which produced the  $J/\psi$  decay is not reconstructed and only the nearest reconstructed PV in the event is found.

In the first case, the positions of the reconstructed PV and the true PV are correlated, which results in a Gaussian-like  $t_z$  distribution with width much larger than the detection resolution. However, it is found from simulation that the signals yields are changed very slightly when including a wide Gaussian function in the resolution function because the proportion of this component is quite small, less than 1% as seen from previous study [39]. Therefore, this component is ignored when performing the two-dimensional fit, and the influence is included in the study of the systematic uncertainty resulting from the imperfect modelling of the detector resolution, described in Sec. 7.5 in detail.

In the second case that the true PV is not reconstructed, the true PV and the wrongly associated PV are not correlated, which results in a long tail in the  $t_z$  distribution that can be modelled using the next-event method. The next-event pseudo proper time,  $t_z^{\text{next}}$ , for each candidate in data, is calculated combining the  $J/\psi$  candidate with the closest PV of another (next) event as

$$t_z^{\text{next}} = \frac{z_{J/\psi} - z_{\text{PV}}^{\text{next}}}{p_z/m_{J/\psi}}, \quad (5.4)$$

where  $z_{\text{PV}}^{\text{next}}$  is the  $z$  position of the nearest PV of the next selected event. In Fig. 5.4, the reconstructed  $t_z$  distribution is compared with the one obtained by the next-event method. The region  $-40 < t_z < -10$  ps is dominated by the tail events, and in the plot the tail events are scaled so that the area in this region is the same as that of  $t_z$  distribution. From this plot, it is clearly seen that  $t_z^{\text{next}}$  is a reasonable quantity to model the tail distribution.

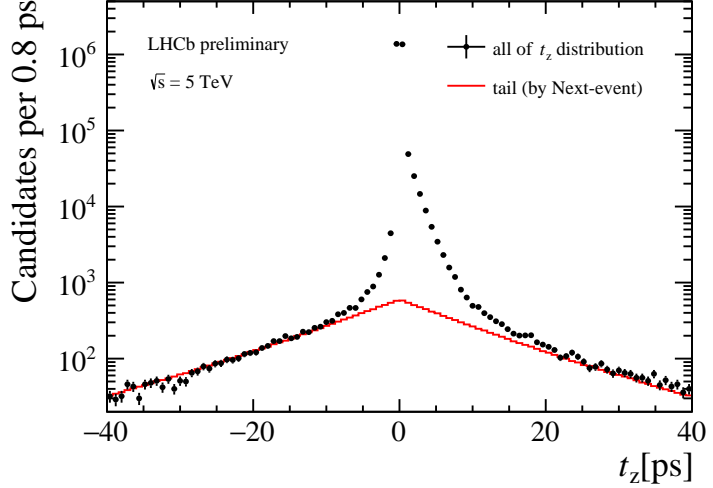


Figure 5.4:  $t_z$  distribution of reconstructed events and the one obtained by the next-event method. The area in the region  $-40 < t_z < -10$  ps is scaled to be the same.

299 The tail distribution is not convolved with the resolution function, and is described by a  
300 histogram  $f_{\text{tail}}(t_z)$ .

301 The  $J/\psi$  candidates in the mass sidebands,  $75 < |m_{\mu^+\mu^-} - m_{J/\psi}| < 150$  MeV/ $c^2$ , are  
302 used to explicitly model the background  $t_z$  distribution. The background consists of  
303 random combinations of muons from semileptonic  $b$  and  $c$  decays which tend to produce  
304 positive  $t_z$  values, as well as misreconstructed tracks from decays-in-flight of kaons and  
305 pions which contribute to both positive and negative  $t_z$  values. The  $t_z$  background is  
306 modelled with an empirical function, composed of a delta function and five exponential  
307 functions (three for positive  $t_z$  and two for negative  $t_z$ , with one positive  $t_z$  and one  
308 negative  $t_z$  sharing the same slope). This function is convolved with the sum of two  
309 Gaussian function as a resolution function, which has different parameters from those of  
310 signals. The empirical function is

$$f_{\text{bkg}}(t_z) = \left[ (1 - f_1 - f_2 - f_3 - f_4)\delta(t_z) + \theta(t_z)\left(\frac{f_1}{\tau_1}e^{-t_z/\tau_1} + \frac{f_2}{\tau_2}e^{-t_z/\tau_2}\right) \right. \\ \left. + \theta(-t_z)\frac{f_3}{\tau_3}e^{t_z/\tau_3} + \frac{f_4}{2\tau_4}e^{-|t_z|/\tau_4} \right] \otimes \left( \frac{\beta'}{\sqrt{2\pi}S'_1\sigma}e^{-\frac{(t_z-\mu)^2}{S'^2_1\sigma^2}} + \frac{1-\beta'}{\sqrt{2\pi}S'_2\sigma}e^{-\frac{(t_z-\mu)^2}{S'^2_2\sigma^2}} \right). \quad (5.5)$$

311 The parameters in Eq. 5.5 are determined by fitting the mass sidebands, and are fixed in  
312 the final two-dimensional fit. In bins with high statistics ( $1 < p_T < 2$  GeV/ $c$ ,  $2.5 < y < 3$   
313 and  $1 < p_T < 2$  GeV/ $c$ ,  $3 < y < 3.5$ ), another exponential function with positive  $t_z$  is  
314 added to the empirical function. In bins with low statistics, several components in Eq.  
315 5.5 are reduced (approximately for bins with number of events less than 30k, except a few  
316 bins that can also be fitted with the full function form successfully). In Fig. 5.5, the  $t_z$   
317 background distribution in the range of  $2 < p_T < 3$  GeV/ $c$ ,  $3 < y < 3.5$  is shown together  
318 with the fit. The plots in all the bins are shown in Appendix F.

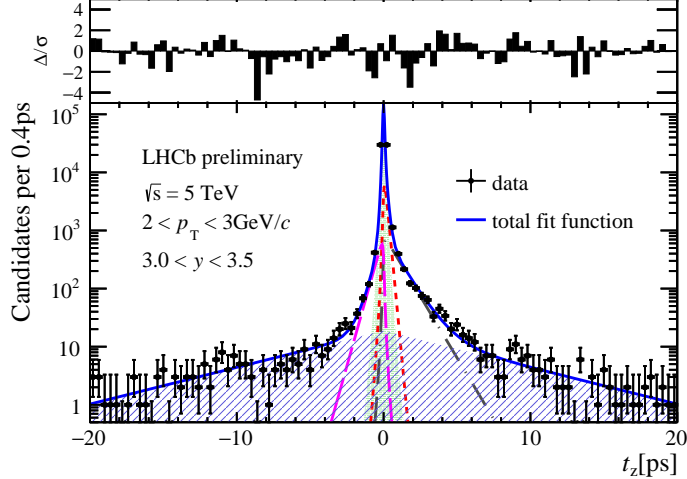


Figure 5.5:  $t_z$  background fit result of  $J/\psi$  candidates with  $2 < p_T < 3 \text{ GeV}/c$ ,  $3 < y < 3.5$ .

319 Finally, the function to describe  $t_z$  is

$$f_{t_z}(t_z; N_{\text{prompt}}, N_{\text{from } b}, N_{\text{bkg}}, N_{\text{tail}}, \tau_b, \mu, S_1, S_2, \beta) = \\ \left( N_{\text{prompt}} \delta(t_z) + \frac{N_{\text{from } b}}{\tau_b} e^{-t_z/\tau_b} \right) \otimes f_{\text{resolution}}(t_z; \mu, S_1, S_2, \beta) + N_{\text{tail}} f_{\text{tail}}(t_z) + N_{\text{bkg}} f_{\text{bkg}}(t_z), \quad (5.6)$$

320 where  $N_{\text{prompt}}$ ,  $N_{\text{from } b}$ ,  $N_{\text{bkg}}$  and  $N_{\text{tail}}$  are the number of prompt  $J/\psi$ ,  $J/\psi$  from  $b$ , back-  
321 ground and wrong PV events respectively. The wrong PV events are still the  $J/\psi$   
322 signals, and it is assumed that the prompt  $J/\psi$  and  $J/\psi$  from  $b$  have equal prob-  
323 ability that the true PV is not reconstructed. Therefore, the extracted number of  
324 prompt  $J/\psi$  is  $N_{\text{prompt}} + N_{\text{tail}} \frac{N_{\text{prompt}}}{N_{\text{prompt}} + N_{\text{from } b}}$ , and the extracted number of  $J/\psi$  from  $b$  is  
325  $N_{\text{from } b} + N_{\text{tail}} \frac{N_{\text{from } b}}{N_{\text{prompt}} + N_{\text{from } b}}$ , since the efficiencies for prompt  $J/\psi$  and  $J/\psi$  from  $b$  are  
326 almost the same.

327 In the range of  $2 \text{ GeV}/c < p_T < 3 \text{ GeV}/c$ ,  $3 < y < 3.5$ , the two-dimensional fit results  
328 are shown in Fig. 5.6. The plots of  $t_z$  fit result in all the bins are shown in Appendix D.  
329 The two-dimensional pull distributions of the fit in all the bins are shown in Appendix I,  
330 and the fitted parameters are given in Appendix B. To further check the two-dimensional  
331 fit, the pseudo decay times of  $b$ -hadrons  $\tau_b$ , the parameter of the exponential function  
332 defined in Eq. 5.6, obtained in  $(p_T, y)$  bins are shown in Fig. 5.7. The mean value of  $\tau_b$  is  
333  $1.410 \pm 0.005 \text{ ps}$ , consistent with the previous MC study [53]. In addition, the toy MC  
334 test is performed to check the bias, detailed in Appendix K.

335 The number of prompt  $J/\psi$  and number of  $J/\psi$  from  $b$  in each  $(p_T, y)$  bin are extracted  
336 after performing the two-dimensional fit, as shown in Fig. 5.8.

## 337 6 Efficiency determination

338 The total efficiency  $\varepsilon_{\text{tot}}$  is determined independently in each  $(p_T, y)$  bin and split as the  
339 multiplication of the acceptance, reconstruction-selection efficiency, PID efficiency and

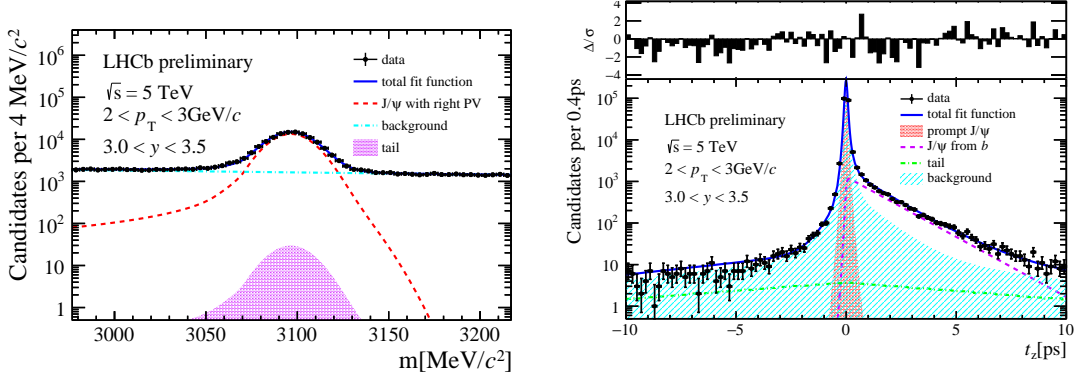


Figure 5.6: Invariant mass (left) and  $t_z$  (right) fit result of  $J/\psi$  candidates with  $2 < p_T < 3 \text{ GeV}/c$ ,  $3.0 < y < 3.5$ .

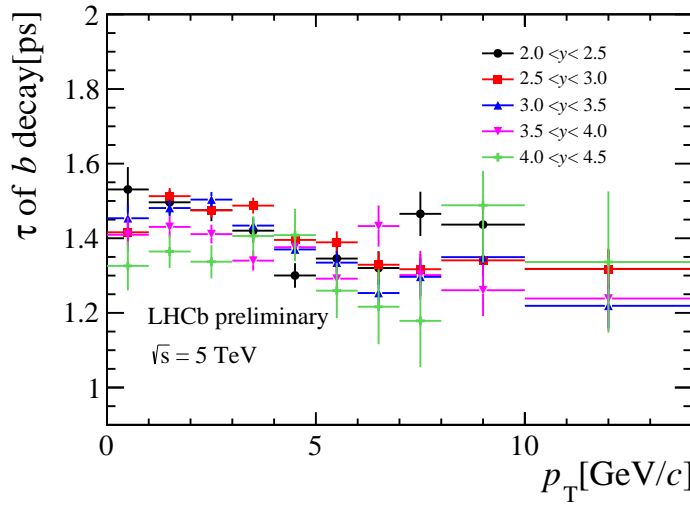


Figure 5.7: The pseudo decay times of  $b$ -hadrons  $\tau_b$  as a function of  $p_T$  in bins of  $y$ .

<sup>340</sup> trigger efficiency.

$$\varepsilon_{\text{tot}} = \varepsilon_{\text{acc}} \times \varepsilon_{\text{rec\&sel}} \times \varepsilon_{\text{PID}} \times \varepsilon_{\text{trig}}. \quad (6.1)$$

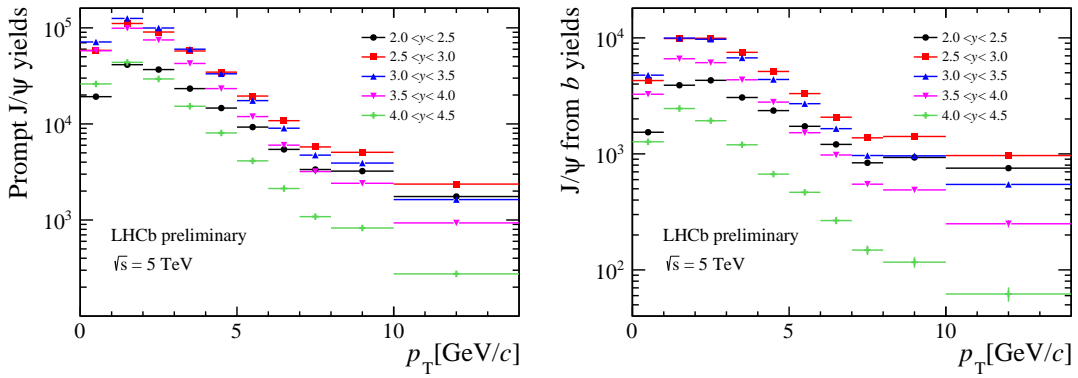


Figure 5.8: The extracted number of prompt  $J/\psi$  (left) and  $J/\psi$  from  $b$  (right) as a function of  $p_T$  in bins of  $y$ .

341 In the simulated sample, the prompt  $J/\psi$  and  $J/\psi$  from  $b$  are separated using the MC  
 342 truth information. For each efficiency, it is calculated independently for prompt  $J/\psi$  and  
 343  $J/\psi$  from  $b$ , and the comparison is also provided. The total efficiency  $\varepsilon_{\text{tot}}$  and each split  
 344 one for prompt  $J/\psi$ ,  $J/\psi$  from  $b$  and the average for both prompt  $J/\psi$  and  $J/\psi$  from  $b$  are  
 345 summarized in Appendix C.

## 346 6.1 Acceptance

347 The acceptance is defined as

$$\varepsilon_{\text{acc}} = \frac{J/\psi \text{ in bin}(p_T, y) \text{ with both } \mu \text{ in LHCb acceptance}}{J/\psi \text{ in bin}(p_T, y)}. \quad (6.2)$$

348 The LHCb acceptance means the polar angle [10, 400] mrad defined with respect to the  
 349 direction of LHCb  $z$ -axis. The acceptance  $\varepsilon_{\text{acc}}$  is determined using a simulation sample at  
 350 the generator level, without any geometrical acceptance requirement. The  $\varepsilon_{\text{acc}}$  in each  
 ( $p_T, y$ ) bin is shown in Fig. 6.1. The difference between the acceptance  $\varepsilon_{\text{acc}}$  of prompt

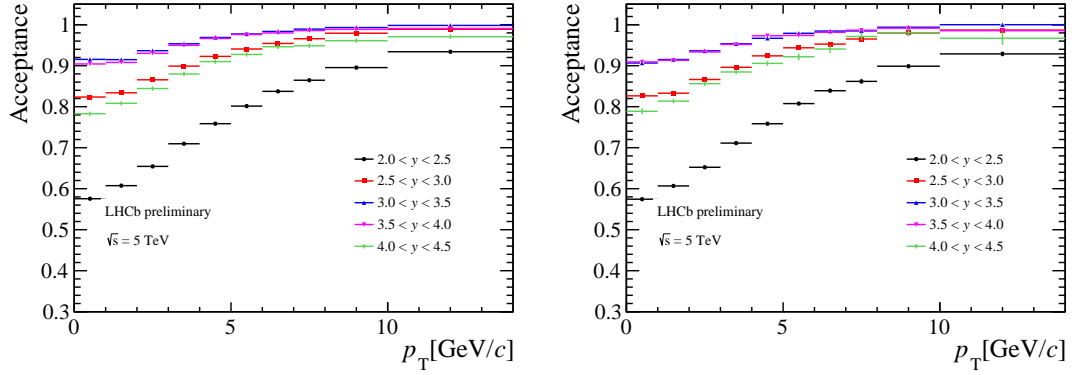


Figure 6.1: The acceptance  $\varepsilon_{\text{acc}}$  of prompt  $J/\psi$  (left) and  $J/\psi$  from  $b$  (right) as a function of  $p_T$  in bins of  $y$ .

351  $J/\psi$  and  $J/\psi$  from  $b$  is shown in Fig. 6.2.

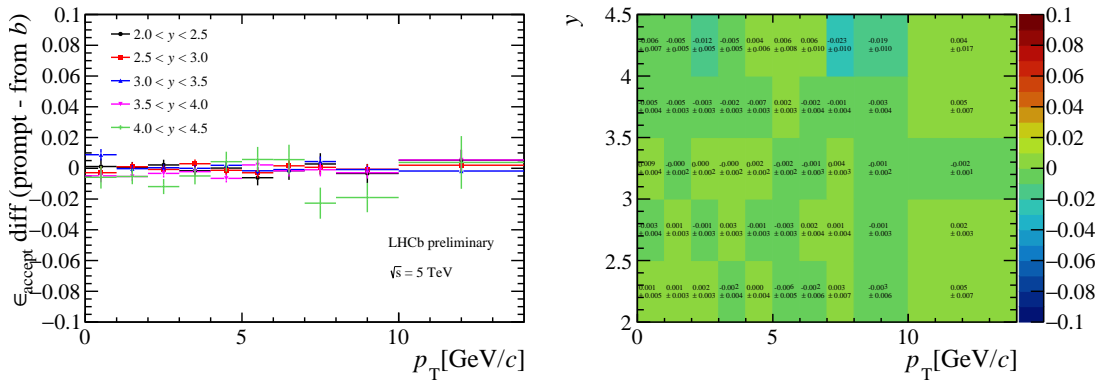


Figure 6.2: The difference of  $\varepsilon_{\text{acc}}$  (prompt  $J/\psi$  -  $J/\psi$  from  $b$ ).

## 353 6.2 Reconstruction-selection efficiency

354 The reconstruction-selection efficiency is defined as

$$\varepsilon_{\text{rec\&sel}} = \frac{J/\psi \text{ selected in bin}(p_T, y) \text{ without PID requirement}}{J/\psi \text{ in bin}(p_T, y) \text{ with both } \mu \text{ in LHCb acceptance}}. \quad (6.3)$$

355 The reconstruction-selection efficiency is determined using the full-simulation sample. It  
 356 includes the efficiency of reconstructing the two muon tracks and the offline selection  
 357 of the  $J/\psi$  signals, with the selections that are listed in Table 4.3 (excluding PID and  
 358 trigger).

359 Studies show that the tracking efficiency is slightly different between simulation and  
 360 data. Therefore, the full-simulation sample is corrected as a function of the kinematics  
 361 of each muon. The correction factors in bins of muon kinematics are obtained from the  
 362 tracking group by comparing the absolute tracking efficiency in data and simulation,  
 shown in Fig. 6.3.

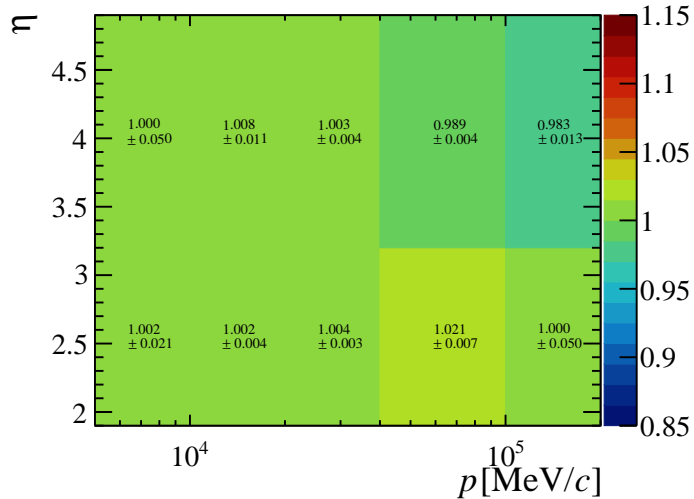


Figure 6.3: Tracking efficiency correction factors in bins of muon kinematics.

363  
 364 The distributions of the number of the SPD hits, used to describe the multiplicity of  
 365 the event, are different between in data and in Monte Carlo, as shown in Fig. 6.4. The  
 366 distribution in data is obtained by using the sPlot method. The correction is necessary  
 367 in the calculation of not only the reconstruction-selection efficiency, but also the PID  
 368 efficiency and the trigger efficiency. In addition, the correction for  $p_T$ - $y$  spectrum is also  
 369 needed in the calculation, as detailed in Appendix H.

370 The  $\varepsilon_{\text{rec\&sel}}$  in each  $(p_T, y)$  bin is shown in Fig. 6.5. The difference between the  
 371 reconstruction-selection efficiency  $\varepsilon_{\text{rec\&sel}}$  of prompt  $J/\psi$  and  $J/\psi$  from  $b$  is shown in Fig.  
 372 6.6.

## 373 6.3 PID efficiency

374 The PID efficiency is defined as

$$\varepsilon_{\text{PID}} = \frac{J/\psi \text{ selected in bin}(p_T, y) \text{ with PID requirement}}{J/\psi \text{ selected in bin}(p_T, y) \text{ without PID requirement}}. \quad (6.4)$$

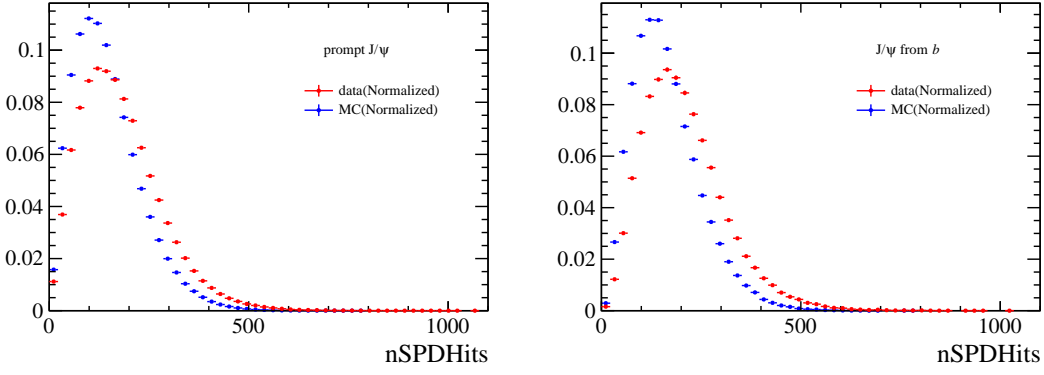


Figure 6.4: The comparison of nSPDhits distributions in data and MC for prompt  $J/\psi$  (left) and  $J/\psi$  from  $b$  (right).

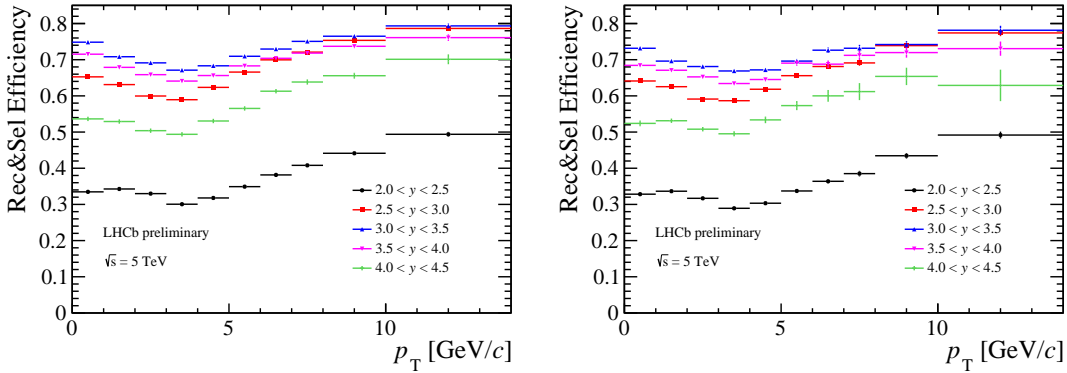


Figure 6.5: The reconstruction-selection efficiency  $\varepsilon_{\text{rec}\&\text{sel}}$  of prompt  $J/\psi$  (left) and  $J/\psi$  from  $b$  (right) as a function of  $p_T$  in bins of  $y$ .

375 The PID efficiency is determined using the full-simulation sample, selected by all the  
 376 selections except the PID and the trigger, calibrated with the data using the PIDCalib  
 377 package. The PID efficiency of the single muon in bins of muon kinematics is obtained  
 378 from the PIDCalib package, shown in Fig. 6.7. When calculating the  $\varepsilon_{\text{PID}}$  in each  $(p_T, y)$   
 379 bin, there are few events with the muon in the empty bin of Fig. 6.7. In this case, the

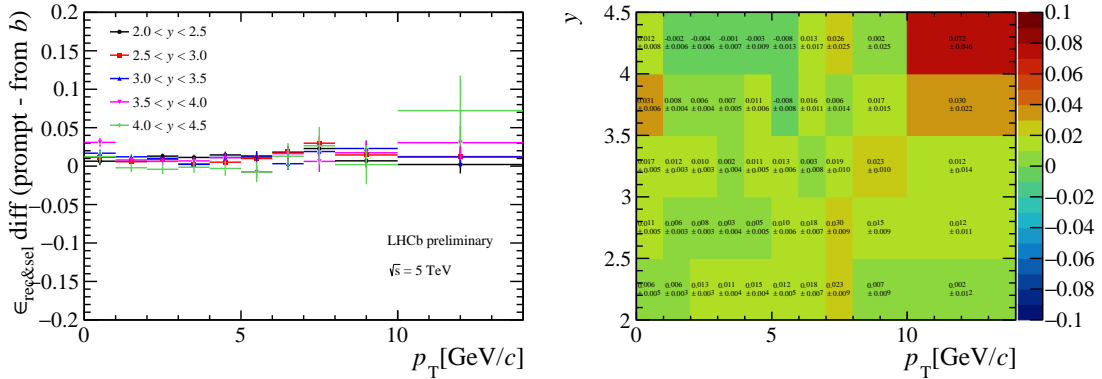


Figure 6.6: The difference of  $\varepsilon_{\text{rec}\&\text{sel}}$  (prompt  $J/\psi$ -  $J/\psi$  from  $b$ ).

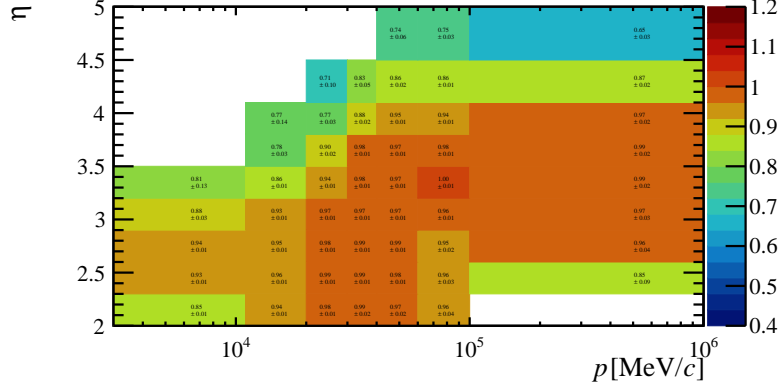


Figure 6.7: PID efficiency of the single muon from the PIDCalib package in bins of muon kinematics.

380 value of the nearest  $p_T$  bin (same  $y$ ) is used. The  $\varepsilon_{\text{PID}}$  in each  $(p_T, y)$  bin is shown in Fig. 6.8. The difference between the PID efficiency  $\varepsilon_{\text{PID}}$  of prompt  $J/\psi$  and  $J/\psi$  from  $b$  is

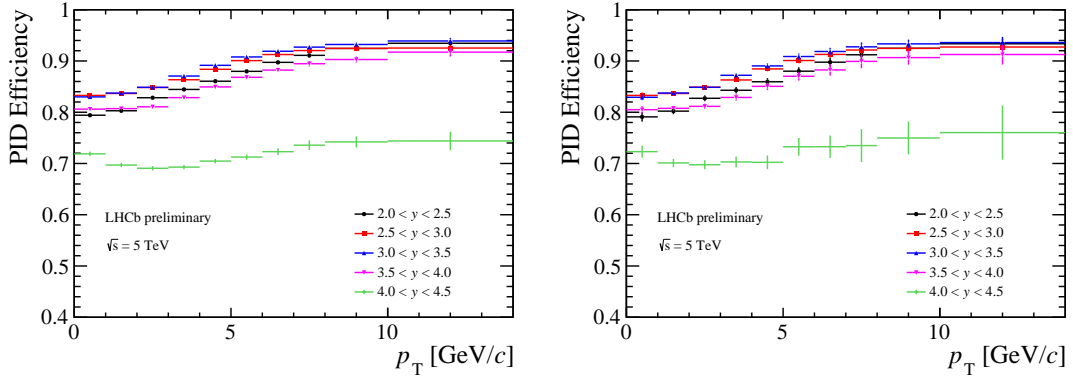


Figure 6.8: The PID efficiency  $\varepsilon_{\text{PID}}$  of prompt  $J/\psi$  (left) and  $J/\psi$  from  $b$  (right) as a function of  $p_T$  in bins of  $y$ .

381 shown in Fig. 6.9.

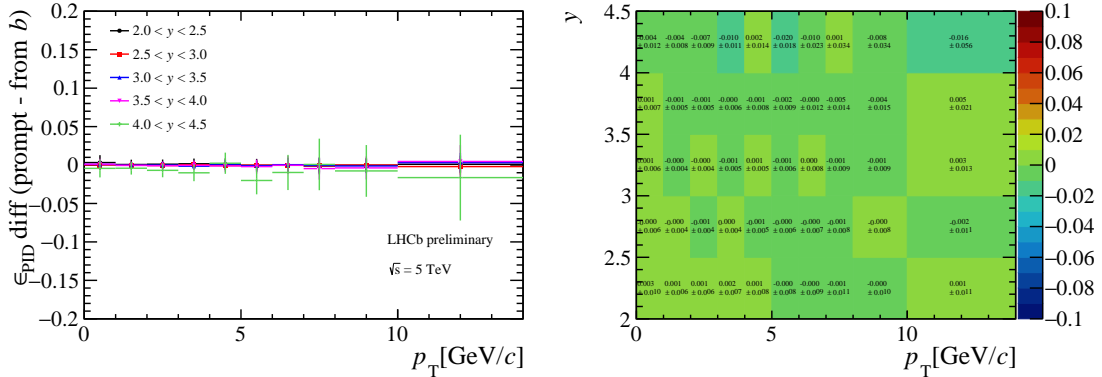


Figure 6.9: The difference of  $\varepsilon_{\text{PID}}$  (prompt  $J/\psi$  -  $J/\psi$  from  $b$ ).

382

## 383 6.4 Trigger efficiency

384 The trigger efficiency is defined as

$$\varepsilon_{\text{trig}} = \frac{J/\psi \text{ triggered in bin}(p_T, y)}{J/\psi \text{ selected in bin}(p_T, y) \text{ with PID requirement}}. \quad (6.5)$$

385 Here the triggers include both TOS requirement of L0DiMuon, Hlt1DiMuonHighMass and  
 386 Hlt2DiMuonJpsiTurbo. Only L0DiMuon and Hlt1DiMuonHighMass contribute actually to  
 387 the efficiency, because the offline selections are tighter than those in Hlt2DiMuonJpsiTurbo.  
 388 The trigger efficiency is determined using the full-simulation sample directly. The  $\varepsilon_{\text{trig}}$  in  
 each  $(p_T, y)$  bin is shown in Fig. 6.10. The difference between the trigger efficiency  $\varepsilon_{\text{trig}}$

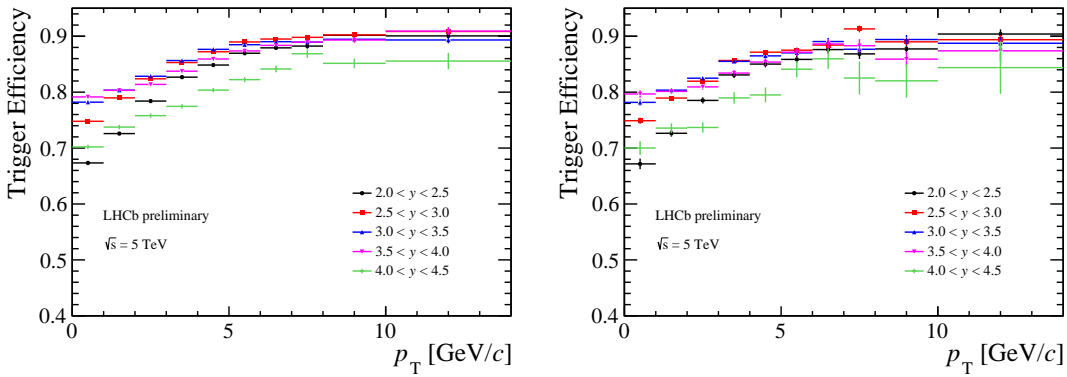


Figure 6.10: The trigger efficiency  $\varepsilon_{\text{trig}}$  of prompt  $J/\psi$  (left) and  $J/\psi$  from  $b$  (right) as a function of  $p_T$  in bins of  $y$ .

389 of prompt  $J/\psi$  and  $J/\psi$  from  $b$  is shown in Fig. 6.11.

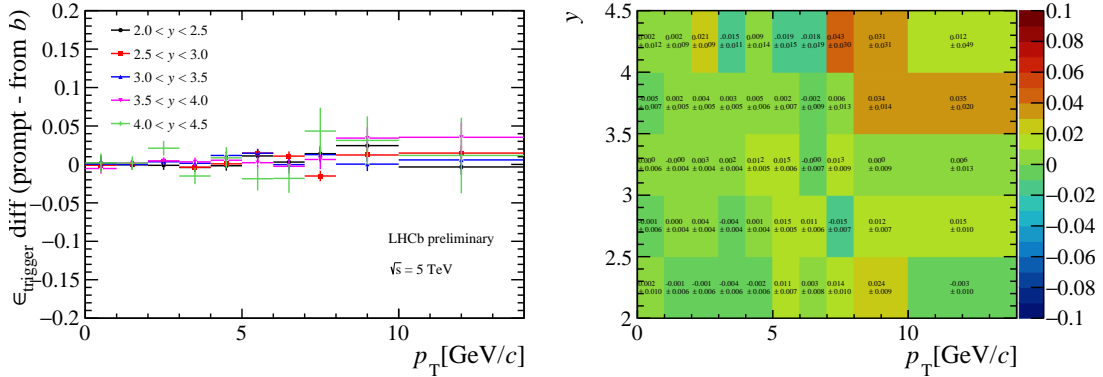


Figure 6.11: The difference of  $\varepsilon_{\text{trig}}$  (prompt  $J/\psi$  -  $J/\psi$  from  $b$ ).

390

## 391 6.5 Total efficiency

392 In principle, the difference in efficiency for prompt  $J/\psi$  and  $J/\psi$  from  $b$  can only present  
 393 in acceptance and reconstruction-selection efficiency (due to the  $t_z$  cut). According to Fig.  
 394 6.9 and Fig. 6.11, the difference for PID efficiency and trigger efficiency between prompt

*J/ψ* and  $J/\psi$  from  $b$  is very small. Therefore, to reduce the uncertainty due to the limited MC sample size, the PID efficiency for inclusive  $J/\psi$  and the trigger efficiency for inclusive  $J/\psi$  are used when calculating the total efficiency for both prompt  $J/\psi$  and  $J/\psi$  from  $b$ .

The  $\varepsilon_{\text{tot}}$  in each  $(p_T, y)$  bin is shown in Fig. 6.12. The difference between the total

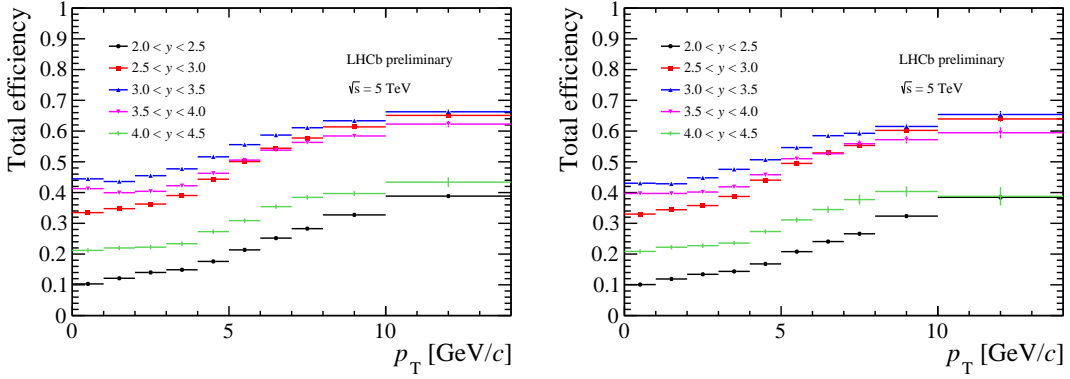


Figure 6.12: The total efficiency  $\varepsilon_{\text{tot}}$  of prompt  $J/\psi$  (left) and  $J/\psi$  from  $b$  (right) as a function of  $p_T$  in bins of  $y$ .

*efficiency  $\varepsilon_{\text{tot}}$  of prompt  $J/\psi$  and  $J/\psi$  from  $b$  is shown in Fig. 6.13.*

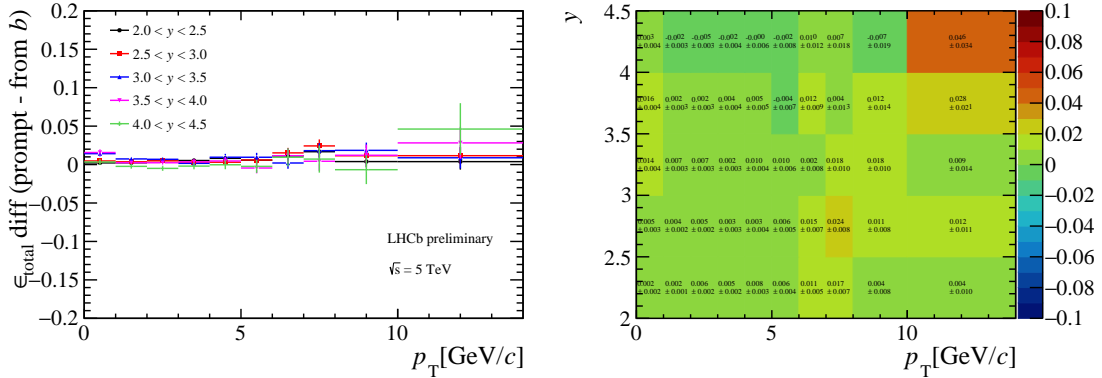


Figure 6.13: The difference of  $\varepsilon_{\text{tot}}$  (prompt  $J/\psi$  -  $J/\psi$  from  $b$ ).

399

## 400 7 Systematic uncertainties

401 The following sources of systematic uncertainties are considered. When considering the  
402 uncertainties about the tracking efficiency, PID efficiency and trigger efficiency, prompt  
403  $J/\psi$  and  $J/\psi$  from  $b$  are combined.

### 404 7.1 Signal model of mass fit

405 Using the sum of two Crystal Ball functions as the signal part of mass fit model could  
406 bias the signal yields. For an alternative, the signal invariant mass is also fitted with  
407 the model which extracted from the kernel-estimated distribution from the MC sample  
408 bin dependently. In order to account for the resolution difference between data and MC,

409 a Gaussian function (the mean is 0 and the sigma is floated during the fit procedure)  
 410 is used to smear the shape of the signals. The study is performed in each kinematic  
 411 bin, and the signal yields from the default fit and the alternative fit are compared.  
 412 The relative difference is about 0.0~2.0%, as shown in Fig. 7.1. which is taken as the  
 413 systematic uncertainty due to the fit model to describe the signal part of the invariant mass  
 414 distribution. It is assumed as uncorrelated between bins because there is no consistent  
 bias in all the bins.

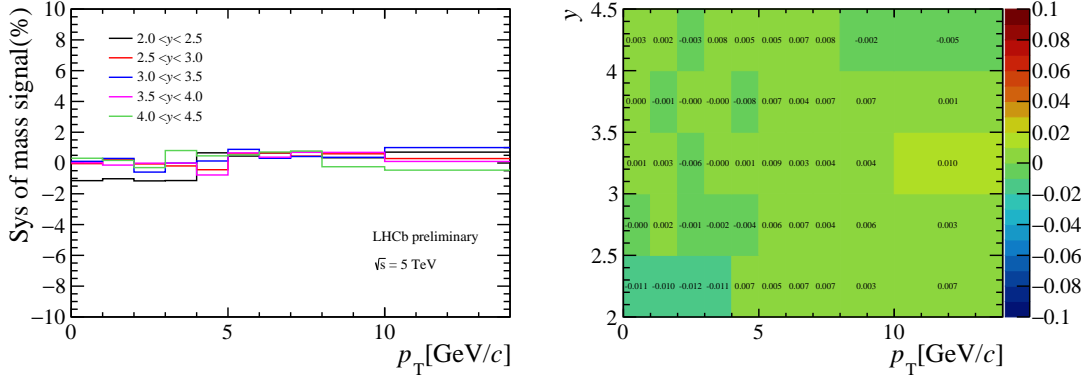


Figure 7.1: The relative difference due to the signal part of mass fit model.

415

## 416 7.2 Background model mass fit

417 Using the exponential function to describe the background in the mass fit also could bias  
 418 the signal yields. As an alternative, a linear function is used. The relative difference, which  
 419 is taken as the systematic uncertainty due to the fit model to describe the background  
 420 part of the invariant mass distribution, is about 0.0~0.7%, as shown in Fig. 7.2. It is  
 421 considered as correlated between bins because the relative differences in all the bins are  
 negative.

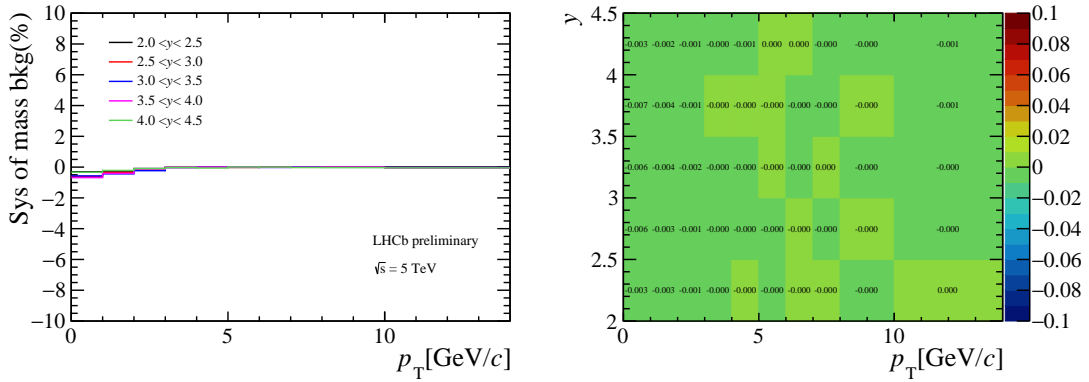


Figure 7.2: The relative difference due to the background part of mass fit model.

422

### 423 7.3 $t_z$ background shape

424 Another source is using mass sidebands to model the  $t_z$  background distribution. An  
 425 alternative approach to describe the  $t_z$  background is the sPlot method. The background  
 426 parameters can also be obtained by fitting to the s-weighted  $t_z$  distribution, and are fixed  
 427 for the  $t_z$  fit. The relative difference is about 0.0~1.2% for prompt  $J/\psi$ , as detailed in Fig.  
 428 7.3, and 0.0~4.0% for  $J/\psi$  from  $b$ , as detailed in Fig. 7.4. It is assumed as uncorrelated  
 between bins since there is no consistent bias in all the bins.

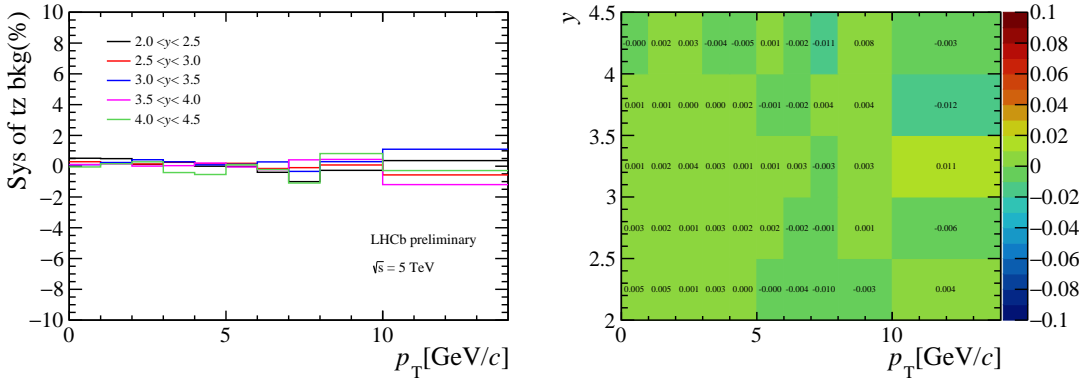


Figure 7.3: The relative difference for prompt  $J/\psi$  due to the description of  $t_z$  background distribution.

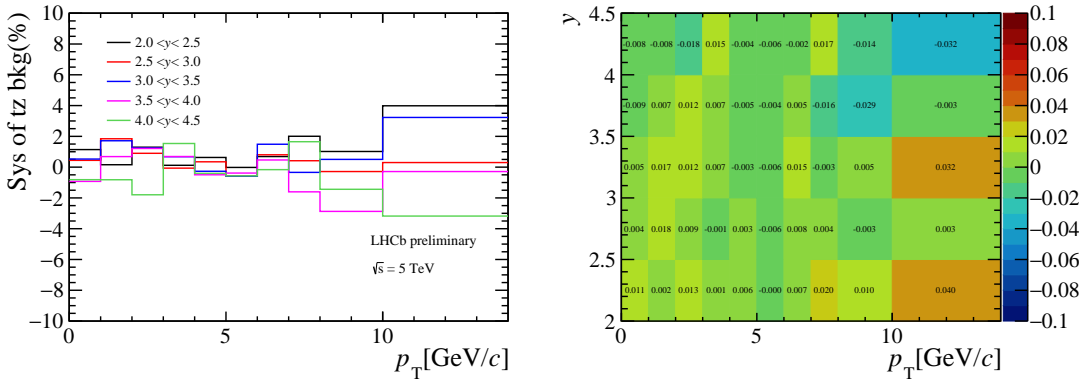


Figure 7.4: The relative difference for  $J/\psi$  from  $b$  due to the description of  $t_z$  background distribution.

429

### 430 7.4 Long tail in $t_z$ distribution

431 For the systematic uncertainty due to the long tail in  $t_z$  distribution, apart from the  
 432 next-event method, a double-sided exponential function is to describe the long tail as  
 433 an alternative, and the relative difference is taken as the systematic uncertainty. The  
 434 parameter of the double-sided exponential function is fixed after using a single-sided  
 435 exponential function to fit  $t_z$  in the range of  $-40 \text{ ps} < t_z < -10 \text{ ps}$ . The relative difference  
 436 is less than 0.04%, which is small due to the fact that the tail is rather small. So, it is  
 437 negligible compared with other sources.

## 438 7.5 Signal model of $t_z$ fit

439 The signal model of  $t_z$  fit, including the imperfect modelling of the detector resolution of  
 440  $t_z$ , the delta function to describe the prompt  $J/\psi$  and one exponential function to describe  
 441 the  $J/\psi$  from  $b$ , could bias the yields, especially for the  $J/\psi$  from  $b$ . To study this effect,  
 442 the  $t_z$  distribution in the truth-matched MC sample is fitted to the same model in all the  
 443 bins, as shown in the Appendix J. According to the fit plots, the yields of  $J/\psi$  from  $b$  will  
 444 be underestimated in the low  $y$  bins, and be overestimated in the high  $y$  bins, especially  
 445 when  $p_T$  is small.

446 The relative difference between the fitted yield and the true number obtained from  
 447 the MC is taken as the systematic uncertainty in each bin. It is 0.0~0.8% for prompt  
 448  $J/\psi$ , as shown in Fig. 7.5, and 0.0~14.7% for  $J/\psi$  from  $b$ , as shown in Fig. 7.6. This  
 449 uncertainty is assumed as correlated between  $p_T$  bins for the consistent bias in all the  $p_T$   
 bins, as uncorrelated between  $y$  bins because of no consistent bias in the  $y$  bins.

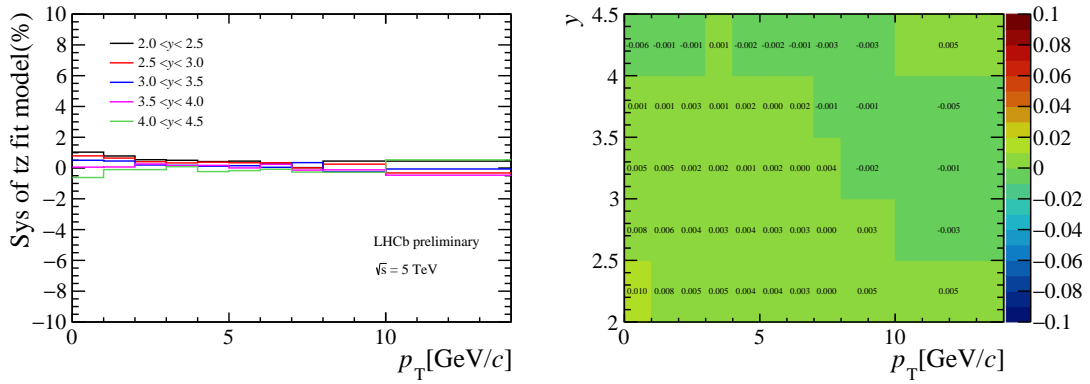


Figure 7.5: The relative difference for prompt  $J/\psi$  due to the signal model of  $t_z$  fit.

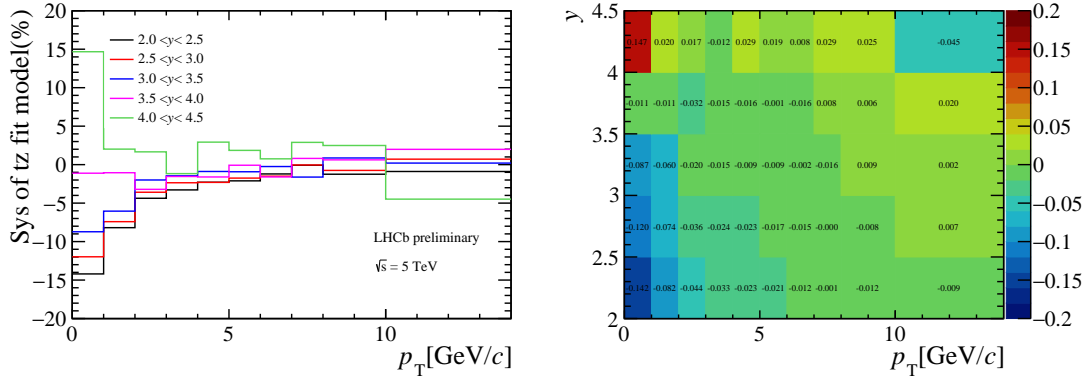


Figure 7.6: The relative difference for  $J/\psi$  from  $b$  due to the signal model of  $t_z$  fit.

450

## 451 7.6 Tracking efficiency

452 There are two sources of systematic uncertainties associated with the track reconstruction  
 453 efficiency.

One is the statistical uncertainty of the ratios due to the limited sample size used to obtain the tracking correction table. This part could be obtained by toy studies: Two hundreds of toy MC experiments were performed where the efficiency for each bin in the  $p$  and  $\eta$  was sampled from 6.3 by Gaussian distributions with the corresponding central value as the mean and the uncertainty as the width. For each experiment, the total efficiency (acceptance is excluded) in different bins could be obtained with the sampled efficiency correction table. Finally, using a Gaussian function to fit to the two hundreds results of each  $(p_T, y)$  bin and the sigma divided by the mean value of the fit result is quoted as the relative uncertainty. The relative uncertainty is around 0.4~3.7%, as shown in Fig. 7.7. The uncertainty in neighboring bins are correlated since they may use the same efficiency correction value. So we assume the uncertainty is correlated between bins.

Another one is the choice of event multiplicity variable. This systematic uncertainty is provided by the tracking group. The tracking experts indicate that choice of the multiplicity variable (nTracks, nSPDhits, or others) is relevant for deciding the systematics. They studied this effect and suggest 0.8% per track, as detailed in Ref. [56].

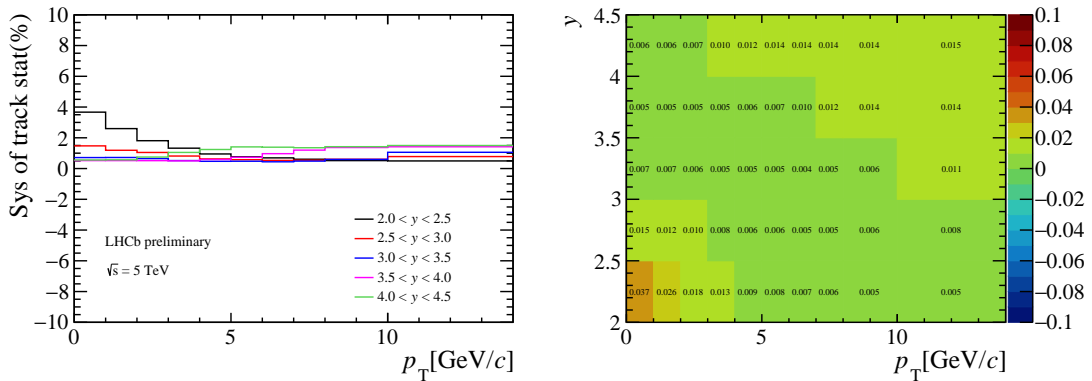


Figure 7.7: The relative difference due to the limited sample size used to obtain the tracking correction table.

468

## 469 7.7 PID efficiency

470 The systematic uncertainty due to PID includes the following two contributions.

471 The first is the statistical uncertainty due to the finite size of the calibration sample. Similarly to the method to estimate the statistical uncertainty of the tracking correction ratios as described in Sec. 7.6, two hundred tables of efficiencies is generated from the original table, where the efficiency in each bin of each table is randomly sampled from a Gaussian distribution using the central value as the mean and the uncertainty as the width. Then, we calculate two hundred efficiency values from the generated efficiency tables, and fit the distribution of the one hundred efficiency values with a Gaussian function. The ratio between the width and the mean value of the fitted Gaussian function is quoted as the systematic uncertainty, which is around 0.4~2.2%, as detailed in Fig. 7.8.

480 The second is the uncertainty due to binning scheme of the calibration sample, studied by varying the binning method in  $p$  and  $\eta$  of muons respectively. The nominal binning scheme of the PID efficiency table used to calculate the PID efficiency of  $J/\psi$  mesons is defined:

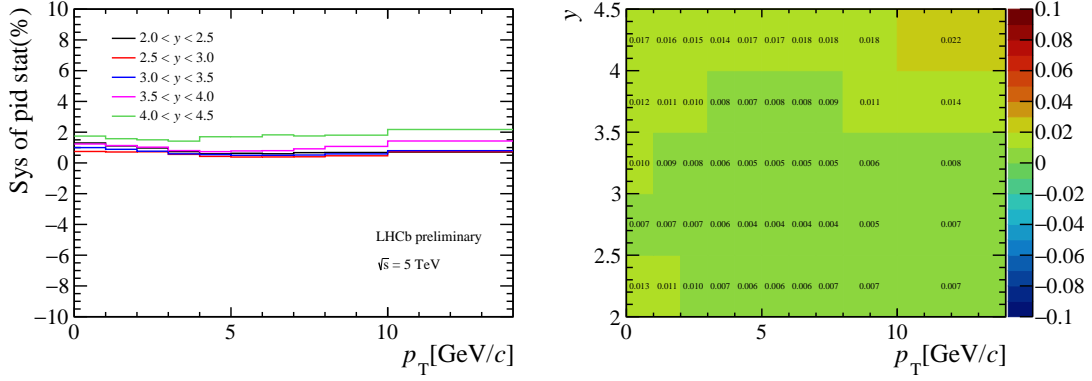


Figure 7.8: The relative difference due to the limited sample size used to obtain the PID calibration table.

- 484  $p$  boundaries [ GeV/c ]: 3, 11, 20, 30, 40, 60, 100, 1000
- 485  $\eta$  boundaries: 2.0, 2.3, 2.6, 2.9, 3.2, 3.5, 3.8, 4.1, 4.5, 5.0
- 486 One of the two alternative binning schemes is defined:
  - 487  $p$  boundaries [ GeV/c ]: 3, 8, 15, 25, 35, 45, 50, 80, 120, 1000
  - 488  $\eta$  boundaries: 2.0, 2.3, 2.6, 2.9, 3.2, 3.5, 3.8, 4.1, 4.5, 5.0

The PID efficiency of the single muon for this binning scheme is shown in Fig. 7.9. The

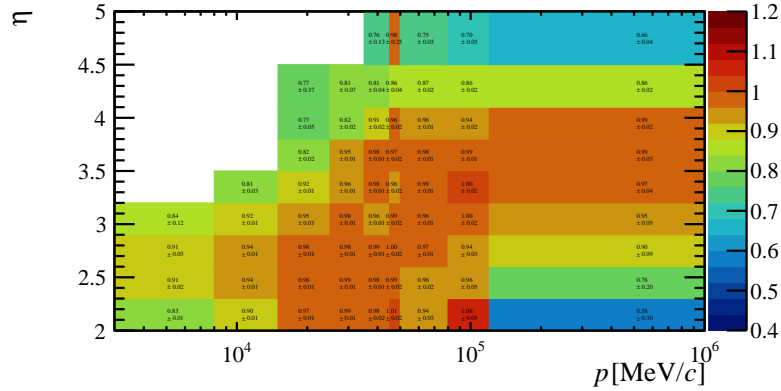


Figure 7.9: PID efficiency of the single muon in bins of muon kinematics for the first alternative binning scheme.

- 489 other one alternative binning scheme is defined:
  - 490  $p$  boundaries [ GeV/c ]: 3, 11, 20, 30, 40, 60, 100, 1000
  - 492  $\eta$  boundaries: 2.0, 2.2, 2.4, 2.7, 3.0, 3.3, 3.6, 4.0, 4.4, 5.0
- 493 The PID efficiency of the single muon for the latter binning scheme is shown in Fig. 7.10.
- 494 Based on the two new muon PID efficiency tables, the PID efficiencies of  $J/\psi$  mesons are
- 495 calculated alternatively. The maximum difference between the two new efficiency and

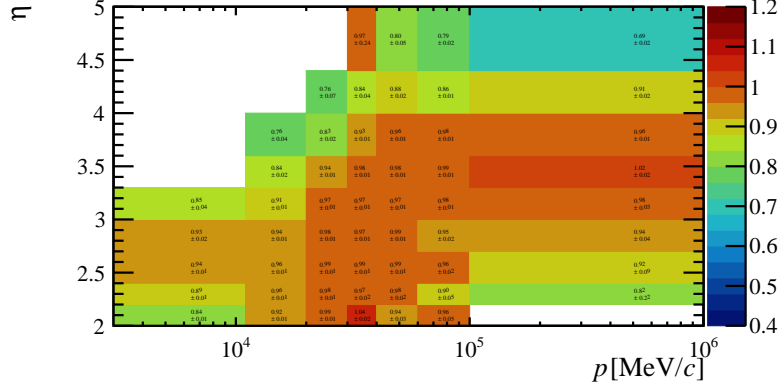


Figure 7.10: PID efficiency of the single muon in bins of muon kinematics for the second alternative binning scheme.

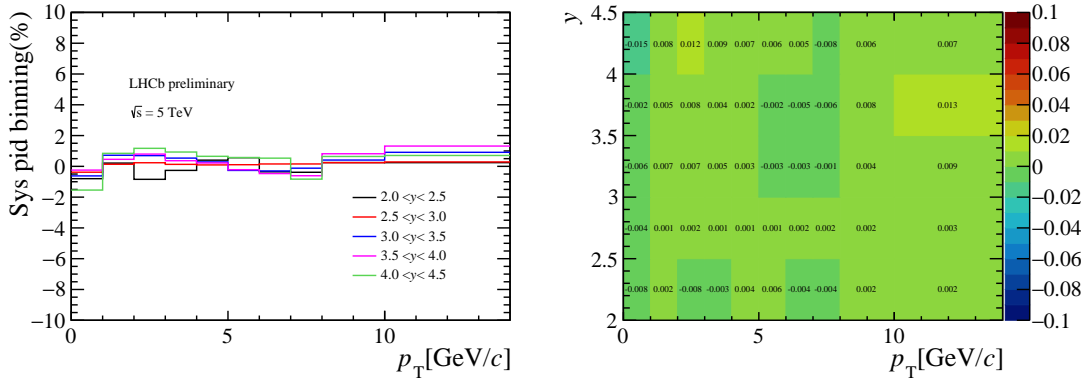


Figure 7.11: The relative difference due to the binning scheme of the calibration sample.

496 the original efficiency is quoted as the systematic uncertainty. The relative uncertainty is  
 497 about  $0.1\sim1.5\%$ , as detailed in Fig. 7.11. We assume the PID efficiency uncertainty is  
 498 correlated between bins because the uncertainty in neighboring bins are highly correlated.

## 499 7.8 Trigger efficiency

500 The trigger efficiency in simulation is cross-checked with data, and the difference between  
 501 simulation and data is quoted as the systematic uncertainty due to trigger. For L0Muon,  
 502 tag-and-probe method is used to extract the single track trigger efficiency in simulation  
 503 and data. The tag-muon is required to fire the L0Muon trigger, and the single track trigger  
 504 efficiency is determined as the fraction of candidates with the probe-muon also firing the  
 505 L0Muon trigger. The single track efficiency is determined in bins of muon transverse  
 506 momentum and pseudo-rapidity as  $\epsilon(p_{T\mu}, \eta_\mu)$ , as shown in Fig. 7.12 and Fig. 7.13 for data  
 507 and simulation respectively.  $\mu^+$  and  $\mu^-$  tracks have different L0Muon efficiency especially  
 508 in low  $p_T$  and high  $\eta$  bins. From the single track L0Muon trigger efficiency, the  $J/\psi$   
 509 L0Muon trigger efficiency is determined as  $\sum\{1-(1-\epsilon(p_{T\mu+}, \eta_{\mu+}))(1-\epsilon(p_{T\mu-}, \eta_{\mu-}))\}/N_{\text{tot}}$ ,  
 510 since at least one muon is required to fire the trigger. The relative difference of  $J/\psi$  L0Muon  
 511 trigger efficiency between data and simulation is quoted as the systematic uncertainty,  
 512 which is about  $0.0\sim1.9\%$ , assumed as correlated between bins, as shown in Fig. 7.14.

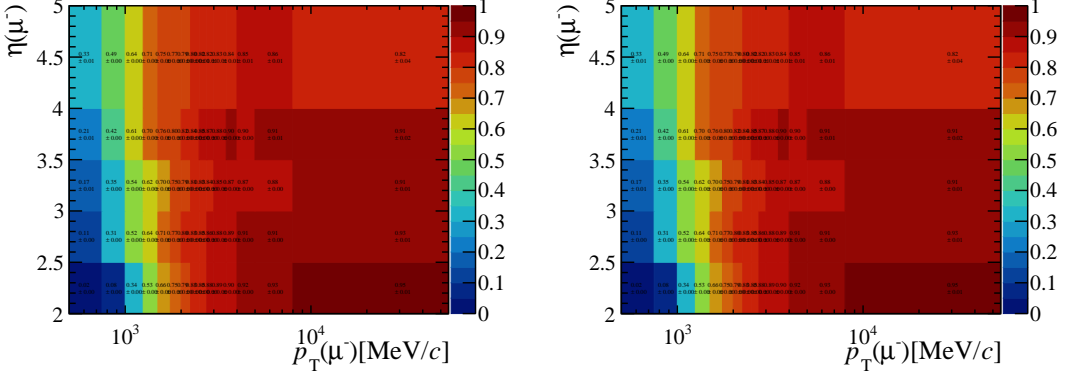


Figure 7.12: The single track L0Muon trigger efficiency determined using tag-and-probe method in data for  $\mu^+$  (left) and  $\mu^-$  (right).

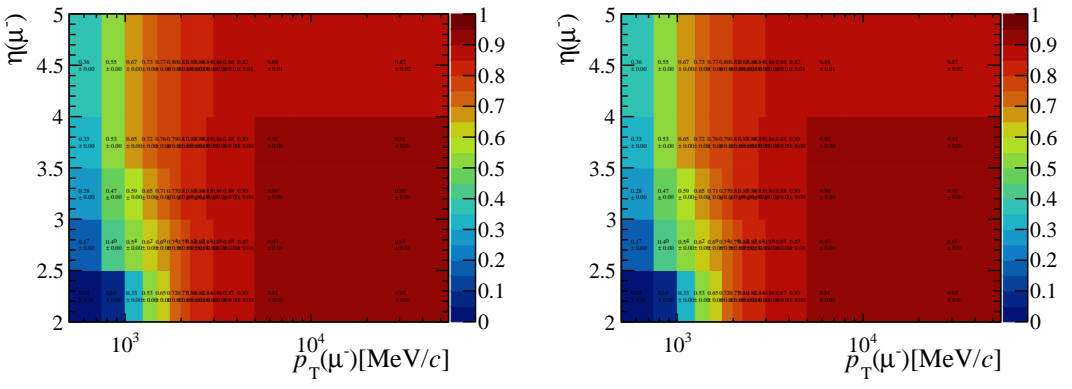


Figure 7.13: The single track L0Muon trigger efficiency determined using tag-and-probe method in simulation for  $\mu^+$  (left) and  $\mu^-$  (right).

513     For Hlt1DiMuonHighMass, the TisTos method is used to evaluate the trigger efficiency  
 514     in data and simulation. Hlt1Global is used as the TIS line. For data, the mass fit is  
 515     performed to extract the  $J/\psi$  signals of the TIS sample and the TIS&&TOS sample. The  
 516     efficiency is the ratio between the number of signals in the TIS&&TOS sample and that in  
 517     the TIS sample. The relative efficiency difference is shown in Fig. 7.15. The distribution

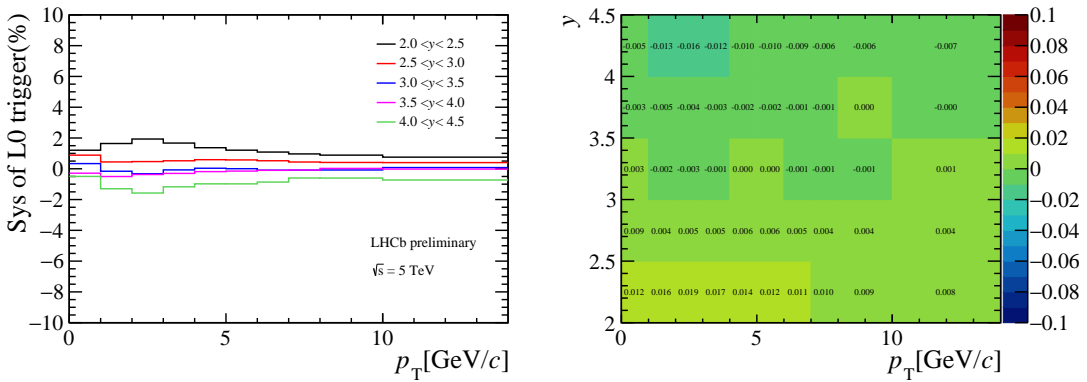


Figure 7.14: The relative difference due to the L0Muon trigger efficiency calculation.

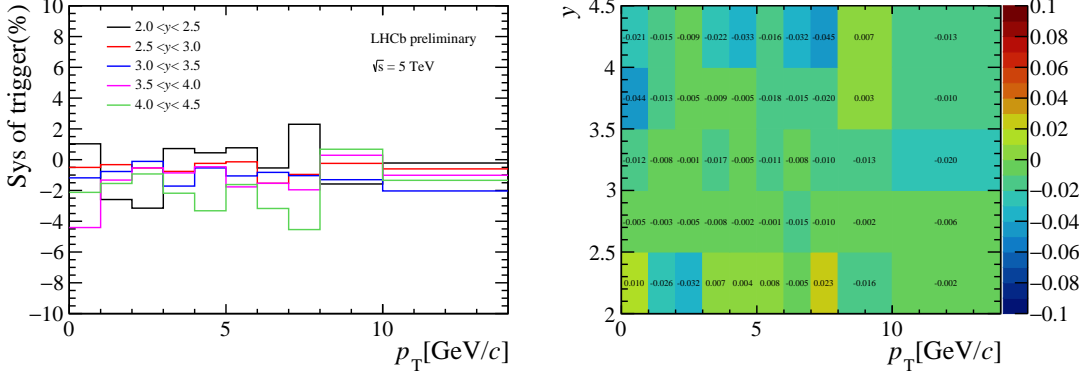


Figure 7.15: The relative difference due to the trigger efficiency calculation.

518 of the ratio between data and simulation for 50 ( $p_T, y$ ) bins suggests a small inconsistency  
of Hlt1 trigger efficiency in simulation and data, as shown in Fig. 7.16. The fit with

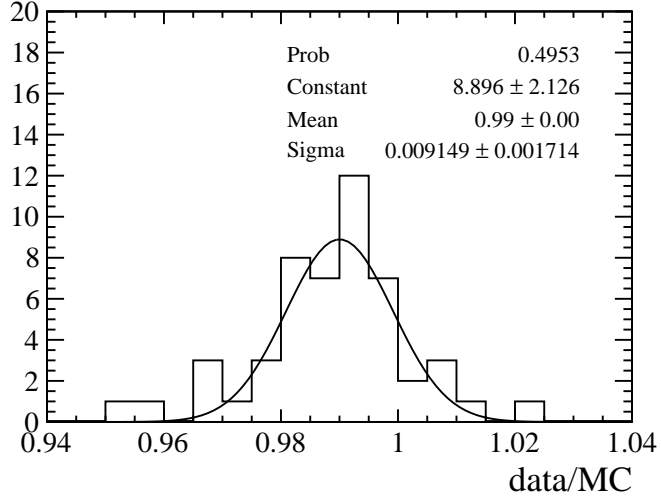


Figure 7.16: The distribution of the ratio between data and simulation for 50 ( $p_T, y$ ) bins.

519 Gaussian is performed and the mean is  $0.990 \pm 0.001$ . We quote a systematic value of  
520 1.0% consistent over bins. The systematic uncertainty quoted this way is consistent with  
521 the relative difference combining all kinematic bins. The efficiency is  $0.880 \pm 0.001$  for  
522 data and  $0.8870 \pm 0.0002$  for simulation.

## 524 7.9 Polarisation

525 The detection efficiency of  $J/\psi$  is affected by the polarisation, especially by the polarisation  
526 parameter  $\lambda_\theta$ . Zero polarisation is assumed in the simulation since there is no prior  
527 knowledge of the polarisation of  $J/\psi$  mesons in  $pp$  collisions at 5 TeV, and only small  
528 longitudinal polarisations have been found in the LHC  $J/\psi$  polarisation analyses [26, 27, 40].  
529 To evaluate the change of results assuming an extreme scenario of polarisation, we  
530 reweight the angular distribution of  $\mu^+$  in the  $J/\psi$  rest frame and calculate the change  
531 of total average efficiency (prompt  $J/\psi$  and  $J/\psi$  from  $b$  are combined). The ratio of the

total efficiency between the extreme scenario of polarisation ( $\lambda_\theta = -1, 1$ ) and the zero polarisation is shown in Fig. 7.17. The increase of the total efficiency is given for a

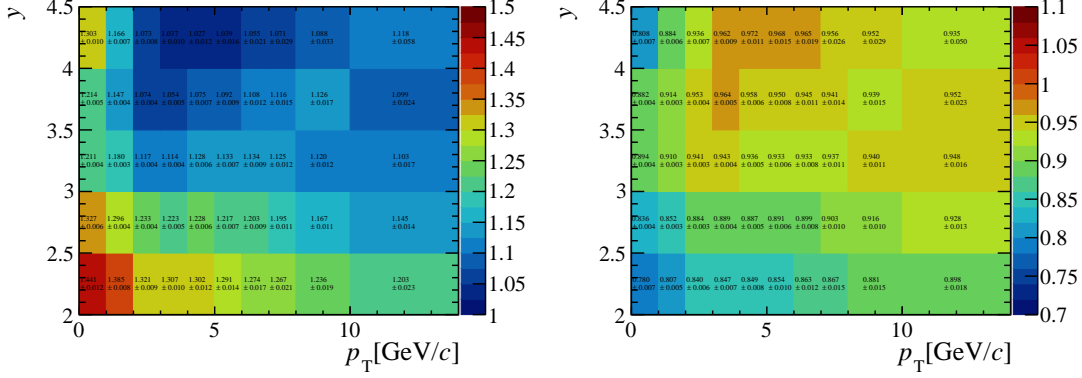


Figure 7.17: The ratio of the total efficiency between  $\lambda_\theta = -1$ (left),  $1$ (right) polarisation and the zero polarisation.

polarisation of  $\lambda_\theta = -0.2$  compared to zero polarisation in  $(p_T, y)$  bins in Table 7.1, and the ratio is shown in Fig. 7.18. We only make the cross-section measurements assuming

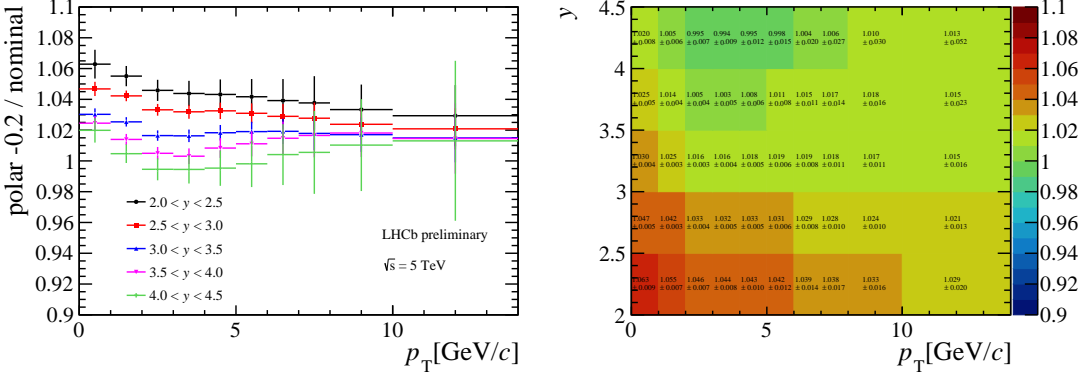


Figure 7.18: The ratio of the total efficiency between  $\lambda_\theta = -0.2$  polarisation and the zero polarisation.

zero polarisation and no corresponding systematic uncertainty is quoted. The difference of the total efficiency for different scenarios of polarisation is given as a reference.

## 7.10 Other sources

- The uncertainty of  $\mathcal{B}(J/\psi \rightarrow \mu^+\mu^-) = 5.961 \pm 0.033\%$  from PDG, is propagated to the cross-section measurement as 0.55%.
- The relative uncertainty of the luminosity is 2.0%, which is propagated to the cross-section results.
- The limited size of the simulation sample used to determine the efficiencies is a source of systematic uncertainties. The uncertainties are 0.2~3.7% for prompt  $J/\psi$  and 0.6~7.7% for  $J/\psi$  from  $b$  depending on the kinematic bins.

Table 7.1: The relative increase of the total efficiency (in %), for a -0.2 polarisation rather than zero, in different bins of  $p_T$  and  $y$ .

$p_T$ ( GeV/c )	$2 < y < 2.5$	$2.5 < y < 3$	$3 < y < 3.5$	$3.5 < y < 4$	$4 < y < 4.5$
0-1	$6.29 \pm 0.93$	$4.68 \pm 0.46$	$3.03 \pm 0.39$	$2.45 \pm 0.45$	$1.99 \pm 0.80$
1-2	$5.51 \pm 0.66$	$4.23 \pm 0.35$	$2.54 \pm 0.30$	$1.40 \pm 0.36$	$0.47 \pm 0.61$
2-3	$4.58 \pm 0.69$	$3.32 \pm 0.38$	$1.65 \pm 0.34$	$0.49 \pm 0.41$	$-0.55 \pm 0.71$
3-4	$4.38 \pm 0.82$	$3.19 \pm 0.45$	$1.63 \pm 0.41$	$0.31 \pm 0.51$	$-0.55 \pm 0.92$
4-5	$4.32 \pm 0.97$	$3.25 \pm 0.53$	$1.83 \pm 0.50$	$0.83 \pm 0.64$	$-0.47 \pm 1.15$
5-6	$4.17 \pm 1.15$	$3.09 \pm 0.64$	$1.90 \pm 0.64$	$1.11 \pm 0.82$	$-0.19 \pm 1.51$
6-7	$3.92 \pm 1.40$	$2.90 \pm 0.80$	$1.92 \pm 0.82$	$1.47 \pm 1.08$	$0.41 \pm 1.98$
7-8	$3.77 \pm 1.74$	$2.77 \pm 1.02$	$1.79 \pm 1.08$	$1.65 \pm 1.42$	$0.55 \pm 2.69$
8-10	$3.33 \pm 1.63$	$2.38 \pm 1.01$	$1.71 \pm 1.12$	$1.81 \pm 1.56$	$1.03 \pm 2.99$
10-14	$2.94 \pm 1.99$	$2.08 \pm 1.34$	$1.49 \pm 1.58$	$1.46 \pm 2.29$	$1.30 \pm 5.20$
14-20			$1.58 \pm 1.93$	$(2 < y < 4.5)$	

Table 7.2: Summary of relative systematic uncertainties (%)

Source	Result (%)	Comment
Signal model of mass fit	$0.0\sim 2.0$	Bin dependent
Background model of mass fit	$0.0\sim 0.7$	Correlated between bins
$t_z$ background shape	$0.0\sim 1.2$ (prompt $J/\psi$ ) $0.0\sim 4.0$ ( $J/\psi$ from $b$ )	Bin dependent
Signal model of $t_z$ fit	$0.0\sim 0.8$ (prompt $J/\psi$ ) $0.0\sim 14.7$ ( $J/\psi$ from $b$ )	$p_T$ bins correlated, $y$ bins uncorrelated
Tracking efficiency	$(0.4\sim 3.7) \oplus (2\times 0.8)$	Correlated between bins
PID efficiency	$(0.4\sim 2.2) \oplus (0.1\sim 1.5)$	Correlated between bins
L0 Trigger efficiency	$0.0\sim 1.9$	Correlated between bins
Hlt1 Trigger efficiency	1.0	Correlated between bins
$\mathcal{B}(J/\psi \rightarrow \mu^+\mu^-)$	0.6	Correlated between bins
Luminosity	2.0	Correlated between bins
MC sample size	$0.2\sim 3.7$ (prompt $J/\psi$ ) $0.6\sim 7.7$ ( $J/\psi$ from $b$ )	Bin dependent
Radiative tail	1.0	Correlated between bins

- 546     • A fraction of events are lost because of the QED radiative tail. The efficiency of the  
 547     mass window is estimated using the simulated sample, and the imperfect modelling  
 548     of the radiative decay is considered as a source of systematic uncertainty. This has  
 549     been studied in previous analysis and the similar effect is expected. Therefore, as in  
 550     RUN-I analysis a value of 1% is quoted.

## 551     7.11 Summary of systematic uncertainties

552     In Table 7.2, the systematic uncertainties are summarized.

## 553 8 Results

### 554 8.1 Cross-sections at 5 TeV

555 With the signal yields determined from the fitting the invariant mass and  $t_z$  distributions,  
 556 the efficiencies estimated from simulation and calibration sample, and the systematic  
 557 uncertainties, the  $J/\psi$  production cross-sections are measured. By integrating the double  
 558 differential results over  $p_T$  ( $y$ ) one can obtain the single differential cross-sections as a  
 559 function of  $y(p_T)$ . The total cross-sections can be obtained by integrating the double  
 560 differential results over  $p_T$  and  $y$  bins as well. For the central value of the integrated  
 561 cross-section, it is the sum of double-differential cross-sections times the bin widths.  
 562 The statistical uncertainties of different bins are added simply in quadrature when  
 563 integrating, as well as the uncorrelated systematic uncertainties. The correlated systematic  
 564 uncertainties of different bins due to the same source are added directly, and then the  
 565 sum of correlated uncertainties due to different sources are added in quadrature. For  
 566 the uncertainty due to the signal model of  $t_z$  fit, which is correlated between  $p_T$  bins  
 567 and uncorrelated between  $y$  bins, the  $p_T$  bins are added directly at first, and then the  $y$   
 568 bins are integrated. It is compared with that with integrating  $y$  bins firstly and  $p_T$  bins  
 569 secondly. The difference is the second-order effect, which is negligible.

570 The measured double differential cross-sections for prompt  $J/\psi$  and  $J/\psi$  from  $b$  are  
 shown in Fig. 8.1 and Fig. 8.2 respectively. The integrated cross-sections for prompt

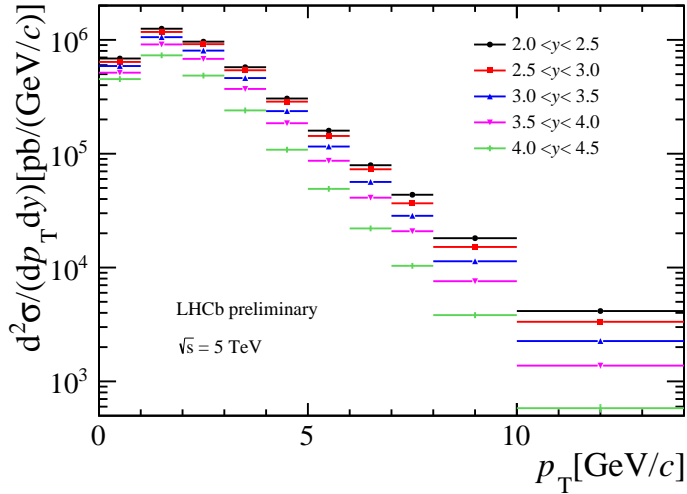


Figure 8.1: Differential cross-sections for prompt  $J/\psi$  as a function of  $p_T$  in bins of  $y$ . Statistical and systematic uncertainties are added in quadrature.

571  
 572  $J/\psi$  and  $J/\psi$  from  $b$  in the range  $0 < p_T < 14 \text{ GeV}/c$  and  $2 < y < 4.5$ , are:

$$\begin{aligned} \sigma_{\text{prompt}} &= 8.150 \pm 0.010(\text{stat}) \pm 0.283(\text{syst}) \mu\text{b}, \\ \sigma_{\text{from } b} &= 0.817 \pm 0.003(\text{stat}) \pm 0.034(\text{syst}) \mu\text{b}, \end{aligned} \quad (8.1)$$

573 where the first uncertainty is statistical and the second one is systematic. In the range  
 574  $0 < p_T < 20 \text{ GeV}/c$  and  $2 < y < 4.5$ , the integrated cross-sections are:

$$\begin{aligned} \sigma_{\text{prompt}} &= 8.154 \pm 0.010(\text{stat}) \pm 0.283(\text{syst}) \mu\text{b}, \\ \sigma_{\text{from } b} &= 0.820 \pm 0.003(\text{stat}) \pm 0.034(\text{syst}) \mu\text{b}, \end{aligned} \quad (8.2)$$

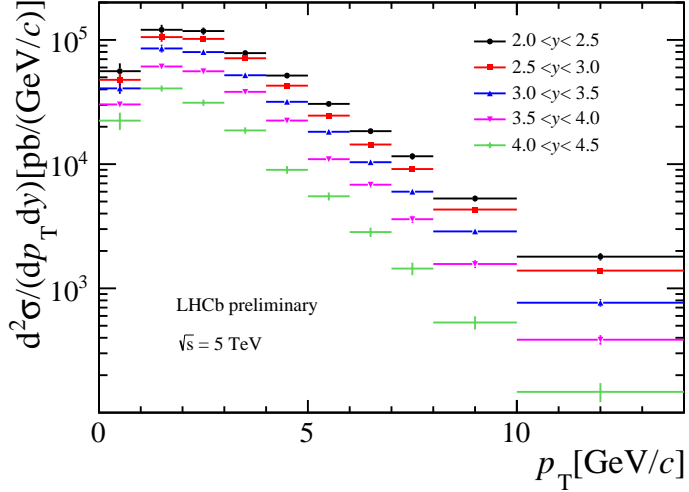


Figure 8.2: Differential cross-sections for  $J/\psi$  from  $b$  as a function of  $p_T$  in bins of  $y$ . Statistical and systematic uncertainties are added in quadrature.

575 The single differential cross-sections as a function of  $p_T$  and  $y$  are shown in Fig. 8.3 for prompt  $J/\psi$  and in Fig. 8.4 for  $J/\psi$  from  $b$ . Tables in Appendix A give the measured

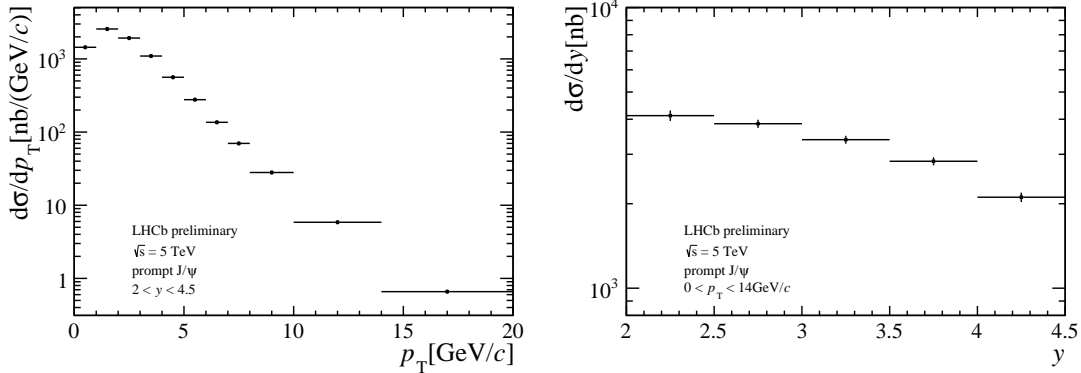


Figure 8.3: The single differential cross-sections as a function of  $p_T$  (left) and  $y$  (right) for prompt  $J/\psi$ .

576  
577 double-differential cross-sections in  $(p_T, y)$  bins, and the single-differential cross-sections.

## 578 8.2 Fraction of $J/\psi$ from $b$

579 The fraction of  $J/\psi$  from  $b$  is shown in Fig. 8.5 and Table 8.1. Most systematic  
580 uncertainties are cancelled. Only the uncertainties due to  $tz$  fit and MC sample size are  
581 included. The fraction increases as a function of  $p_T$ . For a constant  $p_T$ , the fraction  
582 decreases with increasing rapidity, indicating the  $b$ -hadrons are produced less forward  
583 than prompt  $J/\psi$ .

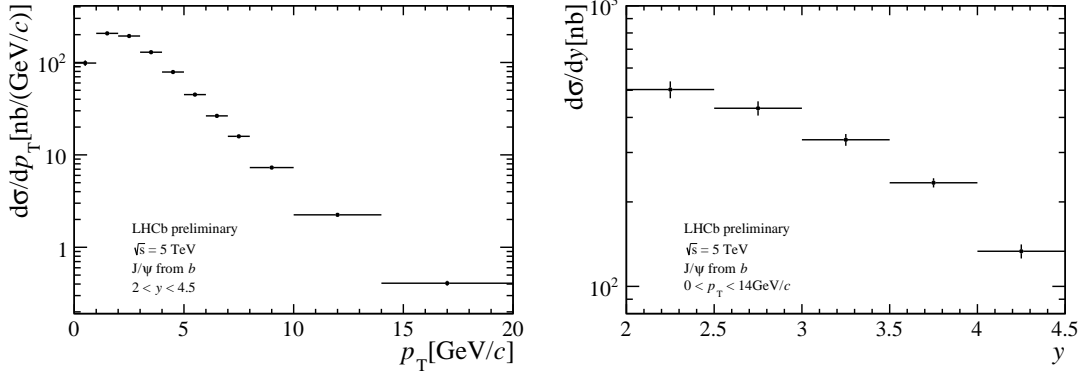


Figure 8.4: The single differential cross-sections as a function of  $p_T$  (left) and  $y$  (right) for  $J/\psi$  from  $b$ .

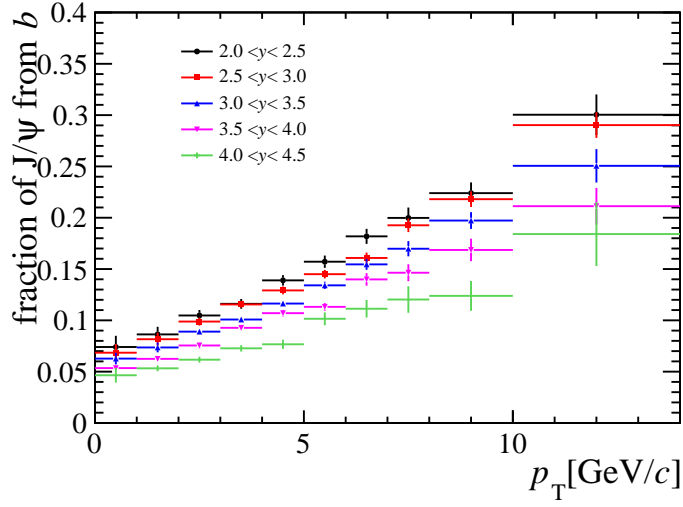


Figure 8.5: The fraction of  $J/\psi$  from  $b$  as a function of  $p_T$  in bins of  $y$ . Statistical and systematic uncertainties are added in quadrature.

Table 8.1: The fraction of  $J/\psi$ -from- $b$  mesons (in %) in  $(p_T, y)$  bins. The first uncertainty is statistical and the second is systematic.

$p_T$ (GeV/c)	$2 < y < 2.5$	$2.5 < y < 3$	$3 < y < 3.5$	$3.5 < y < 4$	$4 < y < 4.5$
0-1	$7.4 \pm 0.3 \pm 1.1$	$6.8 \pm 0.1 \pm 0.8$	$6.3 \pm 0.1 \pm 0.6$	$5.3 \pm 0.1 \pm 0.1$	$4.6 \pm 0.2 \pm 0.7$
1-2	$8.6 \pm 0.2 \pm 0.7$	$8.2 \pm 0.1 \pm 0.6$	$7.4 \pm 0.1 \pm 0.5$	$6.2 \pm 0.1 \pm 0.1$	$5.3 \pm 0.1 \pm 0.1$
2-3	$10.5 \pm 0.2 \pm 0.5$	$9.9 \pm 0.1 \pm 0.4$	$8.9 \pm 0.1 \pm 0.2$	$7.5 \pm 0.1 \pm 0.3$	$6.2 \pm 0.2 \pm 0.2$
3-4	$11.6 \pm 0.3 \pm 0.4$	$11.5 \pm 0.2 \pm 0.3$	$10.1 \pm 0.2 \pm 0.2$	$9.3 \pm 0.2 \pm 0.2$	$7.3 \pm 0.3 \pm 0.2$
4-5	$13.9 \pm 0.4 \pm 0.4$	$12.9 \pm 0.2 \pm 0.3$	$11.6 \pm 0.2 \pm 0.1$	$10.7 \pm 0.2 \pm 0.2$	$7.7 \pm 0.4 \pm 0.2$
5-6	$15.7 \pm 0.5 \pm 0.4$	$14.5 \pm 0.3 \pm 0.3$	$13.4 \pm 0.3 \pm 0.2$	$11.3 \pm 0.4 \pm 0.1$	$10.2 \pm 0.6 \pm 0.2$
6-7	$18.2 \pm 0.6 \pm 0.4$	$16.1 \pm 0.4 \pm 0.3$	$15.5 \pm 0.5 \pm 0.3$	$14.0 \pm 0.5 \pm 0.3$	$11.1 \pm 0.8 \pm 0.2$
7-8	$20.0 \pm 0.8 \pm 0.6$	$19.3 \pm 0.6 \pm 0.2$	$17.0 \pm 0.7 \pm 0.3$	$14.6 \pm 0.8 \pm 0.3$	$12.0 \pm 1.2 \pm 0.5$
8-10	$22.4 \pm 0.9 \pm 0.5$	$21.8 \pm 0.7 \pm 0.3$	$19.7 \pm 0.8 \pm 0.3$	$16.9 \pm 0.9 \pm 0.6$	$12.4 \pm 1.4 \pm 0.5$
10-14	$30.0 \pm 1.4 \pm 1.4$	$29.0 \pm 1.2 \pm 0.5$	$25.1 \pm 1.3 \pm 0.9$	$21.1 \pm 1.7 \pm 0.7$	$18.4 \pm 2.8 \pm 1.4$

### 584 8.3 Extrapolation to the total $b\bar{b}$ cross-section

585 The total  $b\bar{b}$  production cross-section is calculated using:

$$\sigma(pp \rightarrow b\bar{b}X) = \alpha_{4\pi} \frac{\sigma(J/\psi \text{ from } b, p_T < 20 \text{ GeV}/c, 2.0 < y < 4.5)}{2\mathcal{B}(b \rightarrow J/\psi X)}, \quad (8.3)$$

586 where  $\alpha_{4\pi}$  is the extrapolation factor to the full kinematic region and  $\mathcal{B}(b \rightarrow J/\psi X) =$   
 587  $1.16 \pm 0.10\%$  [52] is the inclusive  $b \rightarrow J/\psi X$  branching fraction. The extrapolation factor  
 588 predictions given by simulation (PYTHIA 8) is  $\alpha_{4\pi} = 5.56$  at 5 TeV. The FONLL predictions  
 589 [57, 58] for the extrapolation factor is  $\alpha_{4\pi} \approx \sigma(J/\psi \text{ from } b, p_T < 300 \text{ GeV}/c, -12 < y <$   
 590  $12)/\sigma(J/\psi \text{ from } b, p_T < 20 \text{ GeV}/c, 2.0 < y < 4.5) = 5.30$ . Using the  $\alpha_{4\pi}$  from PYTHIA  
 591 8, the total  $b\bar{b}$  production cross-section is  $\sigma(pp \rightarrow b\bar{b}X) = 196.5 \pm 0.7 \pm 18.7 \mu\text{b}$ , where  
 592 the first uncertainty is statistical and the second one is systematic. The uncertainty is  
 593 dominated by that due to the  $\mathcal{B}(b \rightarrow J/\psi X)$  measurement. No uncertainty on  $\alpha_{4\pi}$  is  
 594 included in this estimate.

### 595 8.4 Comparison with results at 13 TeV

596 A ratio cross-section measurement is made between the results at 13 TeV and 5 TeV to  
 597 reduce the correlated systematic uncertainties. The correlations are evaluated this way:

- 598 • Mass fit. For both analyses, two CB functions are used to describe the signal mass  
 599 shape, and an exponential function to describe the background. But the alternative  
 600 way is different. In addition, the 13 TeV analysis shares the same uncertainty  
 601 value for all the kinematic bins (correlated between bins), while different kinematic  
 602 bins have different uncertainty values for the 5 TeV analysis (bin dependent). For  
 603 simplicity, we assume the correlation is 50% since it is difficult to precisely estimate  
 604 the correlation.
- 605 • Background shape of  $t_z$  fit. There are some correlations between different analyses  
 606 but it is difficult to estimate the exact correlation. The estimated systematic  
 607 uncertainties have large contributions from statistical fluctuations since the numbers  
 608 are determined by comparing the nominal fit and alternative fit in each kinematic  
 609 bin with limited statistics. For a conservative estimation and simplicity, we assume  
 610 it is uncorrelated between different measurements.
- 611 • Signal model of  $t_z$  fit. This uncertainty is only considered in the 5 TeV analysis. We  
 612 assume the correlation is 0 and the systematic uncertainty for 13 TeV is 0 in the  
 613 calculation.
- 614 • PID efficiency. The systematic uncertainty of PID includes two contributions. The  
 615 first is due to finite size of the calibration sample, and second is the uncertainty of  
 616 binning scheme. The first one is totally uncorrelated and the second one is correlated.  
 617 For simplicity, instead of decoupling the uncorrelated and correlated part, we assume  
 618 the total PID systematic uncertainty is 50% correlated.
- 619 • Tracking efficiency. The same discussion for PID systematic uncertainty also applies  
 620 to the tracking systematic uncertainty. We assume the correlation of the total  
 621 tracking systematic uncertainty is 50%.

- Trigger efficiency. The difference between data and simulation is quoted as the uncertainty. For both analyses, the same method is used to estimate the uncertainty: tag-and-probe method for L0Muon and TisTos method for Hlt1DiMuonHighMass. We assume the correlation is 100%.
- $p_T$ - $y$  spectrum. For the 5 TeV analysis, the  $p_T$ - $y$  spectrum correction is performed, as described in Appendix H. For the 13 TeV analysis, it is considered as the systematic uncertainty. There should be some correlations between different analyses, since the same MC generator is used for different samples. But the consistency of the kinematics between simulation and data might be different. So for a conservative estimation and simplicity, we assume the correlation is 0 and the systematic uncertainty for 5 TeV is 0 in the calculation.
- Radiative tail. Both analyses use similar models to describe radiative  $J/\psi$  decays, so this effect totally cancels between different analyses.
- Branching fraction. The correlation is 100%.
- Luminosity. The correlation of luminosity uncertainty between 13 TeV and 8 TeV has been assumed as 50% in the 13 TeV analysis. Similarly, we take the number 50% as the correlation between 13 TeV and 5 TeV.
- MC statistics. It is totally uncorrelated.
- Vertexing. For the 13 TeV analysis, the uncertainty due to the vertex fit quality cut is 0.36%, which is negligible. For the 5 TeV analysis, the vertex fit quality cut is  $J/\psi$  vertex  $\chi^2/\text{ndf} < 8$ . From the Turbo line, the cut is  $J/\psi$  vertex  $\chi^2/\text{ndf} < 25$ . Therefore, we check the difference of the efficiency  $\frac{\text{number of events } J/\psi \text{ vertex } \chi^2/\text{ndf} < 8}{\text{number of events } J/\psi \text{ vertex } \chi^2/\text{ndf} < 25}$  between data and simulation. It is only 0.064%, which is negligible as well. So the systematic uncertainty due to vertexing is negligible.

The result of ratio is shown in Fig. 8.6 (for prompt  $J/\psi$ ) and Fig. 8.7 (for  $J/\psi$  from  $b$ ).

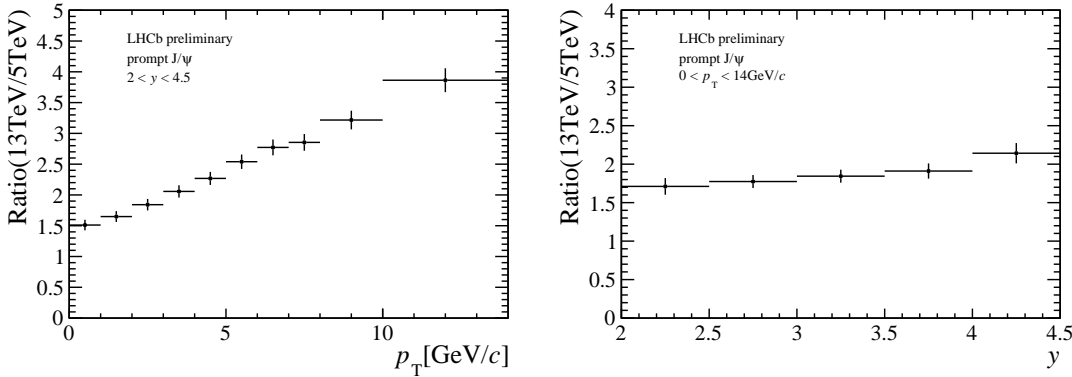


Figure 8.6: The ratio between the results at 13 TeV and 5 TeV for prompt  $J/\psi$  as a function of  $p_T$  (left) and as a function of  $y$  (right).

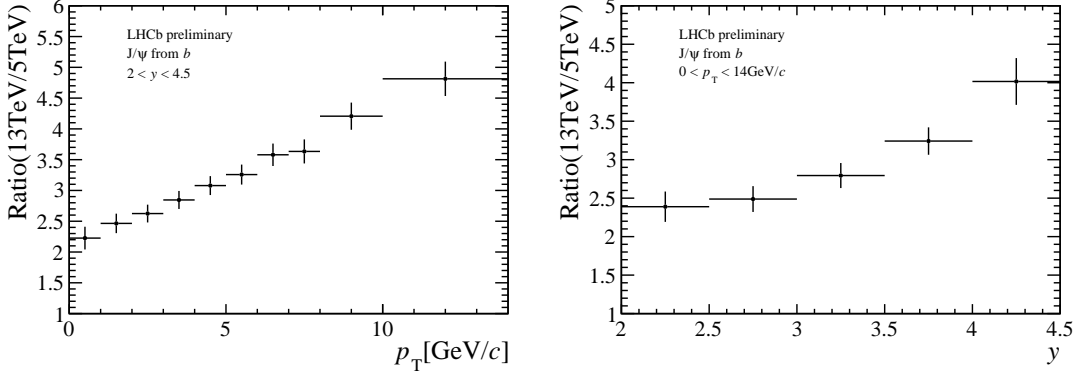


Figure 8.7: The ratio between the results at 13 TeV and 5 TeV for  $J/\psi$  from  $b$  as a function of  $p_T$  (left) and as a function of  $y$  (right).

## 647 8.5 Comparison with results at 8 TeV

648 A ratio cross-section measurement between the results at 8 TeV and 5 TeV is also made to  
 649 reduce the correlated systematic uncertainties. The correlation are evaluated this way:

- 650 • Mass fit. For the 8 TeV analysis, one CB function is used to describe the signal mass  
 651 shape, while two CB functions are used in 5 TeV analysis. And the alternative way  
 652 is different. For simplicity, we assume the correlation is 50% since it is difficult to  
 653 precisely estimate the correlation.
- 654 • Background shape of  $t_z$  fit. Similarly to the discussion in Sec. 8.4, we assume it is  
 655 uncorrelated between different measurements.
- 656 • Signal model of  $t_z$  fit. This uncertainty is only considered in the 5 TeV analysis.  
 657 We assume the correlation is 0 and the systematic uncertainty for 8 TeV is 0 in the  
 658 calculation.
- 659 • PID efficiency. Similarly to the discussion in Sec. 8.4, we assume the total PID  
 660 systematic uncertainty is 50% correlated.
- 661 • Tracking efficiency. Similarly to the discussion in Sec. 8.4, we assume the correlation  
 662 of the total tracking systematic uncertainty is 50%.
- 663 • Trigger efficiency. For the 8 TeV analysis, a value of 4% is quoted for all kinematic  
 664 bins, which comes from comparison of trigger efficiency in data and simulation using  
 665 the TisTos method and comes from the limited statistics. To be simple, we assume  
 666 the correlations are 50% between measurements at 8 TeV and 5 TeV.
- 667 • Radiative tail. This effect totally cancels between different analyses.
- 668 • Branching fraction. The correlation is 100%.
- 669 • Luminosity. The correlation of luminosity uncertainty between 13 TeV and 8 TeV  
 670 has been assumed as 50% in the 13 TeV analysis. Similarly, we take the number  
 671 50% as the correlation between 8 TeV and 5 TeV.

- 672     • MC statistics. It is totally uncorrelated.
- 673     • Vertexing. For the 5 TeV analysis, it is negligible. For the 8 TeV analysis, the value  
674        is 1.0%.
- 675     • Global event cuts (GEC). The uncertainty is only present in the 8 TeV analysis, but  
676        is negligibly small (0.3%).
- 677     • Inter bin cross feed. The uncertainty is also only present in the 8 TeV analysis.  $J/\psi$   
678        can be incorrectly assigned to a wrong bin due to the finite resolution on the  $p_T$   
679        and  $y$ . But the value is 0.5%, which is negligible.

The result of ratio is shown in Fig. 8.8 (for prompt  $J/\psi$ ) and Fig. 8.9 (for  $J/\psi$  from  $b$ ).

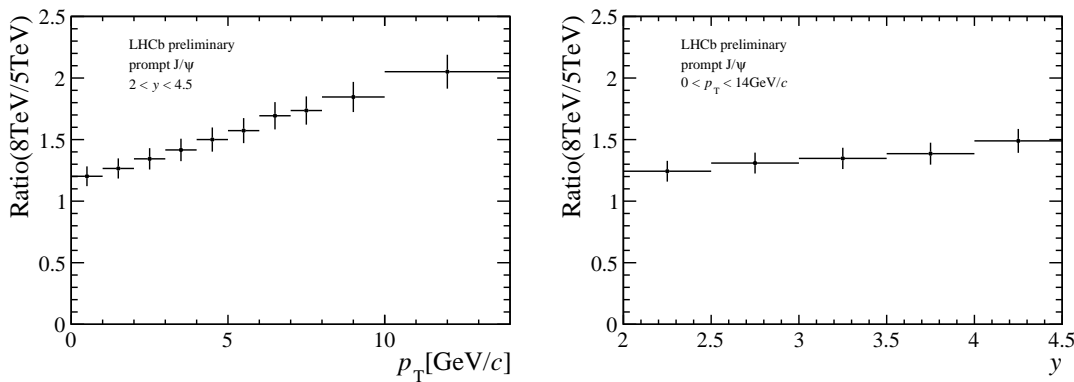


Figure 8.8: The ratio between the results at 8 TeV and 5 TeV for prompt  $J/\psi$  as a function of  $p_T$  (left) and as a function of  $y$  (right).

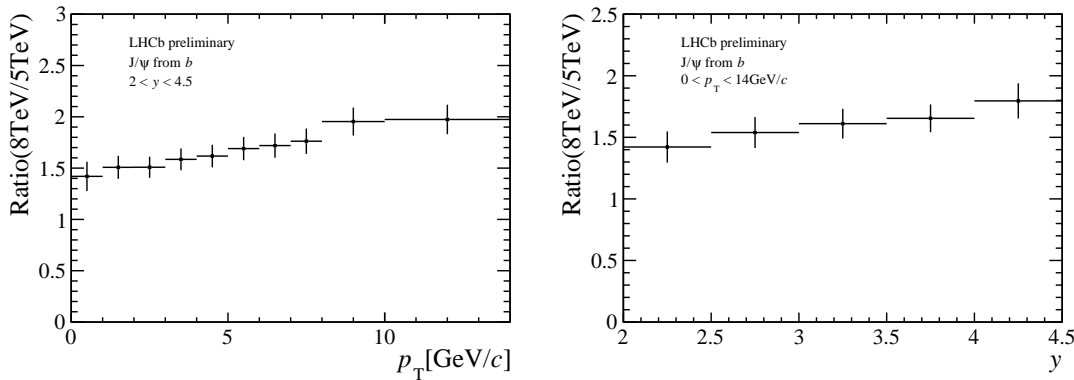


Figure 8.9: The ratio between the results at 8 TeV and 5 TeV for  $J/\psi$  from  $b$  as a function of  $p_T$  (left) and as a function of  $y$  (right).

680

## 681 8.6 Comparison with theory models

682 The single differential cross-sections for prompt  $J/\psi$  have been compared with the theory  
683 models, as shown in Fig. 8.10. Theoretical curves at high  $p_T$  are NLO NRQCD results

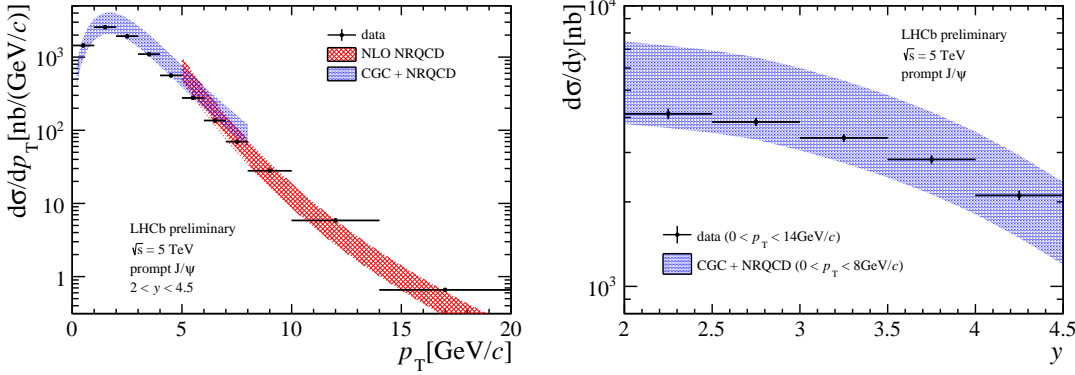


Figure 8.10: The single differential cross-sections as a function of  $p_T$  (left) and  $y$  (right) for prompt  $J/\psi$  compared with the theory models.

with long-distance matrix elements fixed by Tevatron data [59]. Theoretical curves at low  $p_T$  are obtained by combining NRQCD with color glass condensate (CGC) effective theory [60], with long-distance matrix elements fixed by Tevatron data [21] and parameters for color dipole at initial condition fixed from fits to the HERA DIS data [61]. Since the low  $p_T$  part is dominate when integrating the  $p_T$ , the theory predictions for  $d\sigma/dy$  are calculated using CGC + NRQCD both for the low  $p_T$  and high  $p_T$ . the comparisons between experiment results and the theory calculations are shown in Fig. 8.11 for the ratio between 13 TeV and 5 TeV, and in Fig. 8.12 for the ratio between 8 TeV and 5 TeV. For the theoretical ratios, only the uncertainty due to the scales of renormalisation and factorisation is considered. Good agreement is seen between NLO NRQCD calculation

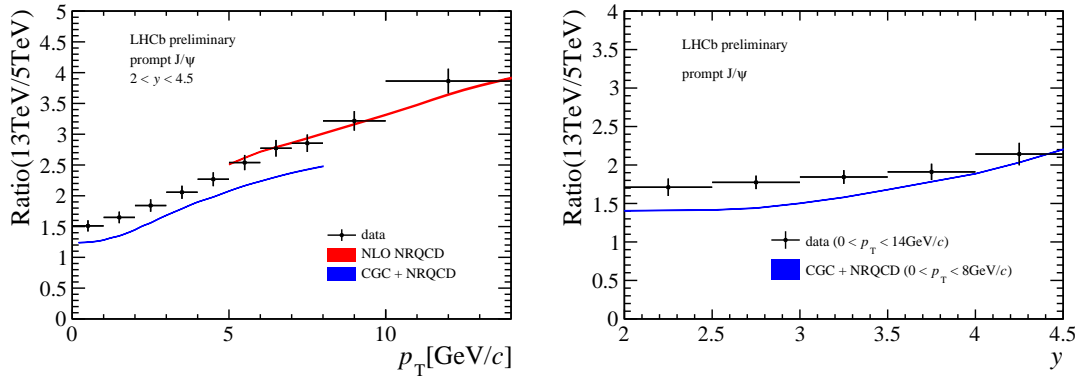


Figure 8.11: The ratio between the results at 13 TeV and 5 TeV for prompt  $J/\psi$  as a function of  $p_T$  (left) and as a function of  $y$  (right) compared with the theory models.

and the measurement at high  $p_T$ . The small tension between data and theory at low  $p_T$  may indicate that fixed order calculation is not enough and Sudakov resummation [62] at low  $p_T$  region is necessary. The comparison of  $d\sigma/dy$  between data and theory shows the small tension as well.

FONLL calculations are compared with the cross-sections for  $J/\psi$  from  $b$ , as shown in Fig. 8.13. The FONLL calculations [57, 58] include the PDFs uncertainties, the uncertainties due to  $b$ -quark mass and the scales of renormalisation and factorisation. FONLL calculations are also compared with the ratio between different energies, as shown

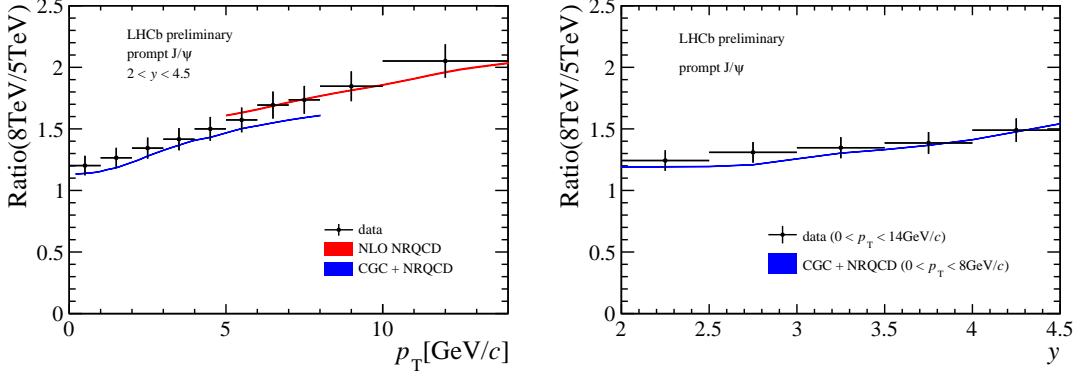


Figure 8.12: The ratio between the results at 8 TeV and 5 TeV for prompt  $J/\psi$  as a function of  $p_T$  (left) and as a function of  $y$  (right) compared with the theory models.

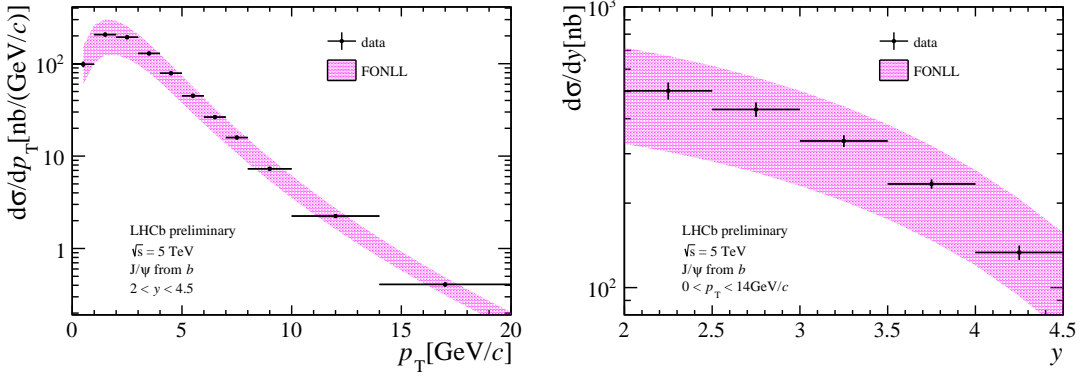


Figure 8.13: The single differential cross-sections as a function of  $p_T$  (left) and  $y$  (right) for  $J/\psi$  from  $b$  compared with FONLL calculations.

702 in Fig. 8.14 for the ratio between 13 TeV and 5 TeV and in Fig. 8.15 for the ratio between  
8 TeV and 5 TeV.

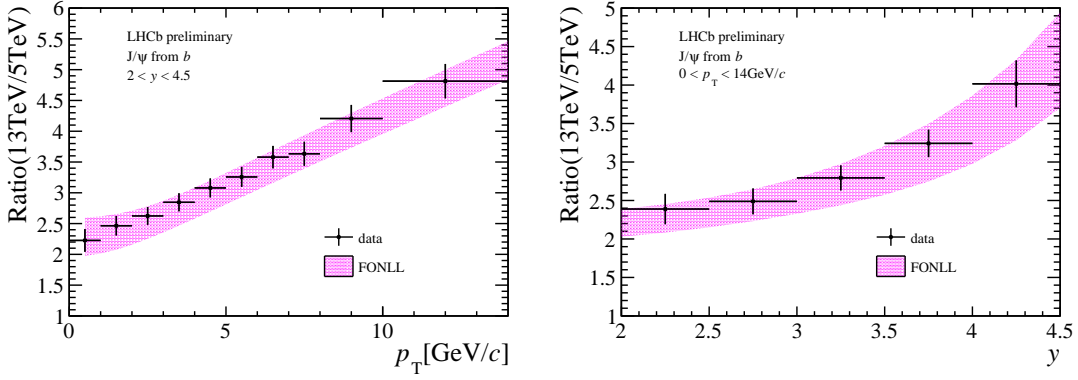


Figure 8.14: The ratio between the results at 13 TeV and 5 TeV for  $J/\psi$  from  $b$  as a function of  $p_T$  (left) and as a function of  $y$  (right) compared with FONLL calculations.

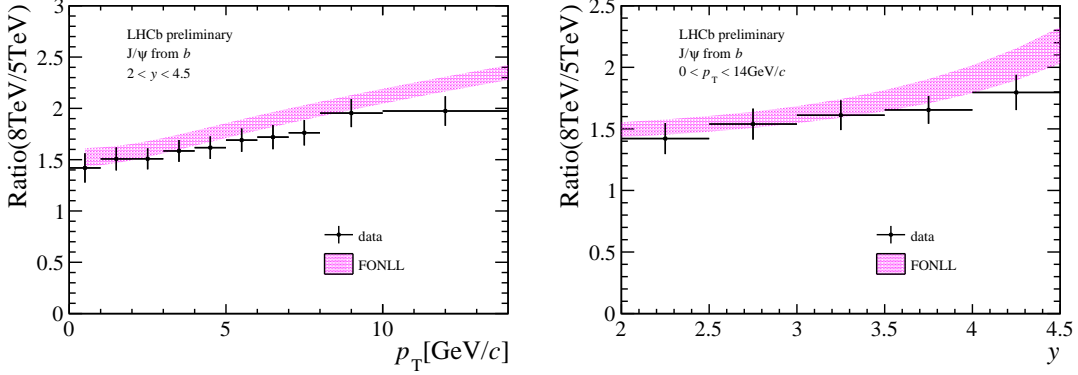


Figure 8.15: The ratio between the results at 8 TeV and 5 TeV for  $J/\psi$  from  $b$  as a function of  $p_T$  (left) and as a function of  $y$  (right) compared with FONLL calculations.

Table 8.2: Fit parameters of the interpolations for the cross-sections of prompt  $J/\psi$  in  $pp$  collisions with  $p_T < 14 \text{ GeV}/c$  and  $2.5 < y < 4.0$ .

fit function	$f(\sqrt{s})$	$p_0$	$p_1$
power low	$(\sqrt{s}/p_1)^{p_0}$	$0.65 \pm 0.06$	$0.43 \pm 0.10$
linear	$p_0 + p_1 \sqrt{s}$	$1.93 \pm 0.31$	$0.59 \pm 0.05$
exponential	$p_0(1 - \exp(-\sqrt{s}/p_1))$	$11.6 \pm 1.7$	$8.9 \pm 1.9$

## 704 8.7 Nuclear modification factor

705 In the analysis of  $J/\psi$  production cross-section in proton-lead collisions at  $\sqrt{s_{NN}} = 5 \text{ TeV}$   
 706 [42], the  $J/\psi$  production cross-section in  $pp$  collisions, used as a reference to determine  
 707 the nuclear modification factor  $R_{p\text{Pb}}$ , is obtained by a power-law interpolation of previous  
 708 LHCb measurements [63]. The interpolated cross-sections for prompt  $J/\psi$  and  $J/\psi$  from  $b$   
 709 in  $pp$  collisions at  $\sqrt{s_{NN}} = 5 \text{ TeV}$ , in the range  $0 < p_T < 14 \text{ GeV}/c$  and  $2.5 < y < 4.0$ , are

$$\begin{aligned} \sigma_{\text{prompt}} &= 4.79 \pm 0.22(\text{stat}) \pm 0.15(\text{syst}) \mu\text{b}, \\ \sigma_{\text{from } b} &= 0.47 \pm 0.04(\text{stat}) \pm 0.01(\text{syst}) \mu\text{b}. \end{aligned} \quad (8.4)$$

710 The cross-sections in this direct measurement are

$$\begin{aligned} \sigma_{\text{prompt}} &= 5.035 \pm 0.006(\text{stat}) \pm 0.164(\text{syst}) \mu\text{b}, \\ \sigma_{\text{from } b} &= 0.499 \pm 0.002(\text{stat}) \pm 0.020(\text{syst}) \mu\text{b}. \end{aligned} \quad (8.5)$$

711 The 5 TeV direct result is consistent with the interpolated one. To further check the  
 712 interpolation, the fit curves and the measurement results are shown in the Fig. 8.16. The  
 713 curves are based on the 2.76 TeV, 7 TeV and 8 TeV data points, which are obtained from  
 714 the  $J/\psi$  analysis in proton-lead collisions, thus the 5 TeV and 13 TeV data points can  
 715 provide good check of the curves. The points agree with the power-law curve very well.  
 716 The same fit is also performed with the data points of all the energies, as shown in Fig.  
 717 8.17, and the results of the fit parameters are summarized in Table 8.2 and Table 8.3.

718 Based on the direct measurement, the nuclear modification factor  $R_{p\text{Pb}}$  as a function  
 719 of  $y$  is updated in Table 8.4, Fig. 8.18 and Fig. 8.19. The nuclear modification factor  
 720  $R_{p\text{Pb}}$  as a function of  $p_T$  is shown in Fig. 8.20.

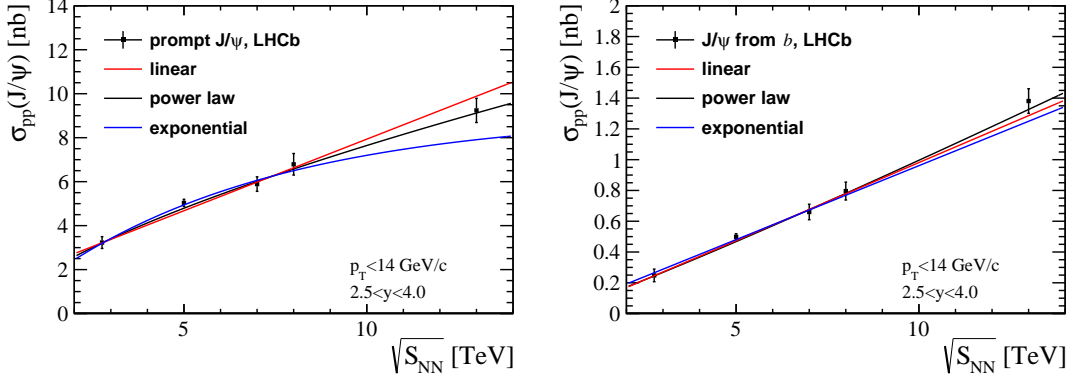


Figure 8.16: Check for the interpolations for the cross-sections of prompt  $J/\psi$  (left) and  $J/\psi$  from  $b$  in  $pp$  collisions at 5 TeV with  $p_T < 14 \text{ GeV}/c$  and  $2.5 < y < 4.0$ . The curves are based on the 2.76 TeV, 7 TeV and 8 TeV data points. The 5 TeV and 13 TeV data points are used to check the curves.

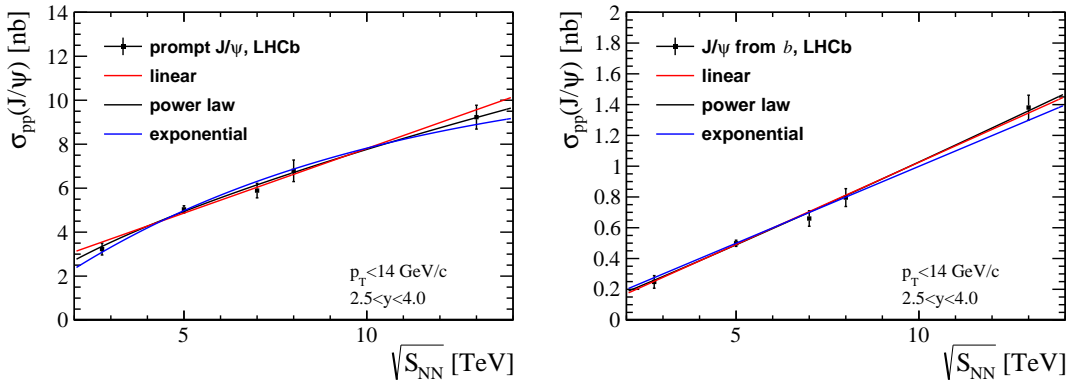


Figure 8.17: The interpolations for the cross-sections of prompt  $J/\psi$  (left) and  $J/\psi$  from  $b$  in  $pp$  collisions with  $p_T < 14 \text{ GeV}/c$  and  $2.5 < y < 4.0$ . The curves are based on the 2.76 TeV, 5 TeV, 7 TeV, 8 TeV and 13 TeV data points.

## 721 9 Conclusion

722 The  $J/\psi$  production cross-sections in proton-proton collisions at a centre-of-mass energy  
 723  $\sqrt{s} = 5 \text{ TeV}$  is studied using a data sample with the integrated luminosity of  $9.18 \pm 0.35 \text{ pb}^{-1}$   
 724 collected by the LHCb detector in LHC operations in 2015. The double differential cross-  
 725 sections, as functions of the transverse momentum  $p_T$  and the rapidity  $y$  of the  $J/\psi$   
 726 mesons, are determined separately for prompt  $J/\psi$  mesons and  $J/\psi$  mesons from  $b$ -hadron

Table 8.3: Fit parameters of the interpolations for the cross-sections of  $J/\psi$  from  $b$  in  $pp$  collisions with  $p_T < 14 \text{ GeV}/c$  and  $2.5 < y < 4.0$ .

fit function	$f(\sqrt{s})$	$p_0$	$p_1$
power low	$(\sqrt{s}/p_1)^{p_0}$	$1.07 \pm 0.07$	$9.75 \pm 0.34$
linear	$p_0 + p_1\sqrt{s}$	$-0.043 \pm 0.045$	$0.107 \pm 0.008$
exponential	$p_0(1 - \exp(-\sqrt{s}/p_1))$	$(5.9 \pm 18.0) \times 10^3$	$(5.9 \pm 18.0) \times 10^4$

Table 8.4: Nuclear modification factor  $R_{p\text{Pb}}$  as a function of  $y$  with  $p_T < 14 \text{ GeV}/c$ . The first uncertainty is statistical, and the second one is the systematic component.

$R_{p\text{Pb}}$	$-4.0 < y < -2.5$	$2.5 < y < 4.0$
prompt $J/\psi$	$0.882 \pm 0.027 \pm 0.060$	$0.586 \pm 0.007 \pm 0.033$
$J/\psi$ from $b$	$0.921 \pm 0.056 \pm 0.072$	$0.777 \pm 0.022 \pm 0.050$
inclusive $J/\psi$	$0.885 \pm 0.025 \pm 0.059$	$0.603 \pm 0.007 \pm 0.034$

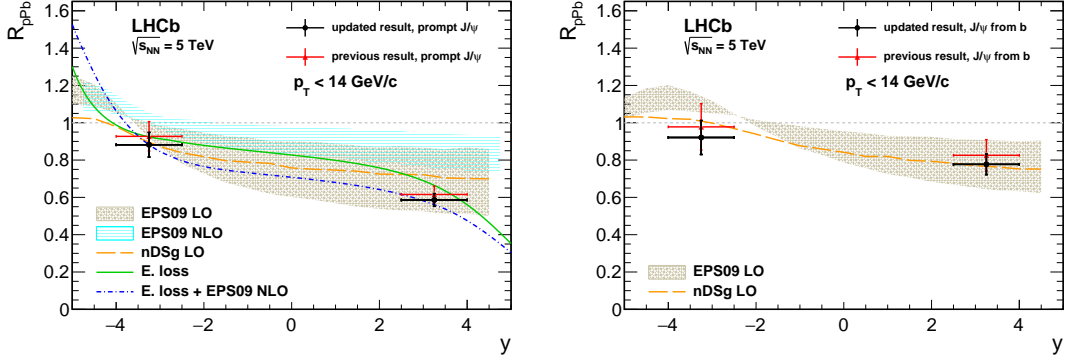


Figure 8.18: Nuclear modification factor  $R_{p\text{Pb}}$  as a function of  $y$  for prompt  $J/\psi$  (left) and  $J/\psi$  from  $b$  (right), together with the theoretical predictions from (yellow dashed line and brown band) Ref. [64], (blue band) Ref. [65], and (green solid and blue dash-dotted lines) Ref. [66]. The red points are previous results in the proton-lead analysis [42]; the black points are updated results in this analysis.

727 decays in the range  $0 < p_T < 14 \text{ GeV}/c$  and  $2 < y < 4.5$ . The production cross-sections  
 728 integrated over the kinematic coverage are

$$\begin{aligned}\sigma(\text{prompt } J/\psi) &= 8.150 \pm 0.010(\text{stat}) \pm 0.283(\text{syst}) \mu\text{b}, \\ \sigma(J/\psi \text{ from } b) &= 0.817 \pm 0.003(\text{stat}) \pm 0.034(\text{syst}) \mu\text{b},\end{aligned}$$

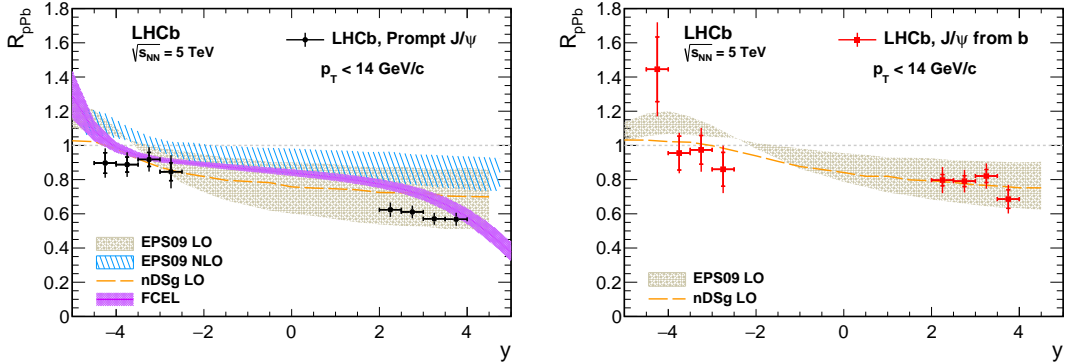


Figure 8.19: Nuclear modification factor  $R_{p\text{Pb}}$  as a function of  $y$  for prompt  $J/\psi$  (left) and  $J/\psi$  from  $b$  (right), together with the theoretical predictions from (yellow dashed line and brown band) Ref. [64], (blue band) Ref. [65], and (green solid and blue dash-dotted lines) Ref. [66]. The inner error bars (delimited by the horizontal lines) show the statistical uncertainties; the outer ones show the statistical and systematic uncertainties added in quadrature.

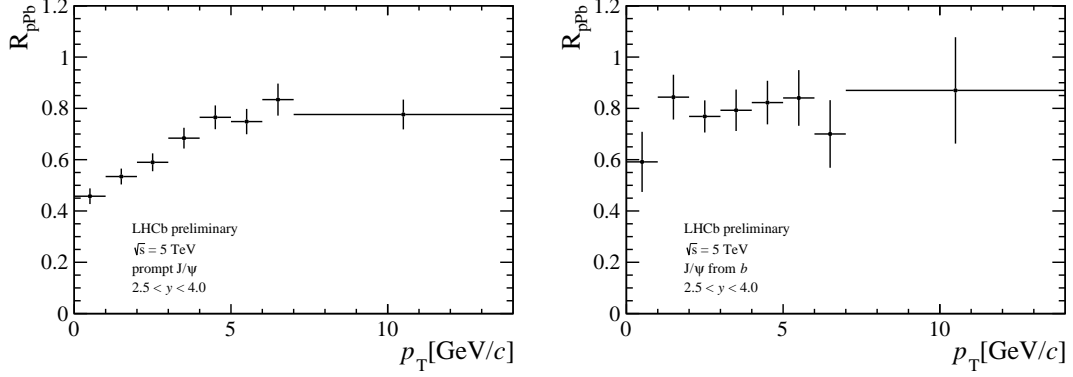


Figure 8.20: Nuclear modification factor  $R_{p\text{Pb}}$  as a function of  $p_T$  for prompt  $J/\psi$  (left) and  $J/\psi$  from  $b$  (right) only for forward rapidity.

729 assuming zero polarization of the  $J/\psi$  mesons. The  $J/\psi$  production cross-section ratios  
 730 between 13 TeV and 5 TeV, and between 8 TeV and 5 TeV are calculated, compared with  
 731 the theory models. The measured prompt  $J/\psi$  results are in good agreement with NLO  
 732 NRQCD calculation at high  $p_T$ . The small tension between data and theory at low  $p_T$   
 733 may indicate that fixed order calculation is not enough and Sudakov resummation at  
 734 low  $p_T$  region is necessary. The measured results for  $J/\psi$  from  $b$  agrees with FONLL  
 735 calculations. The nuclear modification factor  $R_{p\text{Pb}}$  is updated.

<sup>736</sup> **Appendices**

<sup>737</sup> **A Tables of cross-section results**

Table A.1: Double differential production cross-sections  $\frac{d^2\sigma}{dp_T dy} [\text{nb}/(\text{GeV}/c)]$  for prompt  $J/\psi$  in  $(p_T, y)$  bins. The first uncertainties are statistical, the second correlated systematic uncertainties shared between bins and the last are uncorrelated systematic uncertainties.

$p_T$ ( GeV/ $c$ )	$2 < y < 2.5$	$2.5 < y < 3$
0-1	$686.03 \pm 6.80 \pm 35.11 \pm 9.03 \pm 4.92$	$640.03 \pm 3.70 \pm 22.97 \pm 2.78 \pm 5.06$
1-2	$1253.23 \pm 8.66 \pm 55.59 \pm 15.31 \pm 9.82$	$1173.73 \pm 4.95 \pm 39.14 \pm 4.68 \pm 7.58$
2-3	$964.82 \pm 6.79 \pm 40.41 \pm 12.19 \pm 5.23$	$917.24 \pm 4.09 \pm 30.11 \pm 2.86 \pm 3.76$
3-4	$575.26 \pm 4.74 \pm 21.54 \pm 7.51 \pm 2.89$	$540.97 \pm 2.82 \pm 17.21 \pm 2.52 \pm 1.80$
4-5	$305.38 \pm 2.89 \pm 10.65 \pm 2.93 \pm 1.28$	$286.82 \pm 1.76 \pm 8.98 \pm 1.74 \pm 1.10$
5-6	$159.48 \pm 1.84 \pm 5.44 \pm 1.51 \pm 0.72$	$143.21 \pm 1.12 \pm 4.46 \pm 1.11 \pm 0.49$
6-7	$79.23 \pm 1.19 \pm 2.63 \pm 1.02 \pm 0.26$	$73.00 \pm 0.75 \pm 2.26 \pm 0.66 \pm 0.25$
7-8	$43.60 \pm 0.82 \pm 1.43 \pm 0.77 \pm 0.01$	$36.67 \pm 0.52 \pm 1.13 \pm 0.32 \pm 0.00$
8-10	$18.11 \pm 0.34 \pm 0.59 \pm 0.24 \pm 0.08$	$15.17 \pm 0.23 \pm 0.47 \pm 0.15 \pm 0.04$
10-14	$4.15 \pm 0.11 \pm 0.13 \pm 0.07 \pm 0.02$	$3.34 \pm 0.07 \pm 0.11 \pm 0.04 \pm 0.01$
$p_T$ ( GeV/ $c$ )	$3 < y < 3.5$	$3.5 < y < 4$
0-1	$589.31 \pm 3.22 \pm 19.72 \pm 1.82 \pm 2.99$	$515.07 \pm 2.78 \pm 17.29 \pm 1.72 \pm 0.30$
1-2	$1056.67 \pm 4.29 \pm 34.89 \pm 4.63 \pm 4.82$	$911.86 \pm 3.68 \pm 30.29 \pm 2.93 \pm 0.63$
2-3	$804.99 \pm 3.45 \pm 26.10 \pm 6.15 \pm 1.60$	$681.00 \pm 3.04 \pm 22.56 \pm 1.99 \pm 1.78$
3-4	$461.97 \pm 2.24 \pm 14.45 \pm 1.89 \pm 0.81$	$370.70 \pm 2.08 \pm 11.71 \pm 1.36 \pm 0.55$
4-5	$236.68 \pm 1.47 \pm 7.28 \pm 0.94 \pm 0.29$	$185.30 \pm 1.36 \pm 5.81 \pm 1.72 \pm 0.32$
5-6	$115.63 \pm 0.95 \pm 3.55 \pm 1.17 \pm 0.17$	$86.71 \pm 0.86 \pm 2.75 \pm 0.78 \pm 0.01$
6-7	$56.50 \pm 0.64 \pm 1.73 \pm 0.42 \pm 0.03$	$41.09 \pm 0.57 \pm 1.34 \pm 0.38 \pm 0.10$
7-8	$28.48 \pm 0.44 \pm 0.87 \pm 0.28 \pm 0.10$	$20.85 \pm 0.39 \pm 0.71 \pm 0.28 \pm 0.03$
8-10	$11.35 \pm 0.19 \pm 0.35 \pm 0.11 \pm 0.03$	$7.59 \pm 0.16 \pm 0.27 \pm 0.11 \pm 0.01$
10-14	$2.26 \pm 0.06 \pm 0.08 \pm 0.04 \pm 0.00$	$1.38 \pm 0.05 \pm 0.05 \pm 0.03 \pm 0.01$
$p_T$ ( GeV/ $c$ )	$4 < y < 4.5$	
0-1	$452.31 \pm 3.21 \pm 17.49 \pm 2.85 \pm 2.79$	
1-2	$731.38 \pm 4.04 \pm 27.48 \pm 3.52 \pm 0.74$	
2-3	$485.71 \pm 3.25 \pm 19.15 \pm 3.16 \pm 0.50$	
3-4	$240.13 \pm 2.17 \pm 9.05 \pm 2.68 \pm 0.21$	
4-5	$108.46 \pm 1.33 \pm 4.16 \pm 1.18 \pm 0.25$	
5-6	$49.12 \pm 0.84 \pm 1.90 \pm 0.59 \pm 0.08$	
6-7	$22.06 \pm 0.52 \pm 0.86 \pm 0.35 \pm 0.02$	
7-8	$10.36 \pm 0.34 \pm 0.40 \pm 0.24 \pm 0.03$	
8-10	$3.82 \pm 0.14 \pm 0.15 \pm 0.09 \pm 0.01$	
10-14	$0.58 \pm 0.04 \pm 0.02 \pm 0.02 \pm 0.00$	

Table A.2: Double differential production cross-sections  $\frac{d^2\sigma}{dp_T dy} [\text{nb}/(\text{GeV}/c)]$  for  $J/\psi$  from  $b$  in  $(p_T, y)$  bins. The first uncertainties are statistical, the second correlated systematic uncertainties shared between bins and the last are uncorrelated systematic uncertainties.

$p_T$ ( GeV/ $c$ )	$2 < y < 2.5$	$2.5 < y < 3$
0-1	$56.02 \pm 1.88 \pm 2.87 \pm 1.35 \pm 7.96$	$47.72 \pm 1.00 \pm 1.71 \pm 0.48 \pm 5.71$
1-2	$120.67 \pm 2.48 \pm 5.35 \pm 1.88 \pm 9.89$	$105.37 \pm 1.37 \pm 3.51 \pm 2.07 \pm 7.81$
2-3	$117.89 \pm 2.23 \pm 4.94 \pm 2.46 \pm 5.15$	$101.93 \pm 1.26 \pm 3.35 \pm 1.12 \pm 3.66$
3-4	$78.32 \pm 1.67 \pm 2.93 \pm 1.36 \pm 2.57$	$71.20 \pm 0.97 \pm 2.27 \pm 0.52 \pm 1.68$
4-5	$51.65 \pm 1.24 \pm 1.80 \pm 0.89 \pm 1.18$	$42.83 \pm 0.69 \pm 1.34 \pm 0.41 \pm 0.99$
5-6	$30.55 \pm 0.84 \pm 1.04 \pm 0.51 \pm 0.64$	$24.58 \pm 0.48 \pm 0.77 \pm 0.30 \pm 0.43$
6-7	$18.43 \pm 0.60 \pm 0.61 \pm 0.39 \pm 0.22$	$14.39 \pm 0.36 \pm 0.45 \pm 0.22 \pm 0.22$
7-8	$11.57 \pm 0.45 \pm 0.38 \pm 0.36 \pm 0.01$	$9.13 \pm 0.27 \pm 0.28 \pm 0.13 \pm 0.00$
8-10	$5.29 \pm 0.19 \pm 0.17 \pm 0.12 \pm 0.07$	$4.31 \pm 0.13 \pm 0.13 \pm 0.06 \pm 0.03$
10-14	$1.80 \pm 0.07 \pm 0.06 \pm 0.08 \pm 0.02$	$1.39 \pm 0.05 \pm 0.04 \pm 0.02 \pm 0.01$
$p_T$ ( GeV/ $c$ )	$3 < y < 3.5$	$3.5 < y < 4$
0-1	$40.73 \pm 0.84 \pm 1.36 \pm 0.38 \pm 3.55$	$30.25 \pm 0.76 \pm 1.02 \pm 0.40 \pm 0.34$
1-2	$85.36 \pm 1.15 \pm 2.82 \pm 1.56 \pm 5.16$	$61.11 \pm 1.00 \pm 2.03 \pm 0.60 \pm 0.64$
2-3	$79.84 \pm 1.00 \pm 2.59 \pm 1.19 \pm 1.59$	$55.94 \pm 0.89 \pm 1.85 \pm 0.79 \pm 1.80$
3-4	$51.96 \pm 0.75 \pm 1.62 \pm 0.49 \pm 0.75$	$38.20 \pm 0.69 \pm 1.21 \pm 0.42 \pm 0.59$
4-5	$31.75 \pm 0.55 \pm 0.98 \pm 0.27 \pm 0.28$	$22.43 \pm 0.49 \pm 0.70 \pm 0.31 \pm 0.36$
5-6	$18.22 \pm 0.40 \pm 0.56 \pm 0.26 \pm 0.17$	$10.97 \pm 0.33 \pm 0.35 \pm 0.16 \pm 0.01$
6-7	$10.36 \pm 0.29 \pm 0.32 \pm 0.20 \pm 0.03$	$6.83 \pm 0.25 \pm 0.22 \pm 0.12 \pm 0.11$
7-8	$6.00 \pm 0.22 \pm 0.18 \pm 0.09 \pm 0.10$	$3.60 \pm 0.17 \pm 0.12 \pm 0.10 \pm 0.03$
8-10	$2.87 \pm 0.10 \pm 0.09 \pm 0.04 \pm 0.02$	$1.57 \pm 0.08 \pm 0.06 \pm 0.06 \pm 0.01$
10-14	$0.77 \pm 0.04 \pm 0.03 \pm 0.03 \pm 0.00$	$0.39 \pm 0.03 \pm 0.01 \pm 0.01 \pm 0.01$
$p_T$ ( GeV/ $c$ )	$4 < y < 4.5$	
0-1	$22.40 \pm 0.90 \pm 0.87 \pm 0.45 \pm 3.29$	
1-2	$40.68 \pm 1.11 \pm 1.53 \pm 0.61 \pm 0.82$	
2-3	$31.22 \pm 0.91 \pm 1.23 \pm 0.71 \pm 0.52$	
3-4	$18.68 \pm 0.66 \pm 0.70 \pm 0.44 \pm 0.22$	
4-5	$9.00 \pm 0.42 \pm 0.34 \pm 0.18 \pm 0.26$	
5-6	$5.51 \pm 0.30 \pm 0.21 \pm 0.14 \pm 0.10$	
6-7	$2.84 \pm 0.20 \pm 0.11 \pm 0.09 \pm 0.02$	
7-8	$1.44 \pm 0.13 \pm 0.06 \pm 0.07 \pm 0.04$	
8-10	$0.53 \pm 0.06 \pm 0.02 \pm 0.02 \pm 0.01$	
10-14	$0.15 \pm 0.02 \pm 0.01 \pm 0.01 \pm 0.01$	

Table A.3: Single differential production cross-sections  $\frac{d\sigma}{dp_T}$  [nb/(GeV/c)] for prompt  $J/\psi$ . The first uncertainties are statistical, the second correlated systematic uncertainties shared between bins and the last are uncorrelated systematic uncertainties.

$p_T$ (GeV/c)	$2 < y < 4.5$
0-1	$1441.38 \pm 4.70 \pm 53.61 \pm 5.09$
1-2	$2563.43 \pm 6.08 \pm 90.61 \pm 8.64$
2-3	$1926.88 \pm 4.86 \pm 67.32 \pm 7.22$
3-4	$1094.51 \pm 3.34 \pm 36.15 \pm 4.34$
4-5	$561.32 \pm 2.08 \pm 18.10 \pm 2.05$
5-6	$277.07 \pm 1.32 \pm 8.89 \pm 1.21$
6-7	$135.95 \pm 0.86 \pm 4.34 \pm 0.69$
7-8	$69.98 \pm 0.59 \pm 2.23 \pm 0.48$
8-10	$28.02 \pm 0.25 \pm 0.90 \pm 0.17$
10-14	$5.85 \pm 0.08 \pm 0.19 \pm 0.05$
14-20	$0.66 \pm 0.02 \pm 0.02 \pm 0.02$

Table A.4: Single differential production cross-sections  $\frac{d\sigma}{dp_T}$  [nb/(GeV/c)] for  $J/\psi$  from  $b$ . The first uncertainties are statistical, the second correlated systematic uncertainties shared between bins and the last are uncorrelated systematic uncertainties.

$p_T$ (GeV/c)	$2 < y < 4.5$
0-1	$98.56 \pm 1.29 \pm 6.61 \pm 0.80$
1-2	$206.60 \pm 1.70 \pm 10.03 \pm 1.65$
2-3	$193.41 \pm 1.51 \pm 7.58 \pm 1.57$
3-4	$129.17 \pm 1.14 \pm 4.56 \pm 0.83$
4-5	$78.83 \pm 0.83 \pm 2.66 \pm 0.54$
5-6	$44.91 \pm 0.57 \pm 1.49 \pm 0.34$
6-7	$26.43 \pm 0.41 \pm 0.86 \pm 0.25$
7-8	$15.88 \pm 0.31 \pm 0.51 \pm 0.20$
8-10	$7.29 \pm 0.14 \pm 0.24 \pm 0.08$
10-14	$2.24 \pm 0.05 \pm 0.07 \pm 0.05$
14-20	$0.41 \pm 0.02 \pm 0.01 \pm 0.01$

Table A.5: Single differential production cross-sections  $\frac{d\sigma}{dy}$ ( nb) for prompt  $J/\psi$ . The first uncertainties are statistical, the second correlated systematic uncertainties shared between bins and the last are uncorrelated systematic uncertainties.

$y$	$0 < p_T < 14 \text{ GeV}/c$
2.0-2.5	$4119.86 \pm 14.30 \pm 170.61 \pm 34.31$
2.5-3.0	$3855.37 \pm 8.26 \pm 126.79 \pm 21.34$
3.0-3.5	$3381.98 \pm 7.04 \pm 109.07 \pm 13.66$
3.5-4.0	$2833.26 \pm 6.17 \pm 92.56 \pm 5.94$
4.0-4.5	$2109.49 \pm 6.70 \pm 80.02 \pm 7.83$

Table A.6: Single differential production cross-sections  $\frac{d\sigma}{dy}$ ( nb) for  $J/\psi$  from  $b$ . The first uncertainties are statistical, the second correlated systematic uncertainties shared between bins and the last are uncorrelated systematic uncertainties.

$y$	$0 < p_T < 14 \text{ GeV}/c$
2.0-2.5	$502.90 \pm 4.52 \pm 20.00 \pm 28.08$
2.5-3.0	$431.32 \pm 2.53 \pm 14.02 \pm 20.75$
3.0-3.5	$333.04 \pm 2.06 \pm 10.66 \pm 11.88$
3.5-4.0	$234.01 \pm 1.82 \pm 7.61 \pm 4.10$
4.0-4.5	$133.41 \pm 1.92 \pm 5.06 \pm 5.45$

## 738 B Tables of 2D fit results

739 For each kinematic bin of  $J/\psi$  candidates, the 2D fitted value of  $\mu$  (bias of 2D distribution),  
 740  $S_{1,2}$  (scale factor of the first/second Gaussian resolution function convolved with the 2D  
 741 function),  $\beta$  (fraction of the first Gaussian resolution function),  $\tau_b$  (effective  $b$ -hadron  
 742 lifetime),  $\mu_m$  (shared mean value of the two CB functions),  $\sigma_{1,2}$  ( $\sigma$  of the first/second  
 743 CB function),  $f_m$  (fraction of the first CB function),  $\lambda$  (parameter of the exponential  
 744 distribution),  $N_{\text{prompt}}$  (number of prompt  $J/\psi$ ),  $N_{\text{from } b}$  (number of  $J/\psi$  from  $b$ ),  $N_{\text{tail}}$   
 745 (number of wrong PV events),  $N_{\text{bkg}}$  (number of background) will be given in tables.

Table B.1: The parameters of the 2D fit, including the fitted yields and shape parameters for different  $p_T$  bins in the rapidity bin  $2 < y < 2.5$ .

$p_T$ (GeV/c)	$\mu[10^{-3} \text{ ps}]$	$S_1$	$S_2$	$\beta$	$\tau_b[\text{ps}]$
0-1	$-10.6 \pm 0.5$	$1.48 \pm 0.08$	$0.80 \pm 0.03$	$0.32 \pm 0.06$	$1.53 \pm 0.06$
1-2	$-9.4 \pm 0.4$	$1.42 \pm 0.06$	$0.81 \pm 0.02$	$0.34 \pm 0.05$	$1.50 \pm 0.03$
2-3	$-8.5 \pm 0.4$	$1.54 \pm 0.14$	$0.89 \pm 0.03$	$0.20 \pm 0.07$	$1.48 \pm 0.03$
3-4	$-5.9 \pm 0.4$	$1.33 \pm 0.06$	$0.82 \pm 0.03$	$0.38 \pm 0.08$	$1.42 \pm 0.03$
4-5	$-6.3 \pm 0.5$	$1.82 \pm 0.19$	$0.93 \pm 0.02$	$0.09 \pm 0.03$	$1.30 \pm 0.03$
5-6	$-4.9 \pm 0.5$	$0.86 \pm 0.03$	$1.59 \pm 0.12$	$0.78 \pm 0.05$	$1.35 \pm 0.04$
6-7	$-1.5 \pm 0.6$	$1.65 \pm 0.17$	$0.90 \pm 0.03$	$0.19 \pm 0.07$	$1.32 \pm 0.04$
7-8	$-1.7 \pm 0.8$	$2.46 \pm 0.36$	$1.01 \pm 0.03$	$0.08 \pm 0.03$	$1.47 \pm 0.06$
8-10	$-0.2 \pm 0.7$	$1.81 \pm 0.21$	$0.99 \pm 0.04$	$0.18 \pm 0.08$	$1.44 \pm 0.05$
10-14	$-1.8 \pm 0.9$	$2.19 \pm 0.27$	$1.00 \pm 0.06$	$0.20 \pm 0.07$	$1.32 \pm 0.05$
$p_T$ (GeV/c)	$\mu_m[\text{MeV}/c^2]$	$\sigma_1[\text{MeV}/c^2]$	$\sigma_2[\text{MeV}/c^2]$	$f_m$	$\lambda[10^{-3}(\text{MeV}/c^2)^{-1}]$
0-1	$3098.1 \pm 0.1$	$9.42 \pm 0.42$	$16.32 \pm 1.71$	$0.71 \pm 0.10$	$-1.22 \pm 0.09$
1-2	$3097.8 \pm 0.1$	$9.01 \pm 0.36$	$15.10 \pm 1.04$	$0.61 \pm 0.09$	$-1.20 \pm 0.06$
2-3	$3097.6 \pm 0.1$	$9.26 \pm 0.36$	$15.41 \pm 1.08$	$0.64 \pm 0.09$	$-0.74 \pm 0.07$
3-4	$3097.5 \pm 0.1$	$9.97 \pm 0.35$	$16.96 \pm 1.49$	$0.72 \pm 0.08$	$-0.39 \pm 0.11$
4-5	$3097.3 \pm 0.1$	$11.74 \pm 0.10$		1	$-0.39 \pm 0.17$
5-6	$3097.4 \pm 0.1$	$12.30 \pm 0.12$		1	$-0.60 \pm 0.27$
6-7	$3097.5 \pm 0.2$	$12.46 \pm 0.16$		1	$0.05 \pm 0.42$
7-8	$3097.2 \pm 0.2$	$12.86 \pm 0.19$		1	$-0.22 \pm 0.62$
8-10	$3097.4 \pm 0.2$	$13.04 \pm 0.19$		1	$-0.33 \pm 0.67$
10-14	$3097.0 \pm 0.3$	$13.95 \pm 0.27$		1	$0.22 \pm 1.13$
$p_T$ (GeV/c)	$N_{\text{prompt}}$	$N_{\text{from } b}$	$N_{\text{tail}}$	$N_{\text{bkg}}$	
0-1	$19163 \pm 190$	$1532 \pm 51$	$66 \pm 18$	$24476 \pm 207$	
1-2	$41284 \pm 285$	$3899 \pm 80$	$92 \pm 22$	$58144 \pm 320$	
2-3	$36767 \pm 259$	$4301 \pm 81$	$41 \pm 16$	$42372 \pm 273$	
3-4	$23289 \pm 192$	$3058 \pm 65$	$35 \pm 12$	$16992 \pm 179$	
4-5	$14610 \pm 138$	$2358 \pm 57$	$25 \pm 10$	$7469 \pm 110$	
5-6	$9257 \pm 107$	$1726 \pm 47$	$17 \pm 6$	$3113 \pm 73$	
6-7	$5422 \pm 81$	$1205 \pm 39$	$12 \pm 5$	$1414 \pm 51$	
7-8	$3347 \pm 63$	$836 \pm 33$	$9 \pm 5$	$665 \pm 36$	
8-10	$3220 \pm 61$	$929 \pm 34$	$9 \pm 4$	$577 \pm 34$	
10-14	$1754 \pm 45$	$753 \pm 30$	$2 \pm 2$	$226 \pm 23$	

Table B.2: The parameters of the 2D fit, including the fitted yields and shape parameters for different  $p_T$  bins in the rapidity bin  $2.5 < y < 3$ .

$p_T$ ( GeV/c )	$\mu[10^{-3}$ ps]	$S_1$	$S_2$	$\beta$	$\tau_b$ [ ps ]
0-1	$-9.7 \pm 0.3$	$1.40 \pm 0.05$	$0.80 \pm 0.02$	$0.38 \pm 0.05$	$1.42 \pm 0.04$
1-2	$-8.4 \pm 0.2$	$0.80 \pm 0.02$	$1.31 \pm 0.03$	$0.57 \pm 0.04$	$1.51 \pm 0.02$
2-3	$-7.4 \pm 0.2$	$0.81 \pm 0.02$	$1.29 \pm 0.04$	$0.59 \pm 0.05$	$1.48 \pm 0.02$
3-4	$-5.6 \pm 0.2$	$0.84 \pm 0.02$	$1.31 \pm 0.04$	$0.64 \pm 0.05$	$1.49 \pm 0.02$
4-5	$-4.4 \pm 0.3$	$0.91 \pm 0.02$	$1.49 \pm 0.08$	$0.80 \pm 0.05$	$1.40 \pm 0.02$
5-6	$-2.6 \pm 0.3$	$1.46 \pm 0.09$	$0.88 \pm 0.03$	$0.28 \pm 0.08$	$1.39 \pm 0.03$
6-7	$-2.1 \pm 0.4$	$0.96 \pm 0.02$	$1.85 \pm 0.18$	$0.88 \pm 0.04$	$1.33 \pm 0.04$
7-8	$-2.1 \pm 0.5$	$2.00 \pm 0.22$	$0.97 \pm 0.03$	$0.13 \pm 0.04$	$1.32 \pm 0.04$
8-10	$-0.9 \pm 0.5$	$2.15 \pm 0.24$	$0.99 \pm 0.03$	$0.13 \pm 0.04$	$1.34 \pm 0.04$
10-14	$-1.4 \pm 0.6$	$1.00 \pm 0.04$	$2.19 \pm 0.28$	$0.87 \pm 0.05$	$1.32 \pm 0.05$
$p_T$ ( GeV/c )	$\mu_m$ [ MeV/ $c^2$ ]	$\sigma_1$ [ MeV/ $c^2$ ]	$\sigma_2$ [ MeV/ $c^2$ ]	$f_m$	$\lambda[10^{-3}(\text{MeV}/c^2)^{-1}]$
0-1	$3097.1 \pm 0.1$	$9.16 \pm 0.21$	$14.24 \pm 0.48$	$0.61 \pm 0.05$	$-1.63 \pm 0.05$
1-2	$3097.1 \pm 0.0$	$13.19 \pm 0.54$	$8.76 \pm 0.43$	$0.56 \pm 0.10$	$-1.34 \pm 0.03$
2-3	$3096.9 \pm 0.0$	$14.09 \pm 0.78$	$9.50 \pm 0.36$	$0.42 \pm 0.10$	$-0.82 \pm 0.04$
3-4	$3096.8 \pm 0.1$	$10.44 \pm 0.17$	$16.20 \pm 0.87$	$0.75 \pm 0.05$	$-0.53 \pm 0.07$
4-5	$3096.7 \pm 0.1$	$14.33 \pm 0.50$	$9.25 \pm 0.51$	$0.58 \pm 0.09$	$-0.63 \pm 0.13$
5-6	$3096.6 \pm 0.1$	$12.24 \pm 0.08$		1	$-0.77 \pm 0.23$
6-7	$3096.5 \pm 0.1$	$12.38 \pm 0.10$		1	$-0.58 \pm 0.39$
7-8	$3096.2 \pm 0.2$	$12.96 \pm 0.14$		1	$-0.77 \pm 0.56$
8-10	$3096.3 \pm 0.2$	$13.38 \pm 0.16$		1	$0.42 \pm 0.70$
10-14	$3096.8 \pm 0.3$	$13.95 \pm 0.23$		1	$-1.04 \pm 1.11$
$p_T$ ( GeV/c )	$N_{\text{prompt}}$	$N_{\text{from } b}$	$N_{\text{tail}}$	$N_{\text{bkg}}$	
0-1	$58084 \pm 335$	$4269 \pm 89$	$243 \pm 37$	$102538 \pm 402$	
1-2	$110884 \pm 467$	$9852 \pm 128$	$190 \pm 37$	$193064 \pm 557$	
2-3	$90308 \pm 402$	$9903 \pm 122$	$224 \pm 32$	$115546 \pm 439$	
3-4	$57367 \pm 299$	$7490 \pm 102$	$117 \pm 22$	$45353 \pm 283$	
4-5	$34532 \pm 212$	$5122 \pm 82$	$92 \pm 17$	$13826 \pm 158$	
5-6	$19468 \pm 152$	$3301 \pm 65$	$54 \pm 12$	$4632 \pm 91$	
6-7	$10776 \pm 111$	$2065 \pm 51$	$41 \pm 10$	$1689 \pm 58$	
7-8	$5755 \pm 81$	$1373 \pm 41$	$9 \pm 5$	$846 \pm 42$	
8-10	$5052 \pm 76$	$1409 \pm 42$	$18 \pm 7$	$593 \pm 37$	
10-14	$2353 \pm 52$	$962 \pm 34$	$17 \pm 6$	$242 \pm 25$	

Table B.3: The parameters of the 2D fit, including the fitted yields and shape parameters for different  $p_T$  bins in the rapidity bin  $3 < y < 3.5$ .

$p_T$ ( GeV/c )	$\mu[10^{-3}$ ps]	$S_1$	$S_2$	$\beta$	$\tau_b$ [ ps ]
0-1	$-6.0 \pm 0.3$	$1.27 \pm 0.04$	$0.80 \pm 0.03$	$0.44 \pm 0.06$	$1.45 \pm 0.04$
1-2	$-6.0 \pm 0.2$	$1.38 \pm 0.11$	$0.85 \pm 0.03$	$0.29 \pm 0.10$	$1.48 \pm 0.02$
2-3	$-5.3 \pm 0.2$	$1.33 \pm 0.05$	$0.84 \pm 0.02$	$0.33 \pm 0.05$	$1.50 \pm 0.02$
3-4	$-4.4 \pm 0.2$	$0.87 \pm 0.02$	$1.39 \pm 0.06$	$0.73 \pm 0.05$	$1.43 \pm 0.02$
4-5	$-3.3 \pm 0.2$	$1.48 \pm 0.08$	$0.88 \pm 0.02$	$0.22 \pm 0.05$	$1.37 \pm 0.03$
5-6	$-3.5 \pm 0.3$	$0.90 \pm 0.02$	$1.58 \pm 0.12$	$0.83 \pm 0.05$	$1.33 \pm 0.03$
6-7	$-2.6 \pm 0.4$	$0.91 \pm 0.03$	$1.62 \pm 0.22$	$0.85 \pm 0.08$	$1.25 \pm 0.04$
7-8	$-2.9 \pm 0.5$	$0.97 \pm 0.02$	$2.08 \pm 0.34$	$0.93 \pm 0.03$	$1.30 \pm 0.05$
8-10	$-1.9 \pm 0.5$	$2.36 \pm 0.45$	$0.97 \pm 0.02$	$0.04 \pm 0.02$	$1.35 \pm 0.05$
10-14	$-1.7 \pm 0.8$	$1.54 \pm 0.37$	$0.89 \pm 0.12$	$0.30 \pm 0.25$	$1.22 \pm 0.06$
$p_T$ ( GeV/c )	$\mu_m$ [ MeV/ $c^2$ ]	$\sigma_1$ [ MeV/ $c^2$ ]	$\sigma_2$ [ MeV/ $c^2$ ]	$f_m$	$\lambda[10^{-3}(\text{MeV}/c^2)^{-1}]$
0-1	$3096.6 \pm 0.1$	$10.27 \pm 0.40$	$15.60 \pm 0.99$	$0.60 \pm 0.11$	$-1.58 \pm 0.04$
1-2	$3096.5 \pm 0.0$	$10.58 \pm 0.57$	$14.97 \pm 1.11$	$0.56 \pm 0.17$	$-1.46 \pm 0.04$
2-3	$3096.4 \pm 0.0$	$11.81 \pm 0.15$	$19.26 \pm 1.42$	$0.85 \pm 0.04$	$-1.14 \pm 0.05$
3-4	$3096.3 \pm 0.1$	$11.30 \pm 0.32$	$16.34 \pm 0.69$	$0.62 \pm 0.08$	$-0.62 \pm 0.09$
4-5	$3096.2 \pm 0.1$	$10.40 \pm 1.44$	$14.82 \pm 0.89$	$0.32 \pm 0.22$	$-0.55 \pm 0.16$
5-6	$3096.1 \pm 0.1$	$13.77 \pm 0.09$		1	$-0.25 \pm 0.30$
6-7	$3096.1 \pm 0.1$	$13.90 \pm 0.13$		1	$-1.10 \pm 0.47$
7-8	$3095.8 \pm 0.2$	$14.53 \pm 0.18$		1	$0.81 \pm 0.79$
8-10	$3096.2 \pm 0.2$	$14.63 \pm 0.20$		1	$-0.58 \pm 0.87$
10-14	$3095.6 \pm 0.4$	$15.74 \pm 0.32$		1	$0.47 \pm 1.24$
$p_T$ ( GeV/c )	$N_{\text{prompt}}$	$N_{\text{from } b}$	$N_{\text{tail}}$	$N_{\text{bkg}}$	
0-1	$70883 \pm 387$	$4743 \pm 98$	$448 \pm 47$	$123818 \pm 460$	
1-2	$124967 \pm 508$	$9925 \pm 134$	$409 \pm 44$	$174597 \pm 559$	
2-3	$99435 \pm 426$	$9714 \pm 122$	$242 \pm 34$	$98798 \pm 435$	
3-4	$59834 \pm 290$	$6707 \pm 97$	$168 \pm 25$	$31299 \pm 241$	
4-5	$33158 \pm 205$	$4366 \pm 76$	$105 \pm 18$	$8956 \pm 137$	
5-6	$17440 \pm 143$	$2701 \pm 59$	$57 \pm 12$	$2929 \pm 77$	
6-7	$8989 \pm 102$	$1643 \pm 45$	$44 \pm 10$	$1217 \pm 51$	
7-8	$4711 \pm 73$	$963 \pm 35$	$28 \pm 8$	$483 \pm 34$	
8-10	$3908 \pm 66$	$960 \pm 34$	$7 \pm 5$	$388 \pm 31$	
10-14	$1629 \pm 43$	$545 \pm 26$	$2 \pm 2$	$198 \pm 22$	

Table B.4: The parameters of the 2D fit, including the fitted yields and shape parameters for different  $p_T$  bins in the rapidity bin  $3.5 < y < 4$ .

$p_T$ ( GeV/c )	$\mu[10^{-3}$ ps]	$S_1$	$S_2$	$\beta$	$\tau_b$ [ ps ]
0-1	$-2.3 \pm 0.3$	$1.65 \pm 0.09$	$0.91 \pm 0.01$	$0.16 \pm 0.03$	$1.41 \pm 0.05$
1-2	$-2.1 \pm 0.2$	$0.88 \pm 0.01$	$1.50 \pm 0.06$	$0.79 \pm 0.04$	$1.43 \pm 0.03$
2-3	$-1.3 \pm 0.2$	$1.40 \pm 0.06$	$0.86 \pm 0.02$	$0.25 \pm 0.05$	$1.41 \pm 0.03$
3-4	$-1.6 \pm 0.3$	$1.47 \pm 0.09$	$0.87 \pm 0.02$	$0.22 \pm 0.05$	$1.34 \pm 0.03$
4-5	$-1.2 \pm 0.3$	$1.55 \pm 0.12$	$0.87 \pm 0.02$	$0.19 \pm 0.05$	$1.38 \pm 0.03$
5-6	$-0.6 \pm 0.4$	$0.89 \pm 0.03$	$1.57 \pm 0.13$	$0.81 \pm 0.06$	$1.29 \pm 0.04$
6-7	$-1.0 \pm 0.5$	$1.77 \pm 0.24$	$0.92 \pm 0.03$	$0.14 \pm 0.06$	$1.43 \pm 0.06$
7-8	$-1.5 \pm 0.6$	$0.88 \pm 0.04$	$1.66 \pm 0.22$	$0.83 \pm 0.08$	$1.30 \pm 0.07$
8-10	$-0.1 \pm 0.7$	$0.94 \pm 0.03$	$2.10 \pm 0.45$	$0.92 \pm 0.05$	$1.26 \pm 0.07$
10-14	$0.6 \pm 1.0$	$0.91 \pm 0.03$	$2.82 \pm 0.60$	$0.94 \pm 0.03$	$1.24 \pm 0.09$
$p_T$ ( GeV/c )	$\mu_m$ [ MeV/ $c^2$ ]	$\sigma_1$ [ MeV/ $c^2$ ]	$\sigma_2$ [ MeV/ $c^2$ ]	$f_m$	$\lambda[10^{-3}(\text{MeV}/c^2)^{-1}]$
0-1	$3096.2 \pm 0.1$	$11.12 \pm 0.75$	$16.05 \pm 0.76$	$0.41 \pm 0.14$	$-2.09 \pm 0.07$
1-2	$3096.2 \pm 0.1$	$12.24 \pm 0.32$	$17.72 \pm 0.72$	$0.60 \pm 0.08$	$-1.84 \pm 0.06$
2-3	$3096.3 \pm 0.1$	$11.96 \pm 0.62$	$16.98 \pm 0.68$	$0.43 \pm 0.12$	$-1.09 \pm 0.08$
3-4	$3096.0 \pm 0.1$	$12.80 \pm 0.51$	$17.85 \pm 0.71$	$0.50 \pm 0.11$	$-0.35 \pm 0.14$
4-5	$3096.0 \pm 0.1$	$14.22 \pm 0.58$	$20.65 \pm 1.82$	$0.72 \pm 0.13$	$-0.60 \pm 0.26$
5-6	$3096.2 \pm 0.2$	$16.44 \pm 0.14$		1	$-0.67 \pm 0.42$
6-7	$3096.0 \pm 0.2$	$16.91 \pm 0.20$		1	$-0.98 \pm 0.64$
7-8	$3096.2 \pm 0.3$	$17.47 \pm 0.28$		1	$-0.81 \pm 1.03$
8-10	$3096.7 \pm 0.4$	$17.92 \pm 0.31$		1	$-0.76 \pm 1.19$
10-14	$3095.1 \pm 0.7$	$20.39 \pm 0.66$		1	$2.92 \pm 1.96$
$p_T$ ( GeV/c )	$N_{\text{prompt}}$	$N_{\text{from } b}$	$N_{\text{tail}}$	$N_{\text{bkg}}$	
0-1	$57221 \pm 308$	$3232 \pm 81$	$664 \pm 49$	$51151 \pm 305$	
1-2	$98518 \pm 397$	$6563 \pm 107$	$660 \pm 47$	$68244 \pm 365$	
2-3	$74530 \pm 332$	$6086 \pm 97$	$372 \pm 34$	$38437 \pm 278$	
3-4	$42400 \pm 238$	$4332 \pm 79$	$207 \pm 23$	$13023 \pm 168$	
4-5	$23246 \pm 171$	$2785 \pm 61$	$91 \pm 16$	$3963 \pm 103$	
5-6	$11867 \pm 117$	$1514 \pm 45$	$70 \pm 13$	$1533 \pm 61$	
6-7	$6003 \pm 83$	$976 \pm 36$	$15 \pm 7$	$681 \pm 41$	
7-8	$3181 \pm 60$	$546 \pm 26$	$16 \pm 6$	$285 \pm 28$	
8-10	$2407 \pm 52$	$488 \pm 25$	$5 \pm 4$	$215 \pm 24$	
10-14	$933 \pm 34$	$250 \pm 18$	$0 \pm 1$	$109 \pm 20$	

Table B.5: The parameters of the 2D fit, including the fitted yields and shape parameters for different  $p_T$  bins in the rapidity bin  $4 < y < 4.5$ .

$p_T$ ( GeV/c )	$\mu[10^{-3}$ ps]	$S_1$	$S_2$	$\beta$	$\tau_b$ [ ps ]
0-1	$-5.5 \pm 0.5$	$1.71 \pm 0.09$	$0.89 \pm 0.02$	$0.19 \pm 0.03$	$1.33 \pm 0.07$
1-2	$-4.7 \pm 0.4$	$1.77 \pm 0.09$	$0.94 \pm 0.01$	$0.14 \pm 0.02$	$1.36 \pm 0.04$
2-3	$-3.8 \pm 0.4$	$1.65 \pm 0.10$	$0.91 \pm 0.02$	$0.16 \pm 0.04$	$1.34 \pm 0.04$
3-4	$-2.2 \pm 0.5$	$2.73 \pm 0.36$	$0.99 \pm 0.01$	$0.04 \pm 0.01$	$1.41 \pm 0.05$
4-5	$-0.0 \pm 0.6$	$2.25 \pm 0.20$	$0.96 \pm 0.02$	$0.10 \pm 0.02$	$1.41 \pm 0.07$
5-6	$3.6 \pm 0.8$	$0.92 \pm 0.04$	$1.71 \pm 0.17$	$0.77 \pm 0.08$	$1.26 \pm 0.07$
6-7	$1.4 \pm 1.1$	$2.06 \pm 0.26$	$0.97 \pm 0.04$	$0.13 \pm 0.05$	$1.22 \pm 0.10$
7-8	$2.6 \pm 1.5$	$0.68 \pm 0.22$	$1.22 \pm 0.08$	$0.22 \pm 0.18$	$1.18 \pm 0.12$
8-10	$0.6 \pm 1.5$	$1.12 \pm 0.05$	$0.37 \pm 0.18$	$0.93 \pm 0.06$	$1.49 \pm 0.15$
10-14	$5.9 \pm 2.6$	$1.52 \pm 0.22$	$0.80 \pm 0.18$	$0.50 \pm 0.25$	$1.34 \pm 0.19$
$p_T$ ( GeV/c )	$\mu_m$ [ MeV/c <sup>2</sup> ]	$\sigma_1$ [ MeV/c <sup>2</sup> ]	$\sigma_2$ [ MeV/c <sup>2</sup> ]	$f_m$	$\lambda[10^{-3}(\text{MeV}/c^2)^{-1}]$
0-1	$3094.4 \pm 0.1$	$13.79 \pm 0.77$	$19.23 \pm 1.22$	$0.55 \pm 0.16$	$-2.70 \pm 0.19$
1-2	$3094.7 \pm 0.1$	$13.80 \pm 0.65$	$18.79 \pm 0.76$	$0.45 \pm 0.13$	$-2.03 \pm 0.14$
2-3	$3094.9 \pm 0.1$	$14.73 \pm 0.65$	$20.41 \pm 0.88$	$0.49 \pm 0.12$	$-1.43 \pm 0.20$
3-4	$3094.9 \pm 0.2$	$17.99 \pm 0.14$		1	$-0.86 \pm 0.31$
4-5	$3095.3 \pm 0.2$	$19.15 \pm 0.21$		1	$-1.15 \pm 0.52$
5-6	$3096.3 \pm 0.3$	$20.58 \pm 0.30$		1	$0.32 \pm 0.82$
6-7	$3095.5 \pm 0.5$	$21.65 \pm 0.42$		1	$0.05 \pm 1.42$
7-8	$3096.4 \pm 0.7$	$22.70 \pm 0.61$		1	$-1.92 \pm 1.64$
8-10	$3096.2 \pm 0.9$	$23.85 \pm 0.77$		1	$0.98 \pm 2.05$
10-14	$3097.5 \pm 1.7$	$27.27 \pm 1.49$		1	$-0.39 \pm 4.88$
$p_T$ ( GeV/c )	$N_{\text{prompt}}$	$N_{\text{from } b}$	$N_{\text{tail}}$	$N_{\text{bkg}}$	
0-1	$25641 \pm 183$	$1250 \pm 50$	$470 \pm 33$	$6549 \pm 122$	
1-2	$43322 \pm 239$	$2435 \pm 67$	$464 \pm 34$	$11835 \pm 164$	
2-3	$29180 \pm 195$	$1917 \pm 56$	$232 \pm 23$	$6468 \pm 128$	
3-4	$15227 \pm 138$	$1195 \pm 42$	$49 \pm 11$	$2806 \pm 81$	
4-5	$8034 \pm 98$	$667 \pm 31$	$28 \pm 9$	$1063 \pm 53$	
5-6	$4117 \pm 70$	$465 \pm 25$	$12 \pm 6$	$460 \pm 37$	
6-7	$2121 \pm 50$	$266 \pm 19$	$6 \pm 5$	$174 \pm 24$	
7-8	$1080 \pm 36$	$148 \pm 14$	$4 \pm 4$	$117 \pm 18$	
8-10	$825 \pm 31$	$117 \pm 12$	$0 \pm 2$	$84 \pm 16$	
10-14	$275 \pm 18$	$62 \pm 9$	$0 \pm 1$	$18 \pm 8$	

Table B.6: The parameters of the 2D fit, including the fitted yields and shape parameters for  $14 < p_T < 20$  GeV/c and  $2 < y < 4.5$ .

$p_T$ ( GeV/c )	$\mu[10^{-3}$ ps]	$S_1$	$S_2$	$\beta$	$\tau_b$ [ ps ]
14-20	$-0.1 \pm 0.8$	$1.87 \pm 0.26$	$0.93 \pm 0.08$	$0.26 \pm 0.12$	$1.27 \pm 0.05$
$p_T$ ( GeV/c )	$\mu_m$ [ MeV/c <sup>2</sup> ]	$\sigma_1$ [ MeV/c <sup>2</sup> ]	$\sigma_2$ [ MeV/c <sup>2</sup> ]	$f_m$	$\lambda[10^{-3}(\text{MeV}/c^2)^{-1}]$
14-20	$3096.3 \pm 0.4$	$16.20 \pm 0.37$		1	$0.10 \pm 1.20$
$p_T$ ( GeV/c )	$N_{\text{prompt}}$	$N_{\text{from } b}$	$N_{\text{tail}}$	$N_{\text{bkg}}$	
14-20	$1244 \pm 39$	$716 \pm 29$	$12 \pm 5$	$203 \pm 23$	

Table B.7: The parameters of the 2D fit, including the fitted yields and shape parameters for  $0 < p_T < 1 \text{ GeV}/c$  and  $2.0 < y < 2.5$ .

index	$\mu[10^{-3} \text{ ps}]$	$S_1$	$S_2$	$\beta$	$\tau_b[\text{ ps}]$
fit1	$-10.6 \pm 0.5$	$1.48 \pm 0.08$	$0.80 \pm 0.03$	$0.32 \pm 0.06$	$1.53 \pm 0.06$
fit2	$-10.6 \pm 0.5$	$1.48 \pm 0.08$	$0.80 \pm 0.03$	$0.32 \pm 0.06$	$1.53 \pm 0.06$
index	$\mu_m[\text{ MeV}/c^2]$	$\sigma_1[\text{ MeV}/c^2]$	$\sigma_2[\text{ MeV}/c^2]$	$f_m$	$\lambda[10^{-3}(\text{ MeV}/c^2)^{-1}]$
fit1	$3098.1 \pm 0.1$	$9.42 \pm 0.42$	$16.32 \pm 1.71$	$0.71 \pm 0.10$	$-1.22 \pm 0.09$
fit2	$3098.1 \pm 0.1$	$16.30 \pm 1.75$	$9.42 \pm 0.43$	$0.29 \pm 0.10$	$-1.22 \pm 0.09$
index	$N_{\text{prompt}}$	$N_{\text{from } b}$	$N_{\text{tail}}$	$N_{\text{bkg}}$	
fit1	$19163 \pm 190$	$1532 \pm 51$	$66 \pm 18$	$24476 \pm 207$	
fit2	$19162 \pm 190$	$1532 \pm 51$	$66 \pm 18$	$24476 \pm 207$	

Table B.8: The parameters of the 2D fit, including the fitted yields and shape parameters for  $0 < p_T < 1 \text{ GeV}/c$  and  $2.5 < y < 3.0$ .

index	$\mu[10^{-3} \text{ ps}]$	$S_1$	$S_2$	$\beta$	$\tau_b[\text{ ps}]$
fit1	$-9.7 \pm 0.3$	$1.40 \pm 0.05$	$0.80 \pm 0.02$	$0.38 \pm 0.05$	$1.42 \pm 0.04$
fit2	$-9.7 \pm 0.3$	$1.40 \pm 0.04$	$0.80 \pm 0.02$	$0.38 \pm 0.04$	$1.42 \pm 0.04$
index	$\mu_m[\text{ MeV}/c^2]$	$\sigma_1[\text{ MeV}/c^2]$	$\sigma_2[\text{ MeV}/c^2]$	$f_m$	$\lambda[10^{-3}(\text{ MeV}/c^2)^{-1}]$
fit1	$3097.1 \pm 0.1$	$9.16 \pm 0.21$	$14.24 \pm 0.48$	$0.61 \pm 0.05$	$-1.63 \pm 0.05$
fit2	$3097.1 \pm 0.1$	$14.24 \pm 0.89$	$9.16 \pm 0.34$	$0.39 \pm 0.09$	$-1.63 \pm 0.05$
index	$N_{\text{prompt}}$	$N_{\text{from } b}$	$N_{\text{tail}}$	$N_{\text{bkg}}$	
fit1	$58084 \pm 335$	$4269 \pm 89$	$243 \pm 37$	$102538 \pm 402$	
fit2	$58083 \pm 341$	$4270 \pm 89$	$242 \pm 37$	$102537 \pm 407$	

## 746 B.1 Check exchange of $\sigma_1$ and $\sigma_2$

Table B.9: The parameters of the 2D fit, including the fitted yields and shape parameters for  $0 < p_T < 1 \text{ GeV}/c$  and  $3.0 < y < 3.5$ .

index	$\mu[10^{-3} \text{ ps}]$	$S_1$	$S_2$	$\beta$	$\tau_b[\text{ ps}]$
fit1	$-6.0 \pm 0.3$	$1.27 \pm 0.04$	$0.80 \pm 0.03$	$0.44 \pm 0.06$	$1.45 \pm 0.04$
fit2	$-6.0 \pm 0.3$	$1.27 \pm 0.04$	$0.80 \pm 0.03$	$0.44 \pm 0.06$	$1.45 \pm 0.04$
index	$\mu_m[\text{ MeV}/c^2]$	$\sigma_1[\text{ MeV}/c^2]$	$\sigma_2[\text{ MeV}/c^2]$	$f_m$	$\lambda[10^{-3}(\text{ MeV}/c^2)^{-1}]$
fit1	$3096.6 \pm 0.1$	$10.27 \pm 0.40$	$15.60 \pm 0.99$	$0.60 \pm 0.11$	$-1.58 \pm 0.04$
fit2	$3096.6 \pm 0.1$	$15.60 \pm 0.98$	$10.27 \pm 0.40$	$0.40 \pm 0.10$	$-1.58 \pm 0.04$
index	$N_{\text{prompt}}$	$N_{\text{from } b}$	$N_{\text{tail}}$	$N_{\text{bkg}}$	
fit1	$70883 \pm 387$	$4743 \pm 98$	$448 \pm 47$	$123818 \pm 460$	
fit2	$70883 \pm 388$	$4743 \pm 98$	$448 \pm 47$	$123819 \pm 461$	

Table B.10: The parameters of the 2D fit, including the fitted yields and shape parameters for  $0 < p_T < 1 \text{ GeV}/c$  and  $3.5 < y < 4.0$ .

index	$\mu[10^{-3} \text{ ps}]$	$S_1$	$S_2$	$\beta$	$\tau_b[\text{ps}]$
fit1	$-2.3 \pm 0.3$	$1.65 \pm 0.09$	$0.91 \pm 0.01$	$0.16 \pm 0.03$	$1.41 \pm 0.05$
fit2	$-2.3 \pm 0.3$	$1.65 \pm 0.09$	$0.91 \pm 0.01$	$0.16 \pm 0.03$	$1.41 \pm 0.05$
index	$\mu_m[\text{MeV}/c^2]$	$\sigma_1[\text{MeV}/c^2]$	$\sigma_2[\text{MeV}/c^2]$	$f_m$	$\lambda[10^{-3}(\text{MeV}/c^2)^{-1}]$
fit1	$3096.2 \pm 0.1$	$11.12 \pm 0.75$	$16.05 \pm 0.76$	$0.41 \pm 0.14$	$-2.09 \pm 0.07$
fit2	$3096.2 \pm 0.1$	$16.05 \pm 0.73$	$11.12 \pm 0.72$	$0.59 \pm 0.13$	$-2.09 \pm 0.07$
index	$N_{\text{prompt}}$	$N_{\text{from } b}$	$N_{\text{tail}}$	$N_{\text{bkg}}$	
fit1	$57221 \pm 308$	$3232 \pm 81$	$664 \pm 49$	$51151 \pm 305$	
fit2	$57221 \pm 308$	$3232 \pm 81$	$664 \pm 49$	$51151 \pm 305$	

Table B.11: The parameters of the 2D fit, including the fitted yields and shape parameters for  $0 < p_T < 1 \text{ GeV}/c$  and  $4.0 < y < 4.5$ .

index	$\mu[10^{-3} \text{ ps}]$	$S_1$	$S_2$	$\beta$	$\tau_b[\text{ps}]$
fit1	$-5.5 \pm 0.5$	$1.71 \pm 0.09$	$0.89 \pm 0.02$	$0.19 \pm 0.03$	$1.33 \pm 0.07$
fit2	$-5.5 \pm 0.5$	$1.71 \pm 0.09$	$0.89 \pm 0.02$	$0.19 \pm 0.03$	$1.33 \pm 0.07$
index	$\mu_m[\text{MeV}/c^2]$	$\sigma_1[\text{MeV}/c^2]$	$\sigma_2[\text{MeV}/c^2]$	$f_m$	$\lambda[10^{-3}(\text{MeV}/c^2)^{-1}]$
fit1	$3094.4 \pm 0.1$	$13.79 \pm 0.77$	$19.23 \pm 1.22$	$0.55 \pm 0.16$	$-2.70 \pm 0.19$
fit2	$3094.4 \pm 0.1$	$19.23 \pm 1.12$	$13.79 \pm 0.70$	$0.45 \pm 0.15$	$-2.70 \pm 0.19$
index	$N_{\text{prompt}}$	$N_{\text{from } b}$	$N_{\text{tail}}$	$N_{\text{bkg}}$	
fit1	$25641 \pm 183$	$1250 \pm 50$	$470 \pm 33$	$6549 \pm 122$	
fit2	$25642 \pm 182$	$1250 \pm 50$	$470 \pm 33$	$6549 \pm 122$	

Table B.12: The parameters of the 2D fit, including the fitted yields and shape parameters for  $1 < p_T < 2 \text{ GeV}/c$  and  $2.0 < y < 2.5$ .

index	$\mu[10^{-3} \text{ ps}]$	$S_1$	$S_2$	$\beta$	$\tau_b[\text{ps}]$
fit1	$-9.4 \pm 0.4$	$1.42 \pm 0.06$	$0.81 \pm 0.02$	$0.34 \pm 0.05$	$1.50 \pm 0.03$
fit2	$-9.4 \pm 0.4$	$1.42 \pm 0.06$	$0.81 \pm 0.02$	$0.34 \pm 0.05$	$1.50 \pm 0.03$
index	$\mu_m[\text{MeV}/c^2]$	$\sigma_1[\text{MeV}/c^2]$	$\sigma_2[\text{MeV}/c^2]$	$f_m$	$\lambda[10^{-3}(\text{MeV}/c^2)^{-1}]$
fit1	$3097.8 \pm 0.1$	$9.01 \pm 0.36$	$15.10 \pm 1.04$	$0.61 \pm 0.09$	$-1.20 \pm 0.06$
fit2	$3097.8 \pm 0.1$	$15.08 \pm 1.02$	$9.01 \pm 0.35$	$0.39 \pm 0.08$	$-1.20 \pm 0.06$
index	$N_{\text{prompt}}$	$N_{\text{from } b}$	$N_{\text{tail}}$	$N_{\text{bkg}}$	
fit1	$41284 \pm 285$	$3899 \pm 80$	$92 \pm 22$	$58144 \pm 320$	
fit2	$41281 \pm 285$	$3899 \pm 80$	$92 \pm 22$	$58146 \pm 320$	

Table B.13: The parameters of the 2D fit, including the fitted yields and shape parameters for  $1 < p_T < 2 \text{ GeV}/c$  and  $2.5 < y < 3.0$ .

index	$\mu[10^{-3} \text{ ps}]$	$S_1$	$S_2$	$\beta$	$\tau_b[\text{ps}]$
fit1	$-8.4 \pm 0.2$	$0.80 \pm 0.02$	$1.31 \pm 0.03$	$0.57 \pm 0.04$	$1.51 \pm 0.02$
fit2	$-8.4 \pm 0.2$	$0.80 \pm 0.02$	$1.31 \pm 0.03$	$0.57 \pm 0.04$	$1.51 \pm 0.02$
index	$\mu_m[\text{MeV}/c^2]$	$\sigma_1[\text{MeV}/c^2]$	$\sigma_2[\text{MeV}/c^2]$	$f_m$	$\lambda[10^{-3}(\text{MeV}/c^2)^{-1}]$
fit1	$3097.1 \pm 0.0$	$13.19 \pm 0.54$	$8.76 \pm 0.43$	$0.56 \pm 0.10$	$-1.34 \pm 0.03$
fit2	$3097.1 \pm 0.0$	$8.76 \pm 0.41$	$13.19 \pm 0.51$	$0.44 \pm 0.09$	$-1.34 \pm 0.03$
index	$N_{\text{prompt}}$	$N_{\text{from } b}$	$N_{\text{tail}}$	$N_{\text{bkg}}$	
fit1	$110884 \pm 467$	$9852 \pm 128$	$190 \pm 37$	$193064 \pm 557$	
fit2	$110885 \pm 465$	$9852 \pm 128$	$190 \pm 37$	$193064 \pm 555$	

Table B.14: The parameters of the 2D fit, including the fitted yields and shape parameters for  $1 < p_T < 2 \text{ GeV}/c$  and  $3.0 < y < 3.5$ .

index	$\mu[10^{-3} \text{ ps}]$	$S_1$	$S_2$	$\beta$	$\tau_b[\text{ps}]$
fit1	$-6.0 \pm 0.2$	$1.38 \pm 0.11$	$0.85 \pm 0.03$	$0.29 \pm 0.10$	$1.48 \pm 0.02$
fit2	$-6.0 \pm 0.2$	$1.38 \pm 0.04$	$0.85 \pm 0.01$	$0.29 \pm 0.04$	$1.48 \pm 0.02$
index	$\mu_m[\text{MeV}/c^2]$	$\sigma_1[\text{MeV}/c^2]$	$\sigma_2[\text{MeV}/c^2]$	$f_m$	$\lambda[10^{-3}(\text{MeV}/c^2)^{-1}]$
fit1	$3096.5 \pm 0.0$	$10.58 \pm 0.57$	$14.97 \pm 1.11$	$0.56 \pm 0.17$	$-1.46 \pm 0.04$
fit2	$3096.5 \pm 0.0$	$14.99 \pm 0.73$	$10.59 \pm 0.36$	$0.44 \pm 0.11$	$-1.46 \pm 0.04$
index	$N_{\text{prompt}}$	$N_{\text{from } b}$	$N_{\text{tail}}$	$N_{\text{bkg}}$	
fit1	$124967 \pm 508$	$9925 \pm 134$	$409 \pm 44$	$174597 \pm 559$	
fit2	$124969 \pm 490$	$9925 \pm 130$	$409 \pm 44$	$174595 \pm 548$	

Table B.15: The parameters of the 2D fit, including the fitted yields and shape parameters for  $1 < p_T < 2 \text{ GeV}/c$  and  $3.5 < y < 4.0$ .

index	$\mu[10^{-3} \text{ ps}]$	$S_1$	$S_2$	$\beta$	$\tau_b[\text{ps}]$
fit1	$-2.1 \pm 0.2$	$0.88 \pm 0.01$	$1.50 \pm 0.06$	$0.79 \pm 0.04$	$1.43 \pm 0.03$
fit2	$-2.1 \pm 0.2$	$1.50 \pm 0.06$	$0.88 \pm 0.01$	$0.21 \pm 0.04$	$1.43 \pm 0.03$
index	$\mu_m[\text{MeV}/c^2]$	$\sigma_1[\text{MeV}/c^2]$	$\sigma_2[\text{MeV}/c^2]$	$f_m$	$\lambda[10^{-3}(\text{MeV}/c^2)^{-1}]$
fit1	$3096.2 \pm 0.1$	$12.24 \pm 0.32$	$17.72 \pm 0.72$	$0.60 \pm 0.08$	$-1.84 \pm 0.06$
fit2	$3096.2 \pm 0.1$	$17.72 \pm 0.72$	$12.24 \pm 0.32$	$0.40 \pm 0.08$	$-1.84 \pm 0.06$
index	$N_{\text{prompt}}$	$N_{\text{from } b}$	$N_{\text{tail}}$	$N_{\text{bkg}}$	
fit1	$98518 \pm 397$	$6563 \pm 107$	$660 \pm 47$	$68244 \pm 365$	
fit2	$98519 \pm 398$	$6563 \pm 107$	$660 \pm 47$	$68244 \pm 365$	

Table B.16: The parameters of the 2D fit, including the fitted yields and shape parameters for  $1 < p_T < 2 \text{ GeV}/c$  and  $4.0 < y < 4.5$ .

index	$\mu[10^{-3} \text{ ps}]$	$S_1$	$S_2$	$\beta$	$\tau_b[\text{ps}]$
fit1	$-4.7 \pm 0.4$	$1.77 \pm 0.09$	$0.94 \pm 0.01$	$0.14 \pm 0.02$	$1.36 \pm 0.04$
fit2	$-4.7 \pm 0.4$	$1.77 \pm 0.09$	$0.94 \pm 0.01$	$0.14 \pm 0.02$	$1.36 \pm 0.04$
index	$\mu_m[\text{MeV}/c^2]$	$\sigma_1[\text{MeV}/c^2]$	$\sigma_2[\text{MeV}/c^2]$	$f_m$	$\lambda[10^{-3}(\text{MeV}/c^2)^{-1}]$
fit1	$3094.7 \pm 0.1$	$13.80 \pm 0.65$	$18.79 \pm 0.76$	$0.45 \pm 0.13$	$-2.03 \pm 0.14$
fit2	$3094.7 \pm 0.1$	$18.79 \pm 0.75$	$13.80 \pm 0.64$	$0.55 \pm 0.13$	$-2.03 \pm 0.14$
index	$N_{\text{prompt}}$	$N_{\text{from } b}$	$N_{\text{tail}}$	$N_{\text{bkg}}$	
fit1	$43322 \pm 239$	$2435 \pm 67$	$464 \pm 34$	$11835 \pm 164$	
fit2	$43322 \pm 239$	$2435 \pm 67$	$464 \pm 34$	$11834 \pm 164$	

Table B.17: The parameters of the 2D fit, including the fitted yields and shape parameters for  $2 < p_T < 3 \text{ GeV}/c$  and  $2.0 < y < 2.5$ .

index	$\mu[10^{-3} \text{ ps}]$	$S_1$	$S_2$	$\beta$	$\tau_b[\text{ps}]$
fit1	$-8.5 \pm 0.4$	$1.54 \pm 0.14$	$0.89 \pm 0.03$	$0.20 \pm 0.07$	$1.48 \pm 0.03$
fit2	$-8.5 \pm 0.4$	$0.90 \pm 0.03$	$1.54 \pm 0.14$	$0.80 \pm 0.07$	$1.48 \pm 0.03$
index	$\mu_m[\text{MeV}/c^2]$	$\sigma_1[\text{MeV}/c^2]$	$\sigma_2[\text{MeV}/c^2]$	$f_m$	$\lambda[10^{-3}(\text{MeV}/c^2)^{-1}]$
fit1	$3097.6 \pm 0.1$	$9.26 \pm 0.36$	$15.41 \pm 1.08$	$0.64 \pm 0.09$	$-0.74 \pm 0.07$
fit2	$3097.6 \pm 0.1$	$15.42 \pm 1.08$	$9.26 \pm 0.35$	$0.36 \pm 0.08$	$-0.74 \pm 0.07$
index	$N_{\text{prompt}}$	$N_{\text{from } b}$	$N_{\text{tail}}$	$N_{\text{bkg}}$	
fit1	$36767 \pm 259$	$4301 \pm 81$	$41 \pm 16$	$42372 \pm 273$	
fit2	$36768 \pm 259$	$4301 \pm 81$	$41 \pm 16$	$42371 \pm 273$	

Table B.18: The parameters of the 2D fit, including the fitted yields and shape parameters for  $2 < p_T < 3 \text{ GeV}/c$  and  $2.5 < y < 3.0$ .

index	$\mu[10^{-3} \text{ ps}]$	$S_1$	$S_2$	$\beta$	$\tau_b[\text{ps}]$
fit1	$-7.4 \pm 0.2$	$0.81 \pm 0.02$	$1.29 \pm 0.04$	$0.59 \pm 0.05$	$1.48 \pm 0.02$
fit2	$-7.4 \pm 0.2$	$1.29 \pm 0.04$	$0.81 \pm 0.02$	$0.41 \pm 0.05$	$1.48 \pm 0.02$
index	$\mu_m[\text{MeV}/c^2]$	$\sigma_1[\text{MeV}/c^2]$	$\sigma_2[\text{MeV}/c^2]$	$f_m$	$\lambda[10^{-3}(\text{MeV}/c^2)^{-1}]$
fit1	$3096.9 \pm 0.0$	$14.09 \pm 0.78$	$9.50 \pm 0.36$	$0.42 \pm 0.10$	$-0.82 \pm 0.04$
fit2	$3096.9 \pm 0.0$	$9.50 \pm 0.36$	$14.09 \pm 0.77$	$0.58 \pm 0.10$	$-0.82 \pm 0.04$
index	$N_{\text{prompt}}$	$N_{\text{from } b}$	$N_{\text{tail}}$	$N_{\text{bkg}}$	
fit1	$90308 \pm 402$	$9903 \pm 122$	$224 \pm 32$	$115546 \pm 439$	
fit2	$90307 \pm 402$	$9902 \pm 122$	$224 \pm 32$	$115546 \pm 438$	

Table B.19: The parameters of the 2D fit, including the fitted yields and shape parameters for  $2 < p_T < 3 \text{ GeV}/c$  and  $3.0 < y < 3.5$ .

index	$\mu[10^{-3} \text{ ps}]$	$S_1$	$S_2$	$\beta$	$\tau_b[\text{ps}]$
fit1	$-5.3 \pm 0.2$	$1.33 \pm 0.05$	$0.84 \pm 0.02$	$0.33 \pm 0.05$	$1.50 \pm 0.02$
fit2	$-5.3 \pm 0.2$	$1.33 \pm 0.05$	$0.84 \pm 0.02$	$0.33 \pm 0.05$	$1.50 \pm 0.02$
index	$\mu_m[\text{MeV}/c^2]$	$\sigma_1[\text{MeV}/c^2]$	$\sigma_2[\text{MeV}/c^2]$	$f_m$	$\lambda[10^{-3}(\text{MeV}/c^2)^{-1}]$
fit1	$3096.4 \pm 0.0$	$11.81 \pm 0.15$	$19.26 \pm 1.42$	$0.85 \pm 0.04$	$-1.14 \pm 0.05$
fit2	$3096.4 \pm 0.0$	$19.26 \pm 1.35$	$11.80 \pm 0.15$	$0.15 \pm 0.04$	$-1.14 \pm 0.05$
index	$N_{\text{prompt}}$	$N_{\text{from } b}$	$N_{\text{tail}}$	$N_{\text{bkg}}$	
fit1	$99435 \pm 426$	$9714 \pm 122$	$242 \pm 34$	$98798 \pm 435$	
fit2	$99432 \pm 426$	$9714 \pm 122$	$242 \pm 34$	$98800 \pm 435$	

Table B.20: The parameters of the 2D fit, including the fitted yields and shape parameters for  $2 < p_T < 3 \text{ GeV}/c$  and  $3.5 < y < 4.0$ .

index	$\mu[10^{-3} \text{ ps}]$	$S_1$	$S_2$	$\beta$	$\tau_b[\text{ps}]$
fit1	$-1.3 \pm 0.2$	$1.40 \pm 0.06$	$0.86 \pm 0.02$	$0.25 \pm 0.05$	$1.41 \pm 0.03$
fit2	$-1.3 \pm 0.2$	$1.40 \pm 0.06$	$0.86 \pm 0.02$	$0.25 \pm 0.05$	$1.41 \pm 0.03$
index	$\mu_m[\text{MeV}/c^2]$	$\sigma_1[\text{MeV}/c^2]$	$\sigma_2[\text{MeV}/c^2]$	$f_m$	$\lambda[10^{-3}(\text{MeV}/c^2)^{-1}]$
fit1	$3096.3 \pm 0.1$	$11.96 \pm 0.62$	$16.98 \pm 0.68$	$0.43 \pm 0.12$	$-1.09 \pm 0.08$
fit2	$3096.3 \pm 0.1$	$16.96 \pm 0.68$	$11.94 \pm 0.62$	$0.57 \pm 0.12$	$-1.09 \pm 0.08$
index	$N_{\text{prompt}}$	$N_{\text{from } b}$	$N_{\text{tail}}$	$N_{\text{bkg}}$	
fit1	$74530 \pm 332$	$6086 \pm 97$	$372 \pm 34$	$38437 \pm 278$	
fit2	$74528 \pm 332$	$6086 \pm 97$	$372 \pm 34$	$38439 \pm 279$	

Table B.21: The parameters of the 2D fit, including the fitted yields and shape parameters for  $2 < p_T < 3 \text{ GeV}/c$  and  $4.0 < y < 4.5$ .

index	$\mu[10^{-3} \text{ ps}]$	$S_1$	$S_2$	$\beta$	$\tau_b[\text{ps}]$
fit1	$-3.8 \pm 0.4$	$1.65 \pm 0.10$	$0.91 \pm 0.02$	$0.16 \pm 0.04$	$1.34 \pm 0.04$
fit2	$-3.8 \pm 0.4$	$1.65 \pm 0.10$	$0.91 \pm 0.02$	$0.16 \pm 0.03$	$1.34 \pm 0.04$
index	$\mu_m[\text{MeV}/c^2]$	$\sigma_1[\text{MeV}/c^2]$	$\sigma_2[\text{MeV}/c^2]$	$f_m$	$\lambda[10^{-3}(\text{MeV}/c^2)^{-1}]$
fit1	$3094.9 \pm 0.1$	$14.73 \pm 0.65$	$20.41 \pm 0.88$	$0.49 \pm 0.12$	$-1.43 \pm 0.20$
fit2	$3094.9 \pm 0.1$	$20.40 \pm 0.92$	$14.72 \pm 0.68$	$0.51 \pm 0.13$	$-1.43 \pm 0.20$
index	$N_{\text{prompt}}$	$N_{\text{from } b}$	$N_{\text{tail}}$	$N_{\text{bkg}}$	
fit1	$29180 \pm 195$	$1917 \pm 56$	$232 \pm 23$	$6468 \pm 128$	
fit2	$29180 \pm 196$	$1917 \pm 56$	$232 \pm 23$	$6468 \pm 128$	

Table B.22: The parameters of the 2D fit, including the fitted yields and shape parameters for  $3 < p_T < 4 \text{ GeV}/c$  and  $2.0 < y < 2.5$ .

index	$\mu[10^{-3} \text{ ps}]$	$S_1$	$S_2$	$\beta$	$\tau_b[\text{ps}]$
fit1	$-5.9 \pm 0.4$	$1.33 \pm 0.06$	$0.82 \pm 0.03$	$0.38 \pm 0.08$	$1.42 \pm 0.03$
fit2	$-5.9 \pm 0.4$	$0.82 \pm 0.03$	$1.33 \pm 0.06$	$0.62 \pm 0.08$	$1.42 \pm 0.03$
index	$\mu_m[\text{MeV}/c^2]$	$\sigma_1[\text{MeV}/c^2]$	$\sigma_2[\text{MeV}/c^2]$	$f_m$	$\lambda[10^{-3}(\text{MeV}/c^2)^{-1}]$
fit1	$3097.5 \pm 0.1$	$9.97 \pm 0.35$	$16.96 \pm 1.49$	$0.72 \pm 0.08$	$-0.39 \pm 0.11$
fit2	$3097.5 \pm 0.1$	$16.96 \pm 1.40$	$9.97 \pm 0.34$	$0.28 \pm 0.08$	$-0.39 \pm 0.11$
index	$N_{\text{prompt}}$	$N_{\text{from } b}$	$N_{\text{tail}}$	$N_{\text{bkg}}$	
fit1	$23289 \pm 192$	$3058 \pm 65$	$35 \pm 12$	$16992 \pm 179$	
fit2	$23288 \pm 191$	$3059 \pm 65$	$35 \pm 12$	$16992 \pm 178$	

Table B.23: The parameters of the 2D fit, including the fitted yields and shape parameters for  $3 < p_T < 4 \text{ GeV}/c$  and  $2.5 < y < 3.0$ .

index	$\mu[10^{-3} \text{ ps}]$	$S_1$	$S_2$	$\beta$	$\tau_b[\text{ps}]$
fit1	$-5.6 \pm 0.2$	$0.84 \pm 0.02$	$1.31 \pm 0.04$	$0.64 \pm 0.05$	$1.49 \pm 0.02$
fit2	$-5.6 \pm 0.2$	$0.84 \pm 0.02$	$1.31 \pm 0.04$	$0.64 \pm 0.06$	$1.49 \pm 0.02$
index	$\mu_m[\text{MeV}/c^2]$	$\sigma_1[\text{MeV}/c^2]$	$\sigma_2[\text{MeV}/c^2]$	$f_m$	$\lambda[10^{-3}(\text{MeV}/c^2)^{-1}]$
fit1	$3096.8 \pm 0.1$	$10.44 \pm 0.17$	$16.20 \pm 0.87$	$0.75 \pm 0.05$	$-0.53 \pm 0.07$
fit2	$3096.8 \pm 0.1$	$16.20 \pm 1.12$	$10.44 \pm 0.24$	$0.24 \pm 0.07$	$-0.53 \pm 0.07$
index	$N_{\text{prompt}}$	$N_{\text{from } b}$	$N_{\text{tail}}$	$N_{\text{bkg}}$	
fit1	$57367 \pm 299$	$7490 \pm 102$	$117 \pm 22$	$45353 \pm 283$	
fit2	$57368 \pm 300$	$7490 \pm 102$	$117 \pm 22$	$45352 \pm 285$	

Table B.24: The parameters of the 2D fit, including the fitted yields and shape parameters for  $3 < p_T < 4 \text{ GeV}/c$  and  $3.0 < y < 3.5$ .

index	$\mu[10^{-3} \text{ ps}]$	$S_1$	$S_2$	$\beta$	$\tau_b[\text{ps}]$
fit1	$-4.4 \pm 0.2$	$0.87 \pm 0.02$	$1.39 \pm 0.06$	$0.73 \pm 0.05$	$1.43 \pm 0.02$
fit2	$-4.4 \pm 0.2$	$1.39 \pm 0.08$	$0.87 \pm 0.02$	$0.27 \pm 0.07$	$1.43 \pm 0.02$
index	$\mu_m[\text{MeV}/c^2]$	$\sigma_1[\text{MeV}/c^2]$	$\sigma_2[\text{MeV}/c^2]$	$f_m$	$\lambda[10^{-3}(\text{MeV}/c^2)^{-1}]$
fit1	$3096.3 \pm 0.1$	$11.30 \pm 0.32$	$16.34 \pm 0.69$	$0.62 \pm 0.08$	$-0.62 \pm 0.09$
fit2	$3096.3 \pm 0.1$	$16.34 \pm 0.99$	$11.30 \pm 0.35$	$0.38 \pm 0.11$	$-0.61 \pm 0.09$
index	$N_{\text{prompt}}$	$N_{\text{from } b}$	$N_{\text{tail}}$	$N_{\text{bkg}}$	
fit1	$59834 \pm 290$	$6707 \pm 97$	$168 \pm 25$	$31299 \pm 241$	
fit2	$59834 \pm 298$	$6707 \pm 97$	$168 \pm 25$	$31299 \pm 250$	

Table B.25: The parameters of the 2D fit, including the fitted yields and shape parameters for  $3 < p_T < 4 \text{ GeV}/c$  and  $3.5 < y < 4.0$ .

index	$\mu[10^{-3} \text{ ps}]$	$S_1$	$S_2$	$\beta$	$\tau_b[\text{ps}]$
fit1	$-1.6 \pm 0.3$	$1.47 \pm 0.09$	$0.87 \pm 0.02$	$0.22 \pm 0.05$	$1.34 \pm 0.03$
fit2	$-1.6 \pm 0.3$	$1.47 \pm 0.09$	$0.87 \pm 0.02$	$0.22 \pm 0.05$	$1.34 \pm 0.03$
index	$\mu_m[\text{MeV}/c^2]$	$\sigma_1[\text{MeV}/c^2]$	$\sigma_2[\text{MeV}/c^2]$	$f_m$	$\lambda[10^{-3}(\text{MeV}/c^2)^{-1}]$
fit1	$3096.0 \pm 0.1$	$12.80 \pm 0.51$	$17.85 \pm 0.71$	$0.50 \pm 0.11$	$-0.35 \pm 0.14$
fit2	$3096.0 \pm 0.1$	$17.85 \pm 0.71$	$12.80 \pm 0.51$	$0.50 \pm 0.11$	$-0.35 \pm 0.14$
index	$N_{\text{prompt}}$	$N_{\text{from } b}$	$N_{\text{tail}}$	$N_{\text{bkg}}$	
fit1	$42400 \pm 238$	$4332 \pm 79$	$207 \pm 23$	$13023 \pm 168$	
fit2	$42400 \pm 238$	$4332 \pm 79$	$207 \pm 23$	$13023 \pm 168$	

Table B.26: The parameters of the 2D fit, including the fitted yields and shape parameters for  $3 < p_T < 4 \text{ GeV}/c$  and  $4.0 < y < 4.5$ .

index	$\mu[10^{-3} \text{ ps}]$	$S_1$	$S_2$	$\beta$	$\tau_b[\text{ps}]$
fit1	$-2.2 \pm 0.5$	$2.73 \pm 0.36$	$0.99 \pm 0.01$	$0.04 \pm 0.01$	$1.41 \pm 0.05$
fit2	$-2.2 \pm 0.5$	$2.73 \pm 0.36$	$0.99 \pm 0.01$	$0.04 \pm 0.01$	$1.41 \pm 0.05$
index	$\mu_m[\text{MeV}/c^2]$	$\sigma_1[\text{MeV}/c^2]$	$\sigma_2[\text{MeV}/c^2]$	$f_m$	$\lambda[10^{-3}(\text{MeV}/c^2)^{-1}]$
fit1	$3094.9 \pm 0.2$	$17.99 \pm 0.14$	$15.00 \pm 0.00$	$1.00 \pm 0.00$	$-0.86 \pm 0.31$
fit2	$3094.9 \pm 0.2$	$15.00 \pm 0.00$	$17.99 \pm 0.14$	$0.00 \pm 0.00$	$-0.86 \pm 0.31$
index	$N_{\text{prompt}}$	$N_{\text{from } b}$	$N_{\text{tail}}$	$N_{\text{bkg}}$	
fit1	$15227 \pm 138$	$1195 \pm 42$	$49 \pm 11$	$2806 \pm 81$	
fit2	$15227 \pm 138$	$1195 \pm 42$	$49 \pm 11$	$2806 \pm 81$	

Table B.27: The parameters of the 2D fit, including the fitted yields and shape parameters for  $4 < p_T < 5 \text{ GeV}/c$  and  $2.0 < y < 2.5$ .

index	$\mu[10^{-3} \text{ ps}]$	$S_1$	$S_2$	$\beta$	$\tau_b[\text{ps}]$
fit1	$-6.3 \pm 0.5$	$1.82 \pm 0.19$	$0.93 \pm 0.02$	$0.09 \pm 0.03$	$1.30 \pm 0.03$
fit2	$-6.3 \pm 0.5$	$1.82 \pm 0.19$	$0.93 \pm 0.02$	$0.09 \pm 0.03$	$1.30 \pm 0.03$
index	$\mu_m[\text{MeV}/c^2]$	$\sigma_1[\text{MeV}/c^2]$	$\sigma_2[\text{MeV}/c^2]$	$f_m$	$\lambda[10^{-3}(\text{MeV}/c^2)^{-1}]$
fit1	$3097.3 \pm 0.1$	$11.74 \pm 0.10$	$15.00 \pm 0.00$	$1.00 \pm 0.00$	$-0.39 \pm 0.17$
fit2	$3097.3 \pm 0.1$	$15.00 \pm 0.00$	$11.74 \pm 0.10$	$0.00 \pm 0.00$	$-0.39 \pm 0.17$
index	$N_{\text{prompt}}$	$N_{\text{from } b}$	$N_{\text{tail}}$	$N_{\text{bkg}}$	
fit1	$14610 \pm 138$	$2358 \pm 57$	$25 \pm 10$	$7469 \pm 110$	
fit2	$14610 \pm 138$	$2358 \pm 57$	$25 \pm 10$	$7469 \pm 110$	

Table B.28: The parameters of the 2D fit, including the fitted yields and shape parameters for  $4 < p_T < 5 \text{ GeV}/c$  and  $2.5 < y < 3.0$ .

index	$\mu[10^{-3} \text{ ps}]$	$S_1$	$S_2$	$\beta$	$\tau_b[\text{ps}]$
fit1	$-4.4 \pm 0.3$	$0.91 \pm 0.02$	$1.49 \pm 0.08$	$0.80 \pm 0.05$	$1.40 \pm 0.02$
fit2	$-4.4 \pm 0.3$	$0.91 \pm 0.02$	$1.49 \pm 0.08$	$0.80 \pm 0.05$	$1.40 \pm 0.02$
index	$\mu_m[\text{MeV}/c^2]$	$\sigma_1[\text{MeV}/c^2]$	$\sigma_2[\text{MeV}/c^2]$	$f_m$	$\lambda[10^{-3}(\text{MeV}/c^2)^{-1}]$
fit1	$3096.7 \pm 0.1$	$14.33 \pm 0.50$	$9.25 \pm 0.51$	$0.58 \pm 0.09$	$-0.63 \pm 0.13$
fit2	$3096.7 \pm 0.1$	$9.25 \pm 0.53$	$14.34 \pm 0.52$	$0.42 \pm 0.09$	$-0.63 \pm 0.13$
index	$N_{\text{prompt}}$	$N_{\text{from } b}$	$N_{\text{tail}}$	$N_{\text{bkg}}$	
fit1	$34532 \pm 212$	$5122 \pm 82$	$92 \pm 17$	$13826 \pm 158$	
fit2	$34532 \pm 212$	$5122 \pm 82$	$92 \pm 17$	$13826 \pm 158$	

Table B.29: The parameters of the 2D fit, including the fitted yields and shape parameters for  $4 < p_T < 5 \text{ GeV}/c$  and  $3.0 < y < 3.5$ .

index	$\mu[10^{-3} \text{ ps}]$	$S_1$	$S_2$	$\beta$	$\tau_b[\text{ps}]$
fit1	$-3.3 \pm 0.2$	$1.48 \pm 0.08$	$0.88 \pm 0.02$	$0.22 \pm 0.05$	$1.37 \pm 0.03$
fit2	$-3.3 \pm 0.2$	$1.48 \pm 0.08$	$0.88 \pm 0.02$	$0.22 \pm 0.05$	$1.37 \pm 0.03$
index	$\mu_m[\text{MeV}/c^2]$	$\sigma_1[\text{MeV}/c^2]$	$\sigma_2[\text{MeV}/c^2]$	$f_m$	$\lambda[10^{-3}(\text{MeV}/c^2)^{-1}]$
fit1	$3096.2 \pm 0.1$	$10.40 \pm 1.44$	$14.82 \pm 0.89$	$0.32 \pm 0.22$	$-0.55 \pm 0.16$
fit2	$3096.2 \pm 0.1$	$14.83 \pm 0.83$	$10.40 \pm 1.35$	$0.68 \pm 0.21$	$-0.55 \pm 0.16$
index	$N_{\text{prompt}}$	$N_{\text{from } b}$	$N_{\text{tail}}$	$N_{\text{bkg}}$	
fit1	$33158 \pm 205$	$4366 \pm 76$	$105 \pm 18$	$8956 \pm 137$	
fit2	$33158 \pm 205$	$4366 \pm 76$	$105 \pm 18$	$8956 \pm 136$	

Table B.30: The parameters of the 2D fit, including the fitted yields and shape parameters for  $4 < p_T < 5 \text{ GeV}/c$  and  $3.5 < y < 4.0$ .

index	$\mu[10^{-3} \text{ ps}]$	$S_1$	$S_2$	$\beta$	$\tau_b[\text{ps}]$
fit1	$-1.2 \pm 0.3$	$1.55 \pm 0.12$	$0.87 \pm 0.02$	$0.19 \pm 0.05$	$1.38 \pm 0.03$
fit2	$-1.2 \pm 0.3$	$1.55 \pm 0.12$	$0.87 \pm 0.02$	$0.19 \pm 0.05$	$1.38 \pm 0.03$
index	$\mu_m[\text{MeV}/c^2]$	$\sigma_1[\text{MeV}/c^2]$	$\sigma_2[\text{MeV}/c^2]$	$f_m$	$\lambda[10^{-3}(\text{MeV}/c^2)^{-1}]$
fit1	$3096.0 \pm 0.1$	$14.22 \pm 0.58$	$20.65 \pm 1.82$	$0.72 \pm 0.13$	$-0.60 \pm 0.26$
fit2	$3096.0 \pm 0.1$	$20.65 \pm 1.72$	$14.22 \pm 0.55$	$0.28 \pm 0.12$	$-0.60 \pm 0.26$
index	$N_{\text{prompt}}$	$N_{\text{from } b}$	$N_{\text{tail}}$	$N_{\text{bkg}}$	
fit1	$23246 \pm 171$	$2785 \pm 61$	$91 \pm 16$	$3963 \pm 103$	
fit2	$23246 \pm 171$	$2785 \pm 61$	$91 \pm 16$	$3963 \pm 103$	

Table B.31: The parameters of the 2D fit, including the fitted yields and shape parameters for  $4 < p_T < 5 \text{ GeV}/c$  and  $4.0 < y < 4.5$ .

index	$\mu[10^{-3} \text{ ps}]$	$S_1$	$S_2$	$\beta$	$\tau_b[\text{ ps}]$
fit1	$-0.0 \pm 0.6$	$2.25 \pm 0.20$	$0.96 \pm 0.02$	$0.10 \pm 0.02$	$1.41 \pm 0.07$
fit2	$-0.0 \pm 0.6$	$2.25 \pm 0.20$	$0.96 \pm 0.02$	$0.10 \pm 0.02$	$1.41 \pm 0.07$
index	$\mu_m[\text{ MeV}/c^2]$	$\sigma_1[\text{ MeV}/c^2]$	$\sigma_2[\text{ MeV}/c^2]$	$f_m$	$\lambda[10^{-3}(\text{ MeV}/c^2)^{-1}]$
fit1	$3095.3 \pm 0.2$	$19.15 \pm 0.21$	$15.00 \pm 0.00$	$1.00 \pm 0.00$	$-1.15 \pm 0.52$
fit2	$3095.3 \pm 0.2$	$15.00 \pm 0.00$	$19.15 \pm 0.21$	$0.00 \pm 0.00$	$-1.15 \pm 0.52$
index	$N_{\text{prompt}}$	$N_{\text{from } b}$	$N_{\text{tail}}$	$N_{\text{bkg}}$	
fit1	$8034 \pm 98$	$667 \pm 31$	$28 \pm 9$	$1063 \pm 53$	
fit2	$8034 \pm 98$	$667 \pm 31$	$28 \pm 9$	$1063 \pm 53$	

Table B.32: The parameters of the 2D fit, including the fitted yields and shape parameters for  $5 < p_T < 6 \text{ GeV}/c$  and  $2.0 < y < 2.5$ .

index	$\mu[10^{-3} \text{ ps}]$	$S_1$	$S_2$	$\beta$	$\tau_b[\text{ ps}]$
fit1	$-4.9 \pm 0.5$	$0.86 \pm 0.03$	$1.59 \pm 0.12$	$0.78 \pm 0.05$	$1.35 \pm 0.04$
fit2	$-4.9 \pm 0.5$	$0.86 \pm 0.03$	$1.59 \pm 0.12$	$0.78 \pm 0.05$	$1.35 \pm 0.04$
index	$\mu_m[\text{ MeV}/c^2]$	$\sigma_1[\text{ MeV}/c^2]$	$\sigma_2[\text{ MeV}/c^2]$	$f_m$	$\lambda[10^{-3}(\text{ MeV}/c^2)^{-1}]$
fit1	$3097.4 \pm 0.1$	$12.30 \pm 0.12$	$15.00 \pm 0.00$	$1.00 \pm 0.00$	$-0.60 \pm 0.27$
fit2	$3097.4 \pm 0.1$	$15.00 \pm 0.00$	$12.30 \pm 0.12$	$0.00 \pm 0.00$	$-0.60 \pm 0.27$
index	$N_{\text{prompt}}$	$N_{\text{from } b}$	$N_{\text{tail}}$	$N_{\text{bkg}}$	
fit1	$9257 \pm 107$	$1726 \pm 47$	$17 \pm 6$	$3113 \pm 73$	
fit2	$9257 \pm 107$	$1726 \pm 47$	$17 \pm 6$	$3113 \pm 73$	

Table B.33: The parameters of the 2D fit, including the fitted yields and shape parameters for  $5 < p_T < 6 \text{ GeV}/c$  and  $2.5 < y < 3.0$ .

index	$\mu[10^{-3} \text{ ps}]$	$S_1$	$S_2$	$\beta$	$\tau_b[\text{ ps}]$
fit1	$-2.6 \pm 0.3$	$1.46 \pm 0.09$	$0.88 \pm 0.03$	$0.28 \pm 0.08$	$1.39 \pm 0.03$
fit2	$-2.6 \pm 0.3$	$1.46 \pm 0.09$	$0.88 \pm 0.03$	$0.28 \pm 0.08$	$1.39 \pm 0.03$
index	$\mu_m[\text{ MeV}/c^2]$	$\sigma_1[\text{ MeV}/c^2]$	$\sigma_2[\text{ MeV}/c^2]$	$f_m$	$\lambda[10^{-3}(\text{ MeV}/c^2)^{-1}]$
fit1	$3096.6 \pm 0.1$	$12.24 \pm 0.08$	$15.00 \pm 0.00$	$1.00 \pm 0.00$	$-0.77 \pm 0.23$
fit2	$3096.6 \pm 0.1$	$15.00 \pm 0.00$	$12.24 \pm 0.08$	$0.00 \pm 0.00$	$-0.77 \pm 0.23$
index	$N_{\text{prompt}}$	$N_{\text{from } b}$	$N_{\text{tail}}$	$N_{\text{bkg}}$	
fit1	$19468 \pm 152$	$3301 \pm 65$	$54 \pm 12$	$4632 \pm 91$	
fit2	$19468 \pm 152$	$3301 \pm 65$	$54 \pm 12$	$4632 \pm 91$	

Table B.34: The parameters of the 2D fit, including the fitted yields and shape parameters for  $5 < p_T < 6 \text{ GeV}/c$  and  $3.0 < y < 3.5$ .

index	$\mu[10^{-3} \text{ ps}]$	$S_1$	$S_2$	$\beta$	$\tau_b[\text{ps}]$
fit1	$-3.5 \pm 0.3$	$0.90 \pm 0.02$	$1.58 \pm 0.12$	$0.83 \pm 0.05$	$1.33 \pm 0.03$
fit2	$-3.5 \pm 0.3$	$0.90 \pm 0.02$	$1.58 \pm 0.12$	$0.83 \pm 0.05$	$1.33 \pm 0.03$
index	$\mu_m[\text{MeV}/c^2]$	$\sigma_1[\text{MeV}/c^2]$	$\sigma_2[\text{MeV}/c^2]$	$f_m$	$\lambda[10^{-3}(\text{MeV}/c^2)^{-1}]$
fit1	$3096.1 \pm 0.1$	$13.77 \pm 0.09$	$15.00 \pm 0.00$	$1.00 \pm 0.00$	$-0.25 \pm 0.30$
fit2	$3096.1 \pm 0.1$	$15.00 \pm 0.00$	$13.77 \pm 0.09$	$0.00 \pm 0.00$	$-0.25 \pm 0.30$
index	$N_{\text{prompt}}$	$N_{\text{from } b}$	$N_{\text{tail}}$	$N_{\text{bkg}}$	
fit1	$17440 \pm 143$	$2701 \pm 59$	$57 \pm 12$	$2929 \pm 77$	
fit2	$17440 \pm 143$	$2701 \pm 59$	$57 \pm 12$	$2929 \pm 77$	

Table B.35: The parameters of the 2D fit, including the fitted yields and shape parameters for  $5 < p_T < 6 \text{ GeV}/c$  and  $3.5 < y < 4.0$ .

index	$\mu[10^{-3} \text{ ps}]$	$S_1$	$S_2$	$\beta$	$\tau_b[\text{ps}]$
fit1	$-0.6 \pm 0.4$	$0.89 \pm 0.03$	$1.57 \pm 0.13$	$0.81 \pm 0.06$	$1.29 \pm 0.04$
fit2	$-0.6 \pm 0.4$	$0.89 \pm 0.03$	$1.57 \pm 0.13$	$0.81 \pm 0.06$	$1.29 \pm 0.04$
index	$\mu_m[\text{MeV}/c^2]$	$\sigma_1[\text{MeV}/c^2]$	$\sigma_2[\text{MeV}/c^2]$	$f_m$	$\lambda[10^{-3}(\text{MeV}/c^2)^{-1}]$
fit1	$3096.2 \pm 0.2$	$16.44 \pm 0.14$	$15.00 \pm 0.00$	$1.00 \pm 0.00$	$-0.67 \pm 0.42$
fit2	$3096.2 \pm 0.2$	$15.00 \pm 0.00$	$16.44 \pm 0.14$	$0.00 \pm 0.00$	$-0.67 \pm 0.42$
index	$N_{\text{prompt}}$	$N_{\text{from } b}$	$N_{\text{tail}}$	$N_{\text{bkg}}$	
fit1	$11867 \pm 117$	$1514 \pm 45$	$70 \pm 13$	$1533 \pm 61$	
fit2	$11867 \pm 117$	$1514 \pm 45$	$70 \pm 13$	$1533 \pm 61$	

Table B.36: The parameters of the 2D fit, including the fitted yields and shape parameters for  $5 < p_T < 6 \text{ GeV}/c$  and  $4.0 < y < 4.5$ .

index	$\mu[10^{-3} \text{ ps}]$	$S_1$	$S_2$	$\beta$	$\tau_b[\text{ps}]$
fit1	$3.6 \pm 0.8$	$0.92 \pm 0.04$	$1.71 \pm 0.17$	$0.77 \pm 0.08$	$1.26 \pm 0.07$
fit2	$3.6 \pm 0.8$	$0.92 \pm 0.04$	$1.71 \pm 0.17$	$0.77 \pm 0.08$	$1.26 \pm 0.07$
index	$\mu_m[\text{MeV}/c^2]$	$\sigma_1[\text{MeV}/c^2]$	$\sigma_2[\text{MeV}/c^2]$	$f_m$	$\lambda[10^{-3}(\text{MeV}/c^2)^{-1}]$
fit1	$3096.3 \pm 0.3$	$20.58 \pm 0.30$	$15.00 \pm 0.00$	$1.00 \pm 0.00$	$0.32 \pm 0.82$
fit2	$3096.3 \pm 0.3$	$15.00 \pm 0.00$	$20.58 \pm 0.30$	$0.00 \pm 0.00$	$0.32 \pm 0.82$
index	$N_{\text{prompt}}$	$N_{\text{from } b}$	$N_{\text{tail}}$	$N_{\text{bkg}}$	
fit1	$4117 \pm 70$	$465 \pm 25$	$12 \pm 6$	$460 \pm 37$	
fit2	$4117 \pm 70$	$465 \pm 25$	$12 \pm 6$	$460 \pm 37$	

Table B.37: The parameters of the 2D fit, including the fitted yields and shape parameters for  $6 < p_T < 7 \text{ GeV}/c$  and  $2.0 < y < 2.5$ .

index	$\mu[10^{-3} \text{ ps}]$	$S_1$	$S_2$	$\beta$	$\tau_b[\text{ ps}]$
fit1	$-1.5 \pm 0.6$	$1.65 \pm 0.17$	$0.90 \pm 0.03$	$0.19 \pm 0.07$	$1.32 \pm 0.04$
fit2	$-1.5 \pm 0.6$	$1.65 \pm 0.17$	$0.90 \pm 0.03$	$0.19 \pm 0.07$	$1.32 \pm 0.04$
index	$\mu_m[\text{ MeV}/c^2]$	$\sigma_1[\text{ MeV}/c^2]$	$\sigma_2[\text{ MeV}/c^2]$	$f_m$	$\lambda[10^{-3}(\text{ MeV}/c^2)^{-1}]$
fit1	$3097.5 \pm 0.2$	$12.46 \pm 0.16$	$15.00 \pm 0.00$	$1.00 \pm 0.00$	$0.05 \pm 0.42$
fit2	$3097.5 \pm 0.2$	$15.00 \pm 0.00$	$12.46 \pm 0.16$	$0.00 \pm 0.00$	$0.05 \pm 0.42$
index	$N_{\text{prompt}}$	$N_{\text{from } b}$	$N_{\text{tail}}$	$N_{\text{bkg}}$	
fit1	$5422 \pm 81$	$1205 \pm 39$	$12 \pm 5$	$1414 \pm 51$	
fit2	$5422 \pm 81$	$1205 \pm 39$	$12 \pm 5$	$1414 \pm 51$	

Table B.38: The parameters of the 2D fit, including the fitted yields and shape parameters for  $6 < p_T < 7 \text{ GeV}/c$  and  $2.5 < y < 3.0$ .

index	$\mu[10^{-3} \text{ ps}]$	$S_1$	$S_2$	$\beta$	$\tau_b[\text{ ps}]$
fit1	$-2.1 \pm 0.4$	$0.96 \pm 0.02$	$1.85 \pm 0.18$	$0.88 \pm 0.04$	$1.33 \pm 0.04$
fit2	$-2.1 \pm 0.4$	$0.96 \pm 0.02$	$1.85 \pm 0.18$	$0.88 \pm 0.04$	$1.33 \pm 0.04$
index	$\mu_m[\text{ MeV}/c^2]$	$\sigma_1[\text{ MeV}/c^2]$	$\sigma_2[\text{ MeV}/c^2]$	$f_m$	$\lambda[10^{-3}(\text{ MeV}/c^2)^{-1}]$
fit1	$3096.5 \pm 0.1$	$12.38 \pm 0.10$	$15.00 \pm 0.00$	$1.00 \pm 0.00$	$-0.58 \pm 0.39$
fit2	$3096.5 \pm 0.1$	$15.00 \pm 0.00$	$12.38 \pm 0.10$	$0.00 \pm 0.00$	$-0.58 \pm 0.39$
index	$N_{\text{prompt}}$	$N_{\text{from } b}$	$N_{\text{tail}}$	$N_{\text{bkg}}$	
fit1	$10776 \pm 111$	$2065 \pm 51$	$41 \pm 10$	$1689 \pm 58$	
fit2	$10776 \pm 111$	$2065 \pm 51$	$41 \pm 10$	$1689 \pm 58$	

Table B.39: The parameters of the 2D fit, including the fitted yields and shape parameters for  $6 < p_T < 7 \text{ GeV}/c$  and  $3.0 < y < 3.5$ .

index	$\mu[10^{-3} \text{ ps}]$	$S_1$	$S_2$	$\beta$	$\tau_b[\text{ ps}]$
fit1	$-2.6 \pm 0.4$	$0.91 \pm 0.03$	$1.62 \pm 0.22$	$0.85 \pm 0.08$	$1.25 \pm 0.04$
fit2	$-2.6 \pm 0.4$	$0.91 \pm 0.03$	$1.62 \pm 0.22$	$0.85 \pm 0.08$	$1.25 \pm 0.04$
index	$\mu_m[\text{ MeV}/c^2]$	$\sigma_1[\text{ MeV}/c^2]$	$\sigma_2[\text{ MeV}/c^2]$	$f_m$	$\lambda[10^{-3}(\text{ MeV}/c^2)^{-1}]$
fit1	$3096.1 \pm 0.1$	$13.90 \pm 0.13$	$15.00 \pm 0.00$	$1.00 \pm 0.00$	$-1.10 \pm 0.47$
fit2	$3096.1 \pm 0.1$	$15.00 \pm 0.00$	$13.90 \pm 0.13$	$0.00 \pm 0.00$	$-1.10 \pm 0.47$
index	$N_{\text{prompt}}$	$N_{\text{from } b}$	$N_{\text{tail}}$	$N_{\text{bkg}}$	
fit1	$8989 \pm 102$	$1643 \pm 45$	$44 \pm 10$	$1217 \pm 51$	
fit2	$8989 \pm 102$	$1643 \pm 45$	$44 \pm 10$	$1217 \pm 51$	

Table B.40: The parameters of the 2D fit, including the fitted yields and shape parameters for  $6 < p_T < 7 \text{ GeV}/c$  and  $3.5 < y < 4.0$ .

index	$\mu[10^{-3} \text{ ps}]$	$S_1$	$S_2$	$\beta$	$\tau_b[\text{ ps}]$
fit1	$-1.0 \pm 0.5$	$1.77 \pm 0.24$	$0.92 \pm 0.03$	$0.14 \pm 0.06$	$1.43 \pm 0.06$
fit2	$-1.0 \pm 0.5$	$1.77 \pm 0.24$	$0.92 \pm 0.03$	$0.14 \pm 0.06$	$1.43 \pm 0.06$
index	$\mu_m[\text{ MeV}/c^2]$	$\sigma_1[\text{ MeV}/c^2]$	$\sigma_2[\text{ MeV}/c^2]$	$f_m$	$\lambda[10^{-3}(\text{ MeV}/c^2)^{-1}]$
fit1	$3096.0 \pm 0.2$	$16.91 \pm 0.20$	$15.00 \pm 0.00$	$1.00 \pm 0.00$	$-0.98 \pm 0.64$
fit2	$3096.0 \pm 0.2$	$15.00 \pm 0.00$	$16.91 \pm 0.20$	$0.00 \pm 0.00$	$-0.98 \pm 0.64$
index	$N_{\text{prompt}}$	$N_{\text{from } b}$	$N_{\text{tail}}$	$N_{\text{bkg}}$	
fit1	$6003 \pm 83$	$976 \pm 36$	$15 \pm 7$	$681 \pm 41$	
fit2	$6003 \pm 83$	$976 \pm 36$	$15 \pm 7$	$681 \pm 41$	

Table B.41: The parameters of the 2D fit, including the fitted yields and shape parameters for  $6 < p_T < 7 \text{ GeV}/c$  and  $4.0 < y < 4.5$ .

index	$\mu[10^{-3} \text{ ps}]$	$S_1$	$S_2$	$\beta$	$\tau_b[\text{ ps}]$
fit1	$1.4 \pm 1.1$	$2.06 \pm 0.26$	$0.97 \pm 0.04$	$0.13 \pm 0.05$	$1.22 \pm 0.10$
fit2	$1.4 \pm 1.1$	$2.06 \pm 0.26$	$0.97 \pm 0.04$	$0.13 \pm 0.05$	$1.22 \pm 0.10$
index	$\mu_m[\text{ MeV}/c^2]$	$\sigma_1[\text{ MeV}/c^2]$	$\sigma_2[\text{ MeV}/c^2]$	$f_m$	$\lambda[10^{-3}(\text{ MeV}/c^2)^{-1}]$
fit1	$3095.5 \pm 0.5$	$21.65 \pm 0.42$	$15.00 \pm 0.00$	$1.00 \pm 0.00$	$0.05 \pm 1.42$
fit2	$3095.5 \pm 0.5$	$15.00 \pm 0.00$	$21.65 \pm 0.42$	$0.00 \pm 0.00$	$0.05 \pm 1.42$
index	$N_{\text{prompt}}$	$N_{\text{from } b}$	$N_{\text{tail}}$	$N_{\text{bkg}}$	
fit1	$2121 \pm 50$	$266 \pm 19$	$6 \pm 5$	$174 \pm 24$	
fit2	$2121 \pm 50$	$266 \pm 19$	$6 \pm 5$	$174 \pm 24$	

Table B.42: The parameters of the 2D fit, including the fitted yields and shape parameters for  $7 < p_T < 8 \text{ GeV}/c$  and  $2.0 < y < 2.5$ .

index	$\mu[10^{-3} \text{ ps}]$	$S_1$	$S_2$	$\beta$	$\tau_b[\text{ ps}]$
fit1	$-1.7 \pm 0.8$	$2.46 \pm 0.36$	$1.01 \pm 0.03$	$0.08 \pm 0.03$	$1.47 \pm 0.06$
fit2	$-1.7 \pm 0.8$	$2.46 \pm 0.36$	$1.01 \pm 0.03$	$0.08 \pm 0.03$	$1.47 \pm 0.06$
index	$\mu_m[\text{ MeV}/c^2]$	$\sigma_1[\text{ MeV}/c^2]$	$\sigma_2[\text{ MeV}/c^2]$	$f_m$	$\lambda[10^{-3}(\text{ MeV}/c^2)^{-1}]$
fit1	$3097.2 \pm 0.2$	$12.86 \pm 0.19$	$15.00 \pm 0.00$	$1.00 \pm 0.00$	$-0.22 \pm 0.62$
fit2	$3097.2 \pm 0.2$	$15.00 \pm 0.00$	$12.86 \pm 0.19$	$0.00 \pm 0.00$	$-0.22 \pm 0.62$
index	$N_{\text{prompt}}$	$N_{\text{from } b}$	$N_{\text{tail}}$	$N_{\text{bkg}}$	
fit1	$3347 \pm 63$	$836 \pm 33$	$9 \pm 5$	$665 \pm 36$	
fit2	$3347 \pm 63$	$836 \pm 33$	$9 \pm 5$	$665 \pm 36$	

Table B.43: The parameters of the 2D fit, including the fitted yields and shape parameters for  $7 < p_T < 8 \text{ GeV}/c$  and  $2.5 < y < 3.0$ .

index	$\mu[10^{-3} \text{ ps}]$	$S_1$	$S_2$	$\beta$	$\tau_b[\text{ ps}]$
fit1	$-2.1 \pm 0.5$	$2.00 \pm 0.22$	$0.97 \pm 0.03$	$0.13 \pm 0.04$	$1.32 \pm 0.04$
fit2	$-2.1 \pm 0.5$	$2.00 \pm 0.22$	$0.97 \pm 0.03$	$0.13 \pm 0.04$	$1.32 \pm 0.04$
index	$\mu_m[\text{ MeV}/c^2]$	$\sigma_1[\text{ MeV}/c^2]$	$\sigma_2[\text{ MeV}/c^2]$	$f_m$	$\lambda[10^{-3}(\text{ MeV}/c^2)^{-1}]$
fit1	$3096.2 \pm 0.2$	$12.96 \pm 0.14$	$15.00 \pm 0.00$	$1.00 \pm 0.00$	$-0.77 \pm 0.56$
fit2	$3096.2 \pm 0.2$	$15.00 \pm 0.00$	$12.96 \pm 0.14$	$0.00 \pm 0.00$	$-0.77 \pm 0.56$
index	$N_{\text{prompt}}$	$N_{\text{from } b}$	$N_{\text{tail}}$	$N_{\text{bkg}}$	
fit1	$5755 \pm 81$	$1373 \pm 41$	$9 \pm 5$	$846 \pm 42$	
fit2	$5755 \pm 81$	$1373 \pm 41$	$9 \pm 5$	$846 \pm 42$	

Table B.44: The parameters of the 2D fit, including the fitted yields and shape parameters for  $7 < p_T < 8 \text{ GeV}/c$  and  $3.0 < y < 3.5$ .

index	$\mu[10^{-3} \text{ ps}]$	$S_1$	$S_2$	$\beta$	$\tau_b[\text{ ps}]$
fit1	$-2.9 \pm 0.5$	$0.97 \pm 0.02$	$2.08 \pm 0.34$	$0.93 \pm 0.03$	$1.30 \pm 0.05$
fit2	$-2.9 \pm 0.5$	$0.97 \pm 0.02$	$2.08 \pm 0.34$	$0.93 \pm 0.03$	$1.30 \pm 0.05$
index	$\mu_m[\text{ MeV}/c^2]$	$\sigma_1[\text{ MeV}/c^2]$	$\sigma_2[\text{ MeV}/c^2]$	$f_m$	$\lambda[10^{-3}(\text{ MeV}/c^2)^{-1}]$
fit1	$3095.8 \pm 0.2$	$14.53 \pm 0.18$	$15.00 \pm 0.00$	$1.00 \pm 0.00$	$0.81 \pm 0.79$
fit2	$3095.8 \pm 0.2$	$15.00 \pm 0.00$	$14.53 \pm 0.18$	$0.00 \pm 0.00$	$0.81 \pm 0.79$
index	$N_{\text{prompt}}$	$N_{\text{from } b}$	$N_{\text{tail}}$	$N_{\text{bkg}}$	
fit1	$4711 \pm 73$	$963 \pm 35$	$28 \pm 8$	$483 \pm 34$	
fit2	$4711 \pm 73$	$963 \pm 35$	$28 \pm 8$	$483 \pm 34$	

Table B.45: The parameters of the 2D fit, including the fitted yields and shape parameters for  $7 < p_T < 8 \text{ GeV}/c$  and  $3.5 < y < 4.0$ .

index	$\mu[10^{-3} \text{ ps}]$	$S_1$	$S_2$	$\beta$	$\tau_b[\text{ ps}]$
fit1	$-1.5 \pm 0.6$	$0.88 \pm 0.04$	$1.66 \pm 0.22$	$0.83 \pm 0.08$	$1.30 \pm 0.07$
fit2	$-1.5 \pm 0.6$	$0.88 \pm 0.04$	$1.66 \pm 0.22$	$0.83 \pm 0.08$	$1.30 \pm 0.07$
index	$\mu_m[\text{ MeV}/c^2]$	$\sigma_1[\text{ MeV}/c^2]$	$\sigma_2[\text{ MeV}/c^2]$	$f_m$	$\lambda[10^{-3}(\text{ MeV}/c^2)^{-1}]$
fit1	$3096.2 \pm 0.3$	$17.47 \pm 0.28$	$15.00 \pm 0.00$	$1.00 \pm 0.00$	$-0.81 \pm 1.03$
fit2	$3096.2 \pm 0.3$	$15.00 \pm 0.00$	$17.47 \pm 0.28$	$0.00 \pm 0.00$	$-0.81 \pm 1.03$
index	$N_{\text{prompt}}$	$N_{\text{from } b}$	$N_{\text{tail}}$	$N_{\text{bkg}}$	
fit1	$3181 \pm 60$	$546 \pm 26$	$16 \pm 6$	$285 \pm 28$	
fit2	$3181 \pm 60$	$546 \pm 26$	$16 \pm 6$	$285 \pm 28$	

Table B.46: The parameters of the 2D fit, including the fitted yields and shape parameters for  $7 < p_T < 8 \text{ GeV}/c$  and  $4.0 < y < 4.5$ .

index	$\mu[10^{-3} \text{ ps}]$	$S_1$	$S_2$	$\beta$	$\tau_b[\text{ ps}]$
fit1	$2.6 \pm 1.5$	$0.68 \pm 0.22$	$1.22 \pm 0.08$	$0.22 \pm 0.18$	$1.18 \pm 0.12$
fit2	$2.6 \pm 1.5$	$0.68 \pm 0.22$	$1.22 \pm 0.08$	$0.22 \pm 0.18$	$1.18 \pm 0.12$
index	$\mu_m[\text{ MeV}/c^2]$	$\sigma_1[\text{ MeV}/c^2]$	$\sigma_2[\text{ MeV}/c^2]$	$f_m$	$\lambda[10^{-3}(\text{ MeV}/c^2)^{-1}]$
fit1	$3096.4 \pm 0.7$	$22.70 \pm 0.61$	$15.00 \pm 0.00$	$1.00 \pm 0.00$	$-1.92 \pm 1.64$
fit2	$3096.4 \pm 0.7$	$15.00 \pm 0.00$	$22.70 \pm 0.61$	$0.00 \pm 0.00$	$-1.92 \pm 1.64$
index	$N_{\text{prompt}}$	$N_{\text{from } b}$	$N_{\text{tail}}$	$N_{\text{bkg}}$	
fit1	$1080 \pm 36$	$148 \pm 14$	$4 \pm 4$	$117 \pm 18$	
fit2	$1080 \pm 36$	$148 \pm 14$	$4 \pm 4$	$117 \pm 18$	

Table B.47: The parameters of the 2D fit, including the fitted yields and shape parameters for  $8 < p_T < 10 \text{ GeV}/c$  and  $2.0 < y < 2.5$ .

index	$\mu[10^{-3} \text{ ps}]$	$S_1$	$S_2$	$\beta$	$\tau_b[\text{ ps}]$
fit1	$-0.2 \pm 0.7$	$1.81 \pm 0.21$	$0.99 \pm 0.04$	$0.18 \pm 0.08$	$1.44 \pm 0.05$
fit2	$-0.2 \pm 0.7$	$1.81 \pm 0.21$	$0.99 \pm 0.04$	$0.18 \pm 0.08$	$1.44 \pm 0.05$
index	$\mu_m[\text{ MeV}/c^2]$	$\sigma_1[\text{ MeV}/c^2]$	$\sigma_2[\text{ MeV}/c^2]$	$f_m$	$\lambda[10^{-3}(\text{ MeV}/c^2)^{-1}]$
fit1	$3097.4 \pm 0.2$	$13.04 \pm 0.19$	$15.00 \pm 0.00$	$1.00 \pm 0.00$	$-0.33 \pm 0.67$
fit2	$3097.4 \pm 0.2$	$15.00 \pm 0.00$	$13.04 \pm 0.19$	$0.00 \pm 0.00$	$-0.33 \pm 0.67$
index	$N_{\text{prompt}}$	$N_{\text{from } b}$	$N_{\text{tail}}$	$N_{\text{bkg}}$	
fit1	$3220 \pm 61$	$929 \pm 34$	$9 \pm 4$	$577 \pm 34$	
fit2	$3220 \pm 61$	$929 \pm 34$	$9 \pm 4$	$577 \pm 34$	

Table B.48: The parameters of the 2D fit, including the fitted yields and shape parameters for  $8 < p_T < 10 \text{ GeV}/c$  and  $2.5 < y < 3.0$ .

index	$\mu[10^{-3} \text{ ps}]$	$S_1$	$S_2$	$\beta$	$\tau_b[\text{ ps}]$
fit1	$-0.9 \pm 0.5$	$2.15 \pm 0.24$	$0.99 \pm 0.03$	$0.13 \pm 0.04$	$1.34 \pm 0.04$
fit2	$-0.9 \pm 0.5$	$2.15 \pm 0.24$	$0.99 \pm 0.03$	$0.13 \pm 0.04$	$1.34 \pm 0.04$
index	$\mu_m[\text{ MeV}/c^2]$	$\sigma_1[\text{ MeV}/c^2]$	$\sigma_2[\text{ MeV}/c^2]$	$f_m$	$\lambda[10^{-3}(\text{ MeV}/c^2)^{-1}]$
fit1	$3096.3 \pm 0.2$	$13.38 \pm 0.16$	$15.00 \pm 0.00$	$1.00 \pm 0.00$	$0.42 \pm 0.70$
fit2	$3096.3 \pm 0.2$	$15.00 \pm 0.00$	$13.38 \pm 0.16$	$0.00 \pm 0.00$	$0.42 \pm 0.70$
index	$N_{\text{prompt}}$	$N_{\text{from } b}$	$N_{\text{tail}}$	$N_{\text{bkg}}$	
fit1	$5052 \pm 76$	$1409 \pm 42$	$18 \pm 7$	$593 \pm 37$	
fit2	$5052 \pm 76$	$1409 \pm 42$	$18 \pm 7$	$593 \pm 37$	

Table B.49: The parameters of the 2D fit, including the fitted yields and shape parameters for  $8 < p_T < 10 \text{ GeV}/c$  and  $3.0 < y < 3.5$ .

index	$\mu[10^{-3} \text{ ps}]$	$S_1$	$S_2$	$\beta$	$\tau_b[\text{ps}]$
fit1	$-1.9 \pm 0.5$	$2.36 \pm 0.45$	$0.97 \pm 0.02$	$0.04 \pm 0.02$	$1.35 \pm 0.05$
fit2	$-1.9 \pm 0.5$	$2.36 \pm 0.45$	$0.97 \pm 0.02$	$0.04 \pm 0.02$	$1.35 \pm 0.05$
index	$\mu_m[\text{MeV}/c^2]$	$\sigma_1[\text{MeV}/c^2]$	$\sigma_2[\text{MeV}/c^2]$	$f_m$	$\lambda[10^{-3}(\text{MeV}/c^2)^{-1}]$
fit1	$3096.2 \pm 0.2$	$14.63 \pm 0.20$	$15.00 \pm 0.00$	$1.00 \pm 0.00$	$-0.58 \pm 0.87$
fit2	$3096.2 \pm 0.2$	$15.00 \pm 0.00$	$14.63 \pm 0.20$	$0.00 \pm 0.00$	$-0.58 \pm 0.87$
index	$N_{\text{prompt}}$	$N_{\text{from } b}$	$N_{\text{tail}}$	$N_{\text{bkg}}$	
fit1	$3908 \pm 66$	$960 \pm 34$	$7 \pm 5$	$388 \pm 31$	
fit2	$3908 \pm 66$	$960 \pm 34$	$7 \pm 5$	$388 \pm 31$	

Table B.50: The parameters of the 2D fit, including the fitted yields and shape parameters for  $8 < p_T < 10 \text{ GeV}/c$  and  $3.5 < y < 4.0$ .

index	$\mu[10^{-3} \text{ ps}]$	$S_1$	$S_2$	$\beta$	$\tau_b[\text{ps}]$
fit1	$-0.1 \pm 0.7$	$0.94 \pm 0.03$	$2.10 \pm 0.45$	$0.92 \pm 0.05$	$1.26 \pm 0.07$
fit2	$-0.1 \pm 0.7$	$0.94 \pm 0.03$	$2.10 \pm 0.45$	$0.92 \pm 0.05$	$1.26 \pm 0.07$
index	$\mu_m[\text{MeV}/c^2]$	$\sigma_1[\text{MeV}/c^2]$	$\sigma_2[\text{MeV}/c^2]$	$f_m$	$\lambda[10^{-3}(\text{MeV}/c^2)^{-1}]$
fit1	$3096.7 \pm 0.4$	$17.92 \pm 0.31$	$15.00 \pm 0.00$	$1.00 \pm 0.00$	$-0.76 \pm 1.19$
fit2	$3096.7 \pm 0.4$	$15.00 \pm 0.00$	$17.92 \pm 0.31$	$0.00 \pm 0.00$	$-0.76 \pm 1.19$
index	$N_{\text{prompt}}$	$N_{\text{from } b}$	$N_{\text{tail}}$	$N_{\text{bkg}}$	
fit1	$2407 \pm 52$	$488 \pm 25$	$5 \pm 4$	$215 \pm 24$	
fit2	$2407 \pm 52$	$488 \pm 25$	$5 \pm 4$	$215 \pm 24$	

Table B.51: The parameters of the 2D fit, including the fitted yields and shape parameters for  $8 < p_T < 10 \text{ GeV}/c$  and  $4.0 < y < 4.5$ .

index	$\mu[10^{-3} \text{ ps}]$	$S_1$	$S_2$	$\beta$	$\tau_b[\text{ps}]$
fit1	$0.6 \pm 1.5$	$1.12 \pm 0.05$	$0.37 \pm 0.18$	$0.93 \pm 0.06$	$1.49 \pm 0.15$
fit2	$0.6 \pm 1.5$	$1.12 \pm 0.05$	$0.37 \pm 0.18$	$0.93 \pm 0.06$	$1.49 \pm 0.15$
index	$\mu_m[\text{MeV}/c^2]$	$\sigma_1[\text{MeV}/c^2]$	$\sigma_2[\text{MeV}/c^2]$	$f_m$	$\lambda[10^{-3}(\text{MeV}/c^2)^{-1}]$
fit1	$3096.2 \pm 0.9$	$23.85 \pm 0.77$	$15.00 \pm 0.00$	$1.00 \pm 0.00$	$0.98 \pm 2.05$
fit2	$3096.2 \pm 0.9$	$15.00 \pm 0.00$	$23.85 \pm 0.77$	$0.00 \pm 0.00$	$0.98 \pm 2.05$
index	$N_{\text{prompt}}$	$N_{\text{from } b}$	$N_{\text{tail}}$	$N_{\text{bkg}}$	
fit1	$825 \pm 31$	$117 \pm 12$	$0 \pm 2$	$84 \pm 16$	
fit2	$825 \pm 31$	$117 \pm 12$	$0 \pm 2$	$84 \pm 16$	

Table B.52: The parameters of the 2D fit, including the fitted yields and shape parameters for  $10 < p_T < 14 \text{ GeV}/c$  and  $2.0 < y < 2.5$ .

index	$\mu[10^{-3} \text{ ps}]$	$S_1$	$S_2$	$\beta$	$\tau_b[\text{ps}]$
fit1	$-1.8 \pm 0.9$	$2.19 \pm 0.27$	$1.00 \pm 0.06$	$0.20 \pm 0.07$	$1.32 \pm 0.05$
fit2	$-1.8 \pm 0.9$	$2.19 \pm 0.27$	$1.00 \pm 0.06$	$0.20 \pm 0.07$	$1.32 \pm 0.05$
index	$\mu_m[\text{MeV}/c^2]$	$\sigma_1[\text{MeV}/c^2]$	$\sigma_2[\text{MeV}/c^2]$	$f_m$	$\lambda[10^{-3}(\text{MeV}/c^2)^{-1}]$
fit1	$3097.0 \pm 0.3$	$13.95 \pm 0.27$	$15.00 \pm 0.00$	$1.00 \pm 0.00$	$0.22 \pm 1.13$
fit2	$3097.0 \pm 0.3$	$15.00 \pm 0.00$	$13.95 \pm 0.27$	$0.00 \pm 0.00$	$0.22 \pm 1.13$
index	$N_{\text{prompt}}$	$N_{\text{from } b}$	$N_{\text{tail}}$	$N_{\text{bkg}}$	
fit1	$1754 \pm 45$	$753 \pm 30$	$2 \pm 2$	$226 \pm 23$	
fit2	$1754 \pm 45$	$753 \pm 30$	$2 \pm 2$	$226 \pm 23$	

Table B.53: The parameters of the 2D fit, including the fitted yields and shape parameters for  $10 < p_T < 14 \text{ GeV}/c$  and  $2.5 < y < 3.0$ .

index	$\mu[10^{-3} \text{ ps}]$	$S_1$	$S_2$	$\beta$	$\tau_b[\text{ps}]$
fit1	$-1.4 \pm 0.6$	$1.00 \pm 0.04$	$2.19 \pm 0.28$	$0.87 \pm 0.05$	$1.32 \pm 0.05$
fit2	$-1.4 \pm 0.6$	$1.00 \pm 0.04$	$2.19 \pm 0.28$	$0.87 \pm 0.05$	$1.32 \pm 0.05$
index	$\mu_m[\text{MeV}/c^2]$	$\sigma_1[\text{MeV}/c^2]$	$\sigma_2[\text{MeV}/c^2]$	$f_m$	$\lambda[10^{-3}(\text{MeV}/c^2)^{-1}]$
fit1	$3096.8 \pm 0.3$	$13.95 \pm 0.23$	$15.00 \pm 0.00$	$1.00 \pm 0.00$	$-1.04 \pm 1.11$
fit2	$3096.8 \pm 0.3$	$15.00 \pm 0.00$	$13.95 \pm 0.23$	$0.00 \pm 0.00$	$-1.04 \pm 1.11$
index	$N_{\text{prompt}}$	$N_{\text{from } b}$	$N_{\text{tail}}$	$N_{\text{bkg}}$	
fit1	$2353 \pm 52$	$962 \pm 34$	$17 \pm 6$	$242 \pm 25$	
fit2	$2353 \pm 52$	$962 \pm 34$	$17 \pm 6$	$242 \pm 25$	

Table B.54: The parameters of the 2D fit, including the fitted yields and shape parameters for  $10 < p_T < 14 \text{ GeV}/c$  and  $3.0 < y < 3.5$ .

index	$\mu[10^{-3} \text{ ps}]$	$S_1$	$S_2$	$\beta$	$\tau_b[\text{ps}]$
fit1	$-1.7 \pm 0.8$	$1.54 \pm 0.37$	$0.89 \pm 0.12$	$0.30 \pm 0.25$	$1.22 \pm 0.06$
fit2	$-1.7 \pm 0.8$	$1.54 \pm 0.37$	$0.89 \pm 0.12$	$0.30 \pm 0.25$	$1.22 \pm 0.06$
index	$\mu_m[\text{MeV}/c^2]$	$\sigma_1[\text{MeV}/c^2]$	$\sigma_2[\text{MeV}/c^2]$	$f_m$	$\lambda[10^{-3}(\text{MeV}/c^2)^{-1}]$
fit1	$3095.6 \pm 0.4$	$15.74 \pm 0.32$	$15.00 \pm 0.00$	$1.00 \pm 0.00$	$0.47 \pm 1.24$
fit2	$3095.6 \pm 0.4$	$15.00 \pm 0.00$	$15.74 \pm 0.32$	$0.00 \pm 0.00$	$0.47 \pm 1.24$
index	$N_{\text{prompt}}$	$N_{\text{from } b}$	$N_{\text{tail}}$	$N_{\text{bkg}}$	
fit1	$1629 \pm 43$	$545 \pm 26$	$2 \pm 2$	$198 \pm 22$	
fit2	$1629 \pm 43$	$545 \pm 26$	$2 \pm 2$	$198 \pm 22$	

Table B.55: The parameters of the 2D fit, including the fitted yields and shape parameters for  $10 < p_T < 14 \text{ GeV}/c$  and  $3.5 < y < 4.0$ .

index	$\mu[10^{-3} \text{ ps}]$	$S_1$	$S_2$	$\beta$	$\tau_b[\text{ps}]$
fit1	$0.6 \pm 1.0$	$0.91 \pm 0.03$	$2.82 \pm 0.60$	$0.94 \pm 0.03$	$1.24 \pm 0.09$
fit2	$0.6 \pm 1.0$	$0.91 \pm 0.03$	$2.82 \pm 0.60$	$0.94 \pm 0.03$	$1.24 \pm 0.09$
index	$\mu_m[\text{MeV}/c^2]$	$\sigma_1[\text{MeV}/c^2]$	$\sigma_2[\text{MeV}/c^2]$	$f_m$	$\lambda[10^{-3}(\text{MeV}/c^2)^{-1}]$
fit1	$3095.1 \pm 0.7$	$20.39 \pm 0.66$	$15.00 \pm 0.00$	$1.00 \pm 0.00$	$2.92 \pm 1.96$
fit2	$3095.1 \pm 0.7$	$15.00 \pm 0.00$	$20.39 \pm 0.66$	$0.00 \pm 0.00$	$2.92 \pm 1.96$
index	$N_{\text{prompt}}$	$N_{\text{from } b}$	$N_{\text{tail}}$	$N_{\text{bkg}}$	
fit1	$933 \pm 34$	$250 \pm 18$	$0 \pm 1$	$109 \pm 20$	
fit2	$933 \pm 34$	$250 \pm 18$	$0 \pm 1$	$109 \pm 20$	

Table B.56: The parameters of the 2D fit, including the fitted yields and shape parameters for  $10 < p_T < 14 \text{ GeV}/c$  and  $4.0 < y < 4.5$ .

index	$\mu[10^{-3} \text{ ps}]$	$S_1$	$S_2$	$\beta$	$\tau_b[\text{ps}]$
fit1	$5.9 \pm 2.6$	$1.52 \pm 0.22$	$0.80 \pm 0.18$	$0.50 \pm 0.25$	$1.34 \pm 0.19$
fit2	$5.9 \pm 2.6$	$1.52 \pm 0.22$	$0.80 \pm 0.18$	$0.50 \pm 0.25$	$1.34 \pm 0.19$
index	$\mu_m[\text{MeV}/c^2]$	$\sigma_1[\text{MeV}/c^2]$	$\sigma_2[\text{MeV}/c^2]$	$f_m$	$\lambda[10^{-3}(\text{MeV}/c^2)^{-1}]$
fit1	$3097.5 \pm 1.7$	$27.27 \pm 1.49$	$15.00 \pm 0.00$	$1.00 \pm 0.00$	$-0.39 \pm 4.88$
fit2	$3097.5 \pm 1.7$	$15.00 \pm 0.00$	$27.27 \pm 1.49$	$0.00 \pm 0.00$	$-0.39 \pm 4.88$
index	$N_{\text{prompt}}$	$N_{\text{from } b}$	$N_{\text{tail}}$	$N_{\text{bkg}}$	
fit1	$275 \pm 18$	$62 \pm 9$	$0 \pm 1$	$18 \pm 8$	
fit2	$275 \pm 18$	$62 \pm 9$	$0 \pm 1$	$18 \pm 8$	

Table B.57: The parameters of the 2D fit, including the fitted yields and shape parameters for  $14 < p_T < 20 \text{ GeV}/c$  and  $2.0 < y < 4.5$ .

index	$\mu[10^{-3} \text{ ps}]$	$S_1$	$S_2$	$\beta$	$\tau_b[\text{ps}]$
fit1	$-0.1 \pm 0.8$	$1.87 \pm 0.26$	$0.93 \pm 0.08$	$0.26 \pm 0.12$	$1.27 \pm 0.05$
fit2	$-0.1 \pm 0.8$	$1.87 \pm 0.26$	$0.93 \pm 0.08$	$0.26 \pm 0.12$	$1.27 \pm 0.05$
index	$\mu_m[\text{MeV}/c^2]$	$\sigma_1[\text{MeV}/c^2]$	$\sigma_2[\text{MeV}/c^2]$	$f_m$	$\lambda[10^{-3}(\text{MeV}/c^2)^{-1}]$
fit1	$3096.3 \pm 0.4$	$16.20 \pm 0.37$	$15.00 \pm 0.00$	$1.00 \pm 0.00$	$0.10 \pm 1.20$
fit2	$3096.3 \pm 0.4$	$15.00 \pm 0.00$	$16.20 \pm 0.37$	$0.00 \pm 0.00$	$0.10 \pm 1.20$
index	$N_{\text{prompt}}$	$N_{\text{from } b}$	$N_{\text{tail}}$	$N_{\text{bkg}}$	
fit1	$1244 \pm 39$	$716 \pm 29$	$12 \pm 5$	$203 \pm 23$	
fit2	$1244 \pm 39$	$716 \pm 29$	$12 \pm 5$	$203 \pm 23$	

<sup>747</sup> **C Tables of efficiencies**

Table C.1: The acceptance  $\varepsilon_{\text{acc}}$  in  $(p_{\text{T}}, y)$  bins for prompt  $J/\psi$ .

$p_{\text{T}}$ ( GeV/c )	$2 < y < 2.5$	$2.5 < y < 3$	$3 < y < 3.5$	$3.5 < y < 4$	$4 < y < 4.5$
0-1	$0.576 \pm 0.001$	$0.824 \pm 0.001$	$0.915 \pm 0.001$	$0.904 \pm 0.001$	$0.783 \pm 0.001$
1-2	$0.607 \pm 0.001$	$0.834 \pm 0.001$	$0.915 \pm 0.001$	$0.908 \pm 0.001$	$0.808 \pm 0.001$
2-3	$0.654 \pm 0.001$	$0.866 \pm 0.001$	$0.937 \pm 0.001$	$0.930 \pm 0.001$	$0.844 \pm 0.001$
3-4	$0.710 \pm 0.001$	$0.899 \pm 0.001$	$0.953 \pm 0.001$	$0.950 \pm 0.001$	$0.880 \pm 0.001$
4-5	$0.759 \pm 0.002$	$0.923 \pm 0.001$	$0.969 \pm 0.001$	$0.966 \pm 0.001$	$0.910 \pm 0.002$
5-6	$0.801 \pm 0.002$	$0.941 \pm 0.001$	$0.977 \pm 0.001$	$0.976 \pm 0.001$	$0.928 \pm 0.002$
6-7	$0.837 \pm 0.002$	$0.954 \pm 0.001$	$0.984 \pm 0.001$	$0.980 \pm 0.001$	$0.946 \pm 0.003$
7-8	$0.865 \pm 0.003$	$0.966 \pm 0.002$	$0.989 \pm 0.001$	$0.986 \pm 0.002$	$0.949 \pm 0.004$
8-10	$0.895 \pm 0.003$	$0.979 \pm 0.002$	$0.993 \pm 0.001$	$0.989 \pm 0.002$	$0.961 \pm 0.004$
10-14	$0.934 \pm 0.003$	$0.989 \pm 0.002$	$0.998 \pm 0.001$	$0.991 \pm 0.002$	$0.971 \pm 0.005$
14-20				$0.985 \pm 0.002(2 < y < 4.5)$	

Table C.2: The acceptance  $\varepsilon_{\text{acc}}$  in  $(p_{\text{T}}, y)$  bins for  $J/\psi$  from  $b$ .

$p_{\text{T}}$ ( GeV/c )	$2 < y < 2.5$	$2.5 < y < 3$	$3 < y < 3.5$	$3.5 < y < 4$	$4 < y < 4.5$
0-1	$0.574 \pm 0.005$	$0.826 \pm 0.004$	$0.907 \pm 0.004$	$0.909 \pm 0.004$	$0.789 \pm 0.007$
1-2	$0.607 \pm 0.003$	$0.833 \pm 0.003$	$0.915 \pm 0.002$	$0.913 \pm 0.003$	$0.814 \pm 0.005$
2-3	$0.652 \pm 0.003$	$0.866 \pm 0.003$	$0.936 \pm 0.002$	$0.934 \pm 0.003$	$0.856 \pm 0.005$
3-4	$0.711 \pm 0.004$	$0.896 \pm 0.003$	$0.953 \pm 0.002$	$0.952 \pm 0.003$	$0.885 \pm 0.005$
4-5	$0.758 \pm 0.004$	$0.924 \pm 0.003$	$0.967 \pm 0.002$	$0.973 \pm 0.003$	$0.906 \pm 0.006$
5-6	$0.808 \pm 0.005$	$0.944 \pm 0.003$	$0.979 \pm 0.002$	$0.974 \pm 0.003$	$0.922 \pm 0.008$
6-7	$0.839 \pm 0.005$	$0.953 \pm 0.004$	$0.984 \pm 0.002$	$0.982 \pm 0.004$	$0.941 \pm 0.009$
7-8	$0.862 \pm 0.006$	$0.965 \pm 0.004$	$0.985 \pm 0.003$	$0.987 \pm 0.004$	$0.971 \pm 0.009$
8-10	$0.899 \pm 0.005$	$0.980 \pm 0.003$	$0.994 \pm 0.002$	$0.991 \pm 0.003$	$0.980 \pm 0.009$
10-14	$0.929 \pm 0.006$	$0.987 \pm 0.003$	$1.000 \pm 0.000$	$0.985 \pm 0.006$	$0.967 \pm 0.016$
14-20				$0.979 \pm 0.004(2 < y < 4.5)$	

Table C.3: The acceptance  $\varepsilon_{\text{acc}}$  in  $(p_{\text{T}}, y)$  bins for inclusive  $J/\psi$ .

$p_{\text{T}}$ ( GeV/c )	$2 < y < 2.5$	$2.5 < y < 3$	$3 < y < 3.5$	$3.5 < y < 4$	$4 < y < 4.5$
0-1	$0.576 \pm 0.001$	$0.824 \pm 0.001$	$0.915 \pm 0.001$	$0.904 \pm 0.001$	$0.783 \pm 0.001$
1-2	$0.607 \pm 0.001$	$0.834 \pm 0.001$	$0.915 \pm 0.001$	$0.908 \pm 0.001$	$0.808 \pm 0.001$
2-3	$0.654 \pm 0.001$	$0.866 \pm 0.001$	$0.937 \pm 0.001$	$0.930 \pm 0.001$	$0.845 \pm 0.001$
3-4	$0.710 \pm 0.001$	$0.899 \pm 0.001$	$0.953 \pm 0.001$	$0.950 \pm 0.001$	$0.880 \pm 0.001$
4-5	$0.759 \pm 0.001$	$0.923 \pm 0.001$	$0.969 \pm 0.001$	$0.967 \pm 0.001$	$0.910 \pm 0.002$
5-6	$0.802 \pm 0.002$	$0.941 \pm 0.001$	$0.978 \pm 0.001$	$0.976 \pm 0.001$	$0.927 \pm 0.002$
6-7	$0.838 \pm 0.002$	$0.954 \pm 0.001$	$0.984 \pm 0.001$	$0.980 \pm 0.001$	$0.946 \pm 0.002$
7-8	$0.864 \pm 0.003$	$0.966 \pm 0.002$	$0.989 \pm 0.001$	$0.986 \pm 0.001$	$0.950 \pm 0.003$
8-10	$0.896 \pm 0.003$	$0.979 \pm 0.001$	$0.993 \pm 0.001$	$0.989 \pm 0.001$	$0.963 \pm 0.003$
10-14	$0.933 \pm 0.003$	$0.988 \pm 0.001$	$0.999 \pm 0.001$	$0.990 \pm 0.002$	$0.970 \pm 0.005$
14-20				$0.983 \pm 0.002(2 < y < 4.5)$	

 Table C.4: The reconstruction-selection efficiencies  $\varepsilon_{\text{rec\&sel}}$  in  $(p_{\text{T}}, y)$  bins for prompt  $J/\psi$ .

$p_{\text{T}}$ ( GeV/c )	$2 < y < 2.5$	$2.5 < y < 3$	$3 < y < 3.5$	$3.5 < y < 4$	$4 < y < 4.5$
0-1	$0.335 \pm 0.001$	$0.653 \pm 0.001$	$0.748 \pm 0.001$	$0.715 \pm 0.001$	$0.536 \pm 0.002$
1-2	$0.343 \pm 0.001$	$0.631 \pm 0.001$	$0.708 \pm 0.001$	$0.679 \pm 0.001$	$0.529 \pm 0.001$
2-3	$0.330 \pm 0.001$	$0.600 \pm 0.001$	$0.691 \pm 0.001$	$0.659 \pm 0.001$	$0.504 \pm 0.001$
3-4	$0.301 \pm 0.001$	$0.589 \pm 0.001$	$0.671 \pm 0.001$	$0.641 \pm 0.001$	$0.494 \pm 0.002$
4-5	$0.318 \pm 0.002$	$0.623 \pm 0.002$	$0.683 \pm 0.002$	$0.656 \pm 0.002$	$0.531 \pm 0.002$
5-6	$0.349 \pm 0.002$	$0.666 \pm 0.002$	$0.709 \pm 0.002$	$0.683 \pm 0.003$	$0.565 \pm 0.004$
6-7	$0.382 \pm 0.003$	$0.700 \pm 0.003$	$0.729 \pm 0.003$	$0.704 \pm 0.004$	$0.613 \pm 0.005$
7-8	$0.408 \pm 0.004$	$0.721 \pm 0.004$	$0.751 \pm 0.004$	$0.718 \pm 0.005$	$0.638 \pm 0.007$
8-10	$0.441 \pm 0.005$	$0.753 \pm 0.004$	$0.765 \pm 0.005$	$0.737 \pm 0.006$	$0.656 \pm 0.008$
10-14	$0.494 \pm 0.007$	$0.786 \pm 0.006$	$0.793 \pm 0.007$	$0.761 \pm 0.009$	$0.701 \pm 0.014$
14-20				$0.703 \pm 0.008(2 < y < 4.5)$	

 Table C.5: The reconstruction-selection efficiencies  $\varepsilon_{\text{rec\&sel}}$  in  $(p_{\text{T}}, y)$  bins for  $J/\psi$  from  $b$ .

$p_{\text{T}}$ ( GeV/c )	$2 < y < 2.5$	$2.5 < y < 3$	$3 < y < 3.5$	$3.5 < y < 4$	$4 < y < 4.5$
0-1	$0.328 \pm 0.005$	$0.641 \pm 0.005$	$0.732 \pm 0.005$	$0.684 \pm 0.005$	$0.524 \pm 0.008$
1-2	$0.336 \pm 0.003$	$0.625 \pm 0.003$	$0.696 \pm 0.003$	$0.671 \pm 0.004$	$0.531 \pm 0.005$
2-3	$0.317 \pm 0.003$	$0.591 \pm 0.003$	$0.681 \pm 0.003$	$0.653 \pm 0.004$	$0.508 \pm 0.006$
3-4	$0.289 \pm 0.003$	$0.587 \pm 0.004$	$0.669 \pm 0.004$	$0.634 \pm 0.005$	$0.495 \pm 0.007$
4-5	$0.303 \pm 0.004$	$0.618 \pm 0.004$	$0.672 \pm 0.005$	$0.645 \pm 0.006$	$0.534 \pm 0.009$
5-6	$0.337 \pm 0.005$	$0.656 \pm 0.005$	$0.696 \pm 0.006$	$0.691 \pm 0.008$	$0.573 \pm 0.013$
6-7	$0.364 \pm 0.006$	$0.681 \pm 0.006$	$0.726 \pm 0.007$	$0.688 \pm 0.010$	$0.600 \pm 0.016$
7-8	$0.385 \pm 0.008$	$0.691 \pm 0.008$	$0.732 \pm 0.009$	$0.712 \pm 0.013$	$0.612 \pm 0.023$
8-10	$0.434 \pm 0.008$	$0.739 \pm 0.007$	$0.742 \pm 0.009$	$0.720 \pm 0.014$	$0.654 \pm 0.024$
10-14	$0.492 \pm 0.010$	$0.774 \pm 0.009$	$0.781 \pm 0.012$	$0.731 \pm 0.020$	$0.629 \pm 0.043$
14-20				$0.657 \pm 0.011(2 < y < 4.5)$	

Table C.6: The reconstruction-selection efficiencies  $\varepsilon_{\text{rec}\&\text{sel}}$  in  $(p_T, y)$  bins for inclusive  $J/\psi$ .

$p_T$ ( GeV/c )	$2 < y < 2.5$	$2.5 < y < 3$	$3 < y < 3.5$	$3.5 < y < 4$	$4 < y < 4.5$
0-1	$0.334 \pm 0.001$	$0.652 \pm 0.001$	$0.747 \pm 0.001$	$0.713 \pm 0.001$	$0.536 \pm 0.002$
1-2	$0.342 \pm 0.001$	$0.631 \pm 0.001$	$0.707 \pm 0.001$	$0.678 \pm 0.001$	$0.529 \pm 0.001$
2-3	$0.328 \pm 0.001$	$0.599 \pm 0.001$	$0.690 \pm 0.001$	$0.658 \pm 0.001$	$0.504 \pm 0.001$
3-4	$0.299 \pm 0.001$	$0.589 \pm 0.001$	$0.671 \pm 0.001$	$0.640 \pm 0.001$	$0.494 \pm 0.002$
4-5	$0.316 \pm 0.002$	$0.623 \pm 0.002$	$0.682 \pm 0.002$	$0.655 \pm 0.002$	$0.531 \pm 0.002$
5-6	$0.347 \pm 0.002$	$0.664 \pm 0.002$	$0.708 \pm 0.002$	$0.684 \pm 0.003$	$0.566 \pm 0.003$
6-7	$0.378 \pm 0.003$	$0.696 \pm 0.003$	$0.729 \pm 0.003$	$0.702 \pm 0.004$	$0.611 \pm 0.005$
7-8	$0.403 \pm 0.004$	$0.715 \pm 0.004$	$0.747 \pm 0.004$	$0.717 \pm 0.005$	$0.635 \pm 0.007$
8-10	$0.440 \pm 0.004$	$0.750 \pm 0.004$	$0.760 \pm 0.004$	$0.734 \pm 0.005$	$0.655 \pm 0.008$
10-14	$0.493 \pm 0.005$	$0.783 \pm 0.005$	$0.790 \pm 0.006$	$0.754 \pm 0.008$	$0.685 \pm 0.014$
14-20				$0.682 \pm 0.007$	$(2 < y < 4.5)$

Table C.7: The PID efficiencies  $\varepsilon_{\text{PID}}$  in  $(p_T, y)$  bins for prompt  $J/\psi$ .

$p_T$ ( GeV/c )	$2 < y < 2.5$	$2.5 < y < 3$	$3 < y < 3.5$	$3.5 < y < 4$	$4 < y < 4.5$
0-1	$0.794 \pm 0.002$	$0.833 \pm 0.001$	$0.830 \pm 0.001$	$0.806 \pm 0.002$	$0.719 \pm 0.002$
1-2	$0.803 \pm 0.002$	$0.837 \pm 0.001$	$0.837 \pm 0.001$	$0.807 \pm 0.001$	$0.697 \pm 0.002$
2-3	$0.828 \pm 0.002$	$0.848 \pm 0.001$	$0.849 \pm 0.001$	$0.811 \pm 0.001$	$0.691 \pm 0.002$
3-4	$0.844 \pm 0.002$	$0.863 \pm 0.002$	$0.871 \pm 0.001$	$0.828 \pm 0.002$	$0.693 \pm 0.003$
4-5	$0.861 \pm 0.003$	$0.884 \pm 0.002$	$0.892 \pm 0.002$	$0.849 \pm 0.002$	$0.705 \pm 0.004$
5-6	$0.880 \pm 0.003$	$0.901 \pm 0.002$	$0.908 \pm 0.002$	$0.868 \pm 0.003$	$0.713 \pm 0.005$
6-7	$0.897 \pm 0.004$	$0.913 \pm 0.003$	$0.919 \pm 0.003$	$0.882 \pm 0.004$	$0.723 \pm 0.007$
7-8	$0.911 \pm 0.005$	$0.920 \pm 0.004$	$0.927 \pm 0.004$	$0.895 \pm 0.005$	$0.736 \pm 0.009$
8-10	$0.924 \pm 0.005$	$0.925 \pm 0.004$	$0.932 \pm 0.004$	$0.903 \pm 0.006$	$0.742 \pm 0.011$
10-14	$0.935 \pm 0.006$	$0.925 \pm 0.006$	$0.939 \pm 0.006$	$0.917 \pm 0.009$	$0.744 \pm 0.018$
14-20				$0.930 \pm 0.007$	$(2 < y < 4.5)$

Table C.8: The PID efficiencies  $\varepsilon_{\text{PID}}$  in  $(p_T, y)$  bins for  $J/\psi$  from  $b$ .

$p_T$ ( GeV/c )	$2 < y < 2.5$	$2.5 < y < 3$	$3 < y < 3.5$	$3.5 < y < 4$	$4 < y < 4.5$
0-1	$0.791 \pm 0.009$	$0.833 \pm 0.006$	$0.829 \pm 0.006$	$0.805 \pm 0.007$	$0.723 \pm 0.012$
1-2	$0.802 \pm 0.006$	$0.837 \pm 0.004$	$0.838 \pm 0.004$	$0.808 \pm 0.005$	$0.701 \pm 0.008$
2-3	$0.827 \pm 0.006$	$0.849 \pm 0.004$	$0.849 \pm 0.004$	$0.811 \pm 0.005$	$0.698 \pm 0.009$
3-4	$0.843 \pm 0.006$	$0.863 \pm 0.004$	$0.872 \pm 0.004$	$0.829 \pm 0.006$	$0.703 \pm 0.011$
4-5	$0.859 \pm 0.007$	$0.884 \pm 0.005$	$0.890 \pm 0.005$	$0.850 \pm 0.007$	$0.702 \pm 0.013$
5-6	$0.880 \pm 0.008$	$0.901 \pm 0.005$	$0.909 \pm 0.006$	$0.870 \pm 0.009$	$0.733 \pm 0.017$
6-7	$0.898 \pm 0.009$	$0.913 \pm 0.006$	$0.919 \pm 0.007$	$0.883 \pm 0.011$	$0.733 \pm 0.022$
7-8	$0.912 \pm 0.010$	$0.921 \pm 0.008$	$0.928 \pm 0.009$	$0.899 \pm 0.013$	$0.735 \pm 0.032$
8-10	$0.925 \pm 0.008$	$0.925 \pm 0.007$	$0.933 \pm 0.008$	$0.907 \pm 0.014$	$0.750 \pm 0.032$
10-14	$0.934 \pm 0.009$	$0.927 \pm 0.009$	$0.936 \pm 0.011$	$0.913 \pm 0.020$	$0.760 \pm 0.053$
14-20				$0.932 \pm 0.010$	$(2 < y < 4.5)$

Table C.9: The PID efficiencies  $\varepsilon_{\text{PID}}$  in  $(p_{\text{T}}, y)$  bins for inclusive  $J/\psi$ .

$p_{\text{T}}$ ( GeV/c )	$2 < y < 2.5$	$2.5 < y < 3$	$3 < y < 3.5$	$3.5 < y < 4$	$4 < y < 4.5$
0-1	$0.794 \pm 0.002$	$0.833 \pm 0.001$	$0.830 \pm 0.001$	$0.806 \pm 0.001$	$0.719 \pm 0.002$
1-2	$0.803 \pm 0.002$	$0.837 \pm 0.001$	$0.837 \pm 0.001$	$0.807 \pm 0.001$	$0.697 \pm 0.002$
2-3	$0.828 \pm 0.002$	$0.848 \pm 0.001$	$0.849 \pm 0.001$	$0.811 \pm 0.001$	$0.691 \pm 0.002$
3-4	$0.844 \pm 0.002$	$0.863 \pm 0.001$	$0.871 \pm 0.001$	$0.829 \pm 0.002$	$0.694 \pm 0.003$
4-5	$0.860 \pm 0.003$	$0.884 \pm 0.002$	$0.891 \pm 0.002$	$0.850 \pm 0.002$	$0.704 \pm 0.004$
5-6	$0.880 \pm 0.003$	$0.901 \pm 0.002$	$0.908 \pm 0.002$	$0.868 \pm 0.003$	$0.714 \pm 0.005$
6-7	$0.897 \pm 0.004$	$0.913 \pm 0.003$	$0.919 \pm 0.003$	$0.882 \pm 0.004$	$0.724 \pm 0.007$
7-8	$0.911 \pm 0.005$	$0.921 \pm 0.003$	$0.927 \pm 0.004$	$0.895 \pm 0.005$	$0.736 \pm 0.009$
8-10	$0.925 \pm 0.004$	$0.925 \pm 0.003$	$0.932 \pm 0.004$	$0.904 \pm 0.005$	$0.743 \pm 0.010$
10-14	$0.934 \pm 0.005$	$0.926 \pm 0.005$	$0.938 \pm 0.005$	$0.916 \pm 0.008$	$0.747 \pm 0.018$
14-20				$0.931 \pm 0.006(2 < y < 4.5)$	

 Table C.10: The trigger efficiencies  $\varepsilon_{\text{trig}}$  in  $(p_{\text{T}}, y)$  bins for prompt  $J/\psi$ .

$p_{\text{T}}$ ( GeV/c )	$2 < y < 2.5$	$2.5 < y < 3$	$3 < y < 3.5$	$3.5 < y < 4$	$4 < y < 4.5$
0-1	$0.673 \pm 0.002$	$0.748 \pm 0.001$	$0.782 \pm 0.001$	$0.791 \pm 0.001$	$0.702 \pm 0.002$
1-2	$0.726 \pm 0.002$	$0.790 \pm 0.001$	$0.804 \pm 0.001$	$0.803 \pm 0.001$	$0.738 \pm 0.002$
2-3	$0.784 \pm 0.002$	$0.824 \pm 0.001$	$0.828 \pm 0.001$	$0.814 \pm 0.001$	$0.758 \pm 0.002$
3-4	$0.827 \pm 0.002$	$0.853 \pm 0.001$	$0.857 \pm 0.001$	$0.837 \pm 0.002$	$0.775 \pm 0.003$
4-5	$0.848 \pm 0.002$	$0.872 \pm 0.002$	$0.877 \pm 0.002$	$0.859 \pm 0.002$	$0.804 \pm 0.004$
5-6	$0.870 \pm 0.003$	$0.890 \pm 0.002$	$0.885 \pm 0.002$	$0.874 \pm 0.002$	$0.822 \pm 0.005$
6-7	$0.879 \pm 0.004$	$0.895 \pm 0.002$	$0.890 \pm 0.003$	$0.884 \pm 0.003$	$0.841 \pm 0.006$
7-8	$0.882 \pm 0.005$	$0.898 \pm 0.003$	$0.889 \pm 0.004$	$0.889 \pm 0.004$	$0.869 \pm 0.007$
8-10	$0.902 \pm 0.004$	$0.902 \pm 0.003$	$0.895 \pm 0.004$	$0.893 \pm 0.005$	$0.852 \pm 0.009$
10-14	$0.901 \pm 0.006$	$0.909 \pm 0.005$	$0.893 \pm 0.006$	$0.909 \pm 0.007$	$0.856 \pm 0.015$
14-20				$0.907 \pm 0.006(2 < y < 4.5)$	

 Table C.11: The trigger efficiencies  $\varepsilon_{\text{trig}}$  in  $(p_{\text{T}}, y)$  bins for  $J/\psi$  from  $b$ .

$p_{\text{T}}$ ( GeV/c )	$2 < y < 2.5$	$2.5 < y < 3$	$3 < y < 3.5$	$3.5 < y < 4$	$4 < y < 4.5$
0-1	$0.672 \pm 0.009$	$0.749 \pm 0.006$	$0.782 \pm 0.005$	$0.797 \pm 0.007$	$0.700 \pm 0.012$
1-2	$0.726 \pm 0.006$	$0.789 \pm 0.004$	$0.804 \pm 0.004$	$0.801 \pm 0.005$	$0.736 \pm 0.008$
2-3	$0.785 \pm 0.006$	$0.820 \pm 0.003$	$0.825 \pm 0.004$	$0.809 \pm 0.005$	$0.737 \pm 0.009$
3-4	$0.831 \pm 0.006$	$0.857 \pm 0.004$	$0.855 \pm 0.004$	$0.834 \pm 0.005$	$0.790 \pm 0.010$
4-5	$0.850 \pm 0.006$	$0.871 \pm 0.004$	$0.865 \pm 0.004$	$0.854 \pm 0.006$	$0.795 \pm 0.013$
5-6	$0.859 \pm 0.007$	$0.875 \pm 0.005$	$0.870 \pm 0.005$	$0.871 \pm 0.007$	$0.841 \pm 0.015$
6-7	$0.876 \pm 0.007$	$0.884 \pm 0.006$	$0.891 \pm 0.006$	$0.886 \pm 0.009$	$0.860 \pm 0.018$
7-8	$0.868 \pm 0.009$	$0.913 \pm 0.006$	$0.877 \pm 0.009$	$0.883 \pm 0.012$	$0.825 \pm 0.029$
8-10	$0.877 \pm 0.008$	$0.890 \pm 0.007$	$0.894 \pm 0.008$	$0.859 \pm 0.013$	$0.820 \pm 0.030$
10-14	$0.904 \pm 0.008$	$0.894 \pm 0.008$	$0.887 \pm 0.011$	$0.874 \pm 0.018$	$0.844 \pm 0.047$
14-20				$0.895 \pm 0.009(2 < y < 4.5)$	

Table C.12: The trigger efficiencies  $\varepsilon_{\text{trig}}$  in  $(p_{\text{T}}, y)$  bins for inclusive  $J/\psi$ .

$p_{\text{T}}$ ( GeV/c )	$2 < y < 2.5$	$2.5 < y < 3$	$3 < y < 3.5$	$3.5 < y < 4$	$4 < y < 4.5$
0-1	$0.673 \pm 0.002$	$0.748 \pm 0.001$	$0.782 \pm 0.001$	$0.792 \pm 0.001$	$0.702 \pm 0.002$
1-2	$0.726 \pm 0.002$	$0.790 \pm 0.001$	$0.804 \pm 0.001$	$0.803 \pm 0.001$	$0.737 \pm 0.002$
2-3	$0.784 \pm 0.002$	$0.823 \pm 0.001$	$0.828 \pm 0.001$	$0.813 \pm 0.001$	$0.757 \pm 0.002$
3-4	$0.827 \pm 0.002$	$0.853 \pm 0.001$	$0.856 \pm 0.001$	$0.837 \pm 0.001$	$0.776 \pm 0.003$
4-5	$0.849 \pm 0.002$	$0.872 \pm 0.001$	$0.875 \pm 0.001$	$0.859 \pm 0.002$	$0.803 \pm 0.003$
5-6	$0.868 \pm 0.003$	$0.888 \pm 0.002$	$0.883 \pm 0.002$	$0.873 \pm 0.002$	$0.824 \pm 0.004$
6-7	$0.879 \pm 0.003$	$0.893 \pm 0.002$	$0.890 \pm 0.002$	$0.884 \pm 0.003$	$0.843 \pm 0.006$
7-8	$0.880 \pm 0.004$	$0.901 \pm 0.003$	$0.887 \pm 0.003$	$0.888 \pm 0.004$	$0.863 \pm 0.008$
8-10	$0.896 \pm 0.004$	$0.900 \pm 0.003$	$0.894 \pm 0.004$	$0.887 \pm 0.005$	$0.847 \pm 0.009$
10-14	$0.902 \pm 0.005$	$0.904 \pm 0.004$	$0.892 \pm 0.005$	$0.901 \pm 0.007$	$0.853 \pm 0.015$
14-20			$0.902 \pm 0.005(2 < y < 4.5)$		

 Table C.13: The total efficiencies  $\varepsilon_{\text{tot}}$  in  $(p_{\text{T}}, y)$  bins for prompt  $J/\psi$ .

$p_{\text{T}}$ ( GeV/c )	$2 < y < 2.5$	$2.5 < y < 3$	$3 < y < 3.5$	$3.5 < y < 4$	$4 < y < 4.5$
0-1	$0.103 \pm 0.001$	$0.335 \pm 0.001$	$0.445 \pm 0.001$	$0.413 \pm 0.001$	$0.212 \pm 0.001$
1-2	$0.121 \pm 0.001$	$0.348 \pm 0.001$	$0.436 \pm 0.001$	$0.400 \pm 0.001$	$0.220 \pm 0.001$
2-3	$0.140 \pm 0.001$	$0.363 \pm 0.001$	$0.455 \pm 0.001$	$0.404 \pm 0.001$	$0.222 \pm 0.001$
3-4	$0.149 \pm 0.001$	$0.390 \pm 0.001$	$0.477 \pm 0.001$	$0.422 \pm 0.002$	$0.234 \pm 0.002$
4-5	$0.176 \pm 0.001$	$0.443 \pm 0.002$	$0.516 \pm 0.002$	$0.463 \pm 0.002$	$0.273 \pm 0.002$
5-6	$0.214 \pm 0.002$	$0.501 \pm 0.002$	$0.556 \pm 0.003$	$0.506 \pm 0.003$	$0.309 \pm 0.003$
6-7	$0.252 \pm 0.003$	$0.544 \pm 0.003$	$0.587 \pm 0.004$	$0.538 \pm 0.004$	$0.354 \pm 0.005$
7-8	$0.283 \pm 0.004$	$0.577 \pm 0.004$	$0.611 \pm 0.005$	$0.563 \pm 0.006$	$0.384 \pm 0.007$
8-10	$0.327 \pm 0.004$	$0.614 \pm 0.005$	$0.633 \pm 0.005$	$0.584 \pm 0.007$	$0.397 \pm 0.008$
10-14	$0.389 \pm 0.006$	$0.651 \pm 0.007$	$0.663 \pm 0.008$	$0.623 \pm 0.010$	$0.434 \pm 0.016$
14-20			$0.581 \pm 0.009(2 < y < 4.5)$		

 Table C.14: The total efficiencies  $\varepsilon_{\text{tot}}$  in  $(p_{\text{T}}, y)$  bins for  $J/\psi$  from  $b$ .

$p_{\text{T}}$ ( GeV/c )	$2 < y < 2.5$	$2.5 < y < 3$	$3 < y < 3.5$	$3.5 < y < 4$	$4 < y < 4.5$
0-1	$0.101 \pm 0.002$	$0.330 \pm 0.003$	$0.430 \pm 0.003$	$0.397 \pm 0.004$	$0.209 \pm 0.004$
1-2	$0.119 \pm 0.001$	$0.344 \pm 0.002$	$0.429 \pm 0.002$	$0.397 \pm 0.003$	$0.222 \pm 0.003$
2-3	$0.134 \pm 0.002$	$0.358 \pm 0.002$	$0.448 \pm 0.003$	$0.402 \pm 0.003$	$0.227 \pm 0.003$
3-4	$0.144 \pm 0.002$	$0.387 \pm 0.003$	$0.476 \pm 0.003$	$0.419 \pm 0.004$	$0.236 \pm 0.004$
4-5	$0.168 \pm 0.002$	$0.440 \pm 0.003$	$0.507 \pm 0.004$	$0.458 \pm 0.005$	$0.273 \pm 0.005$
5-6	$0.208 \pm 0.003$	$0.495 \pm 0.004$	$0.546 \pm 0.005$	$0.510 \pm 0.006$	$0.311 \pm 0.008$
6-7	$0.241 \pm 0.005$	$0.529 \pm 0.006$	$0.585 \pm 0.007$	$0.526 \pm 0.009$	$0.345 \pm 0.011$
7-8	$0.266 \pm 0.006$	$0.553 \pm 0.007$	$0.593 \pm 0.008$	$0.559 \pm 0.011$	$0.377 \pm 0.016$
8-10	$0.324 \pm 0.006$	$0.602 \pm 0.007$	$0.615 \pm 0.009$	$0.572 \pm 0.012$	$0.404 \pm 0.017$
10-14	$0.385 \pm 0.008$	$0.639 \pm 0.009$	$0.654 \pm 0.012$	$0.595 \pm 0.018$	$0.388 \pm 0.030$
14-20			$0.540 \pm 0.011(2 < y < 4.5)$		

## D Plots of the $t_z$ fit

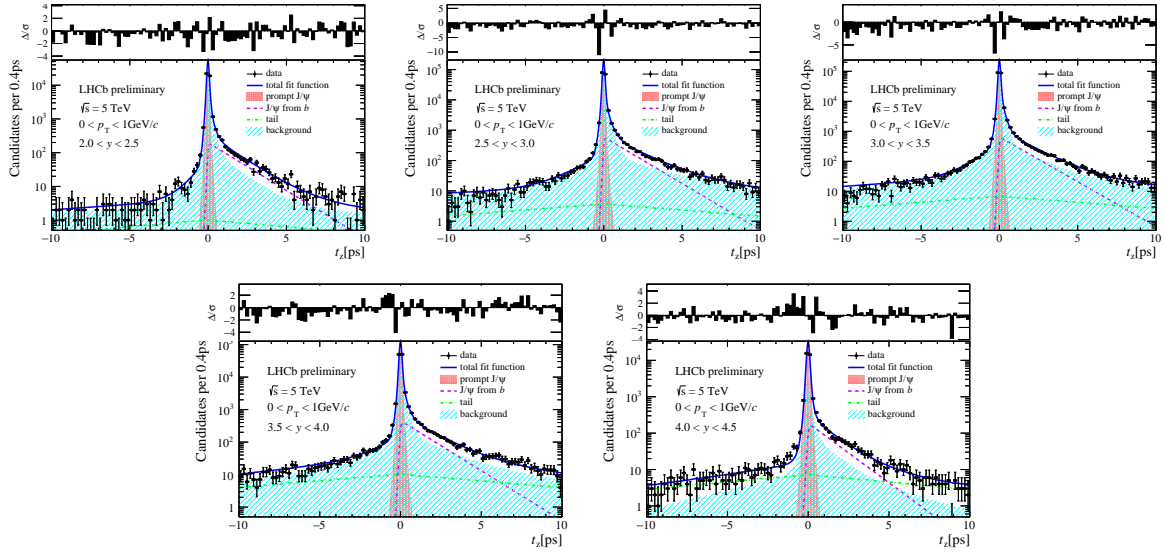


Figure D.1:  $t_z$  fit in bins of  $y$  with  $0 < p_T < 1 \text{ GeV}/c$ .

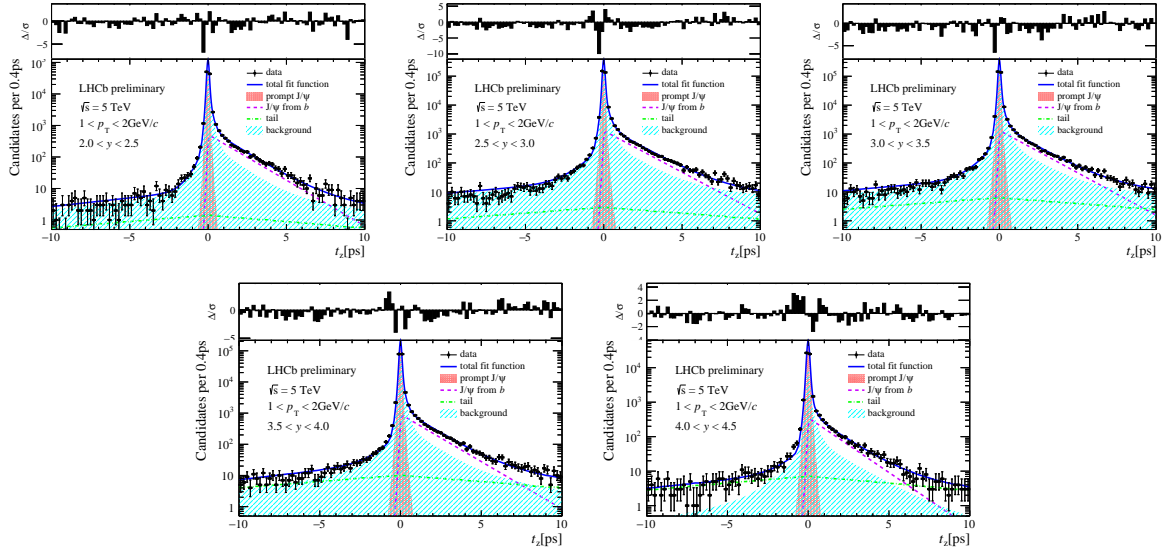


Figure D.2:  $t_z$  fit in bins of  $y$  with  $1 < p_T < 2 \text{ GeV}/c$ .

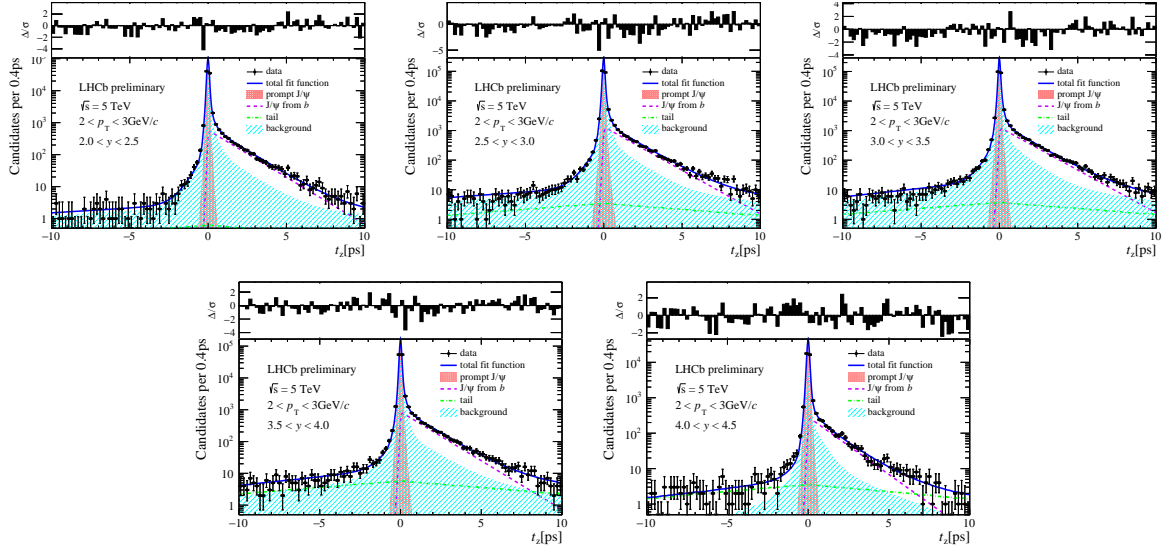


Figure D.3:  $t_z$  fit in bins of  $y$  with  $2 < p_T < 3 \text{ GeV}/c$ .

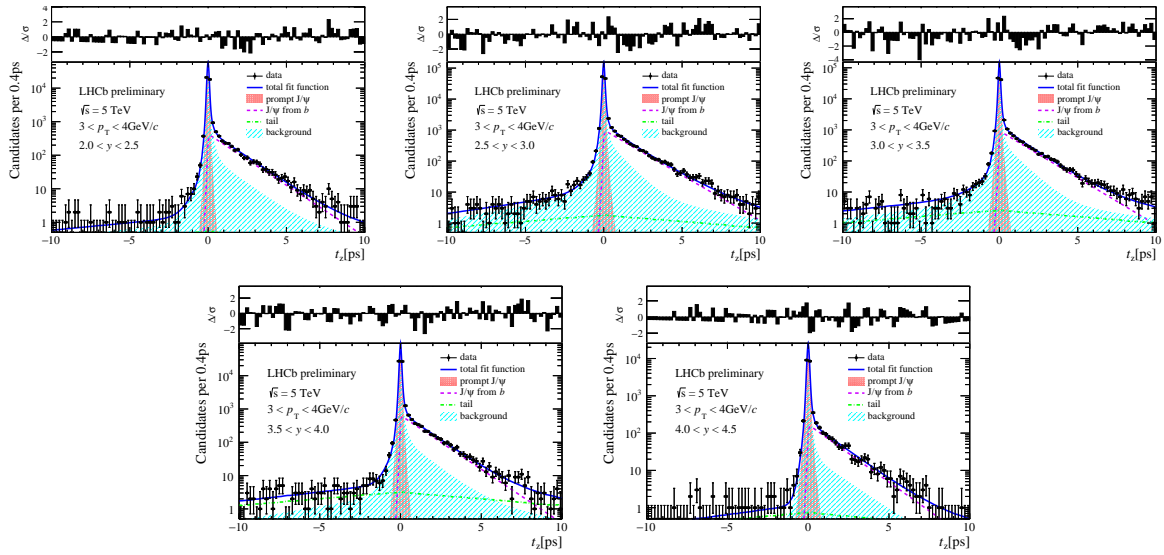


Figure D.4:  $t_z$  fit in bins of  $y$  with  $3 < p_T < 4 \text{ GeV}/c$ .

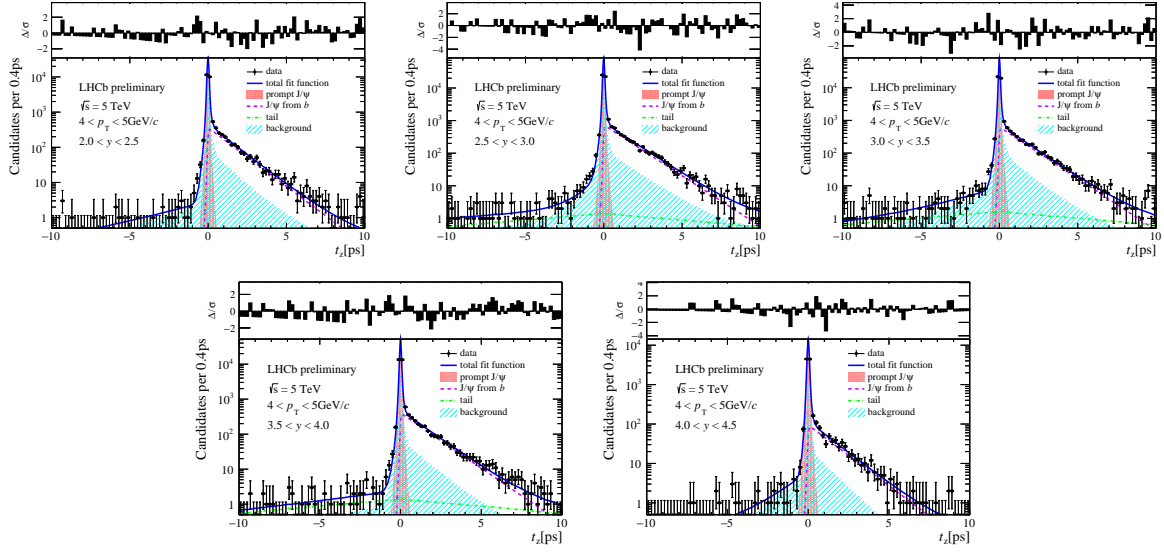


Figure D.5:  $t_z$  fit in bins of  $y$  with  $4 < p_T < 5 \text{ GeV}/c$ .

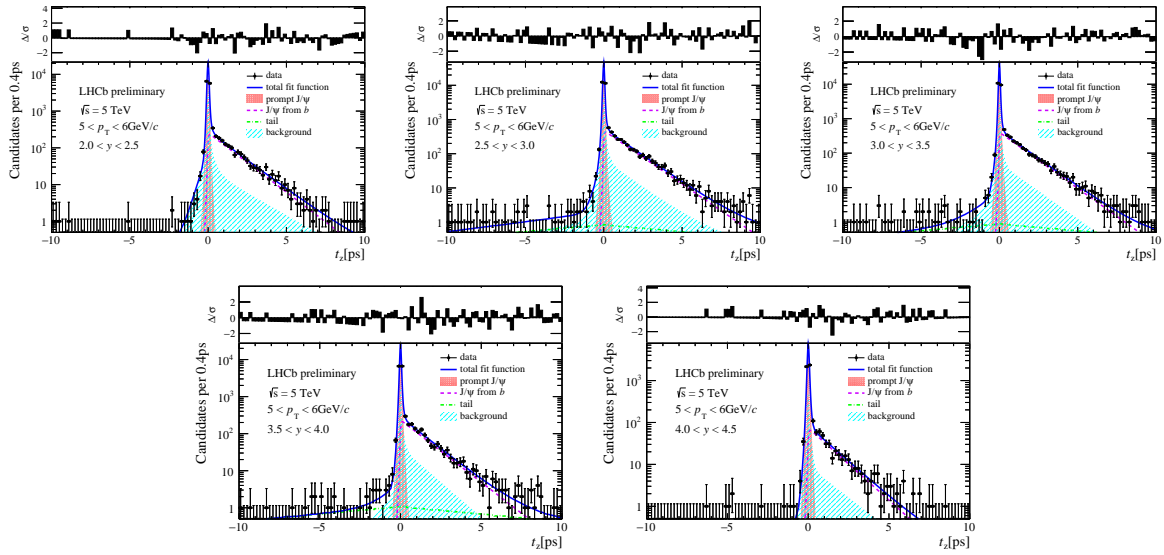


Figure D.6:  $t_z$  fit in bins of  $y$  with  $5 < p_T < 6 \text{ GeV}/c$ .

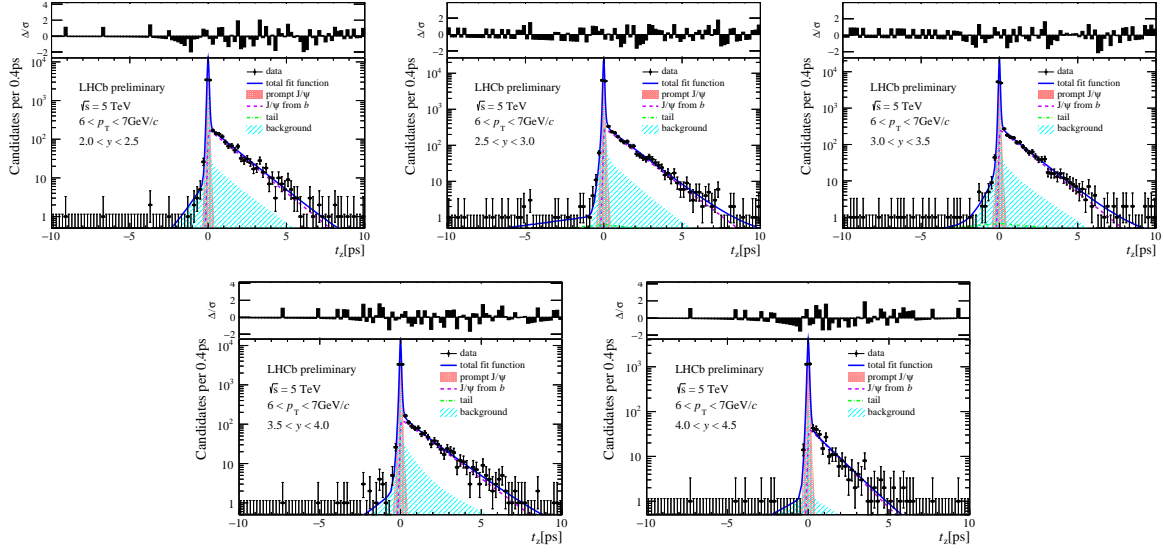


Figure D.7:  $t_z$  fit in bins of  $y$  with  $6 < p_T < 7 \text{ GeV}/c$ .

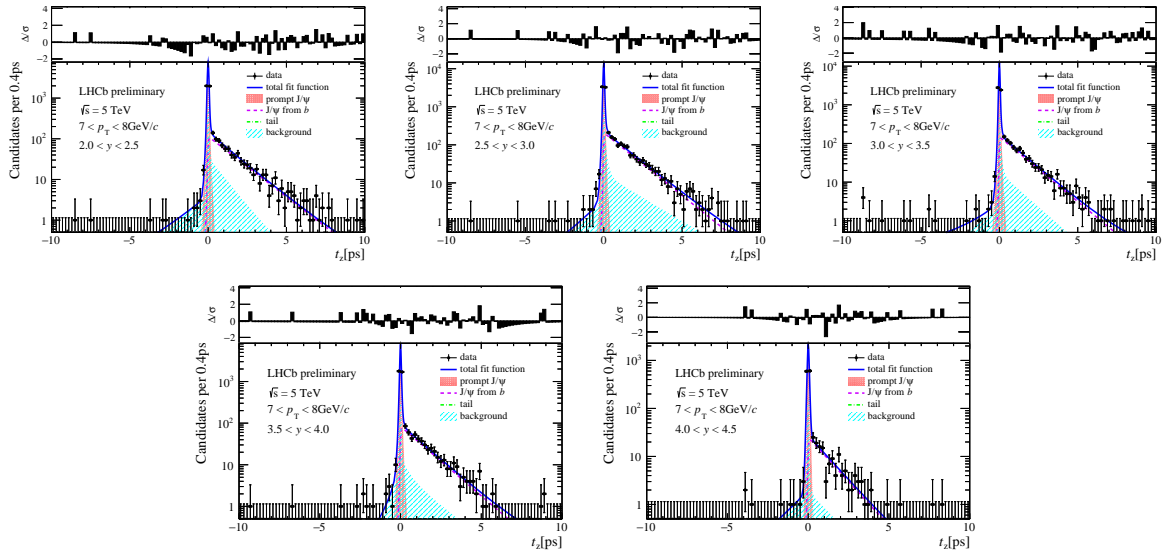


Figure D.8:  $t_z$  fit in bins of  $y$  with  $7 < p_T < 8 \text{ GeV}/c$ .

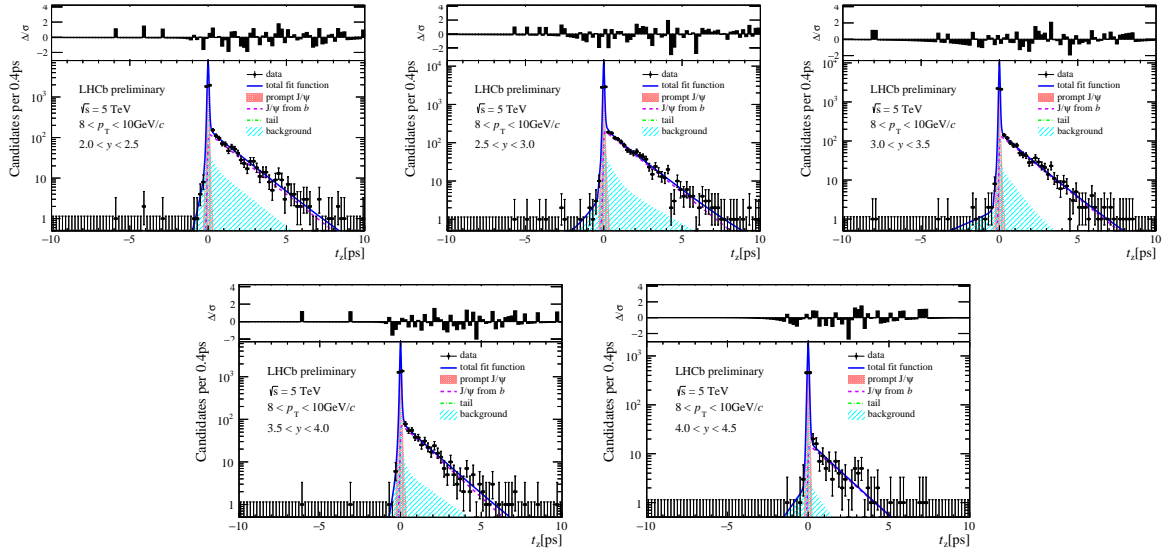


Figure D.9:  $t_z$  fit in bins of  $y$  with  $8 < p_T < 10 \text{ GeV}/c$ .

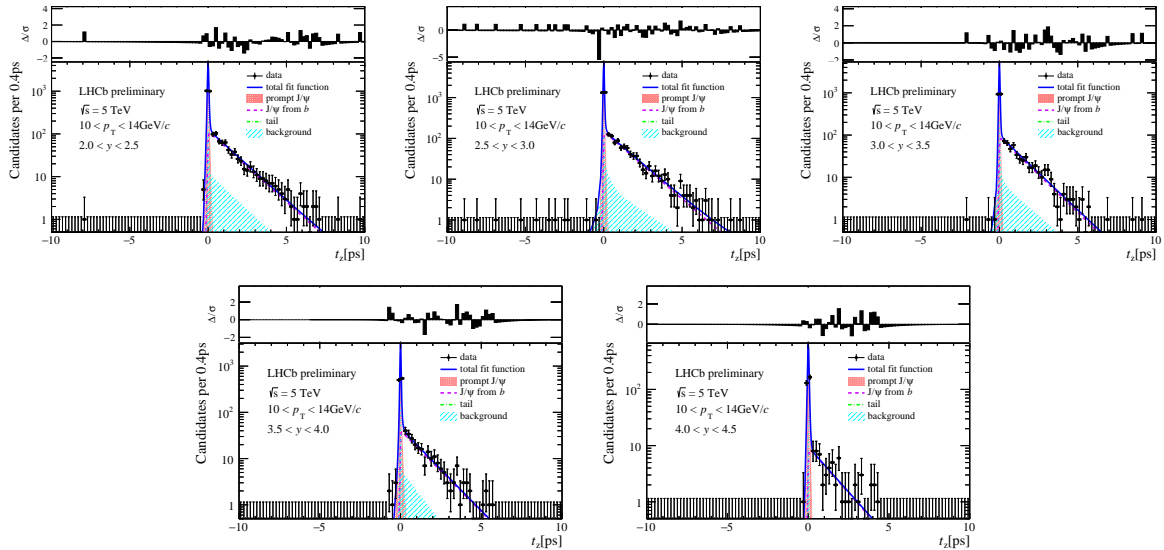


Figure D.10:  $t_z$  fit in bins of  $y$  with  $10 < p_T < 14 \text{ GeV}/c$ .

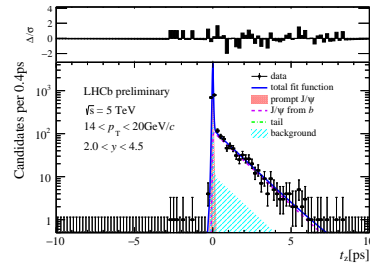


Figure D.11:  $t_z$  fit with  $2.0 < y < 4.5$  and  $14 < p_T < 20 \text{ GeV}/c$ .

## E Plots of the invariant mass fit

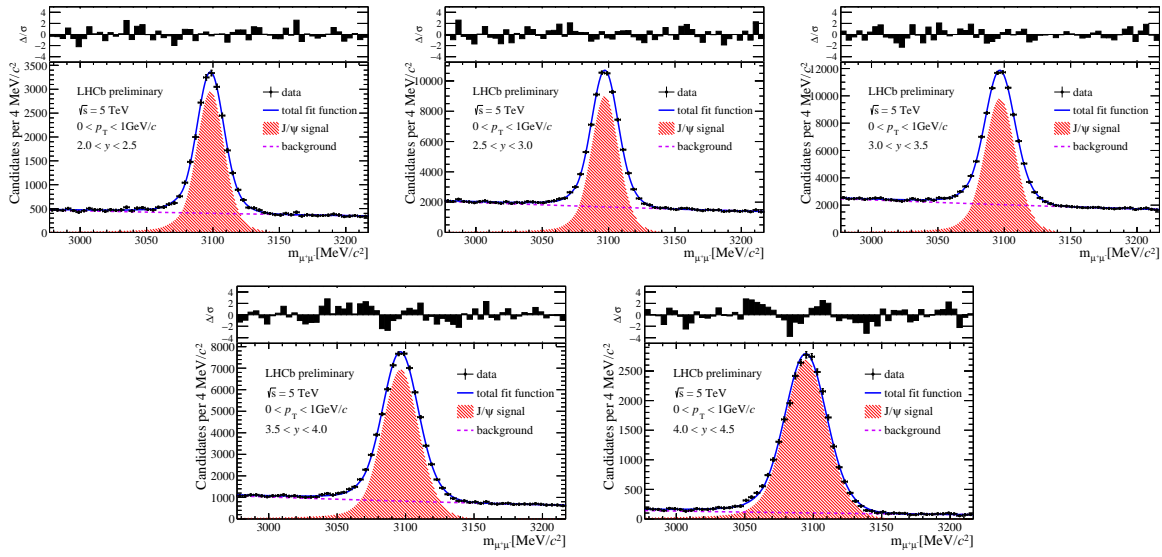


Figure E.1: Invariant mass fit in bins of  $y$  with  $0 < p_T < 1 \text{ GeV}/c$ .

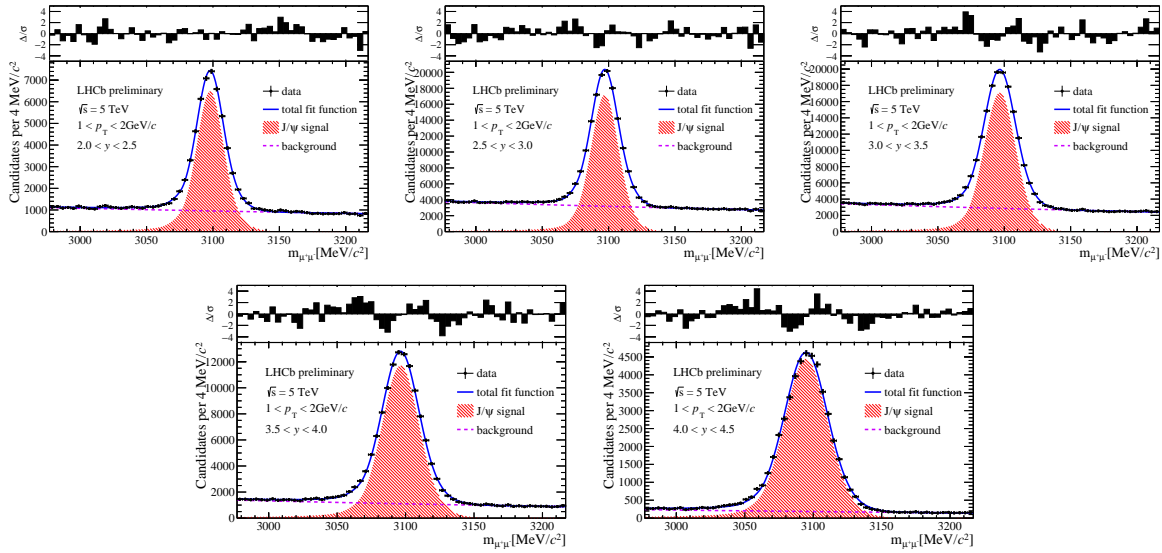


Figure E.2: Invariant mass fit in bins of  $y$  with  $1 < p_T < 2 \text{ GeV}/c$ .

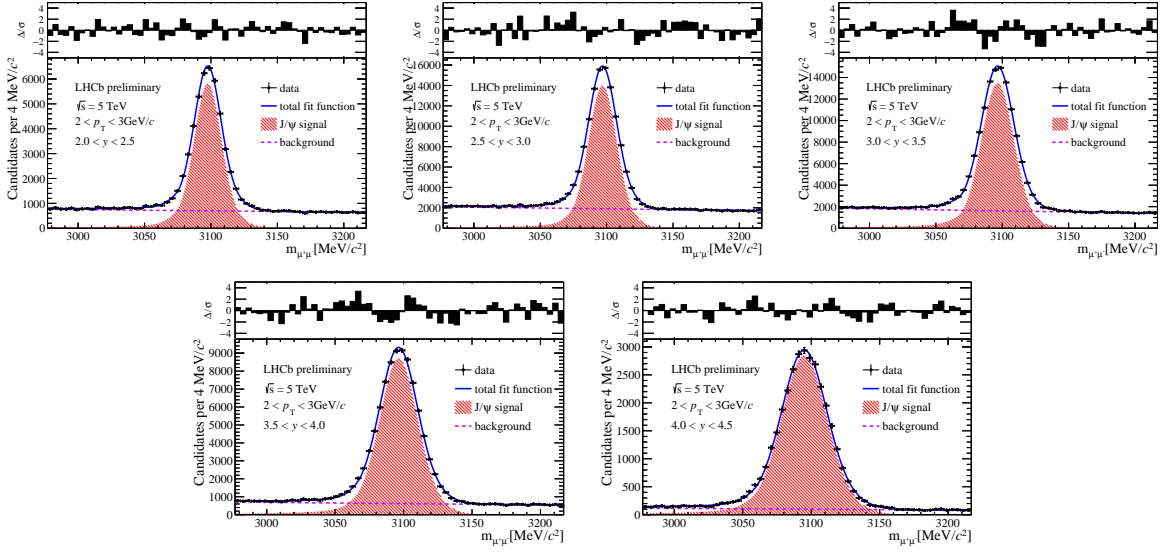


Figure E.3: Invariant mass fit in bins of  $y$  with  $2 < p_T < 3 \text{ GeV}/c$ .

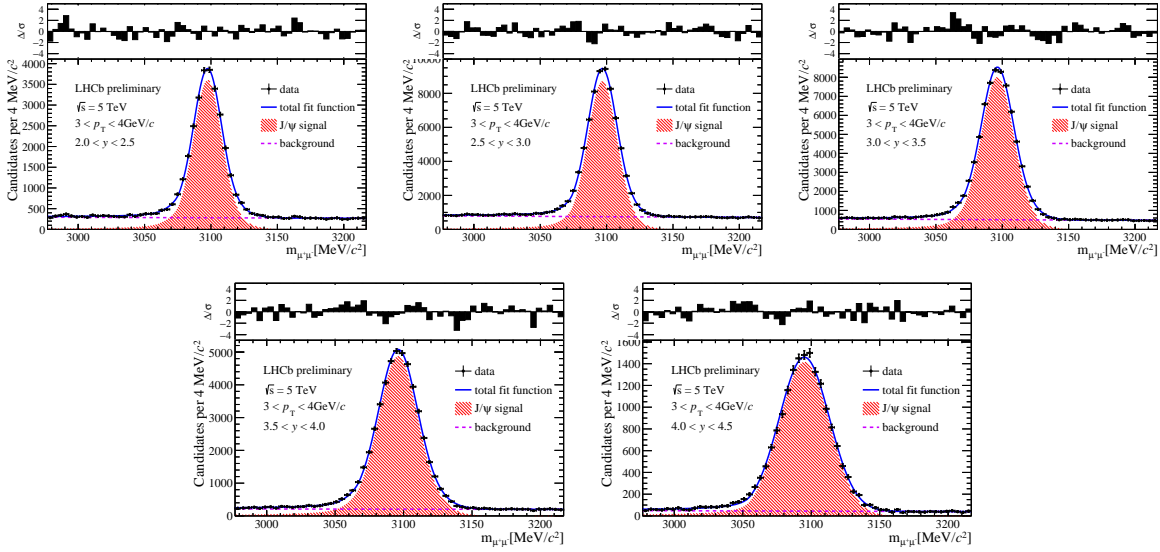


Figure E.4: Invariant mass fit in bins of  $y$  with  $3 < p_T < 4 \text{ GeV}/c$ .

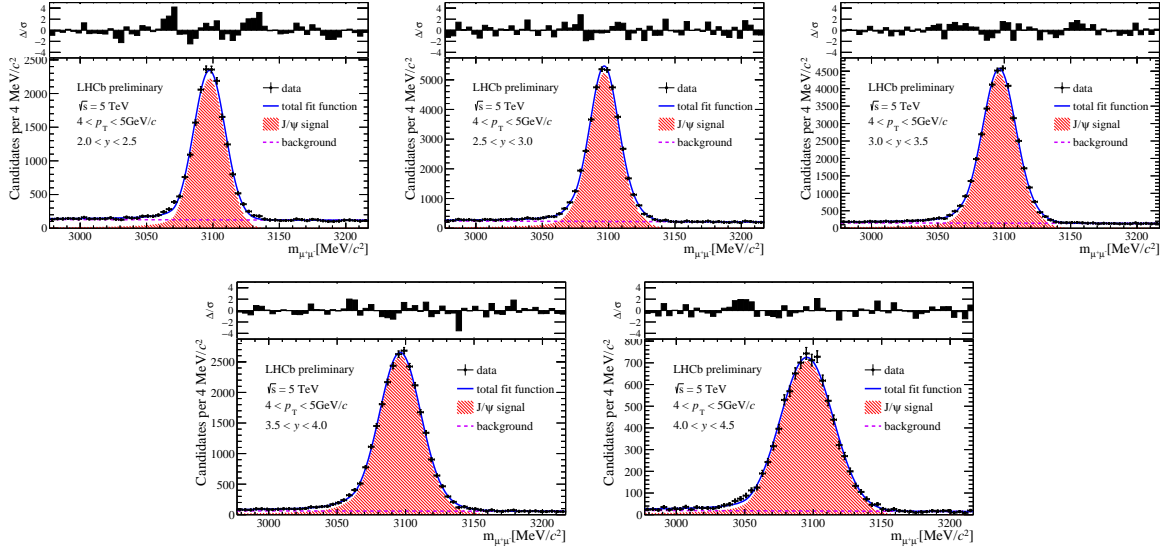


Figure E.5: Invariant mass fit in bins of  $y$  with  $4 < p_T < 5 \text{ GeV}/c$ .

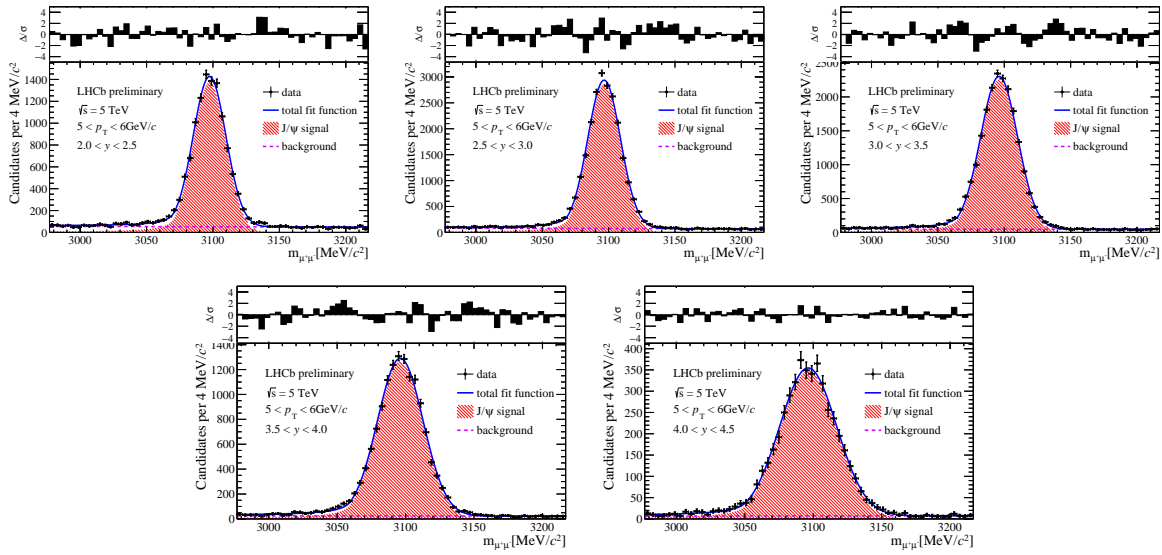


Figure E.6: Invariant mass fit in bins of  $y$  with  $5 < p_T < 6 \text{ GeV}/c$ .

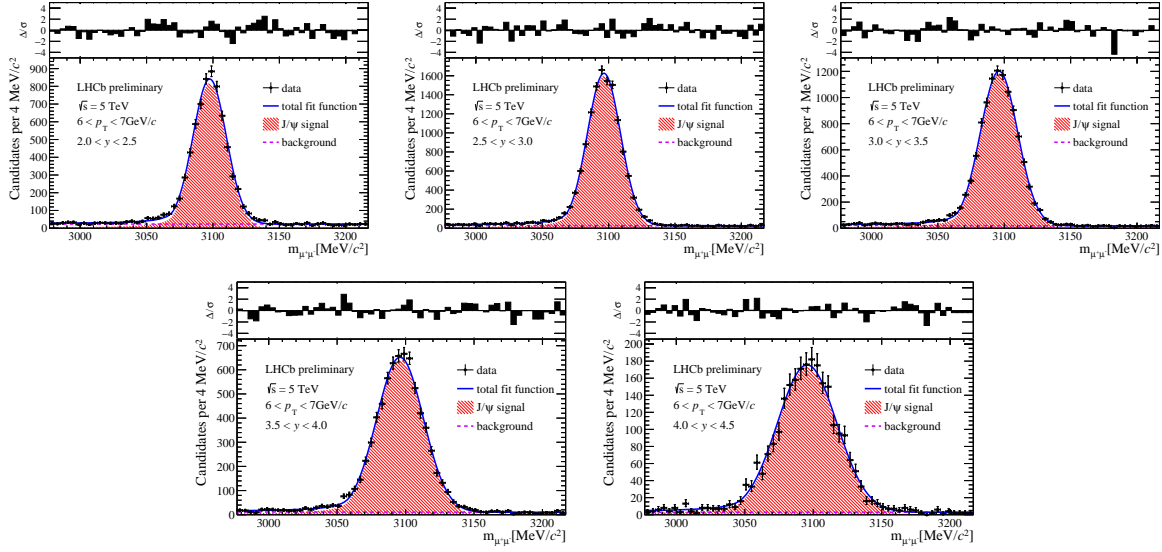


Figure E.7: Invariant mass fit in bins of  $y$  with  $6 < p_T < 7 \text{ GeV}/c$ .

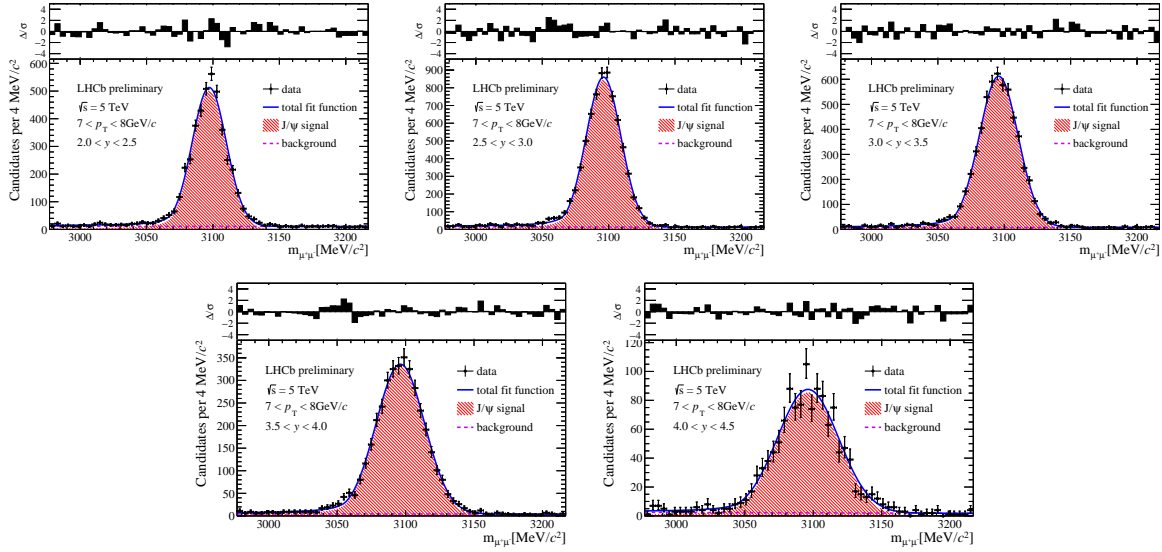


Figure E.8: Invariant mass fit in bins of  $y$  with  $7 < p_T < 8 \text{ GeV}/c$ .

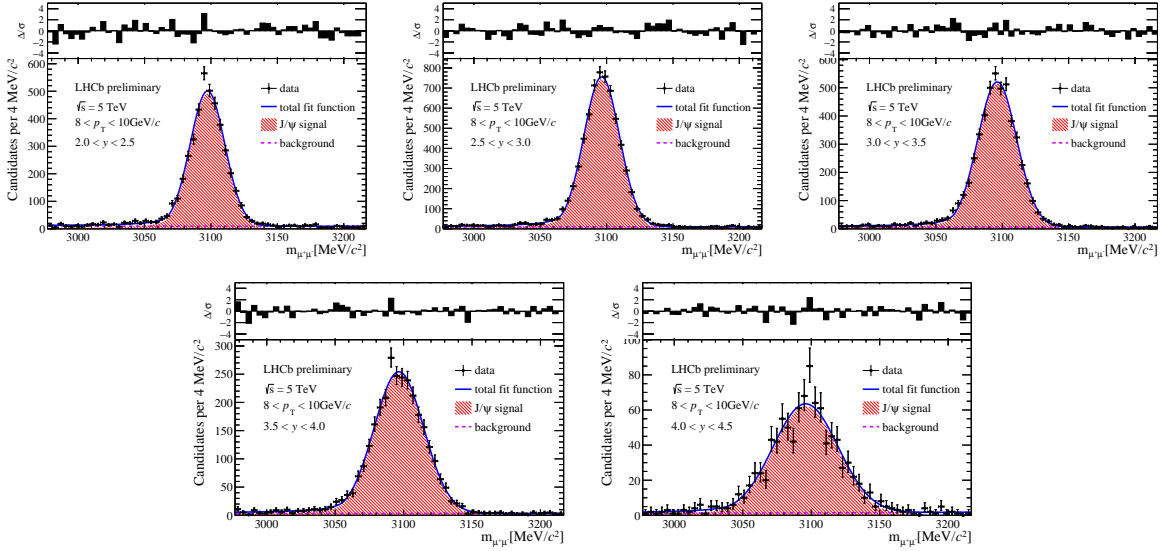


Figure E.9: Invariant mass fit in bins of  $y$  with  $8 < p_T < 10 \text{ GeV}/c$ .

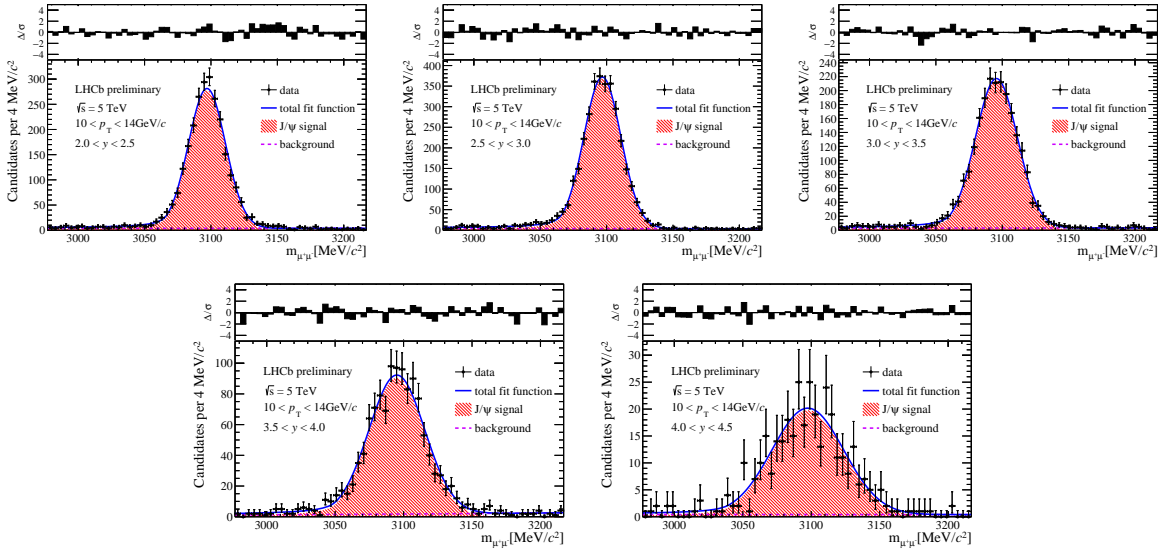


Figure E.10: Invariant mass fit in bins of  $y$  with  $10 < p_T < 14 \text{ GeV}/c$ .

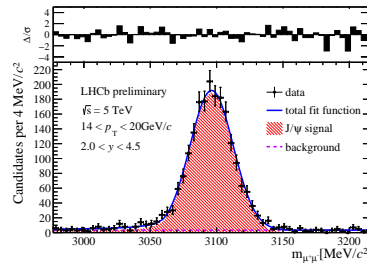


Figure E.11: Invariant mass fit with  $2.0 < y < 4.5$  and  $14 < p_T < 20 \text{ GeV}/c$ .

750 F Plots of the  $t_z$  background fit

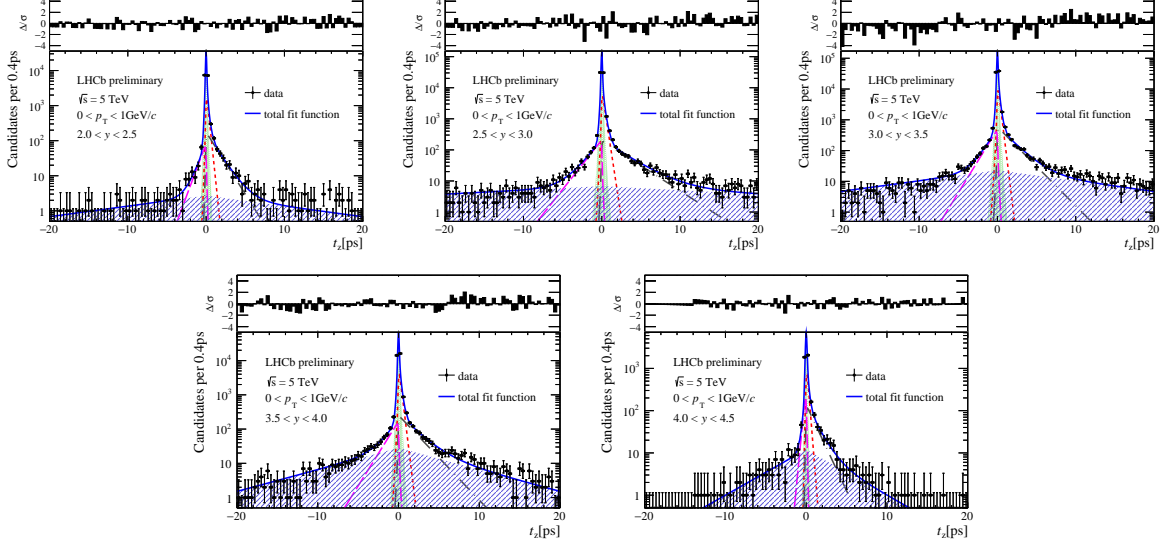


Figure F.1:  $t_z$  background fit in bins of  $y$  with  $0 < p_T < 1 \text{ GeV}/c$ .

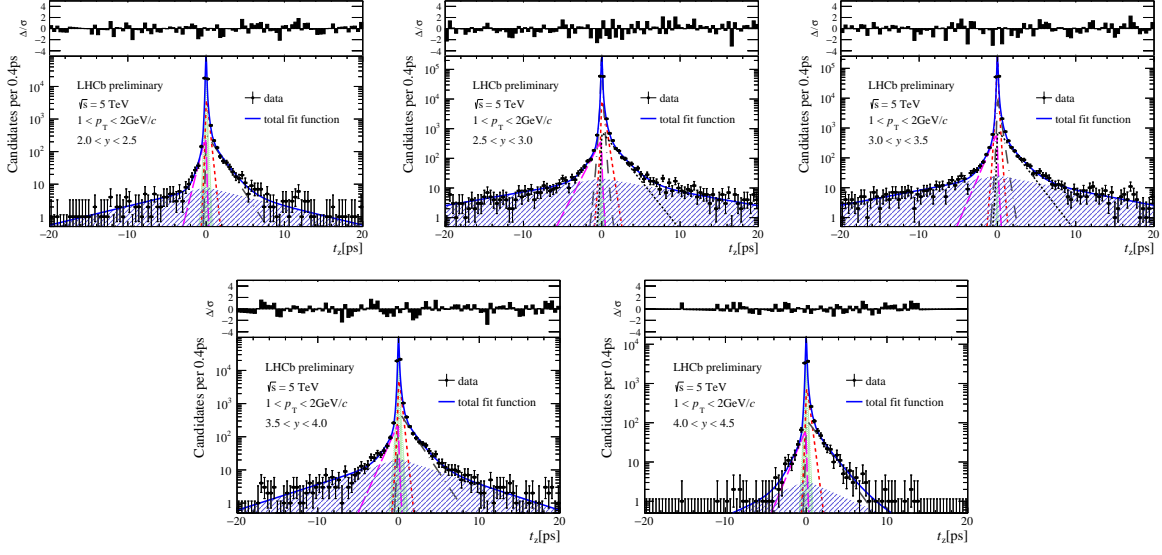


Figure F.2:  $t_z$  background fit in bins of  $y$  with  $1 < p_T < 2 \text{ GeV}/c$ .

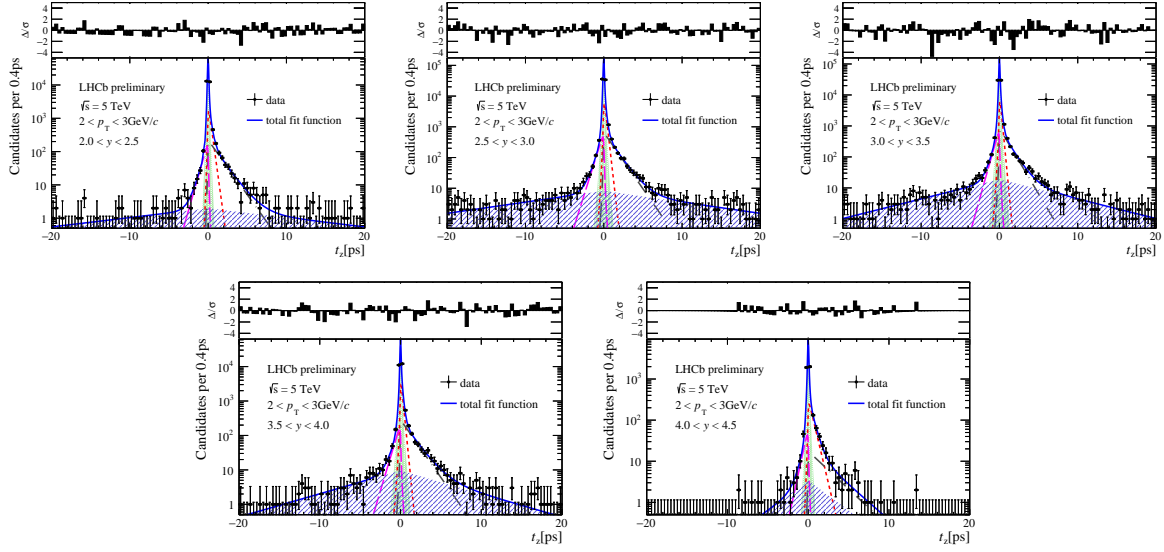


Figure F.3:  $t_z$  background fit in bins of  $y$  with  $2 < p_T < 3 \text{ GeV}/c$ .

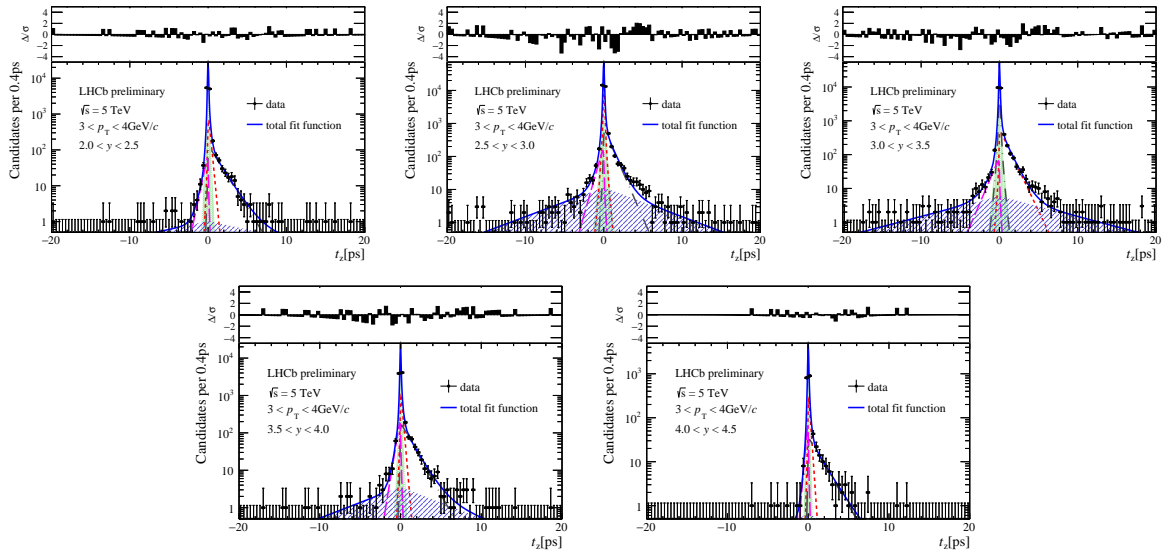


Figure F.4:  $t_z$  background fit in bins of  $y$  with  $3 < p_T < 4 \text{ GeV}/c$ .

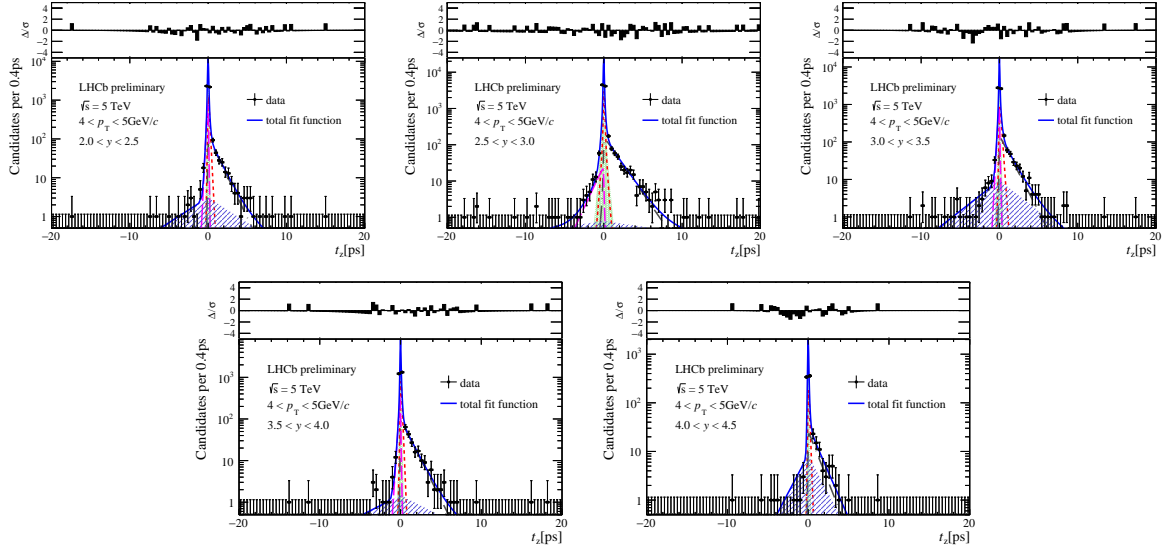


Figure F.5:  $t_z$  background fit in bins of  $y$  with  $4 < p_T < 5 \text{ GeV}/c$ .

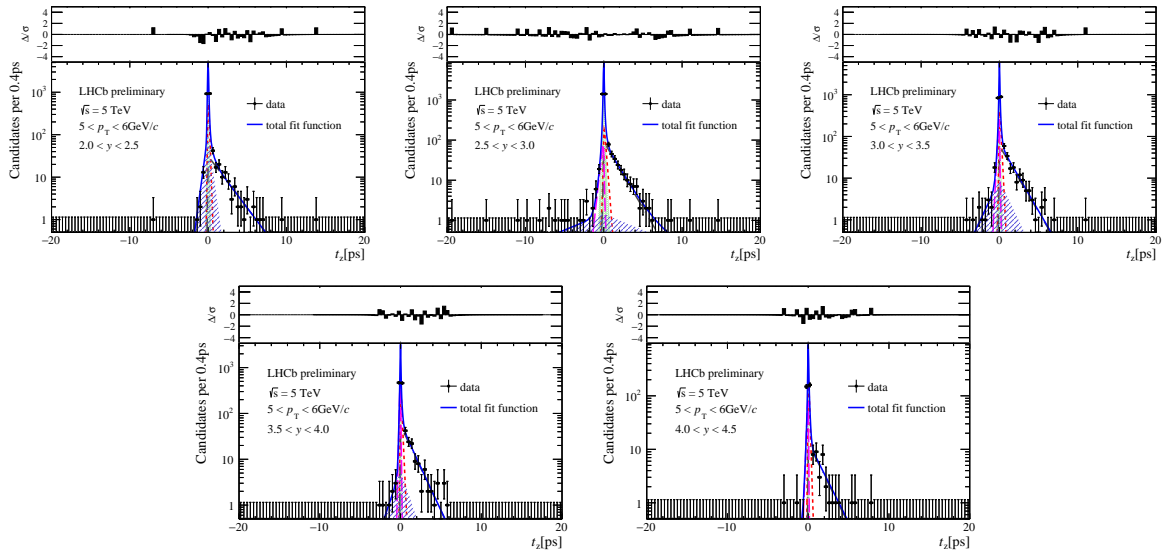


Figure F.6:  $t_z$  background fit in bins of  $y$  with  $5 < p_T < 6 \text{ GeV}/c$ .

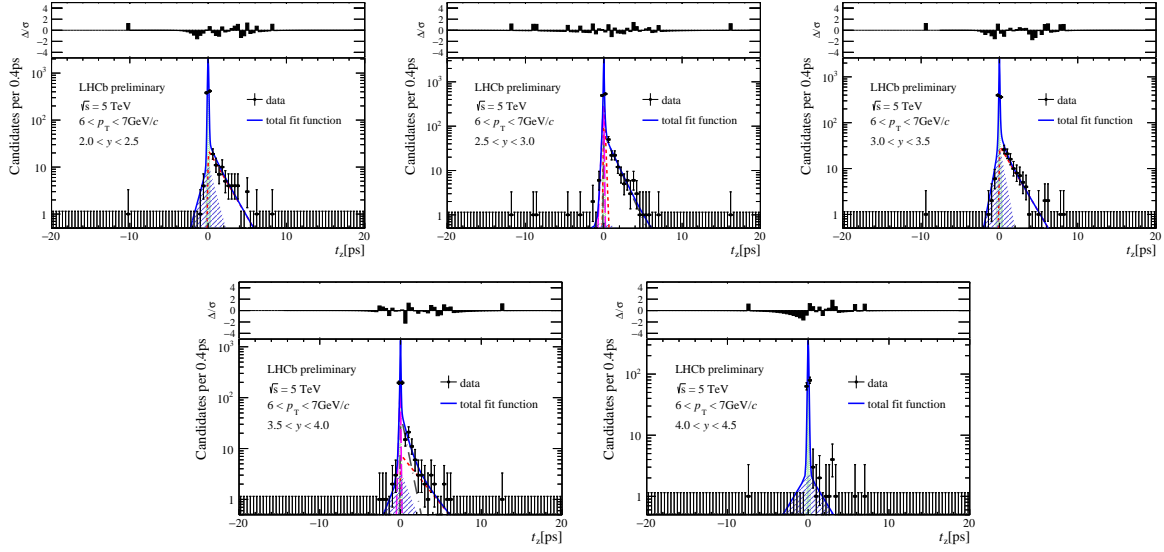


Figure F.7:  $t_z$  background fit in bins of  $y$  with  $6 < p_T < 7 \text{ GeV}/c$ .

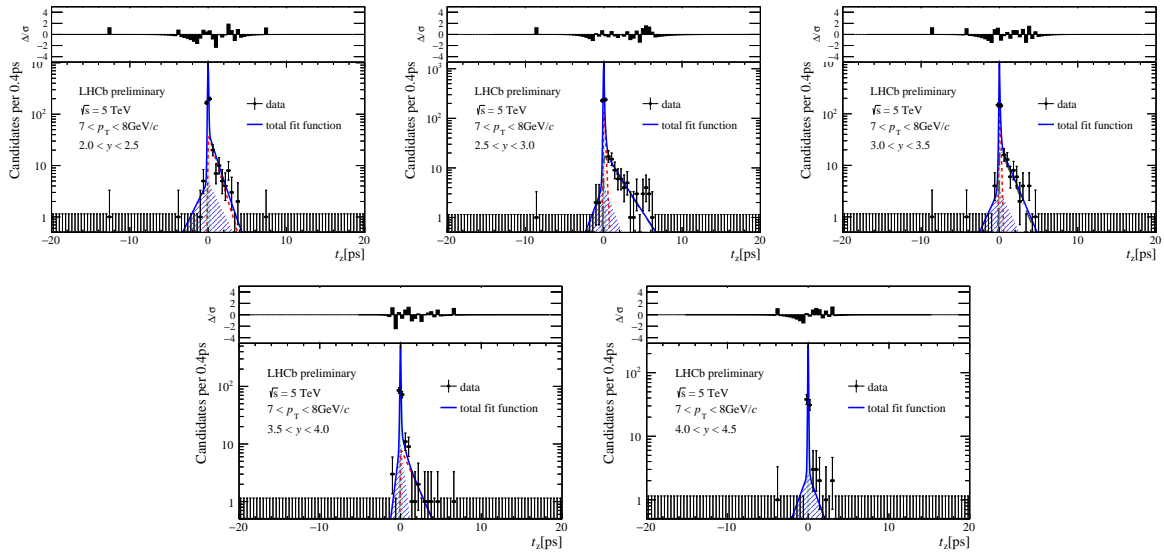


Figure F.8:  $t_z$  background fit in bins of  $y$  with  $7 < p_T < 8 \text{ GeV}/c$ .

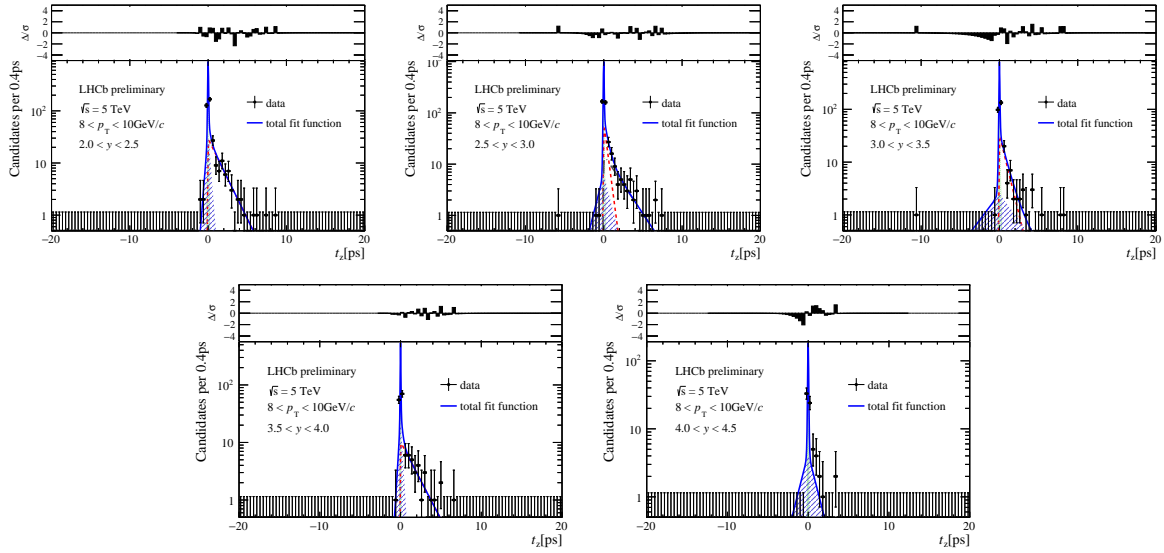


Figure F.9:  $t_z$  background fit in bins of  $y$  with  $8 < p_T < 10 \text{ GeV}/c$ .

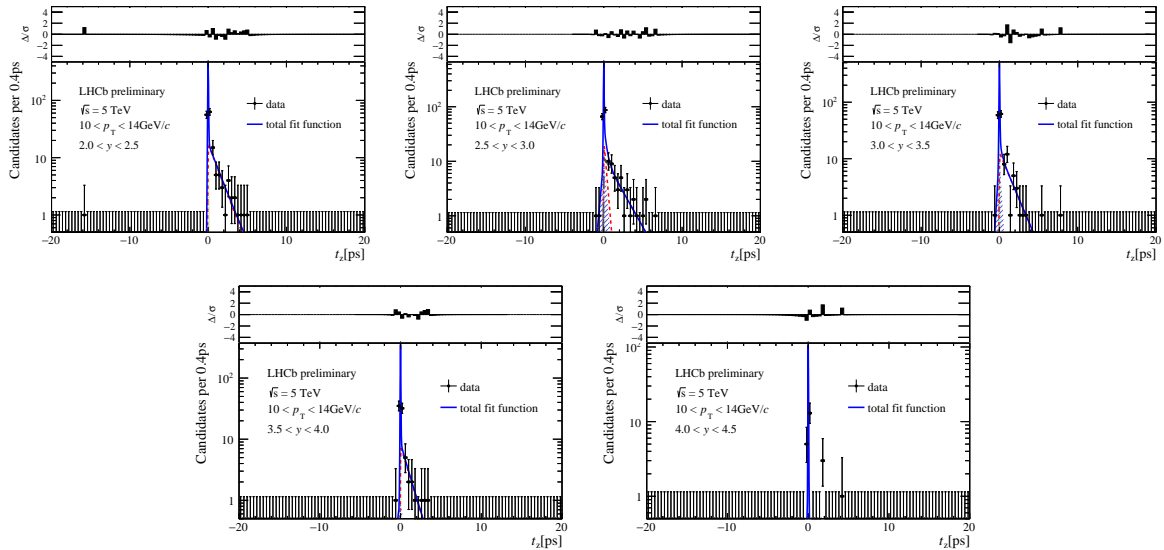


Figure F.10:  $t_z$  background fit in bins of  $y$  with  $10 < p_T < 14 \text{ GeV}/c$ .

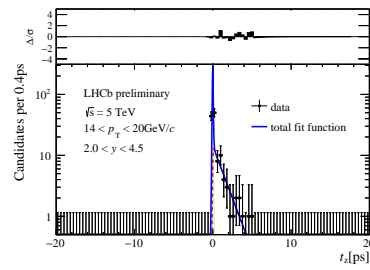


Figure F.11:  $t_z$  background fit with  $2.0 < y < 4.5$  and  $14 < p_T < 20 \text{ GeV}/c$ .

## 751 G Different versions of full-simulation samples

752 For full-simulation samples, 2 M for Sim09b version and 4 M for Sim09h version are  
 753 generated. It is necessary to check whether the two samples can be merged safely.

The comparison of nSPDHits between two versions is shown in Fig. G.1. The

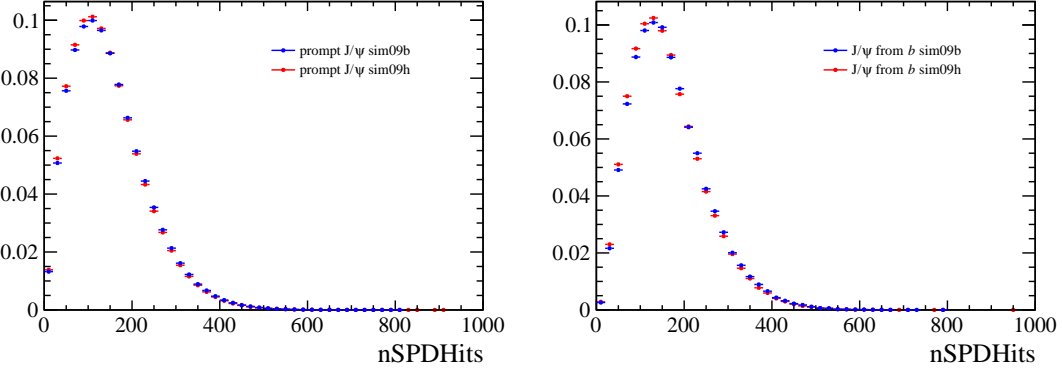


Figure G.1: The comparison of nSPDHits between Sim09b version and Sim09h version for prompt  $J/\psi$  (left) and  $J/\psi$  from  $b$  (right).

754 comparison of  $p_T$  between two versions is shown in Fig. G.2. The comparison of  $y$  between

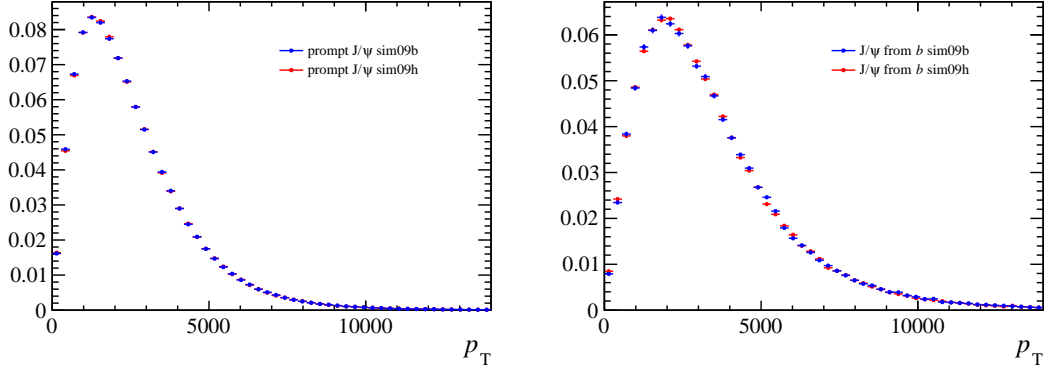


Figure G.2: The comparison of  $p_T$  between Sim09b version and Sim09h version for prompt  $J/\psi$  (left) and  $J/\psi$  from  $b$  (right).

755  
 756 two versions is shown in Fig. G.3. According to these figure, there is not much difference  
 757 between the two versions for the three distributions. Therefore, the two samples are  
 758 merged to calculate the reweight tables for nSPDHits,  $p_T$  and  $y$ .

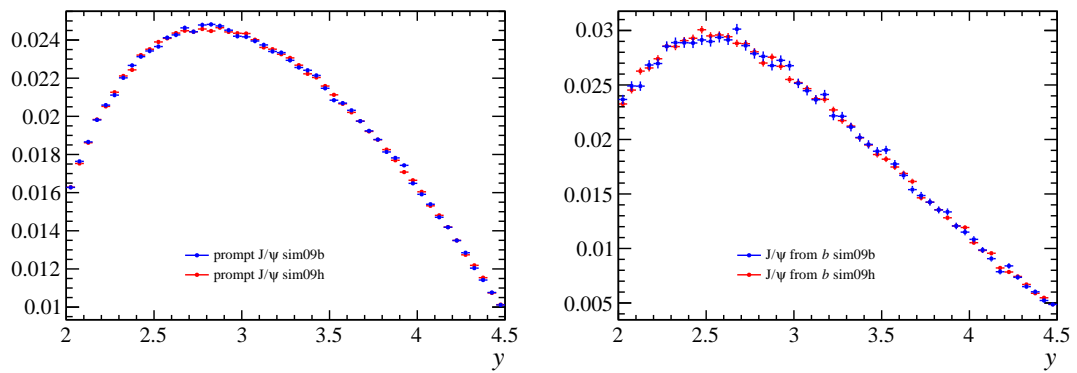


Figure G.3: The comparison of  $y$  between Sim09b version and Sim09h version for prompt  $J/\psi$  (left) and  $J/\psi$  from  $b$  (right).

## 759 H $p_T$ - $y$ spectrum correction

760 The kinematic distributions of  $J/\psi$  mesons in data and simulation could be different even  
 761 though in each  $(p_T, y)$  bin, since the bin size is not infinitely small.

The comparison of  $p_T$  spectra between data and MC is shown in Fig. H.1. The

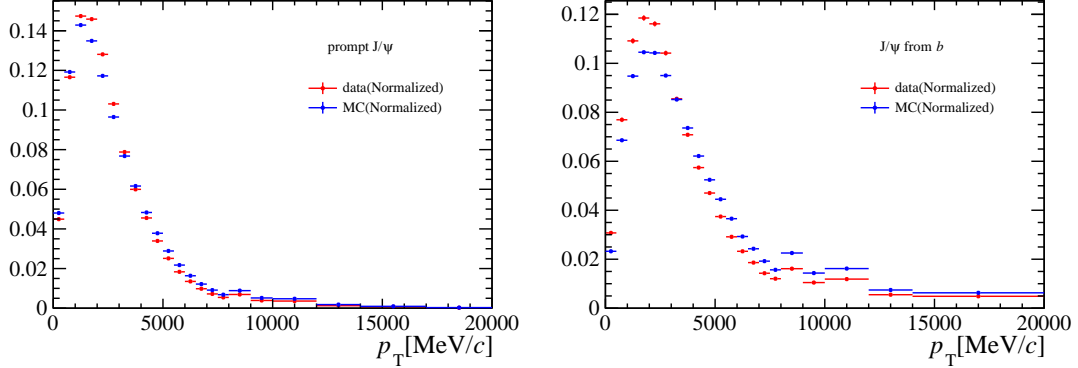


Figure H.1: The comparison of  $p_T$  spectra between data and MC for prompt  $J/\psi$  (left) and  $J/\psi$  from  $b$  (right).

762 comparison of  $y$  spectra between data and MC is shown in Fig. H.2.

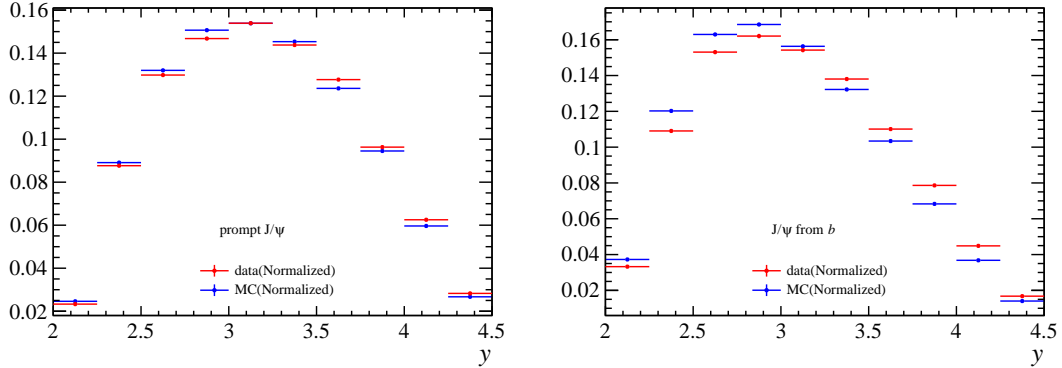


Figure H.2: The comparison of  $y$  spectra between data and MC for prompt  $J/\psi$  (left) and  $J/\psi$  from  $b$  (right).

763 To study how much the difference will affect the efficiencies, the 2D  $p_T$ - $y$  spectrum of  
 764 prompt  $J/\psi$  and  $J/\psi$  from  $b$  in simulation is weighted to that in the background-subtracted  
 765 data. For each original  $(p_T, y)$  bin, it is divided into  $2 \times 2$  parts in further. The efficiencies  
 766 are calculated with the weighted and non-weighted kinematic distributions in each original  
 767 bin, and the relative difference is shown in Fig. H.3. The relative difference is around 1%  
 768 for most  $2 < y < 2.5$  bins, not only for prompt  $J/\psi$ , but also for  $J/\psi$  from  $b$ . Therefore, it  
 770 is better to use the  $p_T$ - $y$ -weighted sample to calculate the efficiencies.

771 Another necessary check is that whether the  $p_T$ - $y$  spectrum reweight will affect the  
 772 nSPDHits distribution, which has been reweighted before. It is shown in Fig. H.4, that  
 773 there is almost no difference for the nSPDHits distribution.

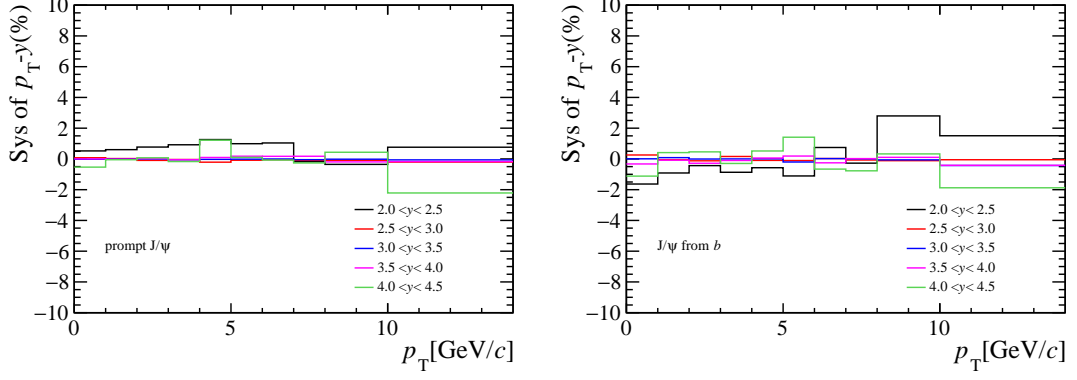


Figure H.3: The relative difference of efficiencies between with weighted and non-weighted kinematic distributions for prompt  $J/\psi$  (left) and  $J/\psi$  from  $b$  (right).

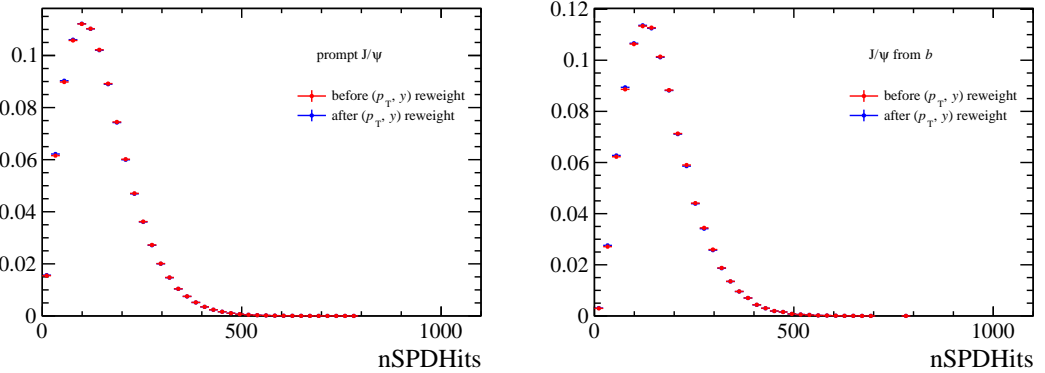


Figure H.4: The comparison of nSPDHits distributions between before and after the  $p_T$ - $y$  spectrum reweight for prompt  $J/\psi$  (left) and  $J/\psi$  from  $b$  (right).

774      The comparison of  $p_T$  spectra between data and MC after the  $p_T$ - $y$  spectrum reweight  
 775      is shown in Fig. H.5. The comparison of  $y$  spectra between data and MC after the  $p_T$ - $y$   
 776      spectrum reweight is shown in Fig. H.6.

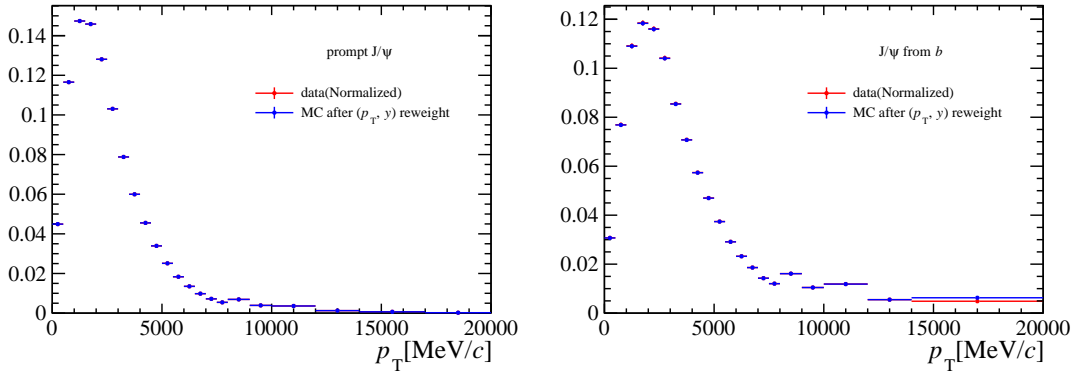


Figure H.5: The comparison of  $p_T$  spectra between data and MC after the  $p_T$ - $y$  spectrum reweight for prompt  $J/\psi$  (left) and  $J/\psi$  from  $b$  (right).

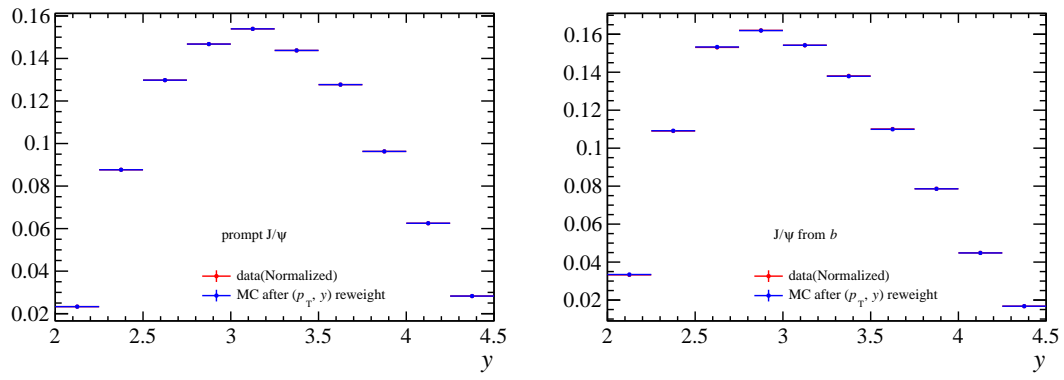


Figure H.6: The comparison of  $y$  spectra between data and MC after the  $p_T$ - $y$  spectrum reweight for prompt  $J/\psi$  (left) and  $J/\psi$  from  $b$  (right).

777 I Plots of 2D pull distributions

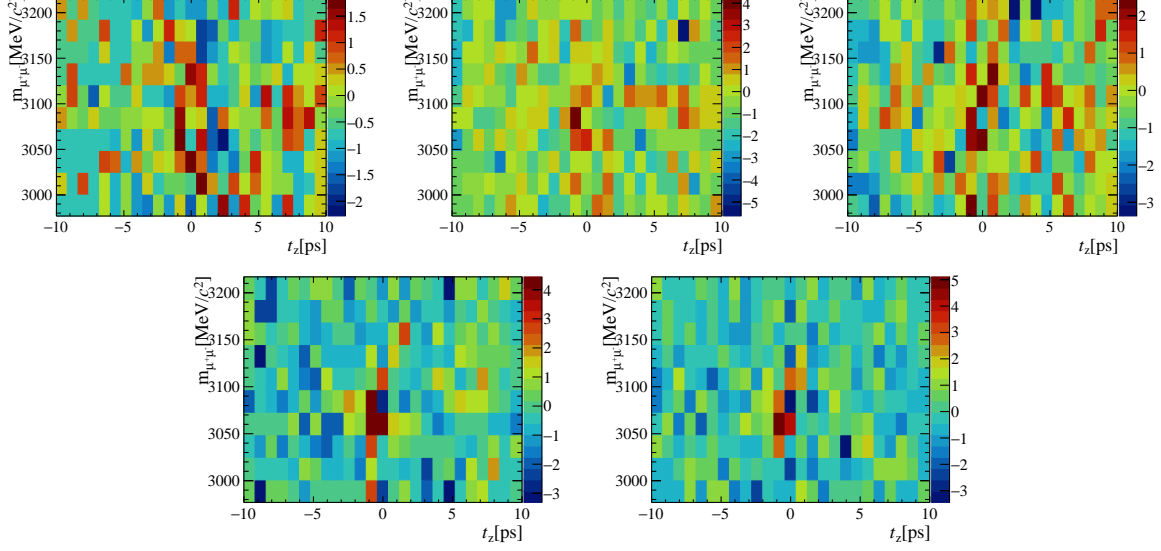


Figure I.1: 2D pull distributions in bins of  $y$  with  $0 < p_T < 1 \text{ GeV}/c$ .

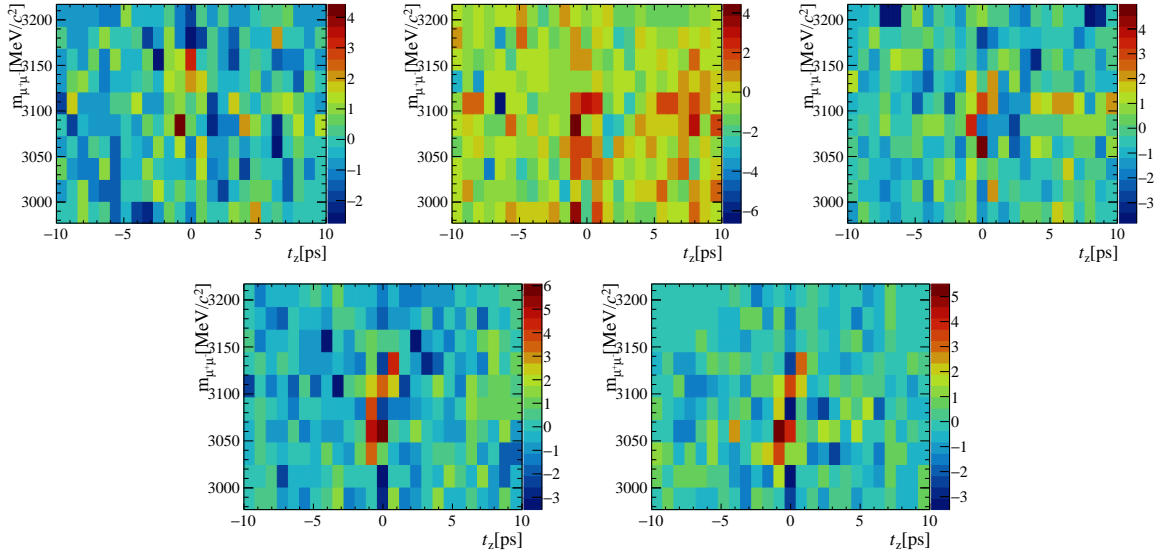


Figure I.2: 2D pull distributions in bins of  $y$  with  $1 < p_T < 2 \text{ GeV}/c$ .

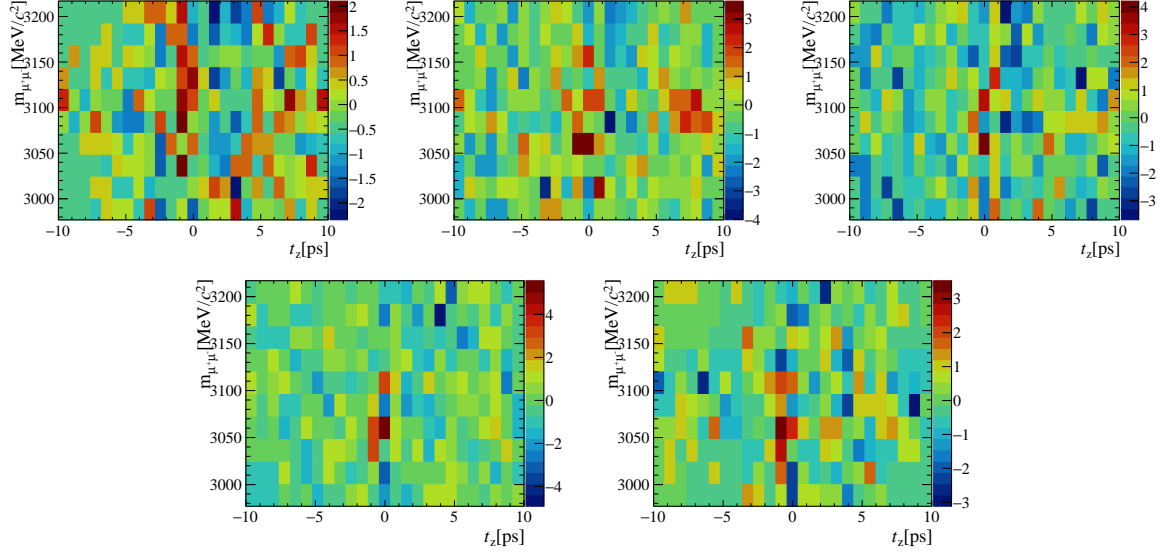


Figure I.3: 2D pull distributions in bins of  $y$  with  $2 < p_T < 3 \text{ GeV}/c$ .

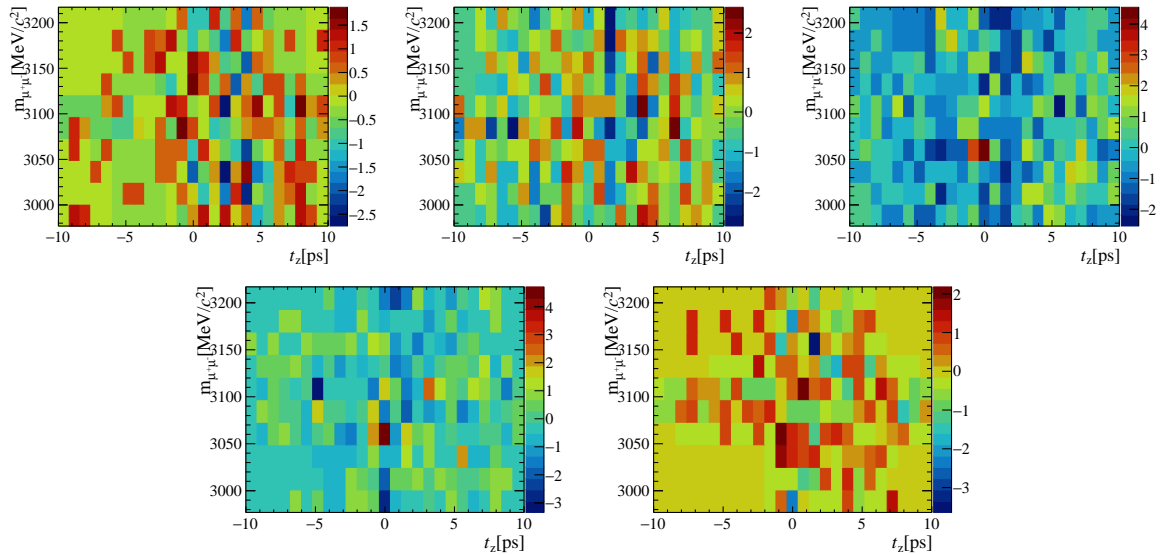


Figure I.4: 2D pull distributions in bins of  $y$  with  $3 < p_T < 4 \text{ GeV}/c$ .

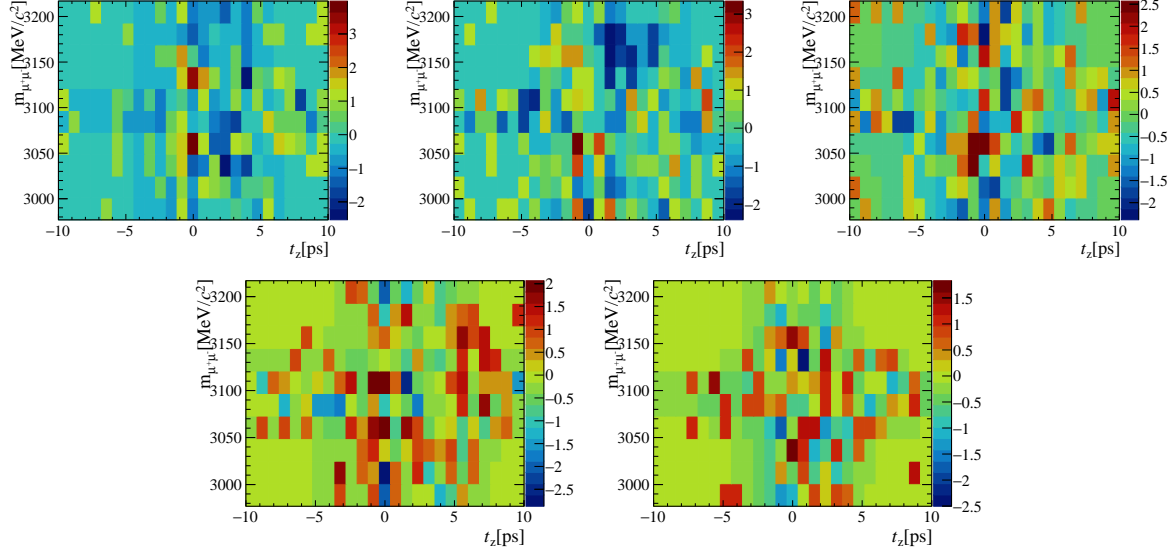


Figure I.5: 2D pull distributions in bins of  $y$  with  $4 < p_T < 5 \text{ GeV}/c$ .

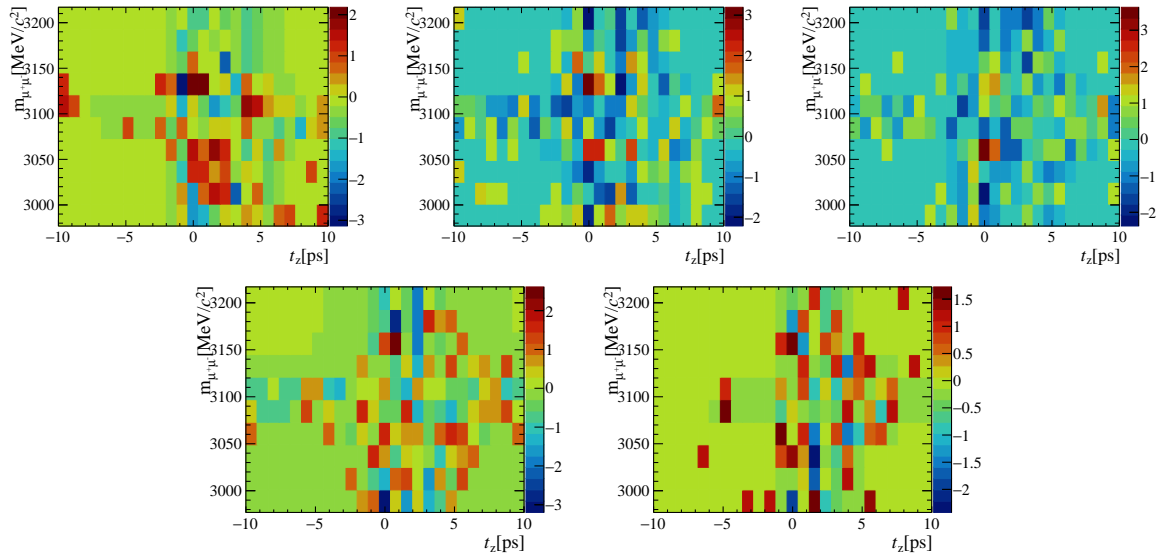


Figure I.6: 2D pull distributions in bins of  $y$  with  $5 < p_T < 6 \text{ GeV}/c$ .

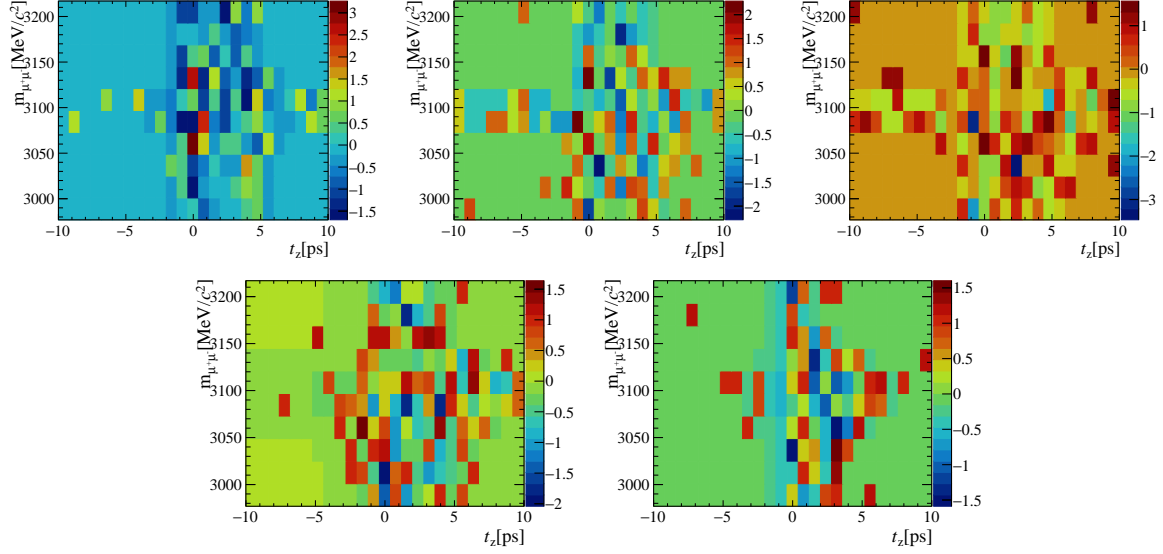


Figure I.7: 2D pull distributions in bins of  $y$  with  $6 < p_T < 7 \text{ GeV}/c$ .

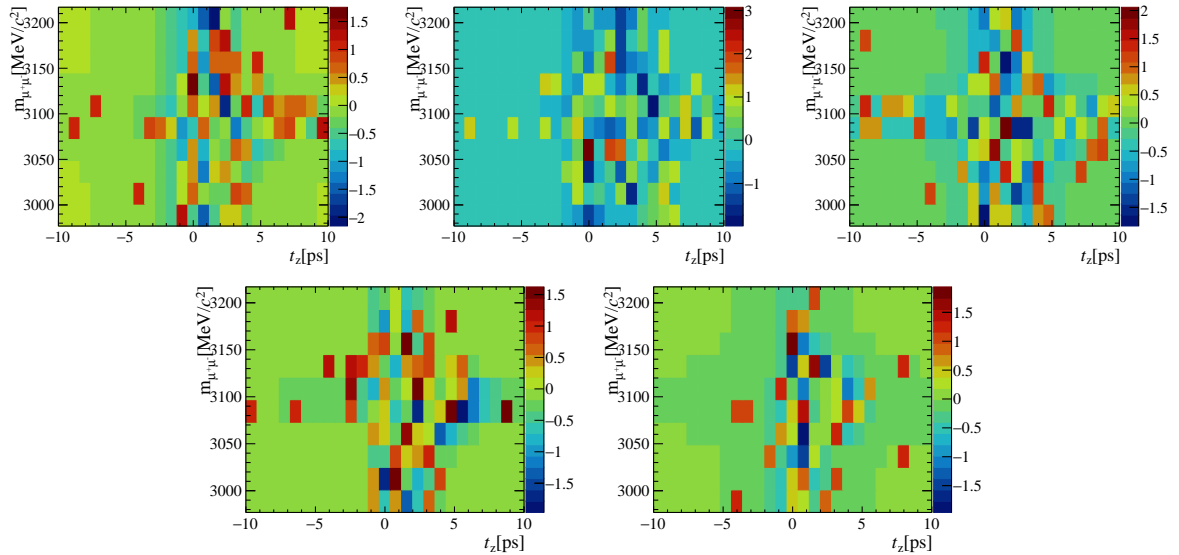


Figure I.8: 2D pull distributions in bins of  $y$  with  $7 < p_T < 8 \text{ GeV}/c$ .

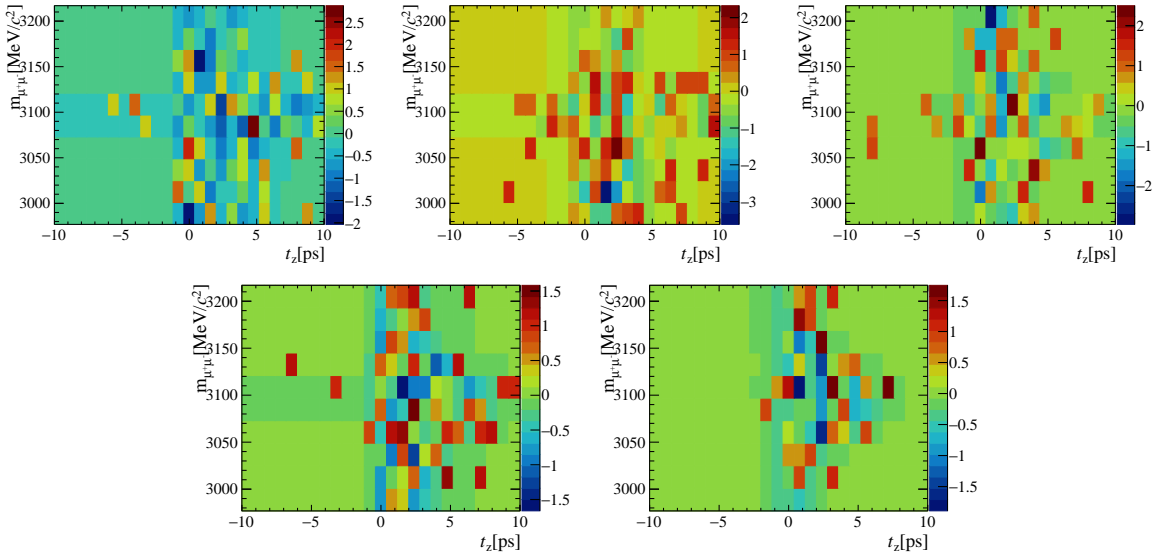


Figure I.9: 2D pull distributions in bins of  $y$  with  $8 < p_T < 10 \text{ GeV}/c$ .

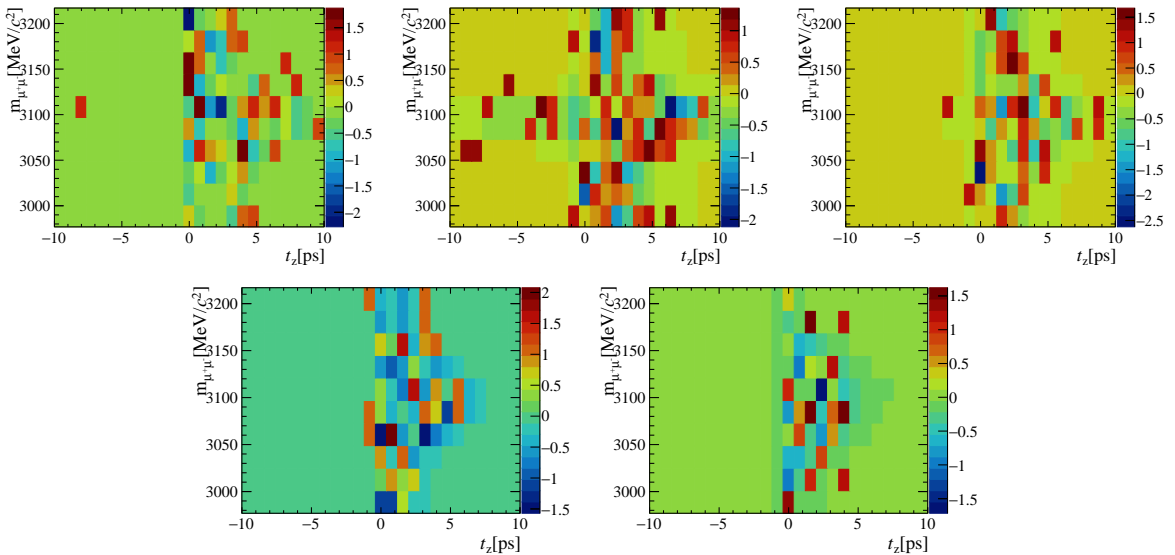


Figure I.10: 2D pull distributions in bins of  $y$  with  $10 < p_T < 14 \text{ GeV}/c$ .

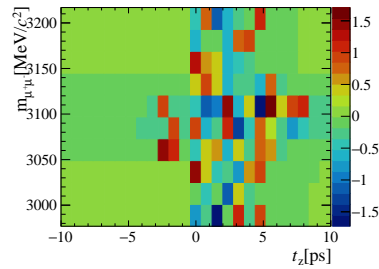


Figure I.11: 2D pull distributions with  $2.0 < y < 4.5$  and  $10 < p_T < 14 \text{ GeV}/c$ .

778 **J** Plots of  $t_z$  fit result in MC

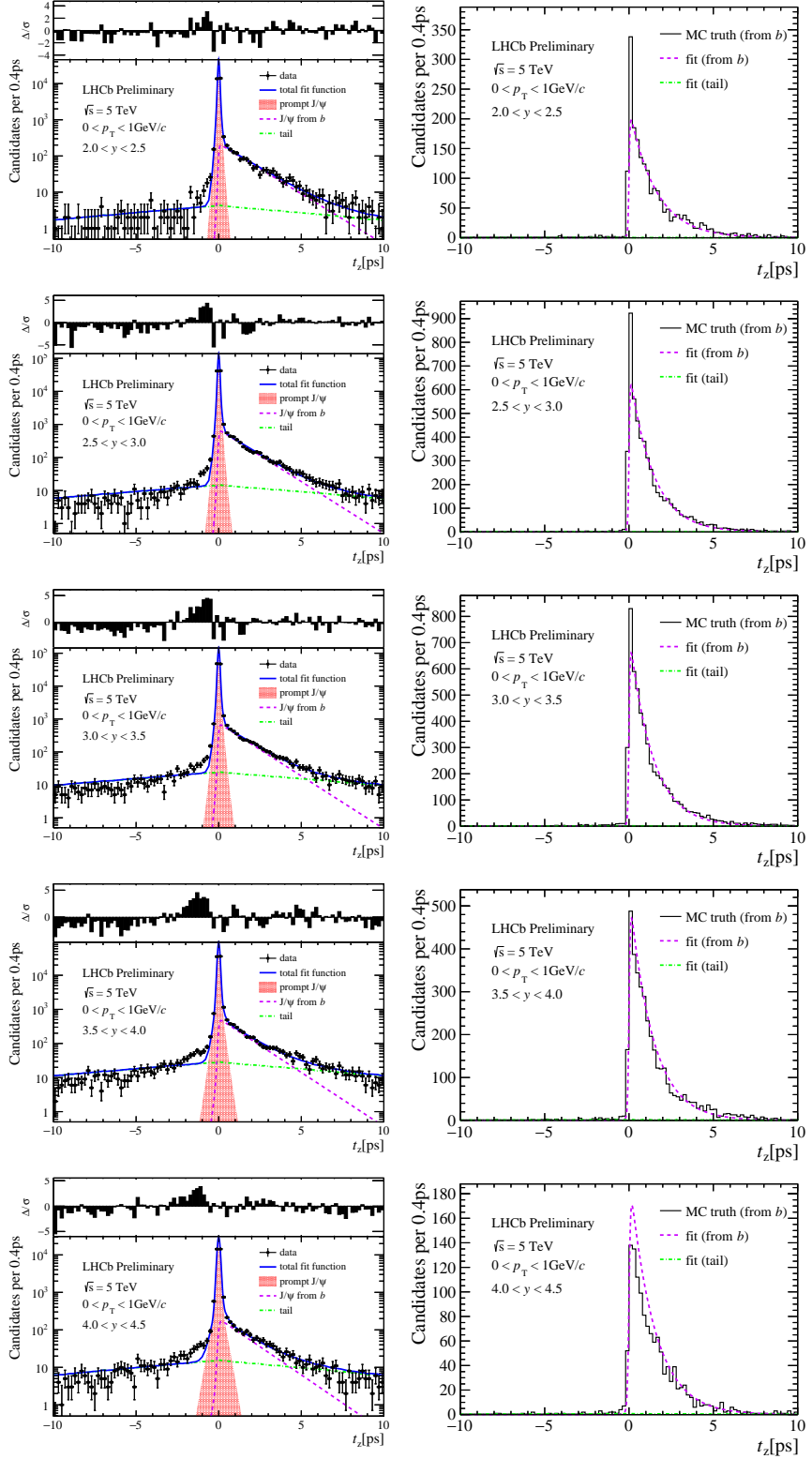


Figure J.1:  $t_z$  fit in MC (left) and the comparison of  $J/\psi$  from  $b$  (right) in bins of  $y$  with  $0 < p_T < 1 \text{ GeV}/c$ .

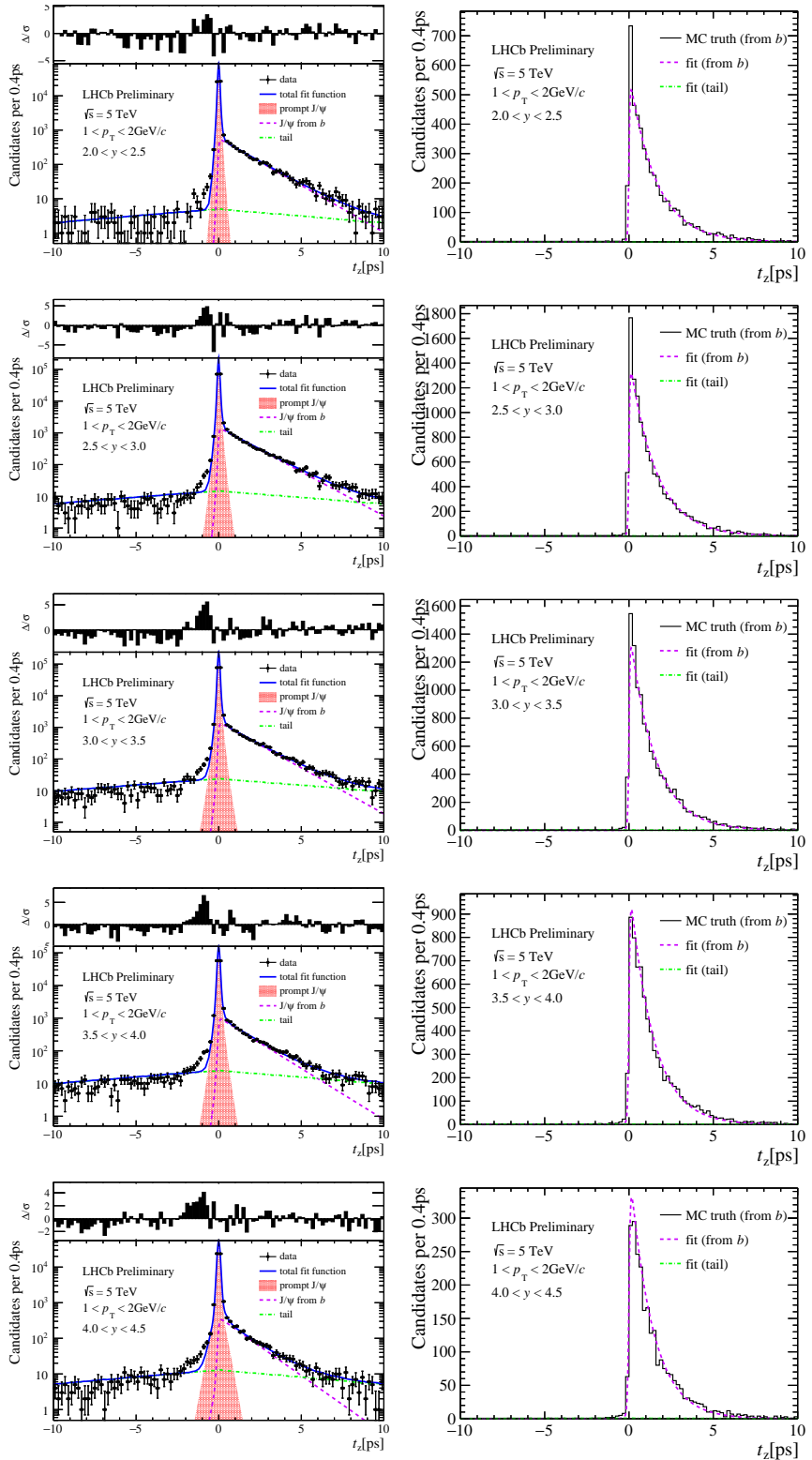


Figure J.2:  $t_z$  fit in MC (left) and the comparison of  $J/\psi$  from  $b$  (right) in bins of  $y$  with  $1 < p_T < 2 \text{ GeV}/c$ .

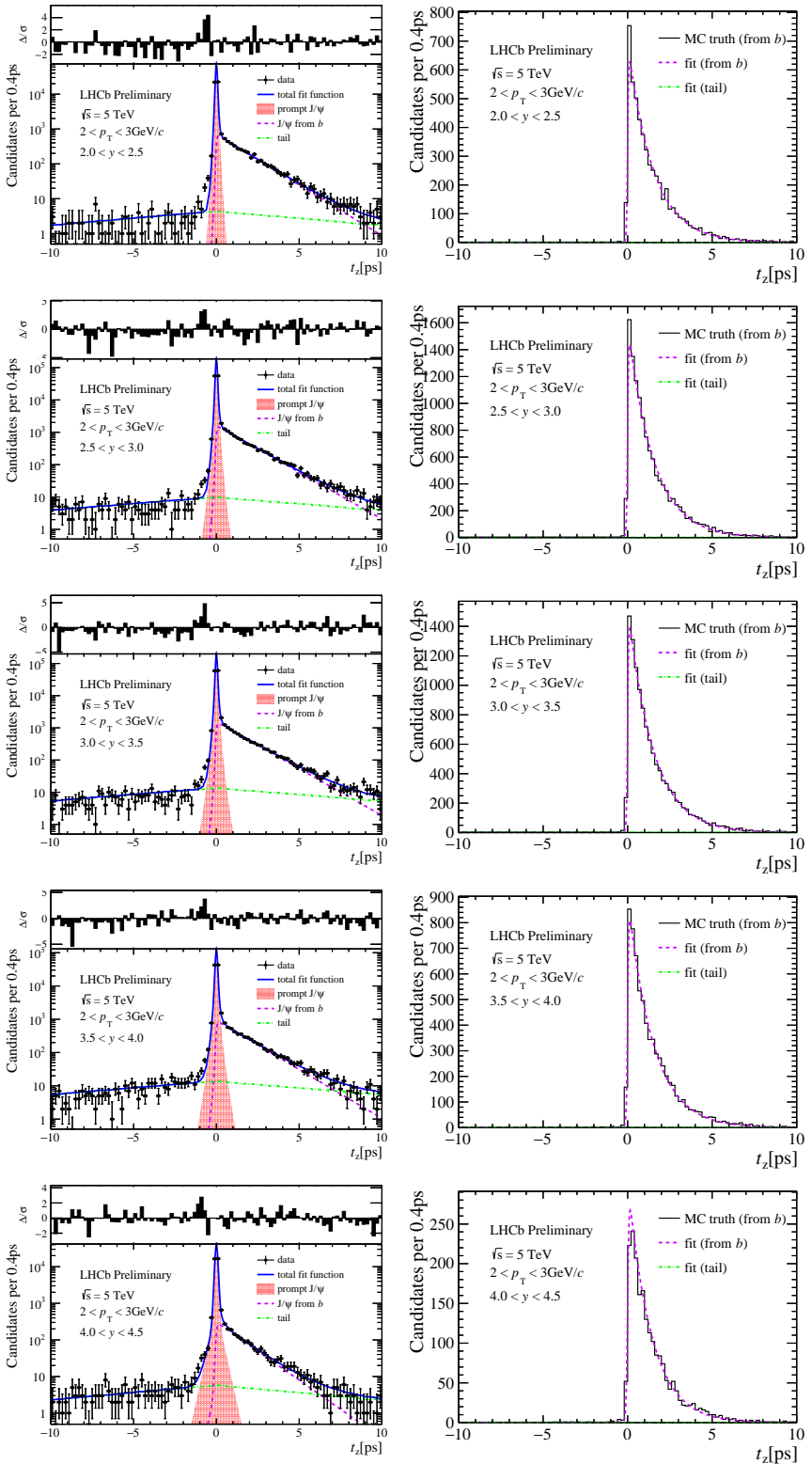


Figure J.3:  $t_z$  fit in MC (left) and the comparison of  $J/\psi$  from  $b$  (right) in bins of  $y$  with  $2 < p_T < 3 \text{ GeV}/c$ .

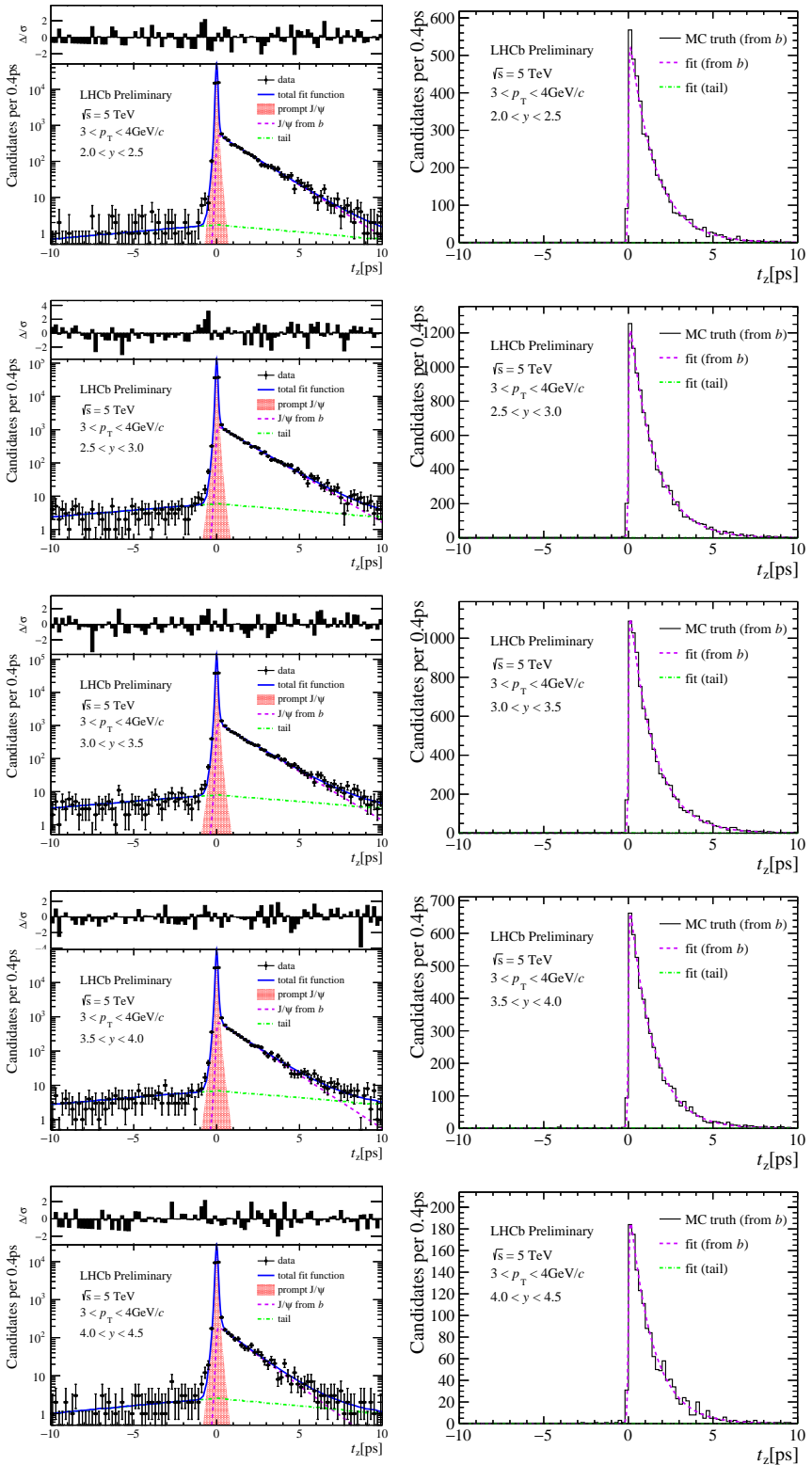


Figure J.4:  $t_z$  fit in MC (left) and the comparison of  $J/\psi$  from  $b$  (right) in bins of  $y$  with  $3 < p_T < 4 \text{ GeV}/c$ .

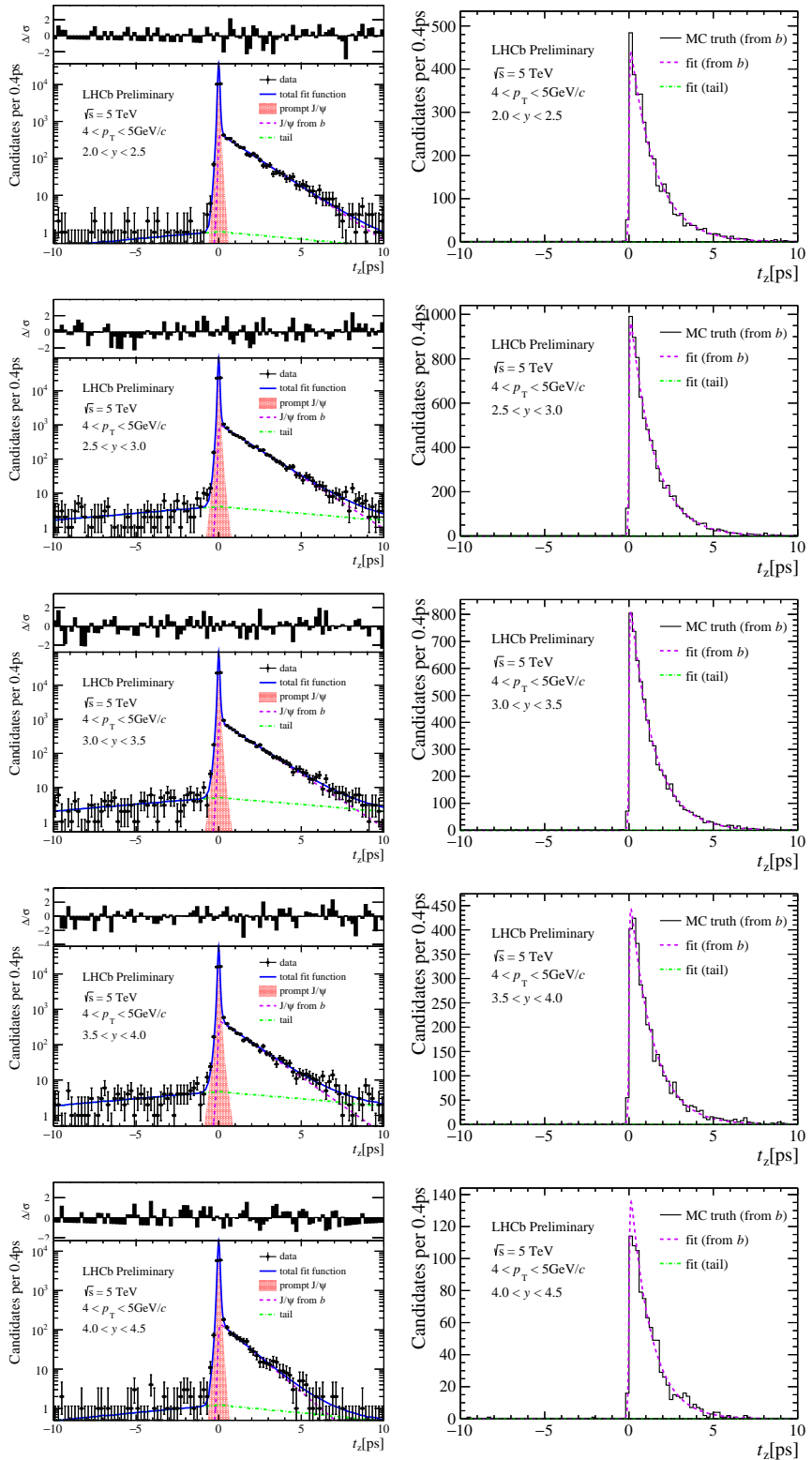


Figure J.5:  $t_z$  fit in MC (left) and the comparison of  $J/\psi$  from  $b$  (right) in bins of  $y$  with  $3 < p_T < 4 \text{ GeV}/c$ .

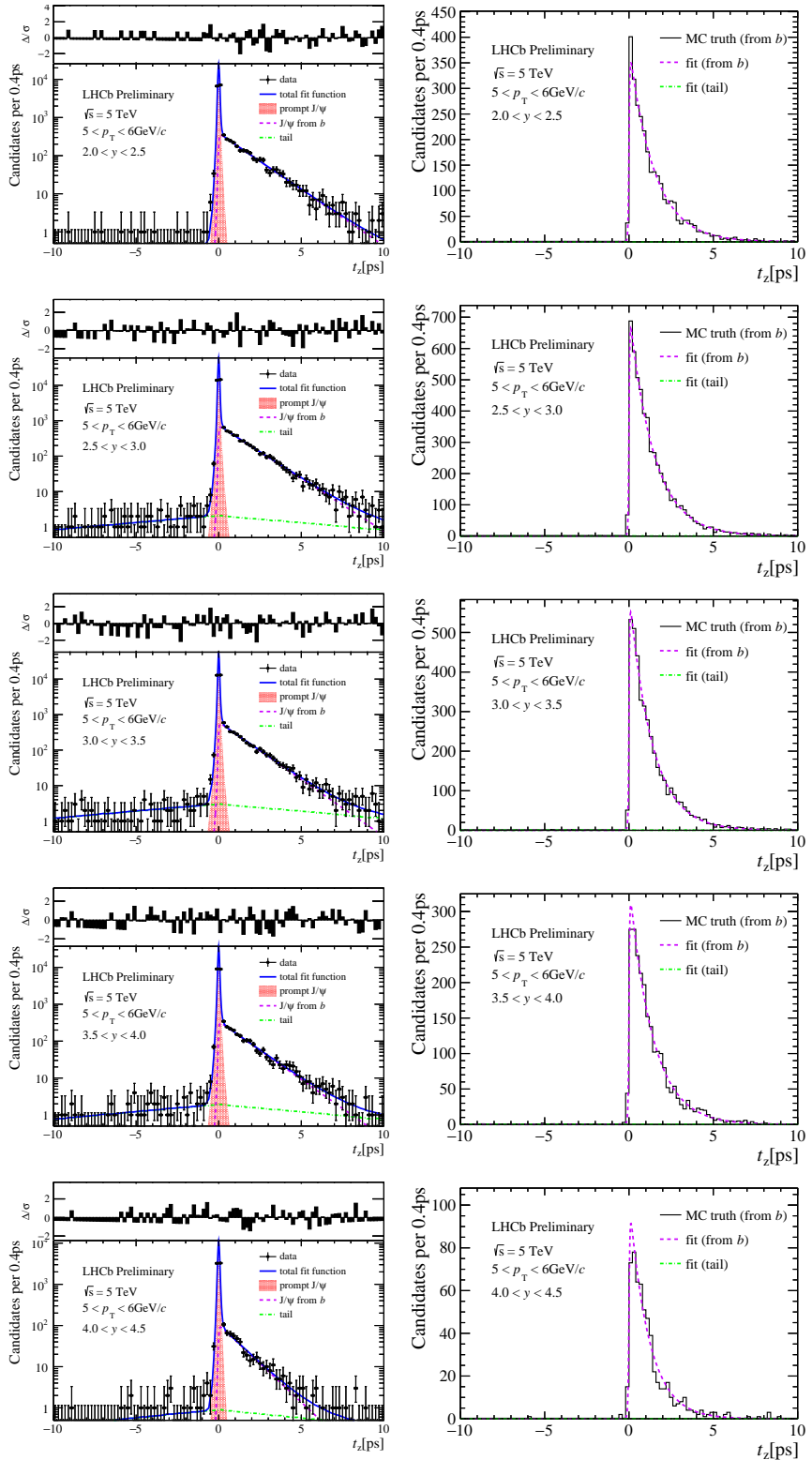


Figure J.6:  $t_z$  fit in MC (left) and the comparison of  $J/\psi$  from  $b$  (right) in bins of  $y$  with  $5 < p_T < 6 \text{ GeV}/c$ .

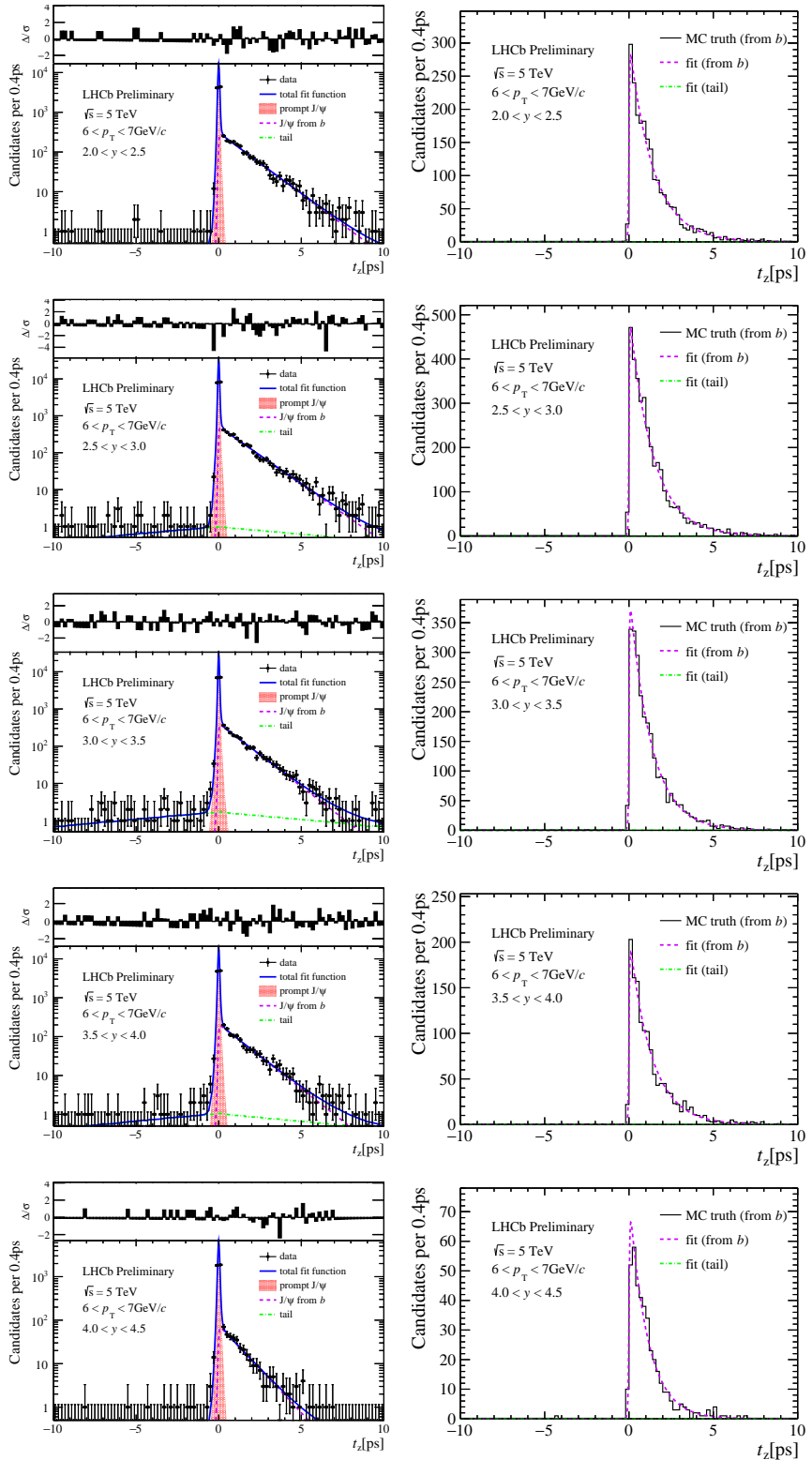


Figure J.7:  $t_z$  fit in MC (left) and the comparison of  $J/\psi$  from  $b$  (right) in bins of  $y$  with  $6 < p_T < 7 \text{ GeV}/c$ .

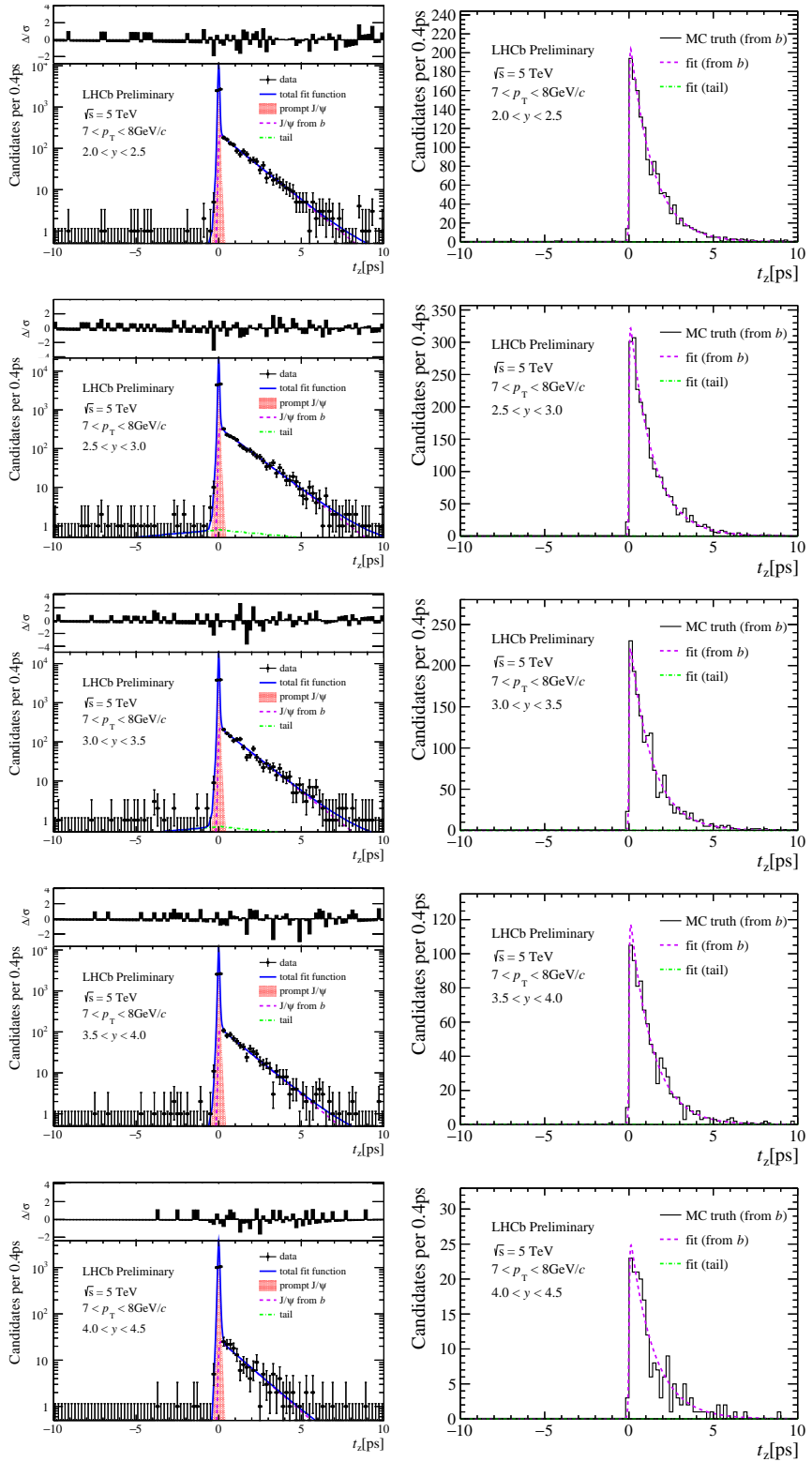


Figure J.8:  $t_z$  fit in MC (left) and the comparison of  $J/\psi$  from  $b$  (right) in bins of  $y$  with  $7 < p_T < 8 \text{ GeV}/c$ .

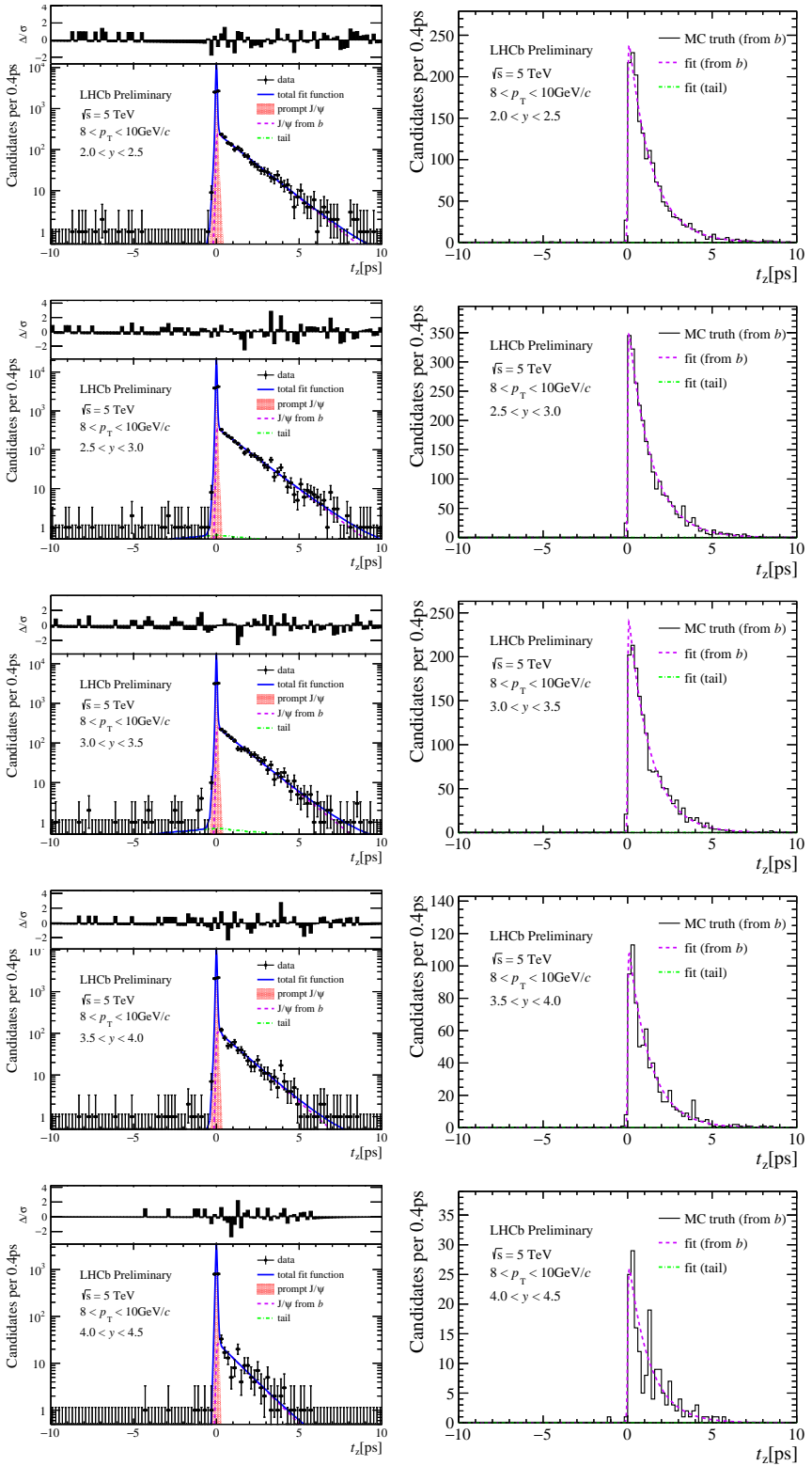


Figure J.9:  $t_z$  fit in MC (left) and the comparison of  $J/\psi$  from  $b$  (right) in bins of  $y$  with  $8 < p_T < 10 \text{ GeV}/c$ .

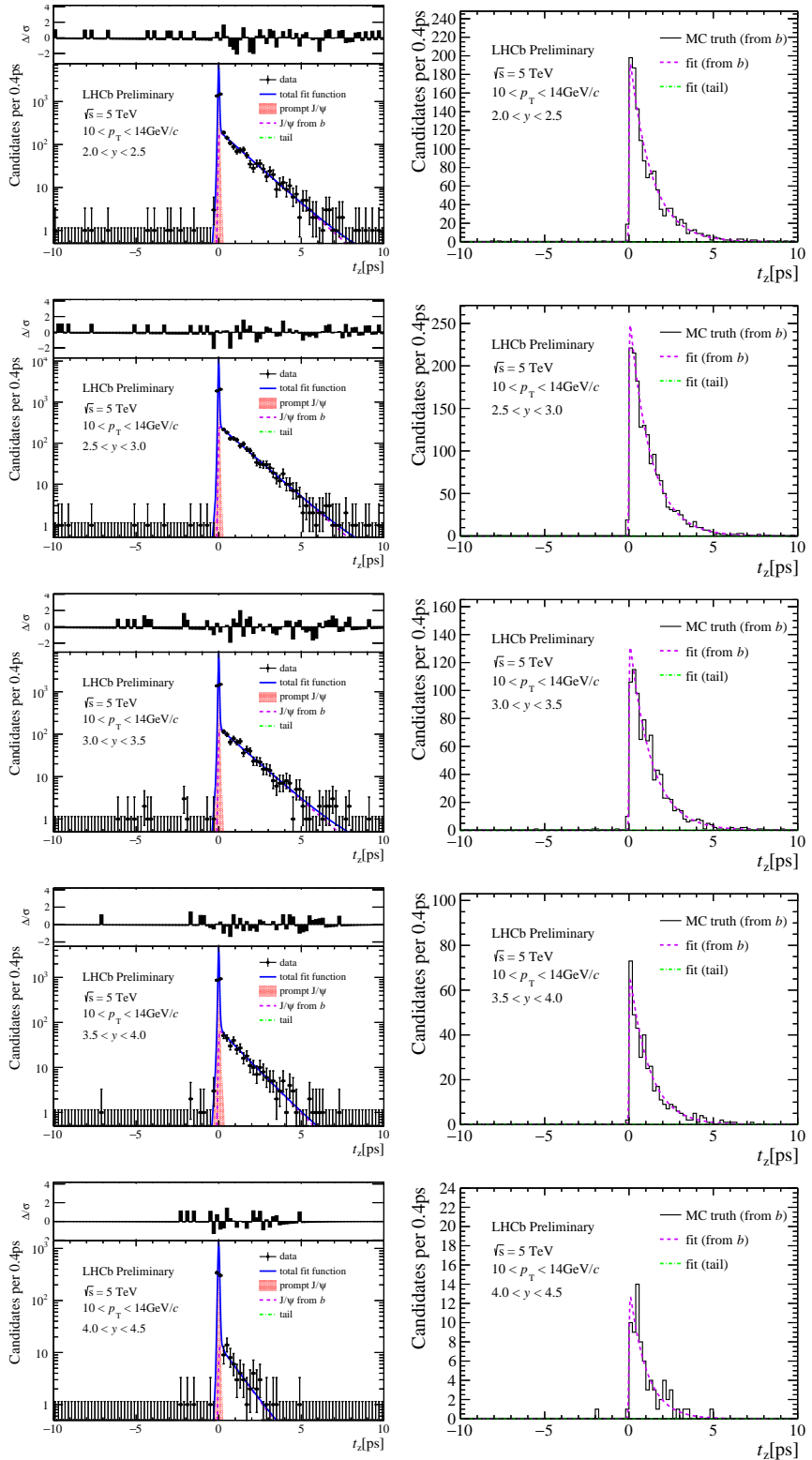


Figure J.10:  $t_z$  fit in MC (left) and the comparison of  $J/\psi$  from  $b$  (right) in bins of  $y$  with  $10 < p_T < 14 \text{ GeV}/c$ .

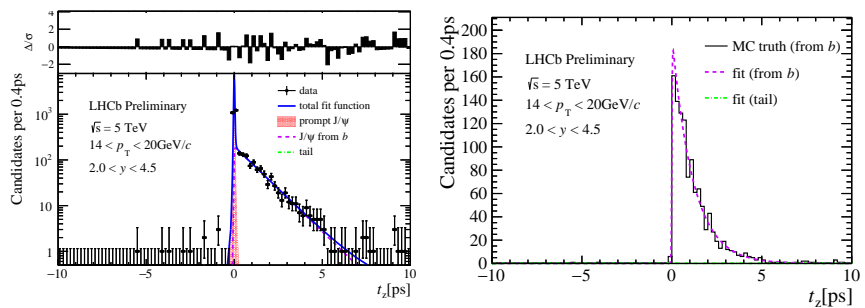


Figure J.11:  $t_z$  fit in MC (left) and the comparison of  $J/\psi$  from  $b$  (right) with  $2.0 < y < 4.5$  and  $14 < p_T < 20 \text{ GeV}/c$ .

## 779 K Check the bias of the 2D fit

780 There are potential pitfalls when performing the unbinned likelihood fit which involves  
 781 complex functions with several components and depends on the event observables [67].  
 782 Such is the case in this analysis when the parameter  $\sigma_{t_z}$ , the event-by-event uncertainty of  
 783  $t_z$  is used in the 2D fit. So, it is necessary to check if there is the bias of the fitted fraction.

784 The distribution of  $t_z$  uncertainty is compared among different components: prompt  
 $J/\psi$ ,  $J/\psi$  from  $b$ , tail and background, as shown in Fig. K.1. The distributions for prompt

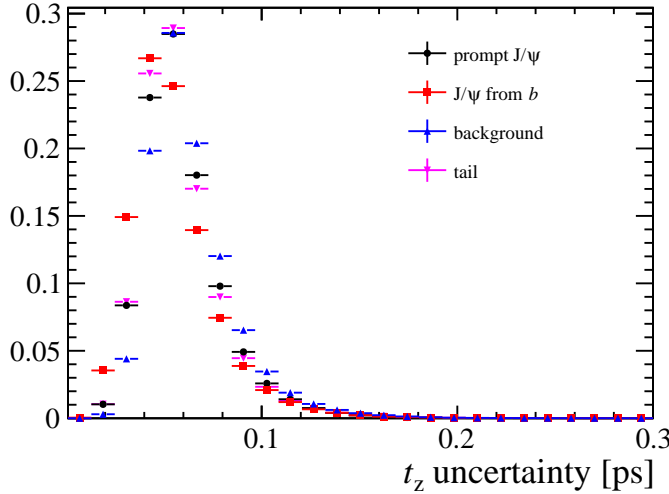


Figure K.1: The comparison of  $t_z$  uncertainty distributions for prompt  $J/\psi$ ,  $J/\psi$  from  $b$ , tail and background.

785  
 786  $J/\psi$  and  $J/\psi$  from  $b$  are obtained from the full-simulation smaple, the distribution for  
 787 background is obtained from the mass sideband of data, and that for tail is obtained from  
 788 the next-event method. There is a little difference among the distributions.

789 To check if there is a bias, we generate 1000 toy MC samples for each  $(p_T, y)$  bin based  
 790 on the 2D fit result to perfrom the test.

791 For each sample, there are four components: prompt  $J/\psi$ ,  $J/\psi$  from  $b$ , background  
 792 and tail. For mass distribtuion,

$$f_{\text{mass}}(m; N_{\text{prompt}}, N_{\text{from } b}, N_{\text{bkg}}, N_{\text{tail}}, \mu_m, \sigma_1, \sigma_2, f_m, \lambda) = \\ (N_{\text{prompt}} + N_{\text{from } b} + N_{\text{tail}}) f_{2\text{CBs}}(m; \mu_m, \sigma_1, \sigma_2, f_m) + N_{\text{bkg}} f_{\text{expo}}(m; \lambda), \quad (\text{K.1})$$

793 and for  $t_z$  distribution,

$$f_{t_z}(t_z; N_{\text{prompt}}, N_{\text{from } b}, N_{\text{bkg}}, N_{\text{tail}}, \tau_b, \mu, S_1, S_2, \beta) = \\ \left( N_{\text{prompt}} \delta(t_z) + \frac{N_{\text{from } b}}{\tau_b} e^{-t_z/\tau_b} \right) \otimes f_{\text{resolution}}(t_z; \mu, S_1, S_2, \beta) + N_{\text{tail}} f_{\text{tail}}(t_z) + N_{\text{bkg}} f_{\text{bkg}}(t_z). \quad (\text{K.2})$$

794 The parameters  $\tau_b, \mu_m, \sigma_1, \sigma_2, f_m, \lambda, \mu, S_1, S_2, \beta$  are obtained from the 2D fit result in  
 795 Appendix B.  $t_z$  uncertainty is obtained from the distributions in Fig. K.1 for each  
 796 component and used to set the PDF parameter  $\sigma_{t_z}$  in  $f_{t_z}$  event by event. The number of  
 797 events  $N_{\text{prompt}}$ ,  $N_{\text{from } b}$ ,  $N_{\text{tail}}$  and  $N_{\text{bkg}}$  for the 1000 samples are assumed as the poisson

random numbers  $N \sim \text{Pois}(n)$ , where  $n$  is the fit result in Appendix B. If  $N_{\text{tail}}$  is less than 10, we omit the tail component in these bins. For these  $N_{\text{tail}} < 10$  bins, the fraction  $N_{\text{tail}}/N_{\text{fromb}}$  is less than 2.6% and the fraction  $N_{\text{tail}}/N_{\text{prompt}}$  is less than 0.4%. So this effect on other components for omitting tail is negligible for these bins.

We perform the fit to the 1000 samples for each bin; only  $N_{\text{prompt}}$ ,  $N_{\text{fromb}}$ ,  $N_{\text{tail}}$ ,  $N_{\text{bkg}}$  and  $\tau_b$  are free. The pull distribution for the 1000 times fit,  $(N_{\text{fit}} - n)/\sigma_{N_{\text{fit}}}$ , are obtained and expected to be  $\text{Gaus}(0,1)$  distribution if there is no bias.

The pull distributions for two bins are taken as examples ( $2 < p_T < 3 \text{ GeV}/c$ ,  $3.0 < y < 3.5$  for high statistic bins,  $14 < p_T < 20 \text{ GeV}/c$ ,  $2.0 < y < 4.5$  for low statistic bins). The Gaussian fit is performed to the pull distributions and the  $\mu$  and  $\sigma$  values are shown in Fig. K.2 and Fig. K.3. For all the bins, the  $\mu$  and  $\sigma$  values for  $N_{\text{prompt}}$ ,  $N_{\text{fromb}}$ ,  $N_{\text{tail}}$ ,  $N_{\text{bkg}}$  and  $\tau_b$  are shown in Fig. K.4, Fig. K.5, Fig. K.6, Fig. K.7 and Fig. K.8. From the four figures, all the  $\sigma$  values are consistent with 1 and most  $\mu$  values are consistent with 0. For a few bins, there seems a little bias between  $\mu$  values and 0, but it is less than the statistical uncertainty of  $N_{\text{fit}}(\mu^2 \ll 1)$ , much less than the systematic uncertainty. Therefore, we think the bias of the 2D fit is negligible.

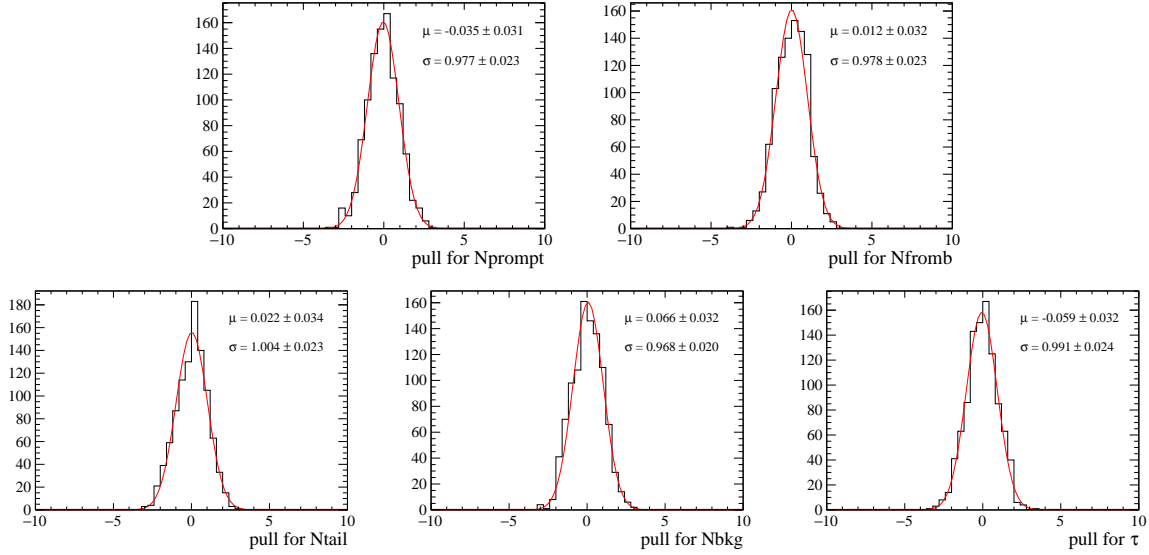


Figure K.2: The pull distributions for  $N_{\text{prompt}}$  (top left),  $N_{\text{fromb}}$  (top right),  $N_{\text{tail}}$  (bottom left),  $N_{\text{bkg}}$  (bottom middle) and  $\tau_b$  (bottom right) in the bin  $2 < p_T < 3 \text{ GeV}/c$ ,  $3.0 < y < 3.5$ .

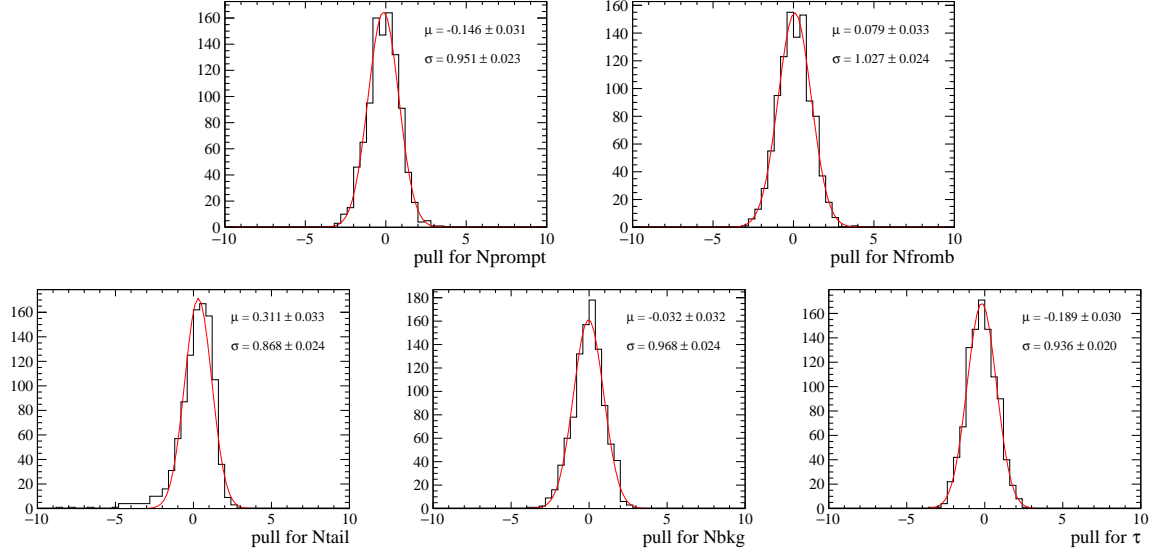


Figure K.3: The pull distributions for  $N_{\text{prompt}}$  (top left),  $N_{\text{fromb}}$  (top right),  $N_{\text{tail}}$  (bottom left),  $N_{\text{bkg}}$  (bottom middle) and  $\tau_b$  (bottom right) in the bin  $14 < p_T < 20 \text{ GeV}/c$ ,  $2.0 < y < 4.5$ .

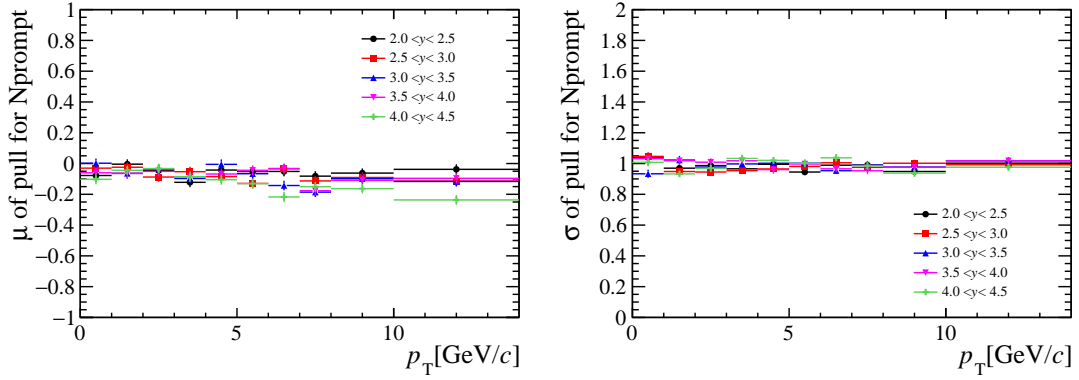


Figure K.4:  $\mu$  (left) and  $\sigma$  (right) of the pull distribution for  $N_{\text{prompt}}$  for all bins.

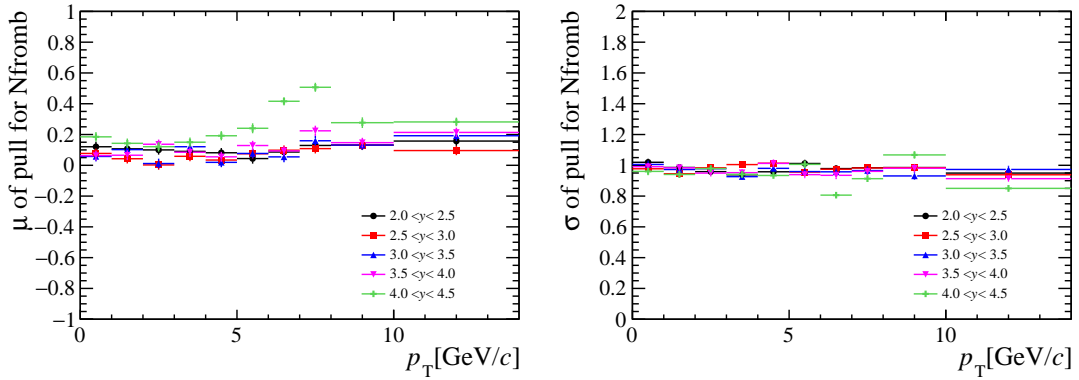


Figure K.5:  $\mu$  (left) and  $\sigma$  (right) of the pull distribution for  $N_{\text{fromb}}$  for all bins.

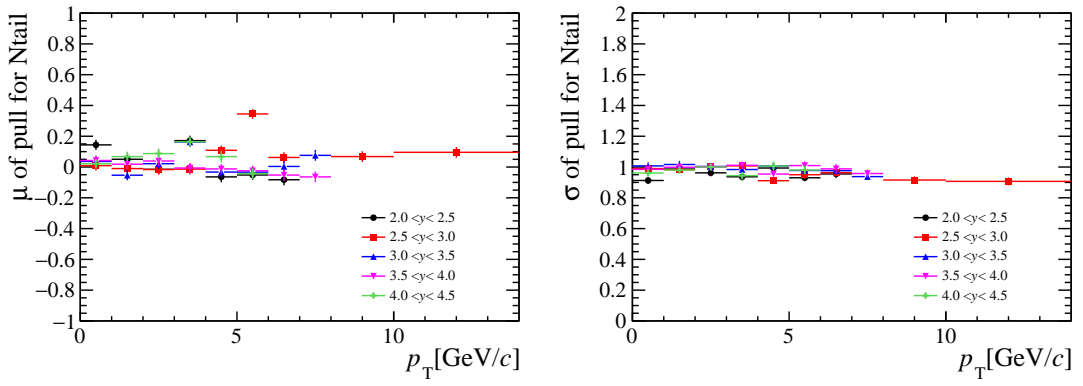


Figure K.6:  $\mu$  (left) and  $\sigma$  (right) of the pull distribution for  $N_{\text{tail}}$  for all bins.

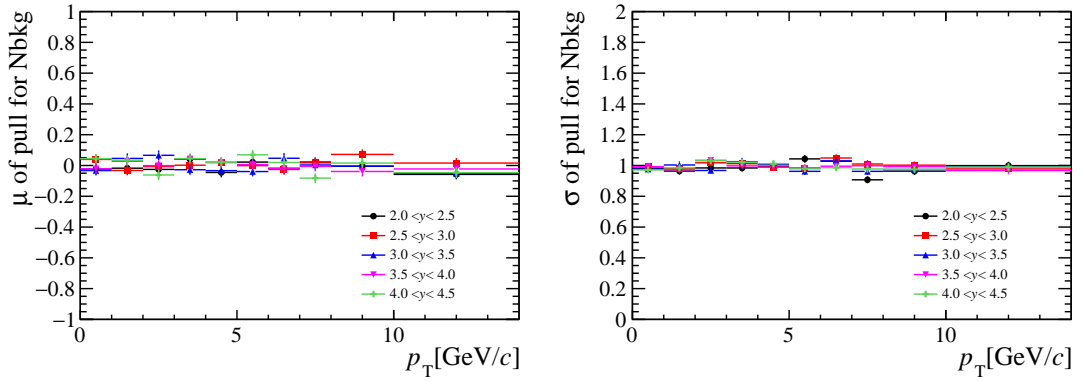


Figure K.7:  $\mu$  (left) and  $\sigma$  (right) of the pull distribution for  $N_{\text{bkg}}$  for all bins.

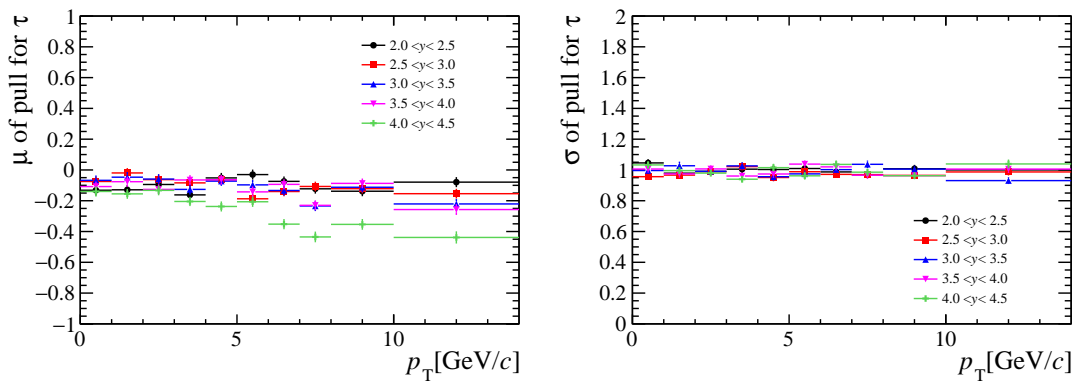


Figure K.8:  $\mu$  (left) and  $\sigma$  (right) of the pull distribution for  $\tau_b$  for all bins.

814 **References**

- 815 [1] C. E. Carlson and R. Suaya, *Hadronic production of  $J/\psi$  mesons*, Phys. Rev. **D14**  
816 (1976) 3115.
- 817 [2] A. Donnachie and P. V. Landshoff, *Production of lepton pairs,  $J/\psi$  and charm with*  
818 *hadron beams*, Nucl. Phys. **B112** (1976) 233.
- 819 [3] S. D. Ellis, M. B. Einhorn, and C. Quigg, *Comment on hadronic production of psions*,  
820 Phys. Rev. Lett. **36** (1976) 1263.
- 821 [4] H. Fritzsch, *Producing heavy quark flavors in hadronic collisions: A test of quantum*  
822 *chromodynamics*, Phys. Lett. **B67** (1977) 217.
- 823 [5] M. Glück, J. F. Owens, and E. Reya, *Gluon contribution to hadronic  $J/\psi$  production*,  
824 Phys. Rev. **D17** (1978) 2324.
- 825 [6] C.-H. Chang, *Hadronic production of  $J/\psi$  associated with a gluon*, Nucl. Phys. **B172**  
826 (1980) 425.
- 827 [7] R. Baier and R. Rückl, *Hadronic production of  $J/\psi$  and  $\Upsilon$ : Transverse momentum*  
828 *distributions*, Phys. Lett. **B102** (1981) 364.
- 829 [8] G. T. Bodwin, E. Braaten, and G. P. Lepage, *Rigorous QCD analysis of inclusive*  
830 *annihilation and production of heavy quarkonium*, Phys. Rev. **D51** (1995) 1125,  
831 arXiv:hep-ph/9407339.
- 832 [9] P. L. Cho and A. K. Leibovich, *Color octet quarkonia production*, Phys. Rev. **D53**  
833 (1996) 150, arXiv:hep-ph/9505329.
- 834 [10] P. L. Cho and A. K. Leibovich, *Color octet quarkonia production. 2.*, Phys. Rev. **D53**  
835 (1996) 6203, arXiv:hep-ph/9511315.
- 836 [11] CDF collaboration, F. Abe *et al.*,  *$J/\psi$  and  $\psi(2S)$  production in  $p\bar{p}$  collisions at*  
837  *$\sqrt{s} = 1.8 \text{ TeV}$* , Phys. Rev. Lett. **79** (1997) 572.
- 838 [12] J. M. Campbell, F. Maltoni, and F. Tramontano, *QCD corrections to  $J/\psi$*   
839 *and  $\Upsilon$  production at hadron colliders*, Phys. Rev. Lett. **98** (2007) 252002,  
840 arXiv:hep-ph/0703113.
- 841 [13] J. P. Lansberg,  *$J/\psi$  production at  $\sqrt{s} = 1.96$  and  $7 \text{ TeV}$ : colour-singlet model*,  
842 *NNLO\** and polarization, J. Phys. **G38** (2011) 124110, arXiv:1107.0292.
- 843 [14] B. Gong and J.-X. Wang, *Next-to-leading-order QCD corrections to  $J/\psi$  polarization*  
844 *at Tevatron and Large-Hadron-Collider energies*, Phys. Rev. Lett. **100** (2008) 232001,  
845 arXiv:0802.3727.
- 846 [15] M. Cacciari, M. Greco, M. L. Mangano, and A. Petrelli, *Charmonium production at*  
847 *the Tevatron*, Phys. Lett. **B356** (1995) 553, arXiv:hep-ph/9505379.
- 848 [16] E. Braaten and S. Fleming, *Color octet fragmentation and the psi-prime surplus at*  
849 *the Tevatron*, Phys. Rev. Lett. **74** (1995) 3327, arXiv:hep-ph/9411365.

- [17] Y.-Q. Ma, K. Wang, and K.-T. Chao, *Complete next-to-leading order calculation of the  $J/\psi$  and  $\psi'$  production at hadron colliders*, Phys. Rev. **D84** (2011) 114001, [arXiv:1012.1030](#).
- [18] B. Gong, X. Q. Li, and J.-X. Wang, *QCD corrections to  $J/\psi$  production via color-octet states at the Tevatron and LHC*, Phys. Lett. **B673** (2009) 197, [arXiv:0805.4751](#).
- [19] M. Butenschoen and B. A. Kniehl, *Reconciling  $J/\psi$  production at HERA, RHIC, Tevatron, and LHC with NRQCD factorization at next-to-leading order*, Phys. Rev. Lett. **106** (2011) 022003, [arXiv:1009.5662](#).
- [20] M. Beneke and I. Z. Rothstein,  *$\psi'$  polarization as a test of color octet quarkonium production*, Phys. Lett. **B372** (1996) 157, [arXiv:hep-ph/9509375](#).
- [21] K.-T. Chao *et al.*,  *$J/\psi$  polarization at hadron colliders in nonrelativistic QCD*, Phys. Rev. Lett. **108** (2012) 242004, [arXiv:1201.2675](#).
- [22] B. Gong, L.-P. Wan, J.-X. Wang, and H.-F. Zhang, *Polarization for prompt  $J/\psi$  and  $\psi(2S)$  production at the Tevatron and LHC*, Phys. Rev. Lett. **110** (2013) 042002, [arXiv:1205.6682](#).
- [23] M. Butenschoen and B. A. Kniehl,  *$J/\psi$  polarization at the Tevatron and the LHC: Nonrelativistic-QCD factorization at the crossroads*, Phys. Rev. Lett. **108** (2012) 172002, [arXiv:1201.1872](#).
- [24] CDF collaboration, A. Abulencia *et al.*, *Polarizations of  $J/\psi$  and  $\psi(2S)$  mesons produced in  $p\bar{p}$  collisions at  $\sqrt{s} = 1.96$  TeV*, Phys. Rev. Lett. **99** (2007) 132001, [arXiv:0704.0638](#).
- [25] D0 collaboration, V. M. Abazov *et al.*, *Measurement of the polarization of the  $\Upsilon(1S)$  and  $\Upsilon(2S)$  states in  $p\bar{p}$  collisions at  $\sqrt{s} = 1.96$  TeV*, Phys. Rev. Lett. **101** (2008) 182004, [arXiv:0804.2799](#).
- [26] ALICE collaboration, B. Abelev *et al.*,  *$J/\psi$  polarization in  $pp$  collisions at  $\sqrt{s} = 7$  TeV*, Phys. Rev. Lett. **108** (2012) 082001, [arXiv:1111.1630](#).
- [27] CMS collaboration, S. Chatrchyan *et al.*, *Measurement of the prompt  $J/\psi$  and  $\psi(2S)$  polarizations in  $pp$  collisions at  $\sqrt{s} = 7$  TeV*, Phys. Lett. **B727** (2013) 381, [arXiv:1307.6070](#).
- [28] CMS collaboration, S. Chatrchyan *et al.*, *Measurement of the  $\Upsilon(1S)$ ,  $\Upsilon(2S)$  and  $\Upsilon(3S)$  polarizations in  $pp$  collisions at  $\sqrt{s} = 7$  TeV*, Phys. Rev. Lett. **110** (2013) 081802, [arXiv:1209.2922](#).
- [29] LHCb, R. Aaij *et al.*, *Measurement of  $J/\psi$  polarization in  $pp$  collisions at  $\sqrt{s} = 7$  TeV*, Eur. Phys. J. **C73** (2013) 2631, [arXiv:1307.6379](#).
- [30] LHCb, R. Aaij *et al.*, *Measurement of  $\psi(2S)$  polarisation in  $pp$  collisions at  $\sqrt{s} = 7$  TeV*, Eur. Phys. J. **C74** (2014) 2872, [arXiv:1403.1339](#).
- [31] ALICE collaboration, B. Abelev *et al.*, *Inclusive  $J/\psi$  production in  $pp$  collisions at  $\sqrt{s} = 2.76$  TeV*, Phys. Lett. **B718** (2012) 295, [arXiv:1203.3641](#).

- [32] LHCb collaboration, R. Aaij *et al.*, *Measurement of  $J/\psi$  production in  $pp$  collisions at  $\sqrt{s} = 2.76 \text{ TeV}$* , JHEP **02** (2013) 041, [arXiv:1212.1045](#).
- [33] LHCb collaboration, R. Aaij *et al.*, *Measurement of  $J/\psi$  production in  $pp$  collisions at  $\sqrt{s} = 7 \text{ TeV}$* , Eur. Phys. J. **C71** (2011) 1645, [arXiv:1103.0423](#).
- [34] CMS collaboration, V. Khachatryan *et al.*, *Prompt and non-prompt  $J/\psi$  production in  $pp$  collisions at  $\sqrt{s} = 7 \text{ TeV}$* , Eur. Phys. J. **C71** (2011) 1575, [arXiv:1011.4193](#).
- [35] ATLAS collaboration, G. Aad *et al.*, *Measurement of the differential cross-sections of inclusive, prompt and non-prompt  $J/\psi$  production in proton-proton collisions at  $\sqrt{s} = 7 \text{ TeV}$* , Nucl. Phys. **B850** (2011) 387, [arXiv:1104.3038](#).
- [36] ALICE collaboration, K. Aamodt *et al.*, *Rapidity and transverse momentum dependence of inclusive  $J/\psi$  production in  $pp$  collisions at  $\sqrt{s} = 7 \text{ TeV}$* , Phys. Lett. **B704** (2011) 442, [arXiv:1105.0380](#).
- [37] CMS collaboration, S. Chatrchyan *et al.*,  *$J/\psi$  and  $\psi(2S)$  production in  $pp$  collisions at  $\sqrt{s} = 7 \text{ TeV}$* , JHEP **02** (2012) 011, [arXiv:1111.1557](#).
- [38] LHCb collaboration, R. Aaij *et al.*, *Production of  $J/\psi$  and  $\Upsilon$  mesons in  $pp$  collisions at  $\sqrt{s} = 8 \text{ TeV}$* , JHEP **06** (2013) 064, [arXiv:1304.6977](#).
- [39] LHCb collaboration, R. Aaij *et al.*, *Measurement of forward  $J/\psi$  production cross-sections in  $pp$  collisions at  $\sqrt{s} = 13 \text{ TeV}$* , JHEP **10** (2015) 172, Erratum *ibid.* **05** (2017) 063, [arXiv:1509.00771](#).
- [40] LHCb collaboration, R. Aaij *et al.*, *Measurement of  $J/\psi$  polarization in  $pp$  collisions at  $\sqrt{s} = 7 \text{ TeV}$* , Eur. Phys. J. **C73** (2013) 2631, [arXiv:1307.6379](#).
- [41] M. Cacciari, M. Greco, and P. Nason, *The  $P(T)$  spectrum in heavy flavor hadroproduction*, JHEP **9805** (1998) 007, [arXiv:hep-ph/9803400](#).
- [42] LHCb, R. Aaij *et al.*, *Study of  $J/\psi$  production and cold nuclear matter effects in  $pPb$  collisions at  $\sqrt{s_{NN}} = 5 \text{ TeV}$* , JHEP **02** (2014) 072, [arXiv:1308.6729](#).
- [43] V. Balagura, *Lhcb luminosity project*, Update of Run 2 luminosity values for  $pp$  at 13 and 5.02 TeV (2021-02-22).
- [44] T. Sjöstrand, S. Mrenna, and P. Skands, *PYTHIA 6.4 physics and manual*, JHEP **05** (2006) 026, [arXiv:hep-ph/0603175](#).
- [45] I. Belyaev *et al.*, *Handling of the generation of primary events in Gauss, the LHCb simulation framework*, J. Phys. Conf. Ser. **331** (2011) 032047.
- [46] D. J. Lange, *The EvtGen particle decay simulation package*, Nucl. Instrum. Meth. **A462** (2001) 152.
- [47] P. Golonka and Z. Was, *PHOTOS Monte Carlo: A precision tool for QED corrections in  $Z$  and  $W$  decays*, Eur. Phys. J. **C45** (2006) 97, [arXiv:hep-ph/0506026](#).
- [48] Geant4 collaboration, S. Agostinelli *et al.*, *Geant4: A simulation toolkit*, Nucl. Instrum. Meth. **A506** (2003) 250.

- [49] Geant4 collaboration, J. Allison *et al.*, *Geant4 developments and applications*, IEEE Trans. Nucl. Sci. **53** (2006) 270.
- [50] M. Clemencic *et al.*, *The LHCb simulation application, Gauss: Design, evolution and experience*, J. Phys. Conf. Ser. **331** (2011) 032023.
- [51] M. Bargiotti and V. Vagnoni, *Heavy quarkonia sector in PYTHIA 6.324: Tuning, validation and perspectives at LHC(b)*, CERN-LHCB-2007-042.
- [52] Particle Data Group, P. A. Z. *et al.* , *Review of particle physics*, Progress of Theoretical and Experimental Physics **2020** (2020).
- [53] W. Qian, *J/ $\psi$  Production Study at the LHCb Experiment*, CERN-THESIS-2010-116, 2010. Presented on 02 Sep 2010.
- [54] T. Skwarnicki, *A study of the radiative cascade transitions between the Upsilon-prime and Upsilon resonances*, PhD thesis, Institute of Nuclear Physics, Krakow, 1986, DESY-F31-86-02.
- [55] J. Lefrancous, *Crystal ball fits*, link.
- [56] *Tracking correction table*, twiki page link.
- [57] M. Cacciari *et al.*, *Theoretical predictions for charm and bottom production at the LHC*, JHEP **10** (2012) 137, arXiv:1205.6344.
- [58] M. Cacciari, M. L. Mangano, and P. Nason, *Gluon PDF constraints from the ratio of forward heavy-quark production at the LHC at  $\sqrt{S} = 7$  and 13 TeV*, Eur. Phys. J. **C75** (2015) 610, arXiv:1507.06197.
- [59] Y.-Q. Ma, K. Wang, and K.-T. Chao,  *$J/\psi(\psi')$  production at the Tevatron and LHC at  $\mathcal{O}(\alpha_s^4 v^4)$  in nonrelativistic QCD*, Phys. Rev. Lett. **106** (2011) 042002, arXiv:1009.3655.
- [60] Y.-Q. Ma and R. Venugopalan, *Comprehensive Description of  $J/\psi$  Production in Proton-Proton Collisions at Collider Energies*, Phys. Rev. Lett. **113** (2014) 192301, arXiv:1408.4075.
- [61] J. L. Albacete, A. Dumitru, H. Fujii, and Y. Nara, *CGC predictions for  $p + Pb$  collisions at the LHC*, Nucl. Phys. **A897** (2013) 1, arXiv:1209.2001.
- [62] K. Watanabe and B.-W. Xiao, *Forward Heavy Quarkonium Productions at the LHC*, Phys. Rev. **D92** (2015) 111502, arXiv:1507.06564.
- [63] ALICE and LHCb collaborations, *Reference pp cross-sections for  $J/\psi$  studies in proton-lead collisions at  $\sqrt{s_{NN}} = 5.02$  TeV and comparisons between ALICE and LHCb results*, Dec, 2013. LHCb-CONF-2013-013, ALICE-PUBLIC-2013-002.
- [64] E. G. Ferreiro, F. Fleuret, J. P. Lansberg, and A. Rakotozafindrabe, *Impact of the Nuclear Modification of the Gluon Densities on  $J/\psi$  production in  $pPb$  collisions at  $\sqrt{s_{NN}} = 5$  TeV*, Phys. Rev. **C88** (2013) 047901, arXiv:1305.4569.

- 961 [65] J. L. Albacete *et al.*, *Predictions for  $p+Pb$  Collisions at  $\sqrt{s_{NN}} = 5$  TeV*, Int. J. Mod.  
962 Phys. **E22** (2013) 1330007, [arXiv:1301.3395](#).
- 963 [66] F. Arleo and S. Peigne, *Heavy-quarkonium suppression in  $p-A$  collisions from parton  
964 energy loss in cold QCD matter*, JHEP **03** (2013) 122, [arXiv:1212.0434](#).
- 965 [67] G. Punzi, *Comments on likelihood fits with variable resolution*, eConf **C030908**  
966 (2003) WELT002, [arXiv:physics/0401045](#).